Angle-resolved photoemission studies of the cuprate superconductors

Andrea Damascelli*

Stanford Synchrotron Radiation Laboratory, Stanford University, Stanford, California 94305

Zahid Hussain

Advanced Light Source, Lawrence Berkeley National Laboratory, Berkeley, California 94720

Zhi-Xun Shen

Department of Physics, Applied Physics and Stanford Synchrotron Radiation Laboratory, Stanford University, Stanford, California 94305

(Published 17 April 2003)

The last decade witnessed significant progress in angle-resolved photoemission spectroscopy (ARPES) and its applications. Today, ARPES experiments with 2-meV energy resolution and 0.2° angular resolution are a reality even for photoemission on solids. These technological advances and the improved sample quality have enabled ARPES to emerge as a leading tool in the investigation of the high-T_c superconductors. This paper reviews the most recent ARPES results on the cuprate superconductors and their insulating parent and sister compounds, with the purpose of providing an updated summary of the extensive literature. The low-energy excitations are discussed with emphasis on some of the most relevant issues, such as the Fermi surface and remnant Fermi surface, the superconducting gap, the pseudogap and d-wave-like dispersion, evidence of electronic inhomogeneity and nanoscale phase separation, the emergence of coherent quasiparticles through the superconducting transition, and many-body effects in the one-particle spectral function due to the interaction of the charge with magnetic and/or lattice degrees of freedom. Given the dynamic nature of the field, we chose to focus mainly on reviewing the experimental data, as on the experimental side a general consensus has been reached, whereas interpretations and related theoretical models can vary significantly. The first part of the paper introduces photoemission spectroscopy in the context of strongly interacting systems, along with an update on the state-of-the-art instrumentation. The second part provides an overview of the scientific issues relevant to the investigation of the low-energy electronic structure by ARPES. The rest of the paper is devoted to the experimental results from the cuprates, and the discussion is organized along conceptual lines: normal-state electronic structure, interlayer interaction, superconducting gap, coherent superconducting peak, pseudogap, electron self-energy, and collective modes. Within each topic, ARPES data from the various copper oxides are presented.

CONTENTS

*Present address: Department of Physics & Astronomy, University of British Columbia, 6224 Agricultural Road, Vancouver, British Columbia, Canada V6T 1Z1.

I. INTRODUCTION

The discovery of superconductivity at 30 K in the LaBaCuO ceramics by Bednorz and Müller (1986) opened the era of *high-T_c superconductivity*, changing the history of a phenomenon that had before been confined to very low temperatures [until 1986 the maximum value of T_c was limited to the 23.2 K observed in Nb_3Ge (Gavaler, 1973; Testardi *et al.*, 1974)]. This unexpected result prompted intense activity in the field of ceramic oxides and has led to the synthesis of compounds with increasingly higher T_c, all characterized by a layered crystal structure with one or more CuO_2 planes per unit cell, and a quasi-two-dimensional (2D) electronic structure. By 1987, a T_c of approximately 90 K (i.e., higher than the boiling point of liquid nitrogen at 77 K) was already observed in $YBa_2Cu_3O_{7-\delta}$ (Wu *et al.*, 1987). The record T_c of 133.5 K (at atmospheric pressure) was later obtained in the trilayer system $HgBa_2Ca_2Cu_3O_{8+x}$ (Schilling *et al.*, 1993).

One may wonder whether the impact of the discovery by Bednorz and Müller (1986) would have been somewhat overlooked if MgB_2, with its recently ascertained 39 K T_c, had already been discovered [Nagamatsu *et al.* (2001); for a review see Day (2001)]. However, independent of the values of T_c the observation of superconductivity in the ceramic copper oxides was in itself an unexpected and surprising result. In fact, ceramic materials are typically insulators, and this is also the case for the undoped copper oxides. However, when doped the latter can become poor metals in the normal state and high-temperature superconductors upon reducing the temperature (see in Fig. 1 the phenomenological phase diagram of electron- and hole-doped high-temperature superconductors, here represented by $Nd_{2-x}Ce_xCuO_4$ and $La_{2-x}Sr_xCuO_4$, respectively). In addition, the detailed investigation of their phase diagram revealed that the macroscopic properties of the copper oxides are profoundly influenced by *strong electron-electron correlations* (i.e., large Coulomb repulsion U). Naively, this is not expected to favor the emergence of superconductivity, for which electrons must be bound together to form Cooper pairs. Even though the approximate T^2 dependence of the resistivity observed in the overdoped metallic regime was taken as evidence for *Fermi-liquid behavior*, the applicability of Fermi-liquid theory (which describes electronic excitations in terms of an interacting gas of renormalized quasiparticles; see Sec. II.C) to the "normal" metallic state of high-temperature superconductors is questionable, because many properties do not follow canonical Fermi-liquid behavior (Orenstein and Millis, 2000). This breakdown of Fermi-liquid theory and of the single-particle picture becomes most dramatic upon approaching the undoped line of the phase diagram ($x=0$ in Fig. 1), where one finds the antiferromagnetic Mott insulator (see Sec. III). On top of this complexity, it has long been recognized that also the interplay between electronic and lattice degrees of freedom as well as the tendencies towards phase separation are strong in these componds (Sigmund and Müller, 1993; Müller, 2000).

The cuprate high-temperature superconductors have attracted great interest not only for the obvious application potential related to their high T_c, but also for their scientific significance. This stems from the fact that they highlight a major intellectual crisis in the quantum theory of solids, which, in the form of one-electron band theory, has been very successful in describing good metals (like Cu) but has proven inadequate for strongly correlated electron systems. In turn, the Bardeen-Cooper-Schrieffer (BCS) theory (Bardeen *et al.*, 1957; see also Schrieffer, 1964), which was developed for Fermi-liquid-like metals and has been so successful in describing conventional superconductors, does not seem to have the appropriate foundation for the description of high-T_c superconductivity. In order to address the scope of the current approach in the quantum theory of solids and the validity of the proposed alternative models, a detailed comparison with those experiments that probe the electronic properties and the nature of the elementary excitations is required.

In this context, angle-resolved photoemission spectroscopy (ARPES) plays a major role because it is the most direct method of studying the electronic structure of solids (see Sec. II). Its large impact on the development of many-body theories stems from the fact that this technique provides information on the single-particle Green's function, which can be calculated starting from a

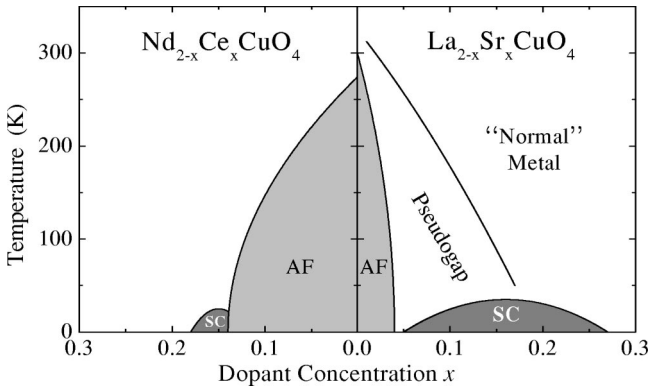

FIG. 1. Phase diagram of n- and p-type superconductors, showing superconductivity (SC), antiferromagnetic (AF), pseudogap, and normal-metal regions.

microscopic Hamiltonian. Driven by the demand, a significant improvement in instrumental resolution and detection efficiency has taken place over the last decade. Owing also to continuously improved sample quality, the stage was set for ARPES to emerge as a leading experimental probe in the study of the high-T_c superconductors. Indeed, many of the ARPES results have broadly impacted the field (Levi, 1990, 1993, 1996; Mitton, 1995, 1998), such as the observation of dispersive electronic features (Takahashi *et al.*, 1988; Olson *et al.*, 1989), of the d-wave superconducting gap (Wells *et al.*, 1992; Shen *et al.*, 1993), of the dispersion of a single hole in the antiferromagnetic insulator (Wells *et al.*, 1995), of the normal-state pseudogap (Ding, Yokoya, *et al.*, 1996; Loeser *et al.*, 1996; Marshall *et al.*, 1996), of spin-charge separation in one-dimensional cuprates (Kim *et al.*, 1996), and of strong electron-proton interaction in p-type cuprates (Lanzara *et al.*, 2001).

In such a rapidly evolving field, one is always presented with a dilemma when deciding whether and how to write a review. On the one hand, it may be premature to proceed with an extensive review, but on the other hand it is helpful for the broader community to have access to a summary of the current state of the subject. It is our intention to present a "snapshot" of the investigation of the high-T_c superconductors by ARPES taken at the time of completion of this article. This will help the readers, especially those who are not photoemission experts, to sort through the extensive literature, learn about the outstanding problems, and become aware of the level of consensus. The downside is that some of the most recent results we discuss may be outpaced by the rapid advance of the field. With this in mind, we limit the scope of our review to ARPES results only, without making detailed comparison with other techniques except when necessary. We shall focus mainly on results reported after 1994, as the previous period has already been extensively reviewed (Shen and Dessau, 1995).[1] In addition, because over the last two years we have witnessed a dramatic improvement of energy and especially momentum resolution with the introduction of the Scienta SES200 electron analyzer, more emphasis will be given to ARPES data obtained with this kind of spectrometer, whenever available. As this review paper will deal mostly with experimental results, we shall refer only to those theoretical concepts and models which are explicitly relevant to the discussion of the ARPES data on the high-temperature superconductors. Furthermore, as the doping evolution is probably the best comparison between theory and experiment, we shall discuss ARPES data on different high-temperature superconductors and on their insulating parent compounds, focusing in particular on systematic changes in the electronic structure which may be relevant to the development of a comprehensive picture for the evolution from Mott insulator to overdoped superconductor.

[1]For more recent reviews see Randeria and Campuzano (1997); Lynch and Olson (1999); Tohyama and Maekawa (2000); Damascelli, Lu, and Shen (2001); Golden *et al.* (2001); Johnson, Fedorov and Valla (2001); Kim (2001).

II. ANGLE-RESOLVED PHOTOEMISSION SPECTROSCOPY

A. General description

Photoelectron spectroscopy is a general term which refers to all techniques based on the photoelectric effect originally observed by Hertz (1887). This was later explained as a manifestation of the quantum nature of light by Einstein (1905), who recognized that when light is incident on a sample an electron can absorb a photon and escape from the material with a maximum kinetic energy $h\nu-\phi$ (where ν is the photon frequency and ϕ, the material work function, is a measure of the potential barrier at the surface that prevents the valence electrons from escaping, typically around 4–5 eV for metals). As a description of the spectroscopic techniques based on the detection of photoemitted electrons is beyond the scope of this review, we shall only summarize the experimental and theoretical aspects relevant to the discussion of the ARPES results presented throughout the paper. For a more detailed description of ARPES and other photoelectron spectroscopies, we refer the reader to the extensive literature available on the subject.[2]

The energetics of the photoemission process and of the geometry of an ARPES experiment are sketched in Figs. 2 and 3(a). A beam of monochromatized radiation supplied either by a gas-discharge lamp or a synchrotron beamline is incident on a sample (which has to be a properly aligned single crystal, in order to perform momentum-resolved measurements). As a result, electrons are emitted by the photoelectric effect and escape into the vacuum in all directions. By collecting the photoelectrons with an electron energy analyzer characterized by a finite acceptance angle, one measures the kinetic energy E_{kin} of the photoelectrons for a given emission angle. This way, the photoelectron momentum **p** is also completely determined: its modulus is given by $p=\sqrt{2mE_{kin}}$ and its components parallel and perpen-

[2]A very detailed list of review articles and books dedicated to photoelectron spectroscopy on solids was recently given by Lynch and Olson (1999) in their book dealing with photoemission spectroscopy on high-temperature superconductors. It is here reproduced with some additions: Smith (1971); Eastman (1972); Carlson (1975); Feuerbacher and Willis (1976); Brundle and Baker (1977, 1978); Cardona and Ley (1978); Feuerbacher *et al.* (1978); Mahan (1978); Wertheim (1978); Ley and Cardona (1979); Nemoshkalenko and Aleshin (1979); Lindau and Spicer (1980); Williams *et al.* (1980); Inglesfield and Holland (1981); Wendin (1981); Leckey (1982); Plummer and Eberhardt (1982); Himpsel (1983); Margaritondo and Weaver (1983); Smith and Himpsel (1983); Courths and Hüfner (1984); Smith and Kevan (1991); Bachrach (1992); Kevan (1992); Hüfner (1995); Shen and Dessau (1995); Braun (1996); Grioni (2001).

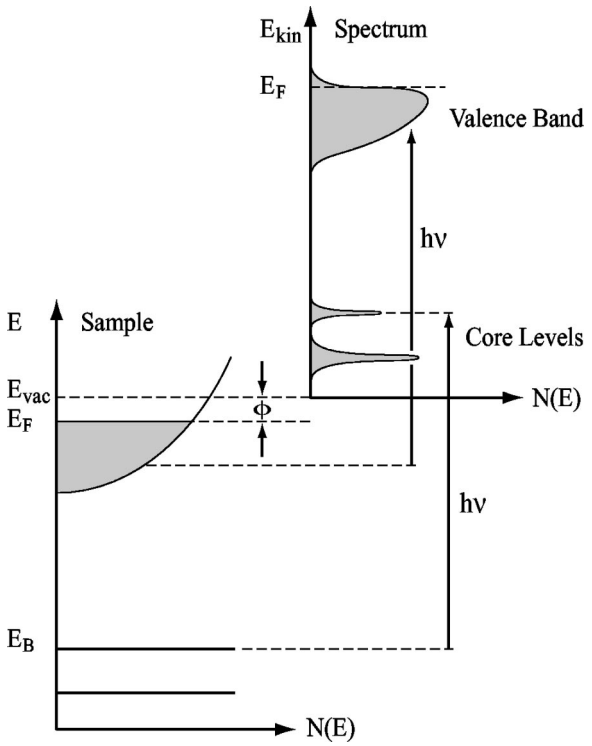

FIG. 2. Energetics of the photoemission process. The electron energy distribution produced by incoming photons and measured as a function of the kinetic energy E_{kin} of the photoelectrons (right) is more conveniently expressed in terms of the binding energy E_B (left) when one refers to the density of states inside the solid ($E_B=0$ at E_F). From Hüfner, 1995.

dicular to the sample surface are obtained from the polar (ϑ) and azimuthal (φ) emission angles.

Within the noninteracting electron picture, and by taking advantage of total energy and momentum conservation laws (note that the photon momentum can be neglected at the low photon energies typically used in ARPES experiments), one can relate the kinetic energy and momentum of the photoelectron to the binding energy E_B and crystal momentum $\hbar\mathbf{k}$ inside the solid:

$$E_{kin}=h\nu-\phi-|E_B|, \tag{1}$$

$$\mathbf{p}_{\parallel}=\hbar\mathbf{k}_{\parallel}=\sqrt{2mE_{kin}}\cdot\sin\vartheta. \tag{2}$$

Here $\hbar\mathbf{k}_{\parallel}$ is the component parallel to the surface of the electron crystal momentum in the *extended* zone scheme. Upon going to larger ϑ angles, one actually probes electrons with $\mathbf{k}$ lying in higher-order Brillouin zones. By subtracting the corresponding reciprocal-lattice vector $\mathbf{G}$, one obtains the *reduced* electron crystal momentum in the first Brillouin zone. Note that the perpendicular component of the wave vector $\mathbf{k}_{\perp}$ is not conserved across the sample surface due to the lack of translational symmetry along the surface normal. This implies that, in general, even experiments performed for all $\mathbf{k}_{\parallel}$ (i.e., by collecting photoelectrons at all possible angles) will not allow a complete determination of the total crystal wave vector $\mathbf{k}$ [unless some *a priori* assumption is made for the dispersion $E(\mathbf{k})$ of the electron final states involved in the photoemission process]. In this regard it has to be mentioned that several specific experimental methods for absolute three-dimensional band mapping have also been developed (see, for example, Hüfner, 1995; Strocov *et al.*, 1997, 1998).

A particular case in which the uncertainty in $\mathbf{k}_{\perp}$ is less relevant is that of the low-dimensional systems characterized by an anisotropic electronic structure and, in particular, a negligible dispersion along the z axis [i.e., along the surface normal; see Fig. 3(a)]. The electronic dispersion is then almost exclusively determined by $\mathbf{k}_{\parallel}$, as in the case of the 2D copper oxide superconductors which we shall focus on throughout this paper [note, however, that possible complications arising from a finite three-dimensionality of the initial and/or final states involved in the photoemission process should always be carefully considered (Lindroos *et al.*, 2002)]. As a result, one can map out in detail the electronic dispersion relations $E(\mathbf{k}_{\parallel})$ simply by tracking, as a function of $\mathbf{p}_{\parallel}$, the energy position of the peaks detected in the ARPES spectra for different takeoff angles [as in Fig. 3(b), where both direct and inverse photoemission spectra for a single band dispersing through the Fermi energy E_F are shown]. As an additional bonus of the lack of z dispersion, one can directly identify the width of the photoemission peaks with the lifetime of the photohole (Smith *et al.*, 1993), which contains information on the intrinsic correlation effects of the system and is formally described by the imaginary part of the electron self-energy (see Sec. II.C). In contrast, in 3D systems the linewidth contains contributions from both photohole and photoelectron lifetimes, with the latter reflecting final-state scattering processes and thus the finite probing depth; as a consequence, isolating the intrinsic many-body effects becomes a much more complicated problem.

Before moving on to the discussion of some theoretical issues, it is worth pointing out that most ARPES experiments are performed at photon energies in the ultraviolet (in particular for $h\nu<100$ eV). The main reason is that by working at lower photon energies it is possible to achieve higher energy and momentum resolution. This is easy to see for the case of the momentum resolution $\Delta\mathbf{k}_{\parallel}$ which, from Eq. (2) and neglecting the contribution due to the finite energy resolution, is

$$\Delta\mathbf{k}_{\parallel}\simeq\sqrt{2mE_{kin}/\hbar^2}\cdot\cos\vartheta\cdot\Delta\vartheta, \tag{3}$$

where $\Delta\vartheta$ corresponds to the finite acceptance angle of the electron analyzer. From Eq. (3) it is clear that the momentum resolution will be better at lower photon energy (i.e., lower E_{kin}), and for larger polar angles ϑ (note that one can effectively improve the momentum resolution by extending the measurements to momenta outside the first Brillouin zone). By working at low photon energies there are also some additional advantages: first, for a typical beamline it is easier to achieve high-energy resolution (see Sec. II.E); second, one can completely disregard the photon momentum $\kappa=2\pi/\lambda$ in Eq. (2), as for 100-eV photons the momentum is 3% ($0.05\ \text{Å}^{-1}$) of the typical Brillouin-zone size of the cuprates ($2\pi/a\simeq1.6\ \text{Å}^{-1}$), and at 21.2 eV (the HeIα line

typically used on ARPES systems equipped with a gas-discharge lamp) it is only 0.5% ($0.008\ \text{Å}^{-1}$). If, on the other hand, the photon momentum is not negligible, the photoemission process does not involve vertical transitions, and κ must be explicitly taken into account in Eq. (2). For example, for 1487-eV photons (the Al K_α line commonly used in x-ray photoemission) $\kappa \simeq 0.76\ \text{Å}^{-1}$, which corresponds to 50% of the zone size.

A major drawback of working at low photon energies is the extreme surface sensitivity. The mean free path for unscattered photoelectrons is characterized by a minimum of approximately 5 Å at 20–100 eV kinetic energies (Seah and Dench, 1979), which are typical values in ARPES experiments. This means that a considerable fraction of the total photoemission intensity will be representative of the topmost surface layer, especially on systems characterized by a large structural/electronic anisotropy and, in particular, by relatively large c-axis lattice parameters, such as the cuprates. Therefore, in order to learn about the bulk electronic structure, ARPES experiments have to be performed on atomically clean and well-ordered systems, which implies that fresh and flat surfaces have to be prepared immediately prior to the experiment in ultrahigh-vacuum conditions (typically at pressures lower than 5×10^{-11} torr). So far, the best ARPES results on copper oxide superconductors have been obtained on samples cleaved *in situ*, which, however, requires a natural cleavage plane for the material under investigation and explains why not all the cuprates are suitable for ARPES experiments.

B. Three-step model and sudden approximation

To develop a formal description of the photoemission process, one has to calculate the transition probability w_{fi} for an optical excitation between the N-electron ground state Ψ_i^N and one of the possible final states Ψ_f^N. This can be approximated by Fermi's golden rule:

$$w_{fi}=\frac{2\pi}{\hbar}|\langle\Psi_f^N|H_{int}|\Psi_i^N\rangle|^2\delta(E_f^N-E_i^N-h\nu), \tag{4}$$

where $E_i^N=E_i^{N-1}-E_B^{\mathbf{k}}$ and $E_f^N=E_f^{N-1}+E_{kin}$ are the initial- and final-state energies of the N-particle system ($E_B^{\mathbf{k}}$ is the binding energy of the photoelectron with kinetic energy E_{kin} and momentum $\mathbf{k}$). The interaction with the photon is treated as a perturbation given by

$$H_{int}=-\frac{e}{2mc}(\mathbf{A}\cdot\mathbf{p}+\mathbf{p}\cdot\mathbf{A})=-\frac{e}{mc}\mathbf{A}\cdot\mathbf{p}, \tag{5}$$

where $\mathbf{p}$ is the electronic momentum operator and $\mathbf{A}$ is the electromagnetic vector potential (note that the gauge $\Phi=0$ was chosen for the scalar potential Φ, and the quadratic term in $\mathbf{A}$ was dropped because in the linear optical regime it is typically negligible with respect to the linear terms). In Eq. (5) we also made use of the commutator relation $[\mathbf{p},\mathbf{A}]=-i\hbar\nabla\cdot\mathbf{A}$ and dipole approximation (i.e., $\mathbf{A}$ constant over atomic dimensions and therefore $\nabla\cdot\mathbf{A}=0$, which holds in the ultraviolet). Although this is a routinely used approximation, it should be noted that $\nabla\cdot\mathbf{A}$ might become important at the surface, where the electromagnetic fields may have a strong spatial dependence, giving rise to a significant intensity for indirect transitions. This surface photoemission contribution, which is proportional to $(\varepsilon-1)$ where ε is the medium dielectric function, can interfere with the bulk contribution, resulting in asymmetric line shapes for the bulk direct-transition peaks.[3] At this point, a more rigorous approach is to proceed with the so-called *one-step model* in which photon absorption, electron removal, and electron detection are treated as a single coherent process.[4] In this case bulk, surface, and vacuum have to be included in the Hamiltonian describing the crystal, which implies that not only bulk states have to be considered, but also surface and evanescent states, as well as surface resonances. However, due to the complexity of the one-step model, photoemission data are usually discussed within the *three-step model*, which, although purely phenomenological, has proven to be rather successful (Fan, 1945; Berglund and Spicer, 1964; Feibelman and Eastman, 1974). Within this approach, the photoemission process is subdivided into three independent and sequential steps:

(i) Optical excitation of the electron in the bulk.
(ii) Travel of the excited electron to the surface.
(iii) Escape of the photoelectron into vacuum.

The total photoemission intensity is then given by the product of three independent terms: the total probability for the optical transition, the scattering probability for the traveling electrons, and the transmission probability through the surface potential barrier. Step (i) contains all the information about the intrinsic electronic structure of the material and will be discussed in detail below. Step (ii) can be described in terms of an effective mean free path, proportional to the probability that the excited electron will reach the surface without scattering (i.e., with no change in energy and momentum). The inelastic-scattering processes, which determine the surface sensitivity of photoemission (as discussed in the previous section), also give rise to a continuous background in the spectra which is usually ignored or subtracted. Step (iii) is described by a transmission probability through the surface, which depends on the energy of the excited electron as well as the material work function ϕ.

In evaluating step (i), and therefore the photoemission intensity in terms of the transition probability w_{fi}, it would be convenient to factorize the wave functions in Eq. (4) into photoelectron and $(N-1)$-electron terms,

[3]For more details on the surface photoemission effects see for example Feuerbacher *et al.* (1978); Miller *et al.* (1996); Hansen *et al.* (1997a, 1997b).

[4]See, for example, Mitchell (1934); Makinson (1949); Buckingham (1950); Mahan (1970); Schaich and Ashcroft (1971); Feibelman and Eastman (1974); Pendry (1975, 1976); Liebsch (1976, 1978); Bansil and Lindroos (1995, 1998, 1999); Lindroos and Bansil (1995, 1996).

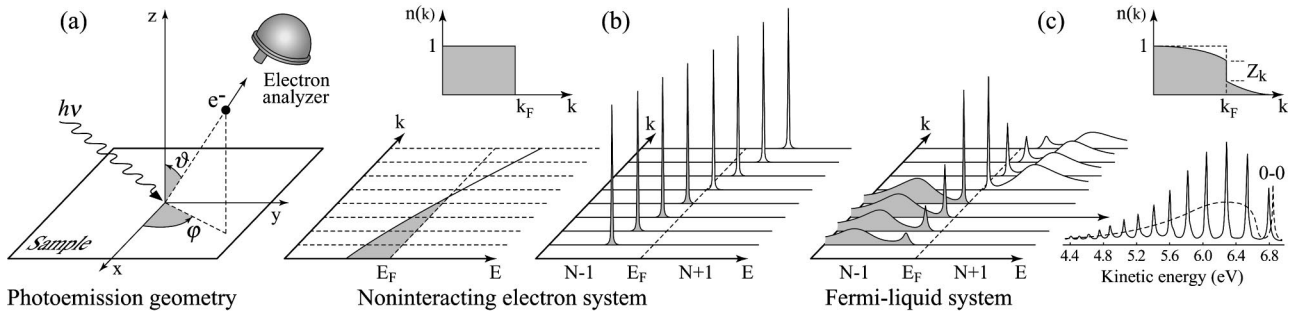

FIG. 3. Angle-resolved photoemission spetroscopy: (a) geometry of an ARPES experiment in which the emission direction of the photoelectron is specified by the polar (ϑ) and azimuthal (φ) angles; (b) momentum-resolved one-electron removal and addition spectra for a noninteracting electron system with a single energy band dispersing across E_F; (c) the same spectra for an interacting Fermi-liquid system (Sawatzky, 1989; Meinders, 1994). For both noninteracting and interacting systems the corresponding ground-state ($T=0$ K) momentum distribution function $n(\mathbf{k})$ is also shown. (c) Lower right, photoelectron spectrum of gaseous hydrogen and the ARPES spectrum of solid hydrogen developed from the gaseous one (Sawatzky, 1989).

as we have done for the corresponding energies. This, however, is far from trivial because during the photoemission process itself the system will relax. The problem simplifies within the *sudden approximation*, which is extensively used in many-body calculations of photoemission spectra from interacting electron systems and which is in principle applicable only to electrons with high kinetic energy. In this limit, the photoemission process is assumed to be *sudden*, with no post-collisional interaction between the photoelectron and the system left behind (in other words, an electron is instantaneously removed and the effective potential of the system changes discontinuously at that instant). The N-particle final state Ψ_f^N can then be written as

$$\Psi_f^N = \mathcal{A}\,\phi_f^{\mathbf{k}}\,\Psi_f^{N-1}, \tag{6}$$

where $\mathcal{A}$ is an antisymmetric operator that properly antisymmetrizes the N-electron wave function so that the Pauli principle is satisfied, $\phi_f^{\mathbf{k}}$ is the wave function of the photoelectron with momentum $\mathbf{k}$, and Ψ_f^{N-1} is the final state wave function of the $(N-1)$-electron system left behind, which can be chosen as an excited state with eigenfunction Ψ_m^{N-1} and energy E_m^{N-1}. The total transition probability is then given by the sum over all possible excited states m. Note, however, that the sudden approximation is inappropriate for photoelectrons with low kinetic energy, which may need longer than the system response time to escape into vacuum. In this case, the so-called *adiabatic limit*, one can no longer factorize Ψ_f^N into two independent parts and the detailed screening of photoelectron and photohole has to be taken into account (Gadzuk and Šunjić, 1975). In this regard, it is important to mention that there is evidence that the sudden approximation is justified for the cuprate high-temperature superconductors even at photon energies as low as 20 eV (Randeria *et al.*, 1995; Sec. II.C).

For the initial state, let us assume for simplicity that Ψ_i^N is a single Slater determinant (i.e., Hartree-Fock formalism), so that we can write it as the product of a one-electron orbital $\phi_i^{\mathbf{k}}$ and an $(N-1)$-particle term:

$$\Psi_i^N = \mathcal{A}\,\phi_i^{\mathbf{k}}\,\Psi_i^{N-1}. \tag{7}$$

More generally, however, Ψ_i^{N-1} should be expressed as $\Psi_i^{N-1}=c_{\mathbf{k}}\Psi_i^N$, where $c_{\mathbf{k}}$ is the annihilation operator for an electron with momentum $\mathbf{k}$. This also shows that Ψ_i^{N-1} is *not* an eigenstate of the $(N-1)$ particle Hamiltonian, but is just what remains of the N-particle wave function after having pulled out one electron. At this point, we can write the matrix elements in Eq. (4) as

$$\langle \Psi_f^N | H_{int} | \Psi_i^N \rangle = \langle \phi_f^{\mathbf{k}} | H_{int} | \phi_i^{\mathbf{k}} \rangle \langle \Psi_m^{N-1} | \Psi_i^{N-1} \rangle, \tag{8}$$

where $\langle \phi_f^{\mathbf{k}} | H_{int} | \phi_i^{\mathbf{k}} \rangle \equiv M_{f,i}^{\mathbf{k}}$ is the one-electron dipole matrix element, and the second term is the $(N-1)$-electron overlap integral. Note that here we replaced Ψ_f^{N-1} with an eigenstate Ψ_m^{N-1}, as discussed above. The total photoemission intensity measured as a function of E_{kin} at a momentum $\mathbf{k}$, namely, $I(\mathbf{k},E_{kin})=\Sigma_{f,i} w_{f,i}$, is then proportional to

$$\sum_{f,i} |M_{f,i}^{\mathbf{k}}|^2 \sum_m |c_{m,i}|^2 \delta(E_{kin} + E_m^{N-1} - E_i^N - h\nu), \tag{9}$$

where $|c_{m,i}|^2 = |\langle \Psi_m^{N-1} | \Psi_i^{N-1} \rangle|^2$ is the probability that the removal of an electron from state i will leave the $(N-1)$-particle system in the excited state m. From this we can see that, if $\Psi_i^{N-1}=\Psi_{m_0}^{N-1}$ for one particular state $m=m_0$, then the corresponding $|c_{m_0,i}|^2$ will be unity and all the other $c_{m,i}$ zero; in this case, if $M_{f,i}^{\mathbf{k}} \neq 0$, the ARPES spectra will be given by a delta function at the Hartree-Fock orbital energy $E_B^{\mathbf{k}} = -\epsilon_{\mathbf{k}}$, as shown in Fig. 3(b) (i.e., the noninteracting particle picture). In strongly correlated systems, however, many of the $|c_{m,i}|^2$ will be different from zero because the removal of the photoelectron results in a strong change of the systems effective potential and, in turn, Ψ_i^{N-1} will overlap with many of the eigenstates Ψ_m^{N-1}. Thus the ARPES spectra will not consist of single delta functions but will show a main line and several satellites according to the number of excited states m created in the process [Fig. 3(c)].

This is very similar to the situation encountered in photoemission from molecular hydrogen (Siegbahn *et al.*, 1969) in which not simply a single peak but many lines separated by a few tenths of eV from each other

are observed [solid line in Fig. 3(c), bottom right]. These so-called "shakeup" peaks correspond to the excitations of the different vibrational states of the H_2^+ molecule. In the case of solid hydrogen [dashed line in Fig. 3(c), bottom right], as discussed by Sawatzky (1989), the vibrational excitations would develop in a broad continuum, while a sharp peak would be observed for the fundamental transition (from the ground state of the H_2 to that of the H_2^+ molecule). Note also that the fundamental line would actually be the only one detected in the adiabatic limit, in which case the $(N-1)$-particle system is left in its ground state.

C. One-particle spectral function

In the discussion of photoemission on solids, and in particular on the correlated electron systems in which many $|c_{m,i}|^2$ in Eq. (9) are different from zero, the most powerful and commonly used approach is based on the Green's-function formalism.[5] In this context, the propagation of a single electron in a many-body system is described by the *time-ordered* one-electron Green's function $\mathcal{G}(t-t')$, which can be interpreted as the probability amplitude that an electron added to the system in a Bloch state with momentum $\mathbf{k}$ at a time zero will still be in the same state after a time $|t-t'|$. By taking the Fourier transform, $\mathcal{G}(t-t')$ can then be expressed in energy-momentum representation resulting in $\mathcal{G}(\mathbf{k},\omega)=G^+(\mathbf{k},\omega)+G^-(\mathbf{k},\omega)$, where $G^+(\mathbf{k},\omega)$ and $G^-(\mathbf{k},\omega)$ are the one-electron addition and removal Green's function, respectively. At $T=0$:

$$G^{\pm}(\mathbf{k},\omega)=\sum_m \frac{|\langle\Psi_m^{N\pm1}|c_{\mathbf{k}}^{\pm}|\Psi_i^N\rangle|^2}{\omega-E_m^{N\pm1}+E_i^N\pm i\eta}, \tag{10}$$

where the operator $c_{\mathbf{k}}^+=c_{\mathbf{k}\sigma}^\dagger$ ($c_{\mathbf{k}}^-=c_{\mathbf{k}\sigma}$) creates (annihilates) an electron with energy ω, momentum $\mathbf{k}$, and spin σ in the N-particle initial state Ψ_i^N, the summation runs over all possible $(N\pm1)$-particle eigenstates $\Psi_m^{N\pm1}$ with eigenvalues $E_m^{N\pm1}$, and η is a positive infinitesimal (note also that from here on we will take $\hbar=1$). In the limit $\eta\to0^+$ one can make use of the identity $(x\pm i\eta)^{-1}=\mathcal{P}(1/x)\mp i\pi\delta(x)$, where $\mathcal{P}$ denotes the principal value, to obtain the *one-particle spectral function* $A(\mathbf{k},\omega)=A^+(\mathbf{k},\omega)+A^-(\mathbf{k},\omega)=-(1/\pi)\,\mathrm{Im}\,G(\mathbf{k},\omega)$, with

$$A^{\pm}(\mathbf{k},\omega)=\sum_m |\langle\Psi_m^{N\pm1}|c_{\mathbf{k}}^{\pm}|\Psi_i^N\rangle|^2\,\delta(\omega-E_m^{N\pm1}+E_i^N) \tag{11}$$

and $G(\mathbf{k},\omega)=G^+(\mathbf{k},\omega)+[G^-(\mathbf{k},\omega)]^*$, which defines the *retarded Green's function*. Note that $A^-(\mathbf{k},\omega)$ and $A^+(\mathbf{k},\omega)$ define the one-electron removal and addition spectra which one can probe with direct and inverse photoemission, respectively. This can be seen, for the direct case, by comparing the expression for $A^-(\mathbf{k},\omega)$ and Eq. (9) for the photoemission intensity (note that in the latter $\Psi_i^{N-1}=c_{\mathbf{k}}\Psi_i^N$, and the energetics of the photoemission process has been explicitly accounted for). Finite-temperature effect can be taken into account by extending the Green's-function formalism just introduced to $T\neq0$ [see, for example, Mahan (1981)]. In the latter case, by invoking once again the sudden approximation, one can write the intensity measured in an ARPES experiment on a 2D single-band system as

$$I(\mathbf{k},\omega)=I_0(\mathbf{k},\nu,\mathbf{A})f(\omega)A(\mathbf{k},\omega), \tag{12}$$

where $\mathbf{k}=\mathbf{k}_\parallel$ is the in-plane electron momentum, ω is the electron energy with respect to the Fermi level, and $I_0(\mathbf{k},\nu,\mathbf{A})$ is proportional to the squared one-electron matrix element $|M_{f,i}^{\mathbf{k}}|^2$ and therefore depends on the electron momentum, and on the energy and polarization of the incoming photon. We also introduced the Fermi function $f(\omega)=(e^{\omega/k_BT}+1)^{-1}$ which accounts for the fact that direct photoemission probes only the occupied electronic states. It has to be mentioned that in Eq. (12) we neglected the presence of any extrinsic background or broadening due to finite energy and momentum resolution, which, however, have to be carefully considered when performing a quantitative analysis of the ARPES spectra [see Sec. II.D and Eq. (21)].

The corrections to the Green's function originating from electron-electron correlations can be conveniently expressed in terms of the electron *proper self-energy* $\Sigma(\mathbf{k},\omega)=\Sigma'(\mathbf{k},\omega)+i\Sigma''(\mathbf{k},\omega)$. Its real and imaginary parts contain all the information on the energy renormalization and lifetime, respectively, of an electron with band energy ϵ_k and momentum $\mathbf{k}$ propagating in a many-body system. The Green's and spectral functions expressed in terms of the self-energy are then given by

$$G(\mathbf{k},\omega)=\frac{1}{\omega-\epsilon_{\mathbf{k}}-\Sigma(\mathbf{k},\omega)}, \tag{13}$$

$$A(\mathbf{k},\omega)=-\frac{1}{\pi}\frac{\Sigma''(\mathbf{k},\omega)}{[\omega-\epsilon_{\mathbf{k}}-\Sigma'(\mathbf{k},\omega)]^2+[\Sigma''(\mathbf{k},\omega)]^2}. \tag{14}$$

It is worth emphasizing that because $G(t,t')$ is a linear response function to an external perturbation, the real and imaginary parts of its Fourier transform $G(\mathbf{k},\omega)$ have to satisfy causality and therefore are related by Kramers-Kronig relations. This implies that if the full $A(\mathbf{k},\omega)=-(1/\pi)\,\mathrm{Im}\,G(\mathbf{k},\omega)$ is available from photoemission and inverse photoemission, one can calculate $\mathrm{Re}\,G(\mathbf{k},\omega)$ and then obtain both the real and imaginary parts of the self-energy directly from Eq. (13). However, due to the lack of high quality inverse photoemission data, this analysis is usually performed only using ARPES spectra by taking advantage of certain approximations (Norman *et al.*, 1999). This will be discussed in more detail in Sec. VIII together with other practical methods used to estimate the self-energy corrections.

In general, the exact calculation of $\Sigma(\mathbf{k},\omega)$ and, in turn, of $A(\mathbf{k},\omega)$ is an extremely difficult task. In the following, as an example we shall briefly consider the interacting *Fermi-liquid* case (Landau, 1956, 1957, 1959).

[5]See, for example, Abrikosov *et al.* (1965); Hedin and Lundqvist (1969); Fetter and Walecka (1971); Mahan (1981); Economou (1983); Rickayzen (1991).

Let us start from the trivial $\Sigma(\mathbf{k},\omega)=0$ noninteracting case. The N-particle eigenfunction Ψ^N is a single Slater determinant and we always end up in a single eigenstate when removing or adding an electron with momentum $\mathbf{k}$. Therefore $G(\mathbf{k},\omega)=1/(\omega-\epsilon_k\pm i\eta)$ has only one pole for each $\mathbf{k}$, and $A(\mathbf{k},\omega)=\delta(\omega-\epsilon_k)$ consists of a single line at the band energy ϵ_k [as in Fig. 3(b)]. In this case, the occupation numbers $n_{\mathbf{k}\sigma}=c^\dagger_{\mathbf{k}\sigma}c_{\mathbf{k}\sigma}$ are good quantum numbers and for a metallic system the *momentum distribution* [i.e., the expectation value $n(\mathbf{k})\equiv\langle n_{\mathbf{k}\sigma}\rangle$, quite generally independent of the spin σ for nonmagnetic systems] is characterized by a sudden drop from 1 to 0 at $\mathbf{k}=\mathbf{k}_F$ [Fig. 3(b), top], which defines a sharp Fermi surface. If we now switch on the electron-electron correlations adiabatically, so that the system remains at equilibrium, any particle added into a Bloch state has a certain probability of being scattered out of it by a collision with another electron, leaving the system in an excited state in which additional electron-hole pairs have been created. The momentum distribution $n(\mathbf{k})$ will now show a discontinuity smaller than 1 at $\mathbf{k}_F$ and a finite occupation probability for $\mathbf{k}>\mathbf{k}_F$ even at $T=0$ [Fig. 3(c), top]. As long as $n(\mathbf{k})$ shows a finite discontinuity $Z_\mathbf{k}>0$ at $\mathbf{k}=\mathbf{k}_F$, we can describe the correlated Fermi sea in terms of well-defined *quasiparticles*, i.e., electrons dressed with a manifold of excited states, which are characterized by a pole structure similar to that of the noninteracting system but with renormalized energy $\varepsilon_\mathbf{k}$ and mass m^*, and a finite lifetime $\tau_\mathbf{k}=1/\Gamma_\mathbf{k}$. In other words, the properties of a Fermi liquid are similar to those of a free-electron gas with damped quasiparticles. Furthermore, because the bare-electron character of the quasiparticle, or pole strength (also called coherence factor), is $Z_\mathbf{k}<1$ and the total spectral weight must be conserved [see Eq. (19)], we can separate $G(\mathbf{k},\omega)$ and $A(\mathbf{k},\omega)$ into a coherent pole part and an incoherent smooth part without poles (Pines and Nozières, 1966):

$$G(\mathbf{k},\omega)=\frac{Z_\mathbf{k}}{\omega-\varepsilon_\mathbf{k}+i\Gamma_\mathbf{k}}+G_{inch}, \tag{15}$$

$$A(\mathbf{k},\omega)=Z_\mathbf{k}\frac{\Gamma_\mathbf{k}/\pi}{(\omega-\varepsilon_\mathbf{k})^2+\Gamma_\mathbf{k}^2}+A_{inch}, \tag{16}$$

where $Z_\mathbf{k}=(1-\partial\Sigma'/\partial\omega)^{-1}$, $\varepsilon_\mathbf{k}=Z_\mathbf{k}(\epsilon_\mathbf{k}+\Sigma')$, and $\Gamma_\mathbf{k}=Z_\mathbf{k}|\Sigma''|$, and the self-energy and its derivatives are evaluated at $\omega=\varepsilon_\mathbf{k}$. It should also be emphasized that the Fermi-liquid description is valid only in proximity to the Fermi surface and rests on the condition $\varepsilon_\mathbf{k}-\mu\gg|\Sigma''|$ for small $(\omega-\mu)$ and $(\mathbf{k}-\mathbf{k}_F)$. Furthermore, $\Gamma_\mathbf{k}\propto[(\pi k_BT)^2+(\varepsilon_\mathbf{k}-\mu)^2]$ for a Fermi-liquid system in two or more dimensions (Lutinger, 1961; Pines and Nozières, 1966), although additional logarithmic corrections should be included in the two-dimensional case (Hodges *et al.*, 1971). When we compare the electron removal and addition spectra for a Fermi liquid of quasiparticles with those of a noninteracting electron system (in the lattice periodic potential), the effect of the self-energy corrections becomes evident [see Figs. 3(c) and (b), respectively]. The quasiparticle peak now has a finite lifetime (due to Σ''), and it sharpens up rapidly, thus emerging from the broad incoherent component upon approaching the Fermi level, where the lifetime is infinite corresponding to a well-defined quasiparticle [note that the coherent and incoherent part of $A(\mathbf{k},\omega)$ represent the main line and satellite structure discussed in the previous section and shown in Fig. 3(c), bottom right]. Furthermore, the peak position is shifted with respect to the bare-band energy $\epsilon_\mathbf{k}$ (due to Σ'): since in the interacting case the quasiparticle mass is larger than the band mass because of the dressing $(m^*>m)$, the total dispersion (or bandwidth) will be smaller $(|\varepsilon_\mathbf{k}|<|\epsilon_\mathbf{k}|)$.

Given that many of the normal-state properties of the cuprate superconductors do not follow the canonical Fermi-liquid behavior, it is worth illustrating the *marginal-Fermi-liquid* (MFL) model, which was specifically proposed as a phenomenological characterization of the high-temperature superconductors as it will be discussed in Sec. VIII.B.2 (Varma *et al.*, 1989, 1990; Abrahams and Varma, 2000). In particular, the motivation of the MFL description was to account for the anomalous responses observed at optimal doping, for example, in electrical resistivity, Raman-scattering intensity, and nuclear-spin relaxation rate. The MFL assumptions are as follows: (i) there are momentum-independent excitations over most of the Brillouin zone that contribute to spin and charge polarizability $\chi(\mathbf{q},\omega,T)$; (ii) the latter has a scale-invariant form as a function of frequency and temperature, namely, $\mathrm{Im}\chi\propto f(\omega/T)$. To visualize the implications of this approach, we compare the MFL and Fermi-liquid self energies, neglecting for simplicity any momentum dependence:

$$\Sigma_{FL}(\omega)=\alpha\omega+i\beta[\omega^2+(\pi k_BT)^2]; \tag{17}$$

$$\Sigma_{MFL}(\omega)=\lambda\left[\omega\ln\frac{x}{\omega_c}-i\frac{\pi}{2}x\right]. \tag{18}$$

Here $x\approx\max(|\omega|,T)$, $\mu=0$, ω_c is an ultraviolet cutoff, and λ is a coupling constant (which could in principle be momentum dependent). From Eqs. (17) and (18) at $T=0$ we see that, while in a Fermi liquid the quasiparticles are well defined because $\Sigma''(\omega)/\Sigma'(\omega)$ vanishes as ω for $\omega\to0$ and $Z_\mathbf{k}$ is finite at $\mathbf{k}=\mathbf{k}_F$, in a marginal Fermi liquid $\Sigma''(\omega)/\Sigma'(\omega)\propto1/\ln\omega$ is only marginally singular for $\omega\to0$, and there are no Fermi-liquid-like quasiparticles because $Z_\mathbf{k}$ vanishes as $1/\ln\omega$ at the Fermi surface (in turn, for $\mathbf{k}=\mathbf{k}_F$ the corresponding Green's and spectral functions are entirely incoherent). As for a MFL description of the high-T_c superconductors, note that from Eq. (18) one obtains a contribution linear in T to the electrical resistivity (i.e., $\omega=0$), consistent with experiments at optimal doping. Furthermore, as we will see in Sec. VIII.B.2, the MFL self-energy has been used for the line-shape analysis of the ARPES spectra from $Bi_2Sr_2CaCu_2O_{8+\delta}$ (Bi2212; Abrahams and Varma, 2000). As a last remark, it should be emphasized that the scale-invariant low-energy excitation spectrum assumed in the MFL model is characteristic of fluctuations associated with a $T=0$ quantum critical point, as also dis-

cussed for the high-T_c superconductors at optimal doping (Varma *et al.*, 1989; Varma, 1999).

Among the general properties of the spectral function there are several sum rules. A fundamental one, which in discussing the Fermi-liquid model was implicitly used to state that $\int d\omega A_{ch} = Z_{\mathbf{k}}$ and $\int d\omega A_{inch} = 1 - Z_{\mathbf{k}}$ (where A_{ch} and A_{inch} refer to coherent and incoherent parts of the spectral function, respectively), is

$$\int_{-\infty}^{+\infty} d\omega A(\mathbf{k},\omega) = 1, \tag{19}$$

which reminds us that $A(\mathbf{k},\omega)$ describes the probability of removing/adding an electron with momentum $\mathbf{k}$ and energy ω to a many-body system. However, as it also requires the knowledge of the electron addition part of the spectral function, it is not so useful in the analysis of ARPES data. A sum rule more relevant to this task is

$$\int_{-\infty}^{+\infty} d\omega f(\omega) A(\mathbf{k},\omega) = n(\mathbf{k}), \tag{20}$$

which relates the one-electron removal spectrum to the momentum distribution $n(\mathbf{k})$. When electronic correlations are important and the occupation numbers are no longer good quantum numbers, the discontinuity at $\mathbf{k}_F$ is reduced (as discussed for the Fermi-liquid case), but a drop in $n(\mathbf{k})$ is usually still observable even for strong correlations (Nozières, 1964). Note, however, that great care is necessary in making use of Eq. (20) because the integral of Eq. (12) does not give simply $n(\mathbf{k})$ but rather $I_0(\mathbf{k},\nu,\mathbf{A})n(\mathbf{k})$. Nevertheless, by tracking in momentum space the *loci* of steepest descent of the experimentally determined $n(\mathbf{k})$, i.e., the maxima in $|\nabla_{\mathbf{k}} n(\mathbf{k})|$, it was possible to identify the Fermi surface in Bi2212 (Campuzano *et al.*, 1996; Sec. IV.C) and also the *remnant* Fermi surface in the insulating parent compound $Ca_2CuO_2Cl_2$ (Ronning *et al.* 1998; Sec. IV.A.2).[6]

An approximate sum rule was proposed by Randeria *et al.* (1995) under the assumptions that at low energies $A(\mathbf{k}_F,-\omega) = A(\mathbf{k}_F,\omega)$, and $I_0(\mathbf{k},\nu,\mathbf{A})$ does not have significant dependence on ν or T (the dependence on $\mathbf{k}$ or $\mathbf{A}$ in this case will appear to be irrelevant). It states that $n(\mathbf{k}_F)$ is independent of temperature (note that here $\mathbf{k} = \mathbf{k}_F$ necessarily, because for $\mathbf{k}$ near but not equal to $\mathbf{k}_F$, different T dependence is expected for states below and above the chemical potential). This approximate sum rule was tested on temperature-dependent ARPES spectra taken on Bi2212 at $\mathbf{k}_F$ near $(\pi,0)$ which, as we shall discuss in detail in Sec. VI.A, are characterized by a remarkable change in line shape below the superconducting phase transition [Fig. 4(a)]. Indeed, as shown in Fig. 4(b), the integrated intensity of the ARPES spectra is temperature independent, which not only satisfies the sum rule but also suggests the validity of the sudden approximation for Bi2212 even at 19-eV photon energy [since it is on this approximation that Eq. (12) and the above analysis rest]. It was also noted that, as the low-energy spectral weight in all the quasi-2D copper oxides is mostly representative of the electronic states belonging to the CuO_2 planes ($Cu\,3d$ and $O\,2p$), the validity of the sudden approximation at this relatively low photon energy and, in turn, of the $A(\mathbf{k},\omega)$ interpretation of the ARPES spectra [Eq. (12)], should be regarded as a general property of this class of compounds (Randeria *et al.*, 1995). However, more experiments on a wide temperature range and in a K-space region where the assumption $A(\mathbf{k}_F,-\omega) = A(\mathbf{k}_F,\omega)$ is not affected by the presence of the Van Hove singularity are needed to further substantiate the validity of this point.

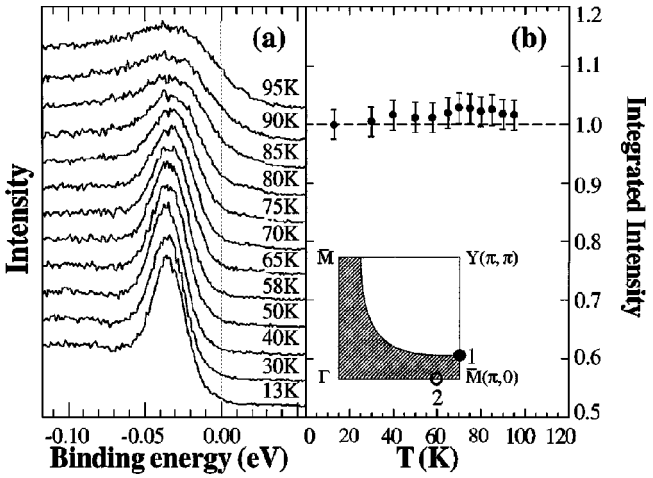

FIG. 4. Temperature dependence of the photoemission data from $Bi_2Sr_2CaCu_2O_{8+\delta}$ ($T_c = 87$ K): (a) ARPES spectra measured at $\mathbf{k} = \mathbf{k}_F$ (point 1 in the Brillouin-zone sketch); (b) integrated intensity. From Randeria *et al.*, 1995.

D. Matrix elements and finite-resolution effects

As discussed in the previous section and summarized by Eq. (12), ARPES directly probes the one-particle spectral function $A(\mathbf{k},\omega)$. However, in extracting quantitative information from the experiment, not only the effect of the matrix element term $I_0(\mathbf{k},\nu,\mathbf{A})$ has to be taken into account, but also the finite experimental resolution and the extrinsic continuous background due to the secondaries (those electrons which escape from the solid after having suffered inelastic-scattering events and, therefore, with a reduced E_{kin}). The latter two effects may be explicitly accounted for by considering a more realistic expression for the photocurrent $I(\mathbf{k},\omega)$:

$$\int d\tilde{\omega} d\tilde{\mathbf{k}}\, I_0(\tilde{\mathbf{k}},\nu,\mathbf{A}) f(\tilde{\omega}) A(\tilde{\mathbf{k}},\tilde{\omega}) R(\omega-\tilde{\omega}) Q(\mathbf{k}-\tilde{\mathbf{k}}) + B, \tag{21}$$

which consists of the convolution of Eq. (12) with energy (R) and momentum (Q) resolution functions (R is typically a Gaussian, Q may be more complicated), and of the background correction B. Of the several possible

[6]For a more extended discussion on the different methods used to determine the Fermi surface experimentally, see Straub *et al.* (1997); Kipp *et al.* (1999); Rossnagel *et al.* (2001).

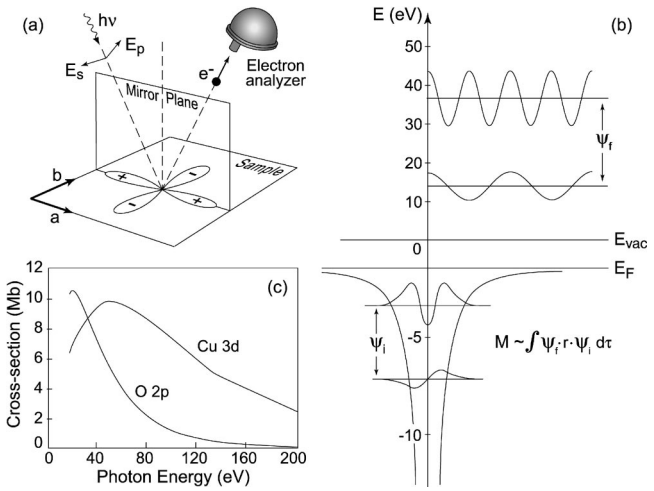

FIG. 5. Schematic representation of the polarization and photon energy effects in the photoemission process: (a) mirror plane emission from a $d_{x^2-y^2}$ orbital; (b) sketch of the optical transition between atomic orbitals with different angular momenta (the wave functions of the harmonic oscillator are here used for simplicity) and free-electron wave functions with different kinetic energies (after Hüfner, 1995); (c) calculated photoionization cross sections for Cu $3d$ and O $2p$ atomic levels (after Yeh and Lindau, 1985).

forms for the background function B (Hüfner, 1995), two are more frequently used: (i) the step-edge background, with three parameters for height, energy position, and width of the step-edge, which reproduces the background observed all the way to E_F in an unoccupied region of momentum space; (ii) the Shirley background $B_{Sh}(\omega) \propto \int_{\omega}^{\mu} d\omega' P(\omega')$, which allows one to extract from the measured photocurrent $I(\omega) = P(\omega) + c_{Sh} B_{Sh}(\omega)$ the contribution $P(\omega)$ due to the unscattered electrons (the only parameter is the constant c_{Sh}; Shirley, 1972).

Let us now very briefly illustrate the effect of the matrix element term $I_0(\mathbf{k},\nu,\mathbf{A}) \propto |M_{f,i}^{\mathbf{k}}|^2$, which is responsible for the dependence of the photoemission data on photon energy and experimental geometry, and may even result in complete suppression of the intensity (Gobeli *et al.*, 1964; Dietz *et al.*, 1976; Hermanson, 1977; Eberhardt and Himpsel, 1980). By using the commutation relation $\hbar\mathbf{p}/m = -i[\mathbf{x},H]$, we can write $|M_{f,i}^{\mathbf{k}}|^2 \propto |\langle \phi_f^{\mathbf{k}} | \boldsymbol{\varepsilon}\cdot\boldsymbol{x} | \phi_i^{\mathbf{k}} \rangle|^2$, where $\boldsymbol{\varepsilon}$ is a unit vector along the polarization direction of the vector potential $\mathbf{A}$. As in Fig. 5(a), let us consider photoemission from a $d_{x^2-y^2}$ orbital, with the detector located in the mirror plane (when the detector is out of the mirror plane, the problem is more complicated because of the lack of an overall well-defined even/odd symmetry). In order to have nonvanishing photoemission intensity, the whole integrand in the overlap integral must be an even function under reflection with respect to the mirror plane. Because odd-parity final states would be zero everywhere on the mirror plane and therefore also at the detector, the final-state wave function $\phi_f^{\mathbf{k}}$ itself must be even. In particular, at the detector the photoelectron is described by an even-parity plane-wave state $e^{i\mathbf{kr}}$ with momentum in the mirror plane and fronts orthogonal to it (Hermanson, 1977). In turn, this implies that $(\boldsymbol{\varepsilon}\cdot\boldsymbol{x})|\phi_i^{\mathbf{k}}\rangle$ must be even. In the case depicted in Fig. 5(a) where $|\phi_i^{\mathbf{k}}\rangle$ is also even, the photoemission process is symmetry allowed for $\mathbf{A}$ even or in-plane (i.e., $\boldsymbol{\varepsilon}_p \cdot \mathbf{x}$ depends only on in-plane coordinates and is therefore even under reflection with respect to the plane) and forbidden for $\mathbf{A}$ odd or normal to the mirror plane (i.e., $\boldsymbol{\varepsilon}_s \cdot \mathbf{x}$ is odd as it depends on normal-to-the-plane coordinates). For a generic initial state of either even or odd symmetry with respect to the mirror plane, the polarization conditions resulting in an overall even matrix element can be summarized as

$$\langle \phi_f^{\mathbf{k}} | \mathbf{A}\cdot\mathbf{p} | \phi_i^{\mathbf{k}} \rangle \begin{cases} \phi_i^{\mathbf{k}} \text{ even} & \langle +|+|+\rangle \Rightarrow \mathbf{A} \text{ even} \\ \phi_i^{\mathbf{k}} \text{ odd} & \langle +|-|-\rangle \Rightarrow \mathbf{A} \text{ odd.} \end{cases} \tag{22}$$

In order to discuss the photon energy dependence, from Eq. (5) and by considering a plane wave $e^{i\mathbf{kr}}$ for the photoelectron at the detector, one may more conveniently write $|M_{f,i}^{\mathbf{k}}|^2 \propto |(\boldsymbol{\varepsilon}\cdot\boldsymbol{k})\langle \phi_i^{\mathbf{k}} | e^{i\mathbf{kr}} \rangle|^2$. The overlap integral, as sketched in Fig. 5(b), strongly depends on the details of the initial-state wave function (peak position of the radial part and oscillating character of it), and on the wavelength of the outgoing plane wave. Upon increasing the photon energy, both E_{kin} and $\mathbf{k}$ increase, and $M_{f,i}^{\mathbf{k}}$ changes in a non-necessarily monotonic fashion [see Fig. 5(c), for the Cu $3d$ and the O $2p$ atomic case]. As a matter of fact, the photoionization cross section is usually characterized by one minimum in free atoms, the so-called Cooper minimum (Cooper, 1962), and a series of them in solids (Molodtsov *et al.*, 2000).

Before concluding this section, it has to be emphasized that the description of photoemission based on the sudden approximation and the three-step model, although artificial and oversimplified, allows an intuitive understanding of the photoemission process. However, for a quantitative analysis of the ARPES spectra, calculations based on the one-step model are generally required. In this case, surface discontinuity, multiple scattering, finite-lifetime effects, and matrix elements for initial- and final-state crystal wave functions are included and accounted for by first-principles calculations, as we shall discuss in Sec. IV.C for the case of Bi2212 (Bansil and Lindroos, 1999).

E. State-of-the-art photoemission

In the early stage of the investigation of the high-temperature superconductors, ARPES proved to be very successful in detecting dispersive electronic features (Takahashi *et al.*, 1988; Olson *et al.*, 1990, 1989), the d-wave superconducting gap (Shen *et al.*, 1993). Over the past decade, a great deal of effort has been invested in further improving this technique. This resulted in an order-of-magnitude improvement in both energy and momentum resolution, thus ushering in a new era in electron spectroscopy and allowing a detailed comparison between theory and experiment. The reasons for this progress are twofold: the availability of dedicated photoemission beamlines on high-flux second- and third-generation synchrotron facilities (for a de-

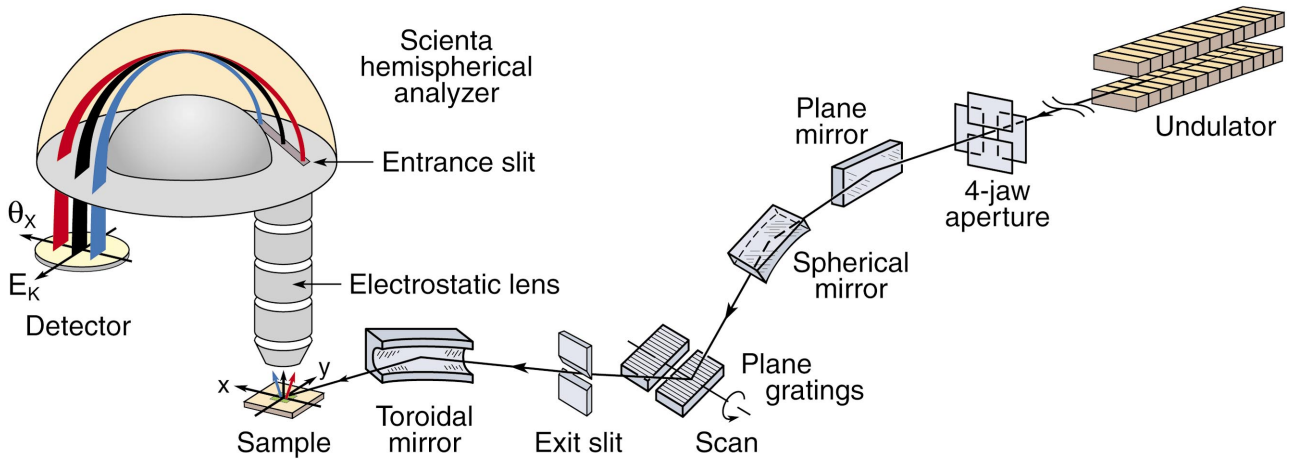

FIG. 6. Generic beamline equipped with a plane grating monochromator and a Scienta electron spectrometer (Color).

scription of synchrotron radiation technology and applications see Koch *et al.*, 1991), and the development of the Scienta electron spectrometers (Beamson *et al.*, 1990; Martensson *et al.*, 1994).

The configuration of a generic angle-resolved photoemission beamline is shown in Fig. 6. A beam of white radiation is produced in a wiggler or an undulator (these so-called "insertion devices" are the straight sections of the electron storage ring where radiation is produced), is monochromatized at the desired photon energy by a grating monochromator, and is focused on the sample. Alternatively, a gas-discharge lamp can be used as a radiation source (once properly monochromatized, to avoid complications due to the presence of different satellites and refocused to a small spot size, essential for high angular resolution). However, synchrotron radiation offers important advantages: it covers a wide spectral range, from the visible to the x-ray region, with an intense and highly polarized continuous spectrum, while a discharge lamp provides only a few unpolarized resonance lines at discrete energies. Photoemitted electrons are then collected by the analyzer, where kinetic energy and emission angle are determined (the whole system is in high vacuum at pressures lower than 5×10^{-11} torr).

A conventional hemispherical analyzer consists of a multielement electrostatic input lens, a hemispherical deflector with entrance and exit slits, and an electron detector (i.e., a channeltron or a multichannel detector). The heart of the analyzer is the deflector, which consists of two concentric hemispheres of radius R_1 and R_2. These are kept at a potential difference ΔV, so that only those electrons reaching the entrance slit with kinetic energy within a narrow range centered at the value $E_{pass}=e\Delta V/(R_1/R_2-R_2/R_1)$ will pass through this hemispherical capacitor, thus reaching the exit slit and then the detector. In this way it is possible to measure the kinetic energy of the photoelectrons with an energy resolution given by $\Delta E_a=E_{pass}(w/R_0+\alpha^2/4)$, where $R_0=(R_1+R_2)/2$, w is the width of the entrance slit, and α is the acceptance angle. The role of the electrostatic lens is to decelerate and focus the photoelectrons onto the entrance slit. By scanning the lens retarding potential one can effectively record the photoemission intensity versus the photoelectron kinetic energy. One of the innovative characteristics of the Scienta analyzer is the two-dimensional position-sensitive detector consisting of two microchannel plates and a phosphor plate in series, followed by a charge-coupled device (CCD) camera. In this case, no exit slit is required: the electrons, which are spread apart along the Y axis of the detector (Fig. 6) as a function of their kinetic energy due to the travel through the hemispherical capacitor, are detected simultaneously. In other words, a range of electron energies is dispersed over one dimension of the detector and can be measured in parallel; scanning the lens voltage is in principle no longer necessary, at least for narrow energy windows (a few percent of E_{pass}). Furthermore, in contrast to a conventional electron analyzer in which the momentum information is averaged over all the photoelectrons within the acceptance angle (typically $\pm1°$), the Scienta system can be operated in angle-resolved mode, which provides energy-momentum information not only at a single k-point but along an extended cut in k space. In particular, the photoelectrons within an angular window of $\sim14°$ along the direction defined by the analyzer entrance slit are focused on different X positions on the detector (Fig. 6). It is thus possible to measure multiple energy distribution curves simultaneously for different photoelectron angles, obtaining a 2D snapshot of energy versus momentum (Fig. 7).

The Scienta SES200 analyzer ($R_0=200$ mm) typically allows energy and angular resolutions of approximately a few meV and 0.2°, respectively [for the 21.2-eV photons of the HeIα line, as one can obtain from Eq. (2), 0.2° corresponds to $\sim1\%$ of the cuprates' Brillouin-zone edge π/a]. Note, however, that in estimating the total energy resolution achievable on a beamline, one also has to take into account ΔE_m of the monochromator, which can be adjusted with entrance and exit slits. The ultimate resolution a monochromator can deliver is given by its resolving power $R=E/\Delta E_m$; it can be as good as 1–2 meV for 20-eV photons but worsens upon increasing photon energy. To maximize the signal intensity at the desired total ΔE, monochromator and

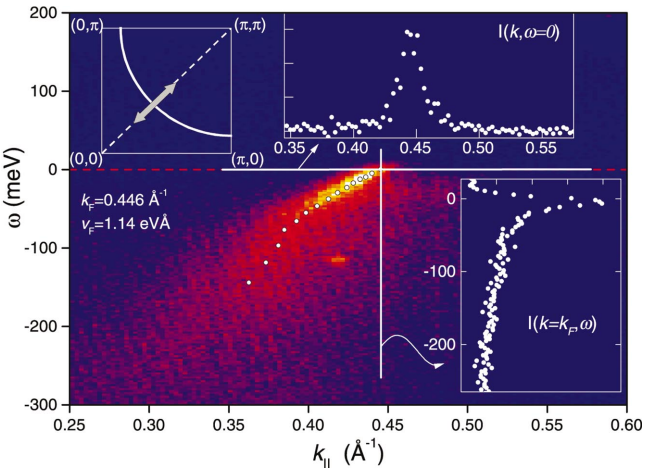

FIG. 7. Energy (ω) vs momentum ($\mathbf{k}_{\parallel}$) image plot of the photoemission intensity from $Bi_2Sr_2CaCu_2O_{8+\delta}$ along (0,0)-(π,π). This k-space cut was taken across the Fermi surface (see sketch of the 2D Brillouin zone upper left) and allows a direct visualization of the photohole spectral function $A(\mathbf{k},\omega)$ (although weighted by Fermi distribution and matrix elements). The quasiparticle dispersion can be clearly followed up to E_F, as emphasized by the white circles. Energy scans at constant momentum (right) and momentum scans at constant energy (upper right) define *energy distribution curves* (EDC's) and *momentum distribution curves* (MDC's), respectively. After Valla, Fedorov, Johnson, Wells, *et al.*, 1999 (Color).

analyzer should be operated at comparable resolutions.

To date, one of the most impressive examples of high energy resolution for a photoemission experiment on a solid sample was reported by Yokoya *et al.* (2000), who performed photoemission measurements on the Ni borocarbides in a system equipped with a Scienta SES2002 electron analyzer (newer version of the SES200), and a Gammadata high-flux discharge lamp combined with a toroidal grating monochromator. With this experimental setup, capable of an energy resolution of 1.5 meV, Yokoya *et al.* (2000) measured angle-integrated photoemission spectra with 2.0-meV resolution on YNi_2B_2C and $Y(Ni_{0.8}Pt_{0.2})_2B_2C$, which are characterized by a superconducting transition at 15.4 and 12.1 K, respectively (see Fig. 8). Due to the extremely high resolution, they successfully detected the opening of the small superconducting gap, as evidenced by the shift to high binding energies of the 6 K spectra leading-edge midpoint (which is instead located at E_F at 20 K, as expected for a metal), and by the appearance of a peak below E_F which directly reflects the piling up of the density of states due to the gap opening. By a detailed analysis of the data, the authors could conclude in favor of an anisotropic s-wave superconducting gap with $\Delta_{max} \simeq 2.2$ and 1.5 meV in the pure and Pt-doped samples, respectively.

It should be emphasized that, when angle-resolved experiments are performed, one has to compromise the energy resolution to improve the angular resolution. Therefore, in angle-resolved experiments, ΔE is typically set in the range of 5–20 meV. To illustrate the capability of state-of-the-art ARPES and how critical the improvement in angle resolution has been, the novel superconductor Sr_2RuO_4 is a particularly good example. This system is isostructural to the archetypal cuprate parent compound La_2CuO_4 (see Fig. 11), but RuO_2 planes replace the CuO_2 planes. Its low-energy electronic structure, as predicted by band-structure calculations is characterized by three bands crossing the chemical potential (Oguchi, 1995; Singh, 1995). These define a complex Fermi surface comprised of two electron pockets and one hole pocket [Fig. 9(d)], which have been clearly observed in de Haas–van Alphen experiments (Mackenzie *et al.*, 1996; Bergemann *et al.*, 2000). On the other hand, early photoemission measurements suggested a different topology (Lu *et al.*, 1996; Yokoya *et al.*, 1996a, 1996b), which generated a certain degree of controversy in the field (Puchkov *et al.*, 1998). This issue was conclusively resolved only by taking advantage of the high energy and momentum resolution of the "new generation" of ARPES data: it was then recognized that a surface reconstruction (Matzdorf *et al.*, 2000) and, in turn, the detection of several direct and folded surface bands were responsible for the conflicting interpretations (Damascelli *et al.*, 2000; Damascelli, Shen, Lu, and Shen, 2001; Damascelli, Shen, *et al.*, 2001; Shen, Damascelli, *et al.*, 2001). Figures 9(a) and 9(b) show high-resolution ($\Delta E = 14$ meV, $\Delta k = 1.5\%$ of the zone edge) ARPES data taken at 10 K with 28-eV photons on a Sr_2RuO_4 single crystal cleaved at 180 K (for Sr_2RuO_4, as recently discovered, the high-temperature cleaving suppresses surface contributions to the photoemission signal and allows one to isolate the bulk electronic structure; Damascelli *et al.*, 2000). Several well-defined quasiparticle peaks disperse towards the Fermi energy and disappear upon crossing E_F. A Fermi energy intensity map [Fig. 9(c)] can then be obtained by integrating the spectra over a narrow energy window about E_F (± 10 meV). As the spectral function (multiplied by the Fermi function) reaches its maximum at E_F when a band crosses the Fermi energy, the Fermi surface is identified by the local maxima of the intensity map. Following this

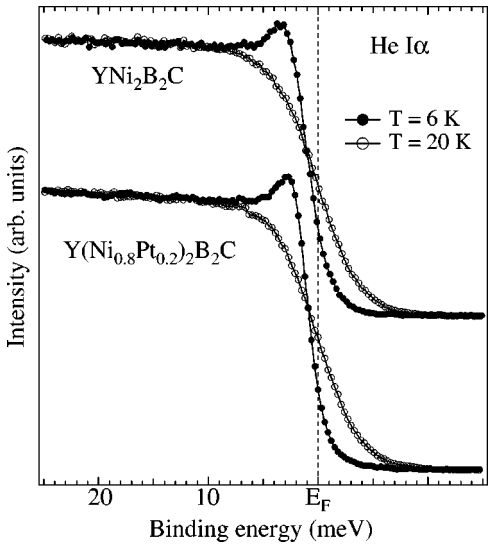

FIG. 8. Angle-integrated photoemission data from Ni borocarbides taken with 2.0-meV resolution. From Yokoya *et al.*, 2000.

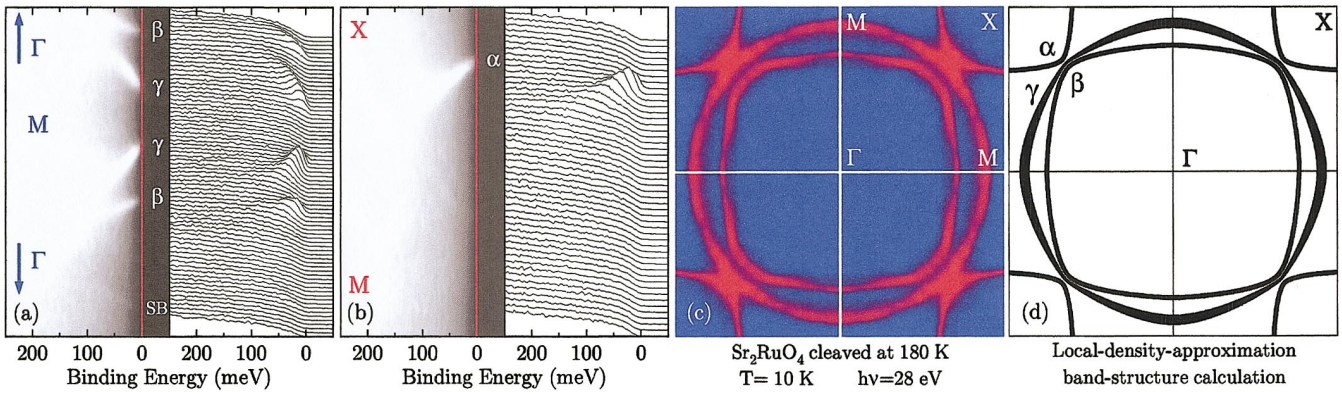

FIG. 9. Photoemission results from Sr_2RuO_4: ARPES spectra and corresponding intensity plot along (a) Γ-M and (b) M-X; (c) measured Fermi surface; (d) calculated Fermi surface (Mazin and Singh, 1997). From Damascelli *et al.*, 2000 (Color).

method, the three sheets of Fermi surface are clearly resolved and are in excellent agreement with the theoretical calculations [Fig. 9(d)].

The improvement in synchrotron-radiation technology results in the availability of high-resolution beamlines operating at increasingly higher photon energies. The significance of this progress is well exemplified by the high photon-energy resonance photoemission experiments on Ce compounds performed by Sekiyama *et al.* (2000) on a high-resolution soft x-ray (500–1500 eV) photoemission system [this consists of a Scienta SES200 spectrometer, combined with a varied line-spacing plane grating monochromator on a high-brilliance beamline at the SPring-8 synchrotron facility (Saitoh *et al.*, 1998)]. Ce compounds are characterized by a very different degree of hybridization between the $4f$ electronic states and other valence bands; the strength of the hybridization is stronger the larger the Kondo temperature T_K. However, although $CeRu_2Si_2$ and $CeRu_2$ are characterized by very different T_K (approximately 22 and 1000 K, respectively), earlier photoemission studies reported similar spectra for the Ce $4f$ electronic states.[7] By performing angle-integrated high-resolution photoemission experiments at the $3d$-$4f$ ($h\nu \simeq 880$ eV, $\Delta E \simeq 100$ meV) and $4d$-$4f$ ($h\nu \simeq 120$ eV, $\Delta E \simeq 50$ meV) resonances (see Fig. 10), Sekiyama *et al.* (2000) observed that, while the spectra for the two compounds are indeed qualitatively similar at 120-eV photon energy, they are remarkably different at 880 eV. As the photoelectron mean free path increases from approximately 5 to almost 20 Å when the photon energy is increased from 120 to 880 eV (Seah and Dench, 1979), it was concluded that the $4d$-$4f$ spectra mainly reflect the surface $4f$ electronic states. These are different from those of the bulk and are not representative of the intrinsic electronic properties of the two compounds, which are more directly probed at 880 eV: the $3d$-$4f$ spectra show a prominent structure corresponding to the tail of a Kondo peak in $CeRu_2Si_2$, and a broader feature reflecting the more itinerant character of the $4f$ electrons in $CeRu_2$ (Sekiyama *et al.*, 2000).

At this point, it is worth emphasizing that while the examples discussed in this section underline certain shortcomings of photoemission and may raise some concerns about the reliability of the ARPES results, on the other hand, they demonstrate that state-of-the-art ARPES, by taking advantage of the momentum and energy resolution as well as of the photon energy range now available, is not only a reliable technique but is also a unique tool for *momentum-space microscopy*.

III. FROM MOTT INSULATOR TO HIGH-T_C SUPERCONDUCTOR

In the following we summarize the basic characteristics of the crystal and electronic structures of the copper

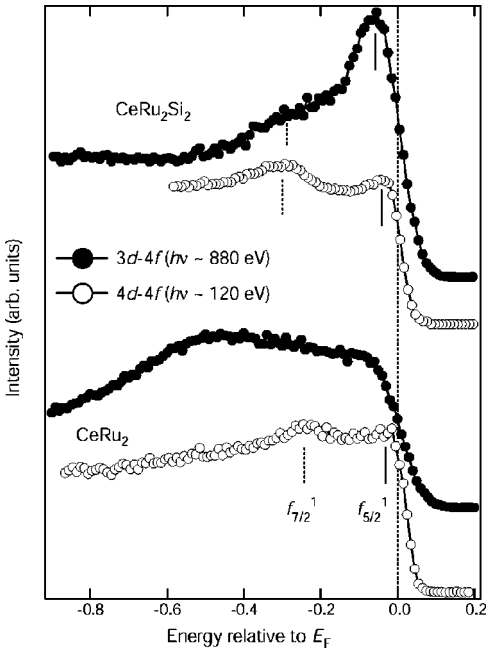

FIG. 10. High-energy angle-integrated photoemission data from Ce compounds at $T = 20$ K. From Sekiyama *et al.*, 2000.

[7]See, for instance, Patthey *et al.* (1990); Weschke *et al.* (1991); Joyce *et al.* (1992); Kaindl *et al.* (1992); Duo *et al.* (1996); Garnier *et al.* (1997).

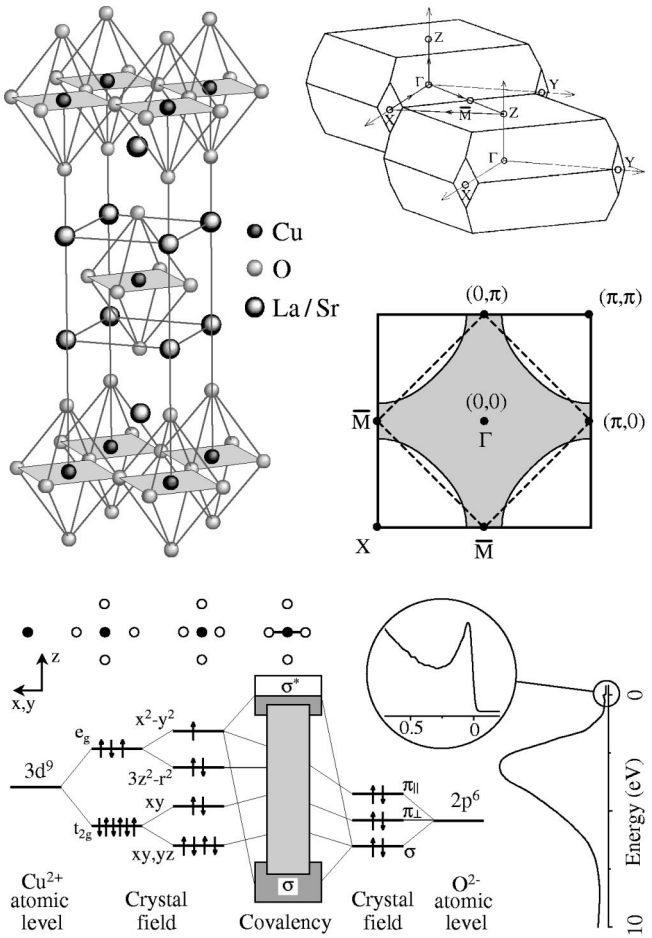

FIG. 11. Crystal structure, Fermi surface, and low-energy electronic configuration of $La_{2-x}Sr_2CuO_4$ (LSCO): Top, crystal structure, 3D Brillouin zone (body-centered tetragonal) and its 2D projection; diamond, Fermi surface at half filling calculated with only the nearest-neighbor hopping; gray area, Fermi surface obtained including also the next-nearest-neighbor hopping. Note that $\bar{M}$ is the midpoint along Γ-Z and not a true symmetry point. Bottom, crystal-field splitting and hybridization giving rise to the Cu-O bands (Fink *et al.*, 1989), and a generic LSCO ARPES spectrum (the circle shows the low-energy scale we shall focus on throughout this review).

oxides.[8] We shall use, as an example, the archetypical cuprate superconductor $La_{2-x}Sr_2CuO_4$ (LSCO) and its parent compound La_2CuO_4 (see Fig. 1), whose undistorted high-temperature tetragonal structure is sketched in Fig. 11. When the temperature is lowered, several structural phase transitions occur, characterized by coherent rotations of the CuO_6 octahedra (see, for example, Kimura *et al.*, 2000). To date, the ARPES data are usually discussed within high-temperature tetragonal notations, which is the approach we will also follow in this review (note however that, with much improved energy and momentum resolution, an important future study will be to test the appropriateness of this description by quantitatively estimating the effects of local and/or long-range structural distortions on the electronic structure). The corresponding three-dimensional Brillouin zone, which is most relevant to the study of the momentum-resolved electronic properties, is also sketched in Fig. 11. However, as the cuprate high-temperature superconductors have a quasi-2D electronic structure with weak dispersion along the z axis, in the discussion of the ARPES data we shall refer to the 2D projected zones as the ones presented in Fig. 11 for LSCO or in Fig. 12 for other systems. As emphasized in Fig. 11, the most important structural element is represented by the CuO_2 planes which form single-layer (as in LSCO) or multilayer blocks separated from each other by the so-called *charge reservoir layers* (La/Sr in Fig. 11). Depending on the number N of CuO_2 planes contained within the characteristic blocks (N is also the number of Cu ions per formula unit), the cuprates are classified into single-layer compounds [e.g., LSCO, $Bi_2Sr_2CuO_{6+\delta}$, $Nd_{2-x}Ce_xCuO_4$, and $(Sr,Ca)_2CuO_2Cl_2$], bilayer compounds (e.g., $Bi_2Sr_2CaCu_2O_{8+\delta}$ and $YBa_2Cu_3O_{7-\delta}$), and trilayer compounds (e.g., $Bi_2Sr_2Ca_2Cu_3O_{10+\delta}$). This structural characteristic profoundly affects the superconducting properties: within each family of cuprates T_c increases with N, at least for $N \leqslant 3$ (Tarascon *et al.*, 1988; Di Stasio *et al.*, 1990). For instance, within the Bi-based cuprate high-temperature superconductors, a maximum T_c of 34, 96, and 110 K is found for $N=1$, 2, and 3, respectively (Eisaki *et al.*, 2002). By substituting different elements in the reservoir layers or by varying their oxygen content (other methods are also possible, depending on the system) one can dope charge carriers into the CuO_2 planes. The latter are believed to be responsible for high-temperature superconductivity as the Cu-O bands are the lowest-energy electronic states and therefore directly determine the macroscopic electronic properties.

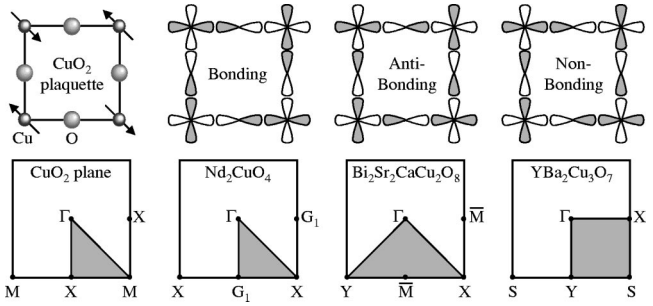

FIG. 12. Cu-O_2 plaquette, phase at (π,π) of Cu $d_{x^2-y^2}$ and O $2p$ orbitals for bonding, antibonding, and nonbonding hybridized wave functions for the bare CuO_2 plane [i.e., square lattice; see also Fig. 13(a)], and 2D projected Brillouin zones with conventional notations for different copper oxides (shaded areas represent the irreducible symmetry units).

[8]For a more detailed description see Pickett (1989); Markiewicz (1991, 1997); Auerbach (1994); Dagotto (1994); Fulde (1995); Rao and Raveau (1995); Imada *et al.* (1998); Orenstein and Millis (2000); Sachdev (2000); Tokura and Nagaosa (2000).

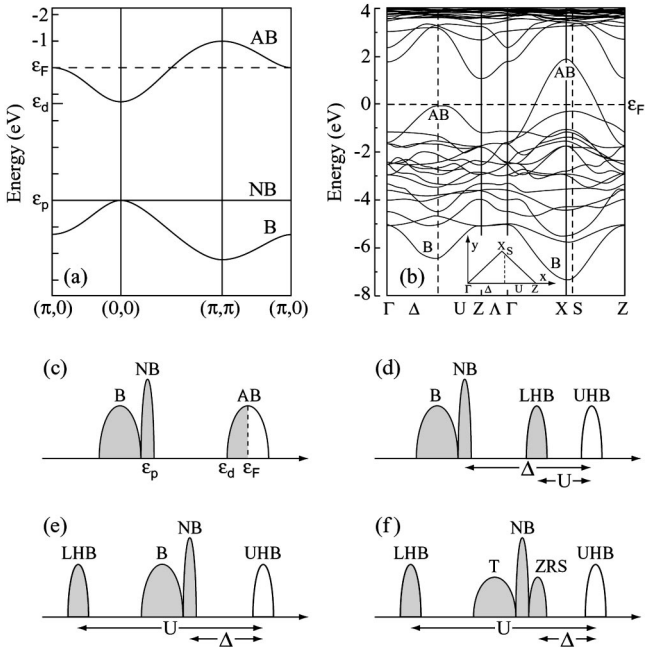

FIG. 13. Opening of a correlation gap in the half-filled correlated metals: (a) bonding (B), antibonding (AB), and nonbonding (NB) bands for the square lattice (Fulde, 1995), and (c) corresponding density of states [(b) band-structure calculations for La_2CuO_4 (Mattheiss, 1987; Horsch *et al.*, 1989; Horsch and Stephan, 1993)]. The system is metallic in the absence of electronic correlations, and becomes (d) a Mott insulator or (e) a charge-transfer insulator, respectively, for $\Delta > U > W$ and $U > \Delta > W$; (f) in the latter case, due to hybridization with the upper Hubbard band, the nonbonding band further splits into triplet and Zhang-Rice singlet states.

For LSCO this is clearly indicated by the local-density approximation (LDA) band-structure calculations presented in Fig. 13(b), where all the bands between E_F and 8-eV binding energy appear to be of Cu $3d$ or O $2p$ character [a schematic picture of the origin of the Cu-O bands in the cuprates is given at the bottom of Fig. 11, where the effect of crystal field splitting and, in particular, Jahn-Teller (Jahn and Teller, 1937) distortion of the octahedron on the Cu e_g and t_{2g} levels is also shown]. Analogous results are obtained for a square lattice with three orbitals (Cu $d_{x^2-y^2}$, and O $2p_x$ and $2p_y$) at half filling (i.e., one electron per Cu $d_{x^2-y^2}$ orbital corresponding to the point $x=0$ in the phase diagram of Fig. 1), which emphasize the presence of one antibonding band at the Fermi level, and of nonbonding and bonding bands at higher binding energy [see Fig. 13(a), and also Figs. 13(c) and 12, where the corresponding metallic density of states and the symmetry of the hybridized wave functions at (π,π) are shown].

The band structures of Figs. 13(a) and (b) imply metallic behavior and a Fermi surface with volume equal to half of the Brillouin zone. In particular, for the calculations of Fig. 13(a) in which only nearest-neighbor hopping (Cu-O, t_{pd}) was considered, a diamondlike Fermi surface is obtained (Fig. 11). A distortion of this surface takes place with the more realistic inclusion of next-nearest-neighbor hopping (O-O, t_{pp}), which results in the Fermi surface given by the gray area in Fig. 11 (Dickinson and Doniach, 1993). These results seem to correspond well to the photoemission spectrum shown in Fig. 11, where a several-eV broad valence band and a low-energy quasiparticle peak are observed (note that the $\sim$500-meV region shown in the enlargement is the energy range that we shall mostly be dealing with throughout this article). However, the experimental spectrum of Fig. 11 was obtained on optimally doped LSCO ($x=0.15$ point in Fig. 1), whereas on the basis of the band-structure results of Fig. 13(b), metallic behavior is also expected for undoped La_2CuO_4 ($x=0$ point in Fig. 1), which, on the contrary, is an antiferromagnetic insulator. This contradiction reflects the failure of the independent-particle picture [assumed in band calculations like those of Figs. 13(a) and (b)] and suggests that the undoped parent compounds of the cuprate superconductors may belong to the class of the *Mott-Hubbard insulators* (Mott, 1949, 1956, 1974; Anderson, 1959; Hubbard, 1964a, 1964b). These systems, because of the odd number of electrons per unit cell, are erroneously predicted by band theory to be paramagnetic metals, with a partially filled d band in the case of transition metal oxides such as CoO. The reason for this failure lies in the on-site electron-electron repulsion U, which is much larger than the bandwidth W. As a consequence, the conduction band splits into upper and lower Hubbard bands and these compounds are rather good insulators with an optical gap U of a few eV between the two Hubbard bands. Similarly in the case of the copper oxides, as the on-site electron-electron repulsion U for the Cu $3d$ electrons is comparable to the bandwidth $W=8t$ (which is the tight-binding result for the square lattice), the antibonding band splits into upper and lower Hubbard bands and charge fluctuations are suppressed [Fig. 13(d)]. It has to be emphasized, however, that in the cuprates the Cu-O charge-transfer energy Δ is smaller than the on-site Coulomb repulsion U [Fig. 13(e)], which characterizes these compounds more precisely as *charge-transfer insulators* (Zaanen *et al.*, 1985).

Therefore the cuprates should be described in terms of the three-band extended Hubbard model (Emery, 1987; Varma *et al.*, 1987a, 1987b), in which Cu $3d_{x^2-y^2}$, as well as O $2p_x$ and $2p_y$ orbitals are explicitly considered. However, because of the finite hybridization between the correlated Cu and the noninteracting-like O orbitals, the first electron removal states correspond to the O-derived Zhang-Rice singlet band (Zhang and Rice, 1988). It was then suggested that the cuprates might be equivalent to an effective single-band Mott-Hubbard system with the Zhang-Rice singlet band playing the role of the lower Hubbard band, and an in-plane Cu-derived band as the upper Hubbard band. These states are separated by an effective Mott gap of the order of Δ [Fig. 13(f)]. Although not universally agreed

upon,[9] this line of thinking is widely used in the literature and supports the early proposal by Anderson (1987) that the essential physics of the cuprates would be captured by the one-band Hubbard model; this contains a single kinetic-energy term proportional to the nearest-neighbor hopping amplitude t, in addition to the Hubbard U term that favors electron localization and results in "frustration" of the kinetic energy:

$$H=-t\sum_{\langle ij\rangle,\sigma}(c_{i\sigma}^{\dagger}c_{j\sigma}+\text{H.c.})+U\sum_{i}n_{i\uparrow}n_{i\downarrow}. \tag{23}$$

Here $c_{i\sigma}^{\dagger}$ ($c_{i\sigma}$) creates (annihilates) an electron or hole on site i with spin σ, $\langle ij\rangle$ identifies nearest-neighbor pairs, and $n_{i\sigma}=c_{i\sigma}^{\dagger}c_{i\sigma}$ is the number operator. In the strong-coupling limit ($U\gg t$) at half filling ($x=0$, i.e., one electron per Cu site in a $3d_{x^2-y^2}$ orbital), the antiferromagnetic state (Anderson, 1950) results from the fact that, when nearest-neighbor spins are antiparallel to each other, the electrons gain kinetic energy by undergoing virtual hopping to neighboring sites (because of the Pauli principle, hopping is forbidden for parallel spins). By projecting out the doubly occupied states at large U (see, for instance, Dagotto, 1994), the Hubbard Hamiltonian simplifies into the t-J Hamiltonian, which is more commonly used in studying the low-lying excitations of the half filled antiferromagnetic insulator:

$$H=-t\sum_{\langle ij\rangle,\sigma}(\tilde{c}_{i\sigma}^{\dagger}\tilde{c}_{j\sigma}+\text{H.c.})+J\sum_{\langle ij\rangle}\left(\mathbf{S}_i\cdot\mathbf{S}_j-\frac{n_in_j}{4}\right), \tag{24}$$

where the operator $\tilde{c}_{i\sigma}=c_{i\sigma}(1-n_{i-\sigma})$ excludes double occupancy, $J=4t^2/U$ is the antiferromagnetic exchange coupling constant, and S_i is the spin operator. At half filling, as charge excitations are gapped, we find at low energy only spin excitations governed by the antiferromagnetic Heisenberg Hamiltonian $H=J\Sigma\mathbf{S}_i\cdot\mathbf{S}_j$ (the constant term $-n_in_j/4$ is usually neglected). Away from half filling, the t-J model describes a so-called *doped antiferromagnet*, i.e., a system of interacting spins and mobile holes. The latter acquire a "magnetic dressing" because they are perturbing the correlations of the spin background that they move through.

As we shall see in greater detail in Sec. IV.A, the ARPES work on undoped insulators provides a starting point for understanding the doping evolution of the electronic structure of the cuprate high-temperature superconductors and emphasizes a fundamental problem in the theoretical description of doped 2D antiferromagnets: the Heisenberg model is so strongly perturbed by the addition of mobile holes that, above a certain doping level, some form of spin liquid may be a better ansatz than the long-range-ordered Néel state. This point is centrally important to high-T_c superconductivity and the high-temperature superconductors, which are poor conductors in the normal state with a behavior fundamentally different from the Fermi-liquid paradigm and are often regarded as doped antiferromagnets (Orenstein and Millis, 2000). For this reason the BCS theory (Bardeen *et al.*, 1957), which was developed for Fermi-liquid-like metals and has been so successful in describing conventional superconductors, is generally considered not to have the appropriate foundation for the description of the high-T_c superconductors. A new approach may therefore be needed, and a necessary requirement for a theory aiming to capture the essential physics of high-T_c superconductivity might be the inclusion of the fundamental ingredients of the physics of the doped antiferromagnets—the competition between antiferromagnetic and Coulomb interactions (which induce localization), and zero-point kinetic energy (which favors delocalization). The most radical electronic models along these lines seem to be those based on (i) the resonating valence bond (RVB) state and the related spin-charge separation picture,[10] (ii) stripes,[11] and (iii) quantum criticality.[12] Although very different, these theoretical approaches have one common denominator: superconductivity is not simply caused by the pairing of two quasiparticles, as in the BCS case, rather it is the process in which the quasiparticles themselves form. Furthermore, contrary to the standard theories of solids, in which any phase transition into a long-range ordered state is driven by the gain in potential energy, in cases (i) and (ii) the driving mechanism for the superconducting phase transition is identified with the gain in kinetic energy, a scenario that has recently received direct support from experimental investigation of the optical conductivity of $Bi_2Sr_2CaCu_2O_{8+\delta}$ (Molegraaf *et al.*, 2002). In the stripe or RVB models the hopping of pairs of holes perturbs the antiferromagnetic spin background less than individual holes. However, it is only when charge fluctuations become phase coherent that the frustration of the kinetic energy is released, and superconductivity sets in.

[9] See Emery (1987) and Varma *et al.* (1987a, 1987b). It should be emphasized, however, that the existence and stability of Zhang-Rice singlets in the cuprates, and in turn the description in terms of an effective one-band Hubbard model, have recently received further support from spin-resolved photoemission experiments on $Bi_2Sr_2CaCu_2O_{8+\delta}$, which suggest the pure singlet character of the first ionization states (Brookes *et al.*, 2001; Tjeng *et al.*, 2001).

[10] See, for example, Anderson (1987, 2000); Affleck and Marston (1988); Kothar and Liu (1988); Maekawa *et al.* (1988); Suzumura *et al.* (1988); Lee and Nagaosa (1992); Ioffe and Millis (1996); Wen and Lee (1996); Laughlin (1997); Balents *et al.* (1998, 1999, 2000); Lee (2000).

[11] See, for example, Zaanen and Gunnarsson (1989); Emery and Kivelson (1993a); Bianconi *et al.* (1996); Salkola *et al.* (1996); Kivelson *et al.* (1998); Emery *et al.* (1999); Ichioka and Machida (1999); Tohyama *et al.* (1999); Zaanen (1999); Chernyshev *et al.* (2000); Fleck *et al.* (2000); Markiewicz (2000); White and Scalapino (2000); Zacher, Eder, *et al.*, (2000); Han *et al.* (2001).

[12] See, for example, Chakravarty *et al.* (1989, 2001); Varma *et al.* (1989); Littlewood and Varma (1991); Sachdev and Ye (1992); Emery and Kivelson (1993b); Sokol and Pines (1993); Castellani *et al.* (1995); Varma (1997).

When the system is doped further, antiferromagnetic correlations are reduced and a metallic state appears. Eventually (i.e., in the optimum and overdoped regime), the antiferromagnetic state is destroyed and a large LDA-like Fermi surface emerges, with a volume which scales as $(1-x)$ counting electrons (x is the concentration of doped holes for p-type high-temperature superconductors), as expected within the Fermi-liquid approach. In this context, the first important question to be answered concerns the way the low-energy states emerge in the very underdoped regime (Fig. 14). For $x \ll 1$, two alternative scenarios have been proposed (see, for example, Allen *et al.*, 1990; Dagotto *et al.*, 1991; van Veenendaal *et al.*, 1994): first, the chemical potential μ is pinned inside the charge-transfer gap Δ as "in-gap states" are created [Fig. 14(b)]; second, the chemical potential moves downwards into the top of the valence band and states are transferred from the upper to the lower Hubbard band because of correlations [Fig. 14(c)].

Another relevant question is: How do the low-lying states evolve upon going from the underdoped to the overdoped regime, where Fermi-liquid-like behavior seems to recover? To better organize the discussion, let us present an overview of some relevant theoretical models. They can be classified as (i) those that preserve the underlying crystalline symmetry, and (ii) those that break this symmetry (note also that the scenarios based on a dynamical breaking of symmetry should be taken into account because ARPES is sensitive to the latter, due to the relatively high excitation energy). The first models to be mentioned among group (i) are the Fermi-liquid and band-structure perspectives (Pines and Nozières, 1966; Pickett, 1989), which sever the connection to the undoped antiferromagnetic insulator by assuming that screening in the doped metal is strong enough for the Fermi-liquid formalism to recover; in this case a well-defined Fermi surface is expected [Fig. 15(a)], with a volume proportional to $(1-x)$ in agreement with Luttinger's theorem (Luttinger, 1960). An alternative scenario considers the breakdown of Fermi-liquid theory due to umklapp scattering (Furukawa and Rice, 1998; Furukawa *et al.*, 1998; Honerkamp *et al.*, 2001). As a result, in the underdoped region of the phase diagram the Fermi surface is truncated near the saddle points at $(\pi,0)$ and $(0,\pi)$, because of the opening of spin and charge gaps. This results in four disconnected arcs of Fermi surface centered at $(\pm\pi/2,\pm\pi/2)$, as shown in Fig. 15(b). In agreement with a generalized form of Luttinger's theorem, the area defined by the four arcs and by the umklapp-gapped Fermi surface [dashed lines in Fig. 15(b)] encloses the full electron density.

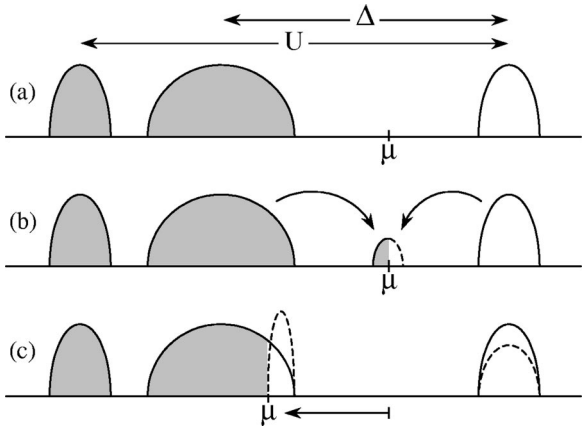

FIG. 14. Doping of a charge-transfer insulator: (a) in the undoped insulator a gap Δ separates the occupied from the unoccupied electronic states; (b) upon doping, μ is pinned inside the charge-transfer gap and states move towards the chemical potential; (c) alternatively, μ shifts to the top of the valence band and spectral weight is transferred as a consequence of electron correlations. From Veenendaal *et al.*, 1994.

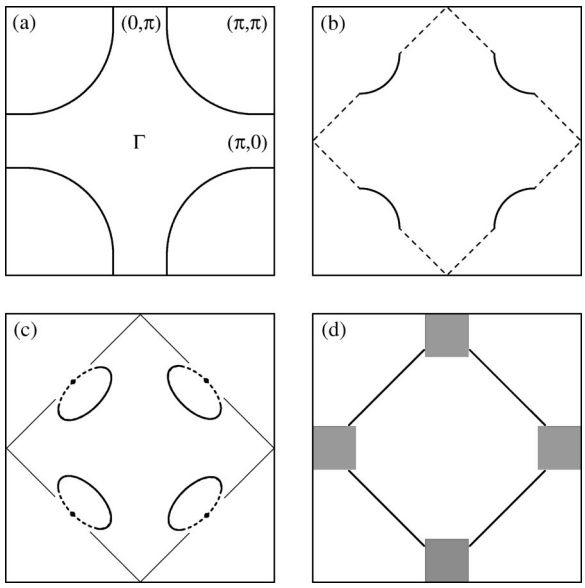

FIG. 15. Calculated Fermi surface for the CuO_2 plane from (a) local-density approximation with next-nearest-neighbor hopping; (b) truncation of a 2D Fermi surface due to umklapp scattering (Furukawa and Rice, 1998); (c) resonating valence bond/flux phase (Wen and Lee, 1996); (d) vertical and horizontal domains of disordered stripes (Salkola *et al.*, 1996).

Among the broken-symmetry models, we find the RVB/flux-phase approach.[13] This predicts a Fermi surface given by four hole pockets close to $(\pm\pi/2,\pm\pi/2)$ with a volume proportional to x, as in Fig. 15(c), which continuously evolve into a large Fermi surface as the hole concentration is increased. Note that this is very similar in spirit to the spin-density-wave picture, which also assumes a dynamical breaking of symmetry (Kampf and Schrieffer, 1990a, 1990b). Another model belonging to group (ii) is the stripe picture, which yields a momentum-space distribution of low-lying excitations (Salkola *et al.*, 1996; Fleck *et al.*, 2000; Markiewicz, 2000). These are represented by the gray patches in Fig. 15(d), where the results obtained for an equal number of vertical and horizontal domains of disordered stripes are qualitatively sketched (in this case the physics, together

[13]See, for example, Affleck and Marston (1988); Kotliar and Liu (1988); Maekawa *et al.* (1988); Suzumura *et al.* (1988); Wen and Lee (1996); Chakravarty *et al.* (2001).

with the superposition of domains, conspires to give the appearance of a large LDA-like Fermi surface).

There is another meaningful way to differentiate the four models discussed above: those depicted in Figs. 15(a)–(c) assume that the system is spatially homogeneous [as far as Fig. 15(b) is concerned, one could talk about phase separation between insulating spin-liquid and metallic regions, but only in momentum space (see Furukawa and Rice, 1998; Furukawa *et al.*, 1998; Honerkamp *et al.*, 2001)]. In contrast, the model in Fig. 15(d) assumes that the system is spatially inhomogeneous: the formation of stripes is defined as the segregation of charge carriers into one-dimensional (1D) domain walls which separate antiferromagnetic spin domains in antiphase with each other (Tranquada *et al.*, 1995). In Fig. 15(d), in particular, disordered stripes are considered (Salkola *et al.*, 1996).

Each of the above pictures seems to capture some of the experimental aspects. Throughout this paper, we shall try to compare ARPES data from various systems with the results of these models, in the hope of identifying the scenario that has the best overlap with the experimental observations. This will also help us to answer the question of whether different materials would favor different scenarios, and to address the relevance of degrees of freedom other than the electronic ones (e.g., lattice degrees of freedom especially in those systems exhibiting stripe instabilities, but also in a wider class of cuprates as we shall discuss in more detail in Sec. VIII).

IV. NORMAL-STATE ELECTRONIC STRUCTURE

A. $Sr_2CuO_2Cl_2$ and $Ca_2CuO_2Cl_2$

The t-J model, briefly discussed in the previous section, is of particular relevance to the low-energy features detected by ARPES on the cuprates. In fact, in ARPES experiments performed on the insulating parent compounds of the high-T_c superconductors, as a result of the photoemission process one photon-excited hole, or *photohole*, is injected in the CuO_2 plane. Therefore this experiment is the practical realization of a "single hole" in an antiferromagnetic insulator, and the comparison of ARPES data and calculations based on the t-J model is particularly meaningful (note that the latter are typically performed on small clusters and hence have difficulties treating charge ordering, which may arise at finite doping; see Sec. IV.B).

1. Single hole in an antiferromagnetic

ARPES spectra and the corresponding energy dispersion for insulating $Sr_2CuO_2Cl_2$ (SCOC) along the nodal direction (0,0)-(π,π) are shown in Figs. 16(a) and (b) (Wells *et al.*, 1995). A more complete quasiparticle dispersion is presented in Fig. 17 (note that throughout the paper we shall use terms like "quasiparticle" in a loose sense for convenience, even though in most cases Fermi-liquid theory may not apply and well-defined quasiparticle peaks cannot be identified in the ARPES spectra). Along (0,0)-(π,π) the dispersion is characterized by a

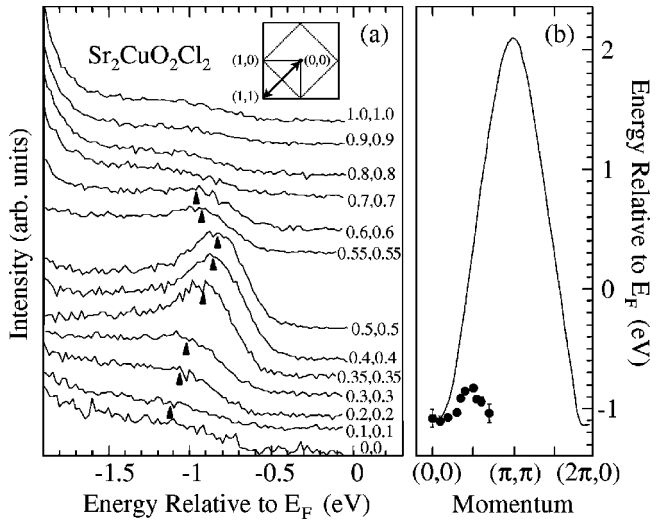

FIG. 16. Photoemission results from SCOC: (a) ARPES spectra from along (0,0)-(π,π) taken at 350 K [note that the Néel temperature is 256 K on this compound; however, for the correlation length indicated by neutron studies (Greven *et al.*, 1994), it was argued that photoemission should still be sensitive to the antiferromagnetic ordering]; (b) comparison between experimental and tight-binding quasiparticle dispersions. After Wells *et al.*, 1995.

bandwidth $W \simeq 0.3$ eV. This is in very good agreement with t-J model calculations (Dagotto, 1994), which show that, independent of the value of $t \simeq 350$ meV, the dressing of the hole moving in the antiferromagnetic background reduces the quasiparticle bandwidth from the square-lattice tight-binding value of $8t \simeq 2.8$ eV [Kittel, 1996; Fig. 16(b)] to $2.2J \simeq 270$ meV [$J \simeq 125$ meV for SCOC as independently deduced from neutron-scattering studies (Greven *et al.*, 1994)].

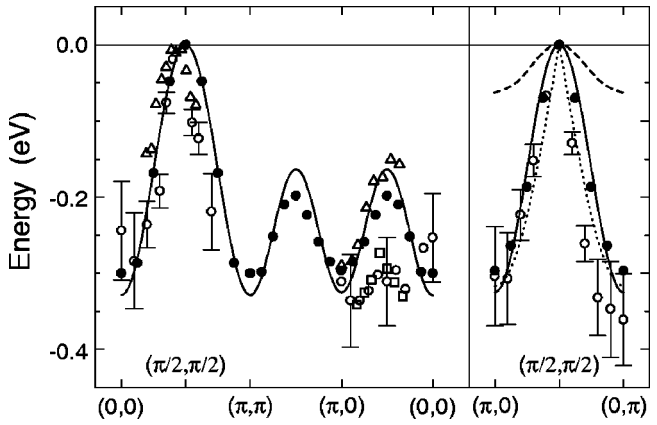

FIG. 17. Electronic dispersion for SCOC ($E=0$ corresponds to the top of the band). Experimental data: ○, Wells *et al.*, 1995; △, La Rosa *et al.*, 1997; □, Kim *et al.*, 1998. Dashed line, t-J model calculations (Wells *et al.*, 1995); ●, self-consistent Born approximation for the t-t'-t''-J model ($t=0.35$ eV, $t'=-0.12$ eV, $t''=0.08$ eV, and $J=0.14$ eV); solid lines, fits of the self-consistent Born approximation data (Tohyama and Maekawa, 2000); dotted line along $(\pi,0)$-$(0,\pi)$, spinon dispersion (Laughlin, 1997).

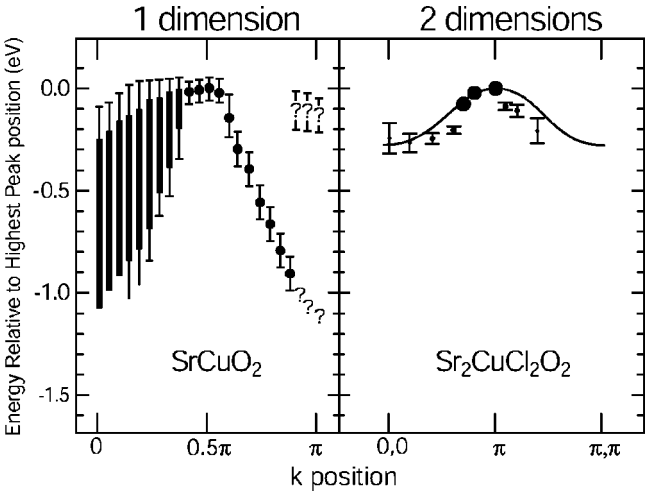

FIG. 18. Experimental dispersion for quasi-1D (Kim *et al.*, 1996) and quasi-2D (Wells *et al.*, 1995) insulating systems.

The ability of t-J model calculations to reproduce the experimentally observed energy-scale renormalization from t to J confirms the importance of many-body effects and, in particular, of the coupling between quasiparticles and magnetic correlations in the (undoped) cuprates. An additional proof of this statement is provided by the comparison between the experimentally determined dispersion for 1D and 2D systems with almost identical structures and Cu-O-Cu bond lengths (e.g., $SrCuO_2$ and SCOC, respectively). The surprising feature in the data presented in Fig. 18 is that the dispersion seen in 1D systems is about three times as large as that in 2D systems (Kim *et al.*, 1996, 1997; Kim, 2001). This violates the noninteracting-particle picture on a qualitative level, as band theory would predict the dispersion in two dimensions ($8t$) to be twice that in one dimension ($4t$). This catastrophic failure of the independent-particle picture can be understood as a consequence of two factors: first, the quasiparticle dispersion in two dimensions is strongly renormalized by the magnetic interaction; second, in one dimension spin-charge separation occurs, and this frees the motion of the holon—an elementary excitation with spin 0 and charge e— from the magnetic interaction (Lieb and Wu, 1968).

On the other hand, the t-J model predicts a relatively flat dispersion (Liu and Manousakis, 1992; Dagotto *et al.*, 1994) along the $(\pi,0)$-$(0,\pi)$ direction (dashed line in Fig. 17), in contrast to the bandwidth $W \simeq 0.3$ eV observed by ARPES around $(\pi/2,\pi/2)$ independent of the direction. Also the poorly defined line shape and the spectral weight suppression observed at $(\pi,0)$, which indicate the lack of integrity of the quasiparticle at those momenta, cannot be reproduced within the simple t-J model calculations (Kim *et al.*, 1998, 2002). Better agreement between the experimental dispersion and the calculations (solid circles and solid line in Fig. 17) is obtained by adding second- and third-nearest-neighbor hopping (t' and t'', respectively) to the t-J Hamiltonian.[14] In fact, as t' and t'' describe hopping within the same magnetic sublattice, they do not alter the antiferromagnetic properties of the system at half filling; at the same time, they are not strongly renormalized by antiferromagnetic correlations but contribute directly to the coherent motion of the hole and, therefore, have a substantial impact on quasiparticle dispersion. Less can be said about the line shape because the broadening is not accounted for by the theory, which is a major limitation of this kind of approach. [This is particularly evident at $(\pi/2, \pi/2)$ where the theory, contrary to what is observed in the experiments (Fig. 16), predicts very sharp peaks as this momentum corresponds to the valence band maximum.] Most importantly the inclusion of t' and t'' accounts for the suppression of the quasiparticle peak at $(\pi,0)$, which may reflect a reduction of antiferromagnetic spin correlations: the additional hopping possibilities represented by t' and t'' induce a spin-liquid state around the photohole with $(\pi,0)$ momentum (Tohayama and Maekawa, 2000; Tohayama *et al.*, 2000). As a consequence, one may expect to find signatures of spin-charge separation in the ARPES data (Anderson, 1987). In this regard, it is interesting to note that the full quasiparticle dispersion observed for SCOC can be very well reproduced by the spinon (an elementary excitation with spin $\hbar/2$ and charge 0) dispersion, as proposed by Laughlin (1997) [the dotted line in Fig. 17 shows the result along $(\pi,0)$-$(0,\pi)$]. Laughlin argued in favor of the decay of the photohole injected in the 2D antiferromagnetic CuO_2 plane into a spinon-holon pair. This is also reminiscent of flux-phase physics,[15] an extension of the early RVB conjecture (Anderson, 1987). We stress here that spin-charge separation in two dimensions, if realized, would have a different impact on the quasiparticle dispersion, as suggested by a comparison with the 1D case in Fig. 18: in two dimensions the holon motion is much less coherent than in one dimension.

2. Remnant Fermi surface

We mentioned above that both the relatively isotropic dispersion at $(\pi/2,\pi/2)$ and the suppression of quasiparticle weight at $(\pi,0)$ observed by ARPES on SCOC and $Ca_2CuO_2Cl_2$ (CCOC), which is similar in many respects to SCOC (Ronning, Kim, *et al.*, 1998, 2003), cannot be explained within the nearest-neighbor-hopping t-J model. Better agreement with experiment is obtained by including in the model longer-range hopping terms. In this way, it is also possible to reproduce the doping dependence of the quasiparticle band structure and, in particular, of the $(\pi,0)$ ARPES spectra (Eder *et al.*, 1997).

[14]See Nazarenko *et al.* (1995); Belinicher *et al.* (1996); Kyung and Ferrell (1996); Xiang and Wheatley (1996); Eder *et al.* (1997); Lee and Shih (1997); Lema and Aligia (1997); Leung *et al.* (1997); Sushkov *et al.* (1997); Kim *et al.* (1998); Tohyama and Maekawa (2000); and Tohyama *et al.* (2000).

[15]See, for example, Affleck and Marston (1988); Kotliar and Liu (1988); Maekawa *et al.* (1988); Suzumura *et al.* (1988); Wen and Lee (1996); Chakravarty *et al.* (2001).

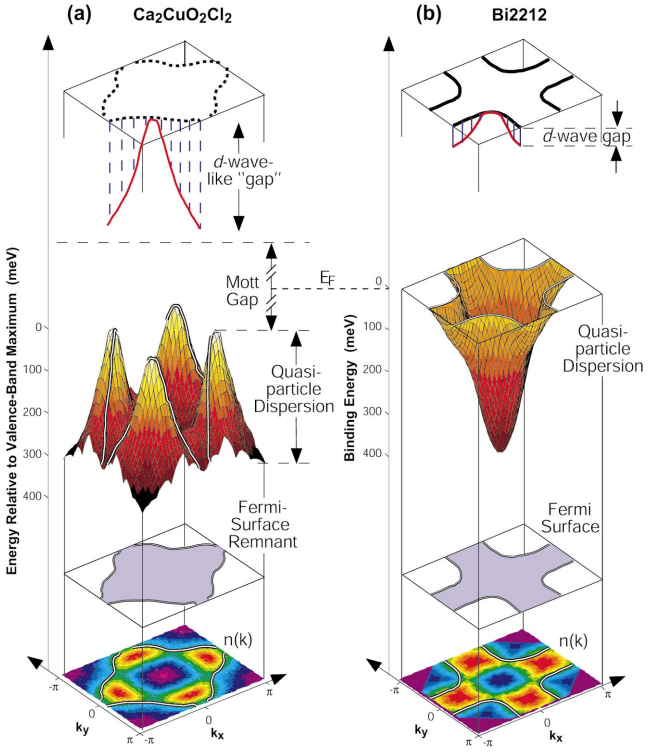

FIG. 19. Comparison of insulating and overdoped regimes: bottom, remnant Fermi surface and Fermi surface obtained from the analysis of $n(k)$ for (a) insulating CCOC and (b) overdoped Bi2212; middle right, while the Fermi surface in Bi2212 corresponds to the isoenergetic contour located at E_F, the remnant Fermi surface is away from E_F (because of the presence of the Mott gap), and (middle left), a large d-wave-like dispersion (300 meV) is found along its contour; top left, the latter defines a d-wave gap for the insulator, similar to (top right) the d-wave pseudogap observed in the underdoped regime. After Ronning *et al.*, 1998 (Color).

However, the t-J model, even in its more extended form, cannot completely account for the strong momentum dependence of the ARPES spectra from the undoped insulator (Eskes and Eder, 1996). In particular, although it predicts a decrease of intensity for the lowest-energy peak upon crossing the antiferromagnetic zone boundary (Bulut *et al.*, 1994; Eskes and Eder, 1996), this is not as sharp as experimentally observed in SCOC [see Fig. 16(a)] or CCOC. This limitation of the t-J model comes from having projected out the doubly occupied states originally contained in the Hubbard model: whereas the momentum occupation number $n(k)$ is a strongly varying function of k in the intermediate-U Hubbard model at half filling, it is trivially equal to 1/2 in the t-J model, which therefore cannot describe the anomalous distribution of spectral weight in the single-particle spectral function. This effect is accounted for by the complete large-U limit of the Hubbard model, as shown on the basis of finite-size cluster calculations by Eskes and Eder (1996), and was referred to by those authors as a *pseudo-Fermi surface*.

A detailed experimental characterization of the k dependence of the ARPES spectral weight for an undoped insulator has been presented by Ronning *et al.* (1998), on the basis of the $n(k)$ mapping obtained by integrating the ARPES spectra from CCOC over an energy window larger than the bandwidth. From the location of the steepest drops in $n(k)$ (see Sec. II.C) a *remnant Fermi surface* was defined for CCOC, which closely follows the antiferromagnetic Brillouin-zone boundary (Fig. 19). Note that matrix element effects also influence the k dependence of the intensity and alter the profile of the remnant Fermi surface (Haffner *et al.*, 2000, 2001). However, the $n(k)$ drop observed at the antiferromagnetic Brillouin-zone boundary both in the experiment and in the numerical results appears to be a robust feature, despite some uncertainties which indeed seem to be caused by matrix element effects (Dürr *et al.*, 2001; Golden *et al.*, 2001; Ronning, Kim, *et al.*, 2003). One has to realize however that the remnant-Fermi surface is not a real Fermi surface (the system has a Mott gap), but identifies the same locus of rapid intensity drop referred to as a pseudo-Fermi surface by Eskes and Eder (1996). It underscores the fact that the system was driven into the insulating state by strong electronic correlations. In addition, it does not even correspond to an isoenergetic contour in the quasiparticle dispersion (Fig. 19), similarly to the Fermi surface determined in the underdoped regime (Sec. VII). The relevance of this approach is that, once a remnant-Fermi surface has been determined, it is also possible to identify a gap along its contour (in addition to the much larger Mott gap) and try to compare it to the high-energy pseudogap of the underdoped cuprates (see Sec. VII).

3. Superconducting $Ca_{2-x}Na_xCuO_2Cl_2$

Although these materials are very difficult to dope up to the onset of superconductivity, recently doping-dependent data from the $(Sr,Ca)_2CuO_2Cl_2$ family have become available. Following earlier success on polycrystalline samples (Hiroi *et al.*, 1994, 1996), Kohsaka *et al.* (2002) have succeeded in growing superconducting single crystals of $Ca_{2-x}Na_xCuO_2Cl_2$ (with maximum $T_c=28$ K at $x=0.15$) by a flux method under a pressure of 4 GPa. This achievement has opened very exciting new opportunities in the systematic investigation of the cuprates: the oxychlorides together with the LSCO family represent the only materials in which a doping range corresponding to the metal-insulator transition can be accessed. Furthermore, since the best ARPES data from insulators have been obtained on this family of compounds, this makes a direct comparison of metal and insulator data more informative.

Figure 20 shows the energy distribution curves measured at 10 K with 25.5-eV photons on 10%-Na-doped CCOC ($T_c=13$ K), along the high-symmetry directions. In going from (0,0) to (π,π), a broad feature disperses up to the Fermi level, as indicated by the clear Fermi edge seen in the spectra near E_F [Fig. 20(b)]. After the band has crossed E_F, one can still follow a feature dispersing backwards (see tick marks) in a fashion very similar to what is expected for magnetic *shadow bands*

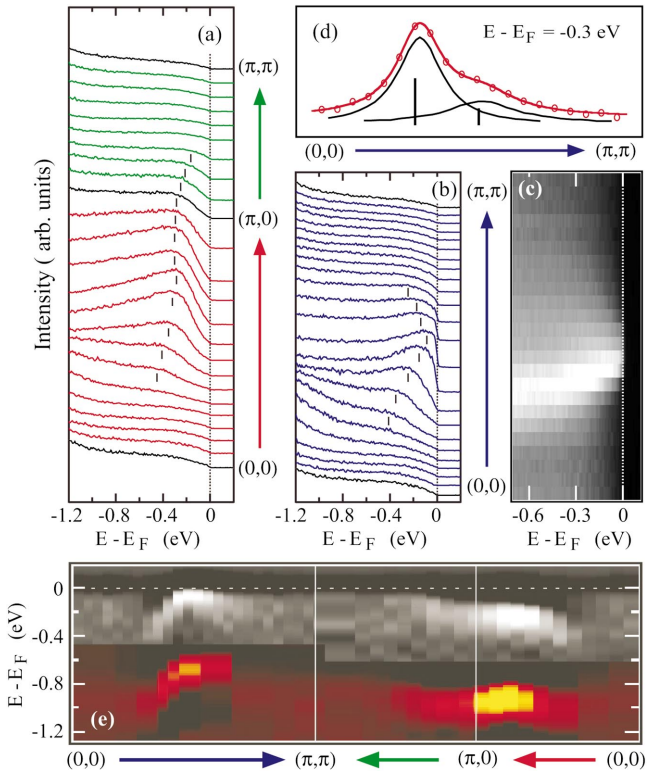

FIG. 20. Photoemission results from Na-doped and Na-free CCOC: (a),(b) ARPES spectra from 10% Na-doped CCOC, taken at $T=10$ K; (c) intensity plot and (d) constant-energy spectra from part (b); (e) second derivative with respect to the binding energy of the ARPES spectra from Na-free (color) and doped (gray) CCOC. After Kohsaka *et al.*, 2002 (Color).

due to spin fluctuations diverging at the antiferromagnetic zone boundary.[16] In the same figure, the constant-energy or momentum distribution curves are also plotted [Fig. 20(d)]. It appears that these cannot be fitted to a single Lorentzian—two Lorentzian peaks are needed. This is probably the most convincing case for the presence of shadow bands, as in this system complications due to structural distortions are not present and, therefore, the origin of the effect is likely magnetic. Figure 20(e) compares the dispersion of insulating CCOC and of the Na-doped superconductor: although in the insulator the top of the valence band is located ~0.7 eV below the chemical potential, there is a striking similarity in the dispersion of the two compounds. This suggests that when the system is doped the chemical potential shifts from inside the gap of the insulator to the top of the valence band near $(\pi/2,\pi/2)$, which is also supported by the similarities between the $(\pi,0)$ ARPES spectra from Na-free and doped CCOC (Ronning, Sasagawa, *et al.*, 2003). Note also that, while according to band theory the dispersive feature in Fig. 20(a) should reach E_F in going from $(\pi,0)$ to (π,π), an unambiguous Fermi crossing is

[16]See Kampf and Schrieffer (1990b); Dagotto (1994); Chubukov (1995); Haas *et al.* (1995); Preuss *et al.* (1995); and Wen and Lee (1996).

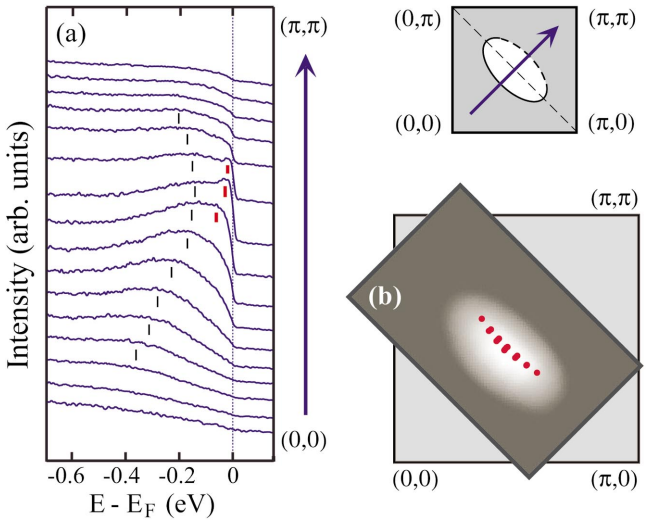

FIG. 21. ARPES data from 10% Na-doped CCOC near $(\pi/2, \pi/2)$: (a) spectra; (b) integrated intensity (over 100 meV). The red dots indicate those momenta at which a sharp peak was observed at E_F. After Kohsaka *et al.*, 2002 (Color).

not seen and near $(\pi,0)$ the band is ~200 meV below E_F, a point that will be discussed in greater detail in the section on the pseudogap (Sec. VII.E).

The results from Na-doped CCOC are consistent with a shift of the chemical potential [as in Fig. 14(c)] and are very suggestive of the two scenarios depicted in Figs. 15(b) or (c), as emphasized in particular by the contour map of the low-lying excitations presented in Fig. 21(b). The task of conclusively distinguishing between the scenarios of Figs. 15(b) and (c) is rather difficult. The key point is whether or not a shadow Fermi surface is detected. Such a surface is marked by the dashed lines in Fig. 15(c), but its presence is not clear in the contour map of Fig. 21(b). This can either mean that a shadow Fermi surface is not present or that one is present but too weak to be detected [the data in Figs. 20(b)–(d) show the presence of a shadow band that disperses away from the Fermi level when passing $(\pi/2,\pi/2)$, but this is not clear at E_F]. Even more difficult would be, at this stage, to distinguish between the scenario of Fig. 15(c) in which the Fermi-surface pockets are not exactly centered at $(\pi/2,\pi/2)$, and the simplest antiferromagnetic/spin-density-wave picture (see, for example, Fulde, 1995), in which the excitation spectrum is symmetric with respect to the antiferromagnetic zone boundary (as in the Brillouin-zone sketch shown in Fig. 21).

A more detailed analysis of the ARPES spectra along the nodal direction reveals additional information (Kohsaka *et al.*, 2002). As shown in Fig. 21, the energy distribution curves near the Fermi energy actually consist of two components: a broader component at higher binding energy that appears to disperse backwards past $(\pi/2,\pi/2)$, defining the shadow band, and a sharp (although weak) component that crosses the Fermi level [its k-space location is indicated by the red dots in Fig. 21(b)]. Note that the sharper low-energy peak is not directly related to superconductivity, as it is seen in the

20-K data of Fig. 21 ($T_c = 13$ K) and, as a matter of fact, was still present at temperatures as high as 75 K (Ronning, Sasagawa *et al.*, 2003). On the one hand, these two components may be thought of as the coherent and incoherent parts of the spectral function, as discussed in Sec. II.C. On the other hand, these results may also indicate that the doping evolution cannot be fully accounted for in terms of a rigid shift of the chemical potential.

4. Summary

It must be stressed that so far only 10%-Na-doped samples have been studied (Kohsaka *et al.*, 2002). Whether the relatively simple behavior (i.e., rigid-band-like) seen for Na-doped CCOC remains true at lower dopings (near the metal-insulator transition boundary) is still an open question, and is of particular relevance to those theories which lead to d-wave superconductivity starting from a rigid-band picture (see, Dagotto *et al.*, 1995). As we shall see in the next section, at first glance the physical picture emerging from LSCO is quite different and is actually more consistent with the scenario in which at low doping levels new states are created inside the gap [Fig. 14(b)]. This could be naturally understood if the system became inhomogeneous at intermediate dopings: in fact two electronic components are observed in LSCO in the underdoped region (5–10 %) and only one in the overdoped regime. However, without data from the very underdoped regime one may also interpret the LSCO doping evolution in terms of a quasirigid band shift with some modifications near the $(\pi,0)$ region. Therefore, until more data on Na-CCOC are available, one cannot conclude whether or not the difference with LSCO is of a qualitative or a quantitative nature.

B. $La_{2-x}Sr_xCuO_4$

In order to study the doping evolution of low-energy electronic properties over the full doping range the most suitable system is $La_{2-x}Sr_xCuO_4$ (LSCO). The hole concentration in the CuO_2 plane can be controlled and determined by the Sr content x, from the undoped insulator ($x=0$) to the heavily overdoped metal ($x\sim0.35$). In addition, LSCO has a simple crystal structure with a single CuO_2 layer (Fig. 11) and none of the complications due to superstructure which are found in Bi2212 (Sec. IV.C). Another interesting feature of this compound is the suppression of T_c at $x=1/8$, which, together with the incommensurate antiferromagnetic long-range order observed by inelastic neutron scattering (Suzuki *et al.*, 1998), has been discussed as evidence for "fluctuating stripes." Similar antiferromagnetic order accompanied by charge ordering was interpreted as a realization of "static stripes" in $La_{1.48}Nd_{0.4}Sr_{0.12}CuO_4$ (Tranquada *et al.*, 1995). Note that, in relation to the specific behavior observed for the two systems, the difference in disorder may also play an important role.

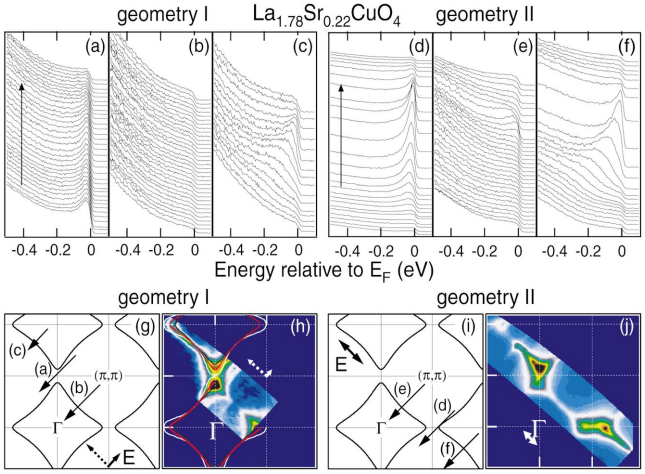

FIG. 22. Photoemission results from overdoped LSCO ($x=0.22$): (a)–(f) ARPES spectra measured at 20 K with 55.5-eV photons in two different experimental geometries; (g), (i) the cut orientation in k-space and field polarization together with the electronlike Fermi surface; (h),(j) E_F intensity map (30-meV integration window). White and black curves are the $k_z=0$ and π/c Fermi surfaces from band calculations (Xu *et al.*, 1987), and red curves the Fermi surface from a tight-binding fit of the data. After Yoshida *et al.*, 2001 (Color).

1. Metal-insulator transition

We begin our discussion with data from $x=0.22$ overdoped LSCO (Yoshida *et al.*, 2001). Because many-body effects such as charge ordering are expected to be weak in the overdoped regime, the results from this sample can be used to test the overall reliability of the ARPES data from LSCO. Figure 22 presents ARPES spectra from two Brillouin zones taken with 55.5-eV photons under different polarization conditions (while in geometry II the electric field was fixed and almost parallel to the sample surface, in geometry I it had only a small in-plane component, which increased at larger momenta). It appears that the spectra from this overdoped sample are very sharp, contrary to the typical data from underdoped LSCO that we shall discuss later. Indeed, the sharpness of the spectra from the second zone is comparable to that observed in Bi2212, at similar doping. Figures 22(h) and (j) present the spectral intensity integrated over a 30-meV energy window at E_F. In general, the E_F intensity map derived from high-resolution data gives a good evaluation of the Fermi surface, provided that matrix element effects are carefully considered (see Secs. II.C and II.E). Yoshida *et al.* (2001) have attempted to account for the photoionization cross-section effects for LSCO by varying the experimental geometry and by performing simulations of the spectral weight distribution, which qualitatively reproduce some of the variation observed in different geometries. From the comparison [Fig. 22(h)] between the experimental E_F intensity maps and the Fermi surfaces obtained from a tight-binding fit to the data and from LDA calculations (Xu *et al.*, 1987), Yoshida *et al.* (2001) concluded that the Fermi surface of overdoped LSCO consists of an electron pocket centered at (0,0), in agreement with band-

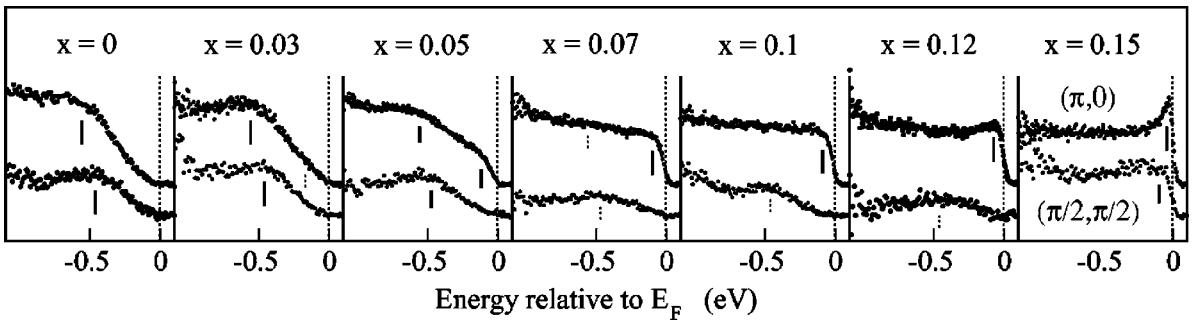

FIG. 23. ARPES data from LSCO for different dopings levels at $(\pi,0)$ and $(\pi/2,\pi/2)$. The spectra were normalized to the integrated intensity of the valence bands, and at $(\pi/2,\pi/2)$ were multiplied by a factor of 2. From Ino *et al.*, 2000.

structure calculations. These results, namely, the observation of sharp spectral features and an LDA-like Fermi surface, as well as the fact that low-energy electron diffraction investigations do not detect any evidence of surface reconstruction, give strong credence to the ARPES data from the LSCO system. Since the quality of LSCO single crystals improves with decreased doping x, these data suggest that the broad spectral features observed in underdoped LSCO are intrinsic in nature.

Let us then move on to the low-doping region, near the metal-insulator transition boundary. Figure 23 presents ARPES spectra at $(\pi,0)$ and $(\pi/2,\pi/2)$ as a function of doping (Ino *et al.*, 2000). The data were recorded under identical experimental geometries so that the photoionization matrix elements are the same. For the insulating samples $(x=0)$, the data are characterized by a high binding energy feature [$\sim$0.5 eV at $(\pi/2,\pi/2)$ and $\sim$0.7 eV at $(\pi,0)$], and are consistent with what we have discussed in Sec. IV.A for insulating SCOC (Wells *et al.*, 1995; Kim *et al.*, 1998), although the features are now broader. The remarkable result is that for $x=0.05$ two features can be identified in the ARPES spectra at the $(\pi,0)$ point (some additional weight at low energy is already observable for $x=0.3$): in addition to the high-energy one, reminiscent of the Zhang-Rice singlet band of an antiferromagnetic insulator, a second shoulder is observable close to E_F. Upon further doping the system with holes, we see a systematic transfer of spectral weight from the high- to the low-energy feature, and a well-defined quasiparticle peak develops near optimal doping. On the other hand, the results obtained at $(\pi/2,\pi/2)$ are very different: first, the data show an overall suppression of weight as compared to $(\pi,0)$ [the spectra plotted in Fig. 23 for $(\pi/2,\pi/2)$ have been multiplied by a factor of 2]; second, in the nodal region [i.e., along (0,0)-(π,π)], a quasiparticle peak is observable only for $x \geqslant 0.15$. As we shall discuss later, with different experimental geometries more spectral weight is detected near E_F in the nodal region, but the overall trend of the doping dependence of the electronic structure is robust.

The dispersion of the LSCO spectral features for different doping levels is summarized in Fig. 24, which presents the second derivative with respect to the binding energy of the ARPES spectra (Ino *et al.*, 2000). Upon increasing doping, we can observe the building of near-E_F weight first at $(\pi,0)$, and then at $(\pi/2,\pi/2)$. One can clearly observe the presence of the flat-band saddle point extensively discussed in the literature. Furthermore, the second derivative emphasizes the presence of a high-energy feature in the heavily underdoped samples (coexisting with a low-energy one, at least for $x=0.05$). This has a 200-meV lower energy at $(\pi/2,\pi/2)$ than at $(\pi,0)$, in qualitative agreement with what is observed in the undoped insulator SCOC (Wells *et al.*, 1995).

The ARPES results from LSCO, and in particular the presence of two electronic components, suggest that the effects of doping on the electronic structure of the correlated insulator cannot be accounted for by a simple

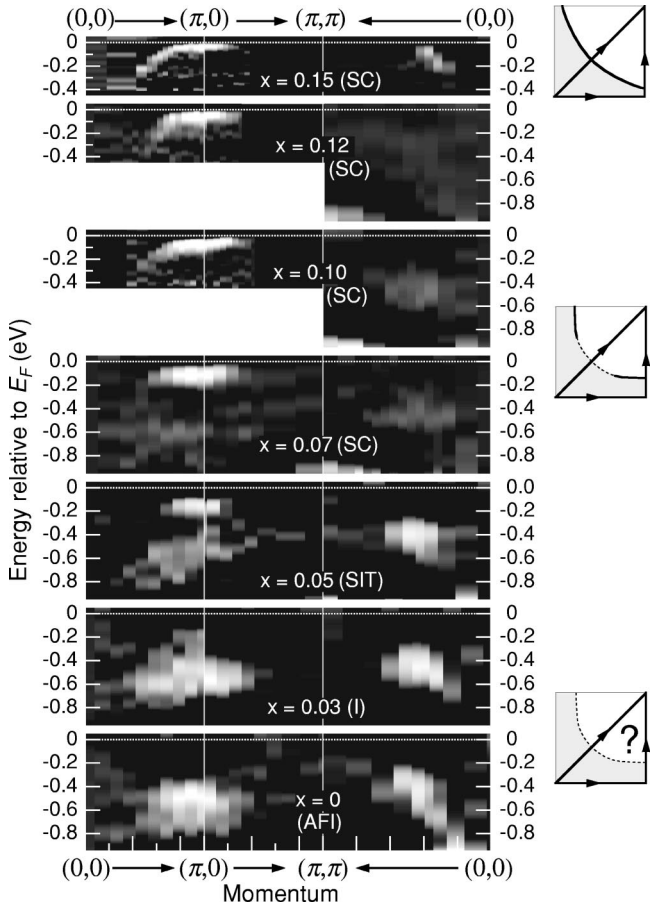

FIG. 24. Second derivative, with respect to the binding energy, of the LSCO ARPES spectra along the high-symmetry directions for many doping levels. From Ino *et al.*, 2000.

shift of the Fermi level in a rigid-band model (Ino *et al.*, 2000). This is in agreement with another observation by Ino *et al.* (1997): from an analysis of direct and inverse angle-integrated photoemission spectra, it was concluded that the chemical potential μ is pinned inside the charge-transfer gap for $x \leqslant 0.10$ and starts shifting downwards significantly only for $x \geqslant 0.15$. The above results seem to indicate that, in the case of LSCO, in-gap states are created upon doping the insulator [Fig. 14(b)].

2. Nanoscale phase separation

Ino *et al.* (2000) suggested that the ARPES results from LSCO may be understood within the stripe picture, which is a particular form of nanoscale phase separation. This would explain the pinning of the chemical potential for $x \leqslant 0.125$ (i.e., the so-called 1/8 doping) as a consequence of the segregation of doped holes into metallic domain walls, which gives rise to the appearance of in-gap states. Furthermore, the suppression of nodal intensity at E_F would be consistent with the vertical and horizontal orientation of the metallic stripes (orthogonal domains are expected for this nanoscale phase separation). Here the conjecture that charge fluctuations would be suppressed along directions crossing the stripes is supported by finite-size cluster calculations (Tohyama *et al.*, 1999). The increase of the spectral weight at E_F for $x \geqslant 1/8$ in the nodal region may indicate that above this doping level the holes overflow from the saturated stripes into the CuO_2 planes.

Concerning the relevancy of the stripe scenario to the ARPES data from the high-T_c superconductors, more insights could come from the investigation of Nd-LSCO, a model compound for which the evidence of spin and charge stripe ordering is the strongest (Tranquada *et al.*, 1995). ARPES data from $La_{1.28}Nd_{0.6}Sr_{0.12}CuO_4$ were reported by Zhou *et al.* (1999). Remarkably, the low-energy spectral weight was mostly concentrated in narrow and straight regions along the (0,0)-(π,0) and (0,0)-(0,π) directions and was confined between lines crossing the axes at $\pm\pi/4$. These straight patches of high intensity are suggestive of almost perfectly nested 1D segments of Fermi surface. Zhou *et al.* (1999) interpreted these results as a signature of a 1D electronic structure related to the presence of static quarter filled charge stripes which, as indicated by neutron and x-ray experiments (Tranquada *et al.*, 1995), at 1/8 doping are separated by antiferromagnetic regions resulting in a pattern with periodicity $4a$ (and characterized by macroscopic orthogonal domains). This interpretation would also explain the origin of the two components seen in the ARPES spectra from LSCO near the metal-insulator transition boundary (Fig. 23): the signal from the antiferromagnetic insulating regions would be pushed to high binding energies because of the Mott gap, while the charge stripes would be responsible for the component near E_F. In this sense, the stripe interpretation is rather appealing (Markiewicz, 2000). On the other hand, there are some aspects which cannot be satisfactorily explained within the idealized stripe picture. For example,

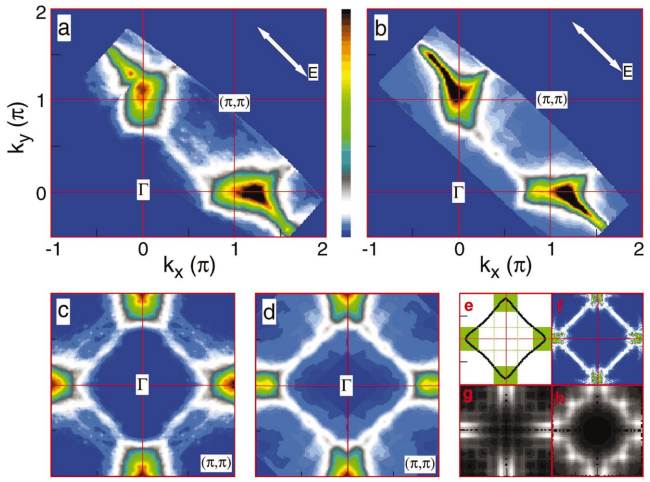

FIG. 25. ARPES data from LSCO and Nd-LSCO: (a),(b) Intensity maps obtained by integrating over 30 meV at E_F the spectra from $x=0.15$ Nd-LSCO and LSCO; (c),(d) corresponding fourfold symmetrization of the first-zone data (white arrows indicate the field polarization); (e) cartoon of the experimental results; calculations for (f) orthogonal domains of disordered or fluctuating stripes [as in Fig. 15(d); Salkola *et al.*, 1996], (g) site-centered and (h) bond-centered stripes (Zacher, Eder, *et al.*, 2000). After Zhou *et al.*, 2001 (Color).

in both LSCO (Fig. 24) and Nd-LSCO (Zhou *et al.*, 1999), the quasiparticle bands along the (0,0)-(π,0) and (0,0)-(0,π) directions are characterized by quite rapid dispersion. This is counter to what one would expect for an ideal 1D system even in the presence of orthogonal domains, as the electronic dispersion should be observed only within and perpendicular to each of the two superimposed 1D Fermi surfaces [for more on this point see Zhou *et al.* (1999)]. Furthermore, possible artifacts due to matrix element effects have to be cautiously considered when interpreting the ARPES data, especially modulations of the integrated spectral weight (Secs. II.C and II.D).

In order to gain more insight into these issues, in particular in relation to the straight segments of Fermi surface observed in Nd-LSCO and to the suppression of the nodal state, Zhou *et al.* (2001) extended the measurements to the second zone and used different polarizations for the incoming electric field. Figure 25 presents data from 15%-doped LSCO and Nd-LSCO recorded in the same geometry as the data of Fig. 22(j) from 22%-doped LSCO. These results confirm the presence of flat bands in extended regions around (π,0) and (0,π). On the other hand, in the second zone appreciable spectral weight is detected at E_F in the nodal region, which appears to become more intense as the Sr concentration is increased in both Nd-LSCO and LSCO and is stronger in Nd-free LSCO for a given Sr content (Fig. 25). This nodal weight was not found in the earlier study of 12%-doped Nd-LSCO (Zhou *et al.*, 1999) and is not expected in calculations considering only rigid stripes (Ichioka and Machida, 1999; Markiewicz, 2000).

Possible descriptions of these results within the stripe context are summarized in Figs. 25(c)–(h) where the low-lying spectral weights from LSCO (c) and Nd-LSCO (d) are compared to the results of model calculations. First, the experimental Fermi surface composed of straight patches at $(\pi,0)$ and $(0,\pi)$ connected by nodal segments [as emphasized in the sketch of Fig. 25(e)] closely resembles the one arising from disorder or fluctuation of the stripes (Salkola *et al.*, 1996), which was sketched in Fig. 15(d) and is here exactly reproduced in Fig. 25(f). Alternatively, the experimental Fermi surface may result from the coexistence of site-centered [Fig. 25(g)] and bond-centered [Fig. 25(h)] stripes (Zacher, Eder, *et al.*, 2000). Both scenarios, as well as more recent calculations performed for various inhomogeneous models for the cuprates (Eroles *et al.*, 2001), suggest that the stripe picture catches the essence of the low-lying physics for the LSCO system. This is also indicated by dynamical mean-field theory results, which are characterized by a 1D dispersive band near E_F and a high-energy incoherent feature in the very underdoped regime (Fleck *et al.*, 2000), as well as by numerical studies of the spin-fermion model, which indicate that both stripe-induced midgap states and valence-band states contribute to the Fermi surface (Moraghebi *et al.*, 2001), consistent with the two electronic components detected by ARPES on LSCO.

3. From hole to electronlike Fermi surface

It was noted that the presence of a sharp structure in momentum space such as a Fermi-surface-like feature does not necessarily imply well-defined one-electron states and, in particular, is not incompatible with the stripe scenario (Orgad *et al.*, 2001). For instance, in a non-Fermi-liquid system like the 1D electron gas, in which the energy distribution curves are typically completely incoherent, the momentum distribution curves near E_F (as defined in Fig. 7) might be very sharp because of more stringent kinematic constraints. Given that the striped system does exhibit a Fermi-surface-like feature (Fig. 25), it is still meaningful to investigate its evolution as a function of doping. In doing so, one must bear in mind that the concept of a Fermi surface is here referred to in a loose manner: in fact, it identifies the momentum-space location where a very broad feature (and not a well-defined peak in energy) crosses E_F, after having defined some kind of band dispersion.

ARPES spectra for underdoped ($x=0.1$) and overdoped ($x=0.3$) LSCO are shown in Fig. 26 (Ino *et al.*, 1999). Although the spectral features from the underdoped samples tend to be broad, which may be related to charge inhomogeneity, as discussed, some clear Fermi crossings are observable in part of the Brillouin zone, especially in overdoped samples. For $x=0.1$, along the direction (0,0)-$(\pi,0)$-$(2\pi,0)$ at 29-eV photon energy [Fig. 26(a)], a broad quasiparticle peak emerges from the background, disperses towards E_F without crossing it, and then pulls back in the second Brillouin zone. Similar results are obtained at 22.4 eV [Fig. 26(b)], the only difference being a decrease of intensity in the first Brillouin zone due to matrix element effects specific to this photon energy (Ino *et al.*, 1999). Along $(\pi,0)$-(π,π) the quasiparticle peak, with maximum binding energy at $(\pi,0)$, disperses almost up to E_F, loses intensity, and disappears [Fig. 26(d)]. The leading-edge midpoint never reaches E_F because of the superconducting gap (~ 8 meV) opened along the Fermi surface at this temperature (as clearly shown in Fig. 66 below). Following Campuzano *et al.* (1996), Ino *et al.* (1999) identified the underlying Fermi surface crossing by the locus of the minimum gap, which is at $(\pi,0.2\pi)$. Along the nodal direction no clear peak was observed [Fig. 26(c)], as discussed above. However, having detected a band below E_F at $(\pi,0)$, the authors concluded that for $x=0.1$ the Fermi surface of LSCO is holelike in character and centered at (π,π). When we compare the spectra from heavily overdoped and underdoped LSCO [Figs. 26(e) and (a)], we see a striking difference: for $x=0.3$, the quasiparticle peak along this cut has almost disappeared at $(\pi,0)$. The decrease of intensity, together with a leading-edge midpoint located above E_F, provides evidence for a quasiparticle peak crossing E_F before $(\pi,0)$. The Fermi surface thus determined for heavily overdoped LSCO is electronlike and centered at (0,0), in agreement with what was discussed in relation to Fig. 22. Careful investigations by Ino *et al.* (2002) indicated that the Fermi surface changes from holelike to electronlike for $x\simeq 0.15$–0.2 as the saddle point moves from below to above E_F, consistent with LDA calculations.

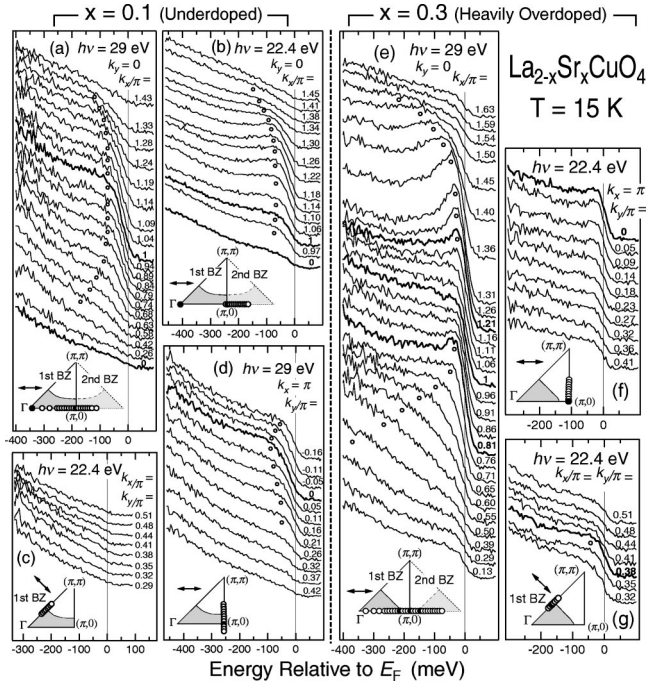

FIG. 26. ARPES spectra from LSCO for different doping levels: (a)–(d) underdoped ($x=0.1$); (e)–(g) heavily overdoped ($x=0.3$). Insets: measured k-space points and incident-light polarization. From Ino *et al.*, 1999.

4. Summary

In summary, what has emerged from the study of the LSCO system is a very complex and intriguing picture,

characterized by some contrasting aspects: neither a simple stripe model nor any of the other models proposed in Fig. 15 can provide a satisfactory explanation for the complete body of available data. As we have discussed, the stripe picture, when disorder/fluctuations and realistic charge disproportionation are considered, has the advantage of qualitatively explaining the data over the entire doping range, including the presence of two electronic components, the straight Fermi-surface segments, and the lack of a chemical potential shift in the very underdoped regime. On the other hand, on a more quantitative level, there are still many open questions. In particular, in order to gain more reliable insights, the effects of matrix elements on the ARPES data should be investigated in more detail. In fact, *ab initio* calculations of the matrix elements are still unavailable for LSCO, and tight-binding fits do not reproduce the results to a satisfactory degree.

As a last remark, it should be mentioned that the very underdoped regime was very recently studied by Yoshida *et al.* (2002). The two-component electronic structure discussed above was also observed for these samples, hinting again at a tendency towards nanoscale phase separation. However, the low-energy component (i.e., from the hole-rich region) defines a Fermi-surface arc reminiscent of an LDA Fermi surface gapped in the $(\pi,0)$ region. Despite this seemingly more conventional behavior, one should not abandon a many-body description of LSCO because a simple band picture cannot explain the basic observation of a two-component low-energy electronic structure.

C. $Bi_2Sr_2CaCu_2O_{8+\delta}$

Let us now turn our attention to $Bi_2Sr_2CaCu_2O_{8+\delta}$ (Bi2212). This is the high-T_c superconductor most intensively investigated by ARPES thanks to the availability of large high quality single crystals, the presence of a natural cleavage plane between the BiO layers, and especially the richness of information that can be obtained by ARPES in both the normal and the superconducting state. Due to sample quality issues most Bi2212 experiments have been carried out near optimal doping, and there is very limited or almost no information on the electronic structure near the metal-insulator transition boundary. In the following we concentrate on cases with a doping of 10% or higher. Therefore we cannot answer the questions of whether the two-component electronic structure observed in LSCO for 5–7 % doping is also present in the Bi2212 case, or how the metallic state emerges in the latter system. Core-level spectroscopy results, however, suggest a behavior intermediate between that seen in LSCO and a simple linear shift of the chemical potential (Harima *et al.*, 2002).

1. Fermi-surface topology

In the following we shall illustrate the normal-state electronic properties of Bi2212, focusing in particular on Fermi-surface topology, a topic that has been marked by intense controversy since the very beginning of its investigation. The main reason for this is the complexity of the electronic structure in the $(\pi,0)$ region of momentum space, which is where the quasiparticle dispersion as determined by ARPES is weakly momentum dependent, giving rise to the so-called *flat bands* (Abrikosov *et al.*, 1993; Dessau *et al.*, 1993; Gofron *et al.*, 1993). The complications arise from the detection of several additional features besides those related to the primary electronic structure. First, there are *shadow bands*, replicas of the main Fermi surface shifted by the wave vector (π,π) in the 2D Brillouin zone (Aebi *et al.*, 1994; see Figs. 27–30). These correspond to the backfolding of the main electronic structure with respect to the mirror planes perpendicular to Γ-X or Γ-Y (in the following we make use of the momentum-space notations defined for Bi2212 in Fig. 12). After the early explanation by Aebi *et al.* (1994) in terms of short-range and dynamic antiferromagnetic correlations resulting in a $(\sqrt{2}\times\sqrt{2})R45°$ superstructure (Kampf and Schrieffer, 1990b), several alternatives have been proposed.[17] These include a structural origin reflecting the presence of two inequivalent Cu sites per CuO_2 plane in the face-centered orthorhombic unit cell (Singh and Pickett, 1995; Ding, Bellman, *et al.*, 1996). A possible, although not yet well-defined, link to superconductivity has also been proposed: recently Kordyuk *et al.* (2002a) observed that the intensity of the shadow bands shows a correlation with T_c, as a function of doping. However, no conclusive picture has been reached so far.

The second additional feature is the *umklapp bands*, which are commonly referred to as originating from the diffraction of the photoelectrons off the superstructure present in the BiO layers, but should rather be considered as a modification of the intrinsic in-plane electronic structure due to the incommensurate distortion of the approximate tetragonal symmetry (Aebi *et al.*, 1995; Osterwalder *et al.*, 1995; Schwaller *et al.*, 1995; Ding, Bellman, *et al.*, 1996). This distortion is characterized by a periodicity of 27 Å along the b axis and results in a unit cell approximately five times larger along this direction (Withers *et al.*, 1988; Yamamoto *et al.*, 1990). This gives rise to two umklapp replicas of the Fermi surface shifted by $\pm(0.21\pi,0.21\pi)$ as shown below in Figs. 28(a), 29, and 30, and even to higher-order ones shifted by $\pm(0.42\pi,0.42\pi)$ and labeled UB2 in Fig. 30(a) (Osterwalder *et al.*, 1995; Fretwell *et al.*, 2000).

The last complications come from the so-called *bilayer band splitting*, that is, the splitting of the CuO_2 plane derived electronic structure in bonding and antibonding bands due to the presence of CuO_2 bilayer blocks in the unit cell of Bi2212. On the basis of symmetry arguments this splitting is expected to be maximum at $(\pi,0)$, while it should vanish along the (0,0)-(π,π) direction (Chakravarty *et al.*, 1993; Andersen *et al.*, 1995). As a

[17] See Chakravarty *et al.* (1995); Haas *et al.* (1995); Singh and Pickett (1995); Ding, Bellman, *et al.* (1996); Salkola *et al.* (1996); and Kordyuk *et al.* (2002a); see also Lynch and Olson (1999), p. 248.

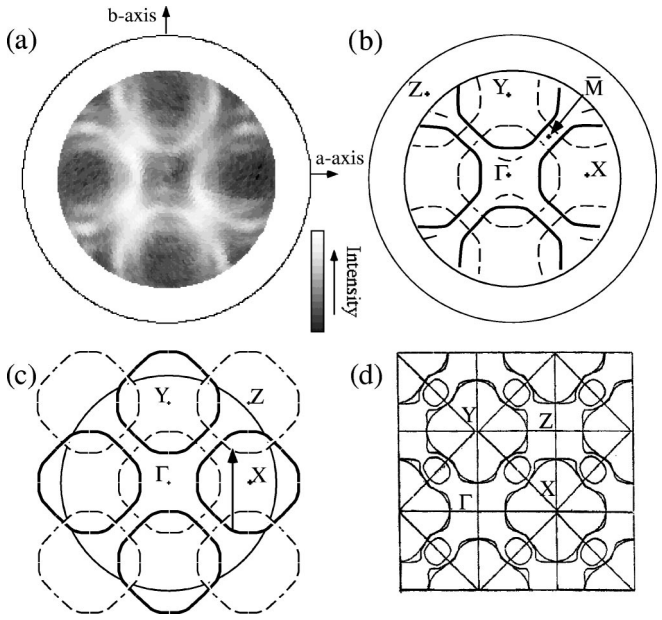

FIG. 27. The Fermi surface of near optimally doped Bi2212: (a) integrated intensity map (10-meV window centered at E_F) for Bi2212 at 300 K obtained with 21.2-eV photons (HeI line); (b),(c) superposition of the main Fermi surface (thick lines) and of its (π,π) translation (thin dashed lines) due to back-folded shadow bands; (d) Fermi surface calculated by Massidda *et al.* (1988). After Aebi *et al.*, 1994.

result, around $(\pi,0)$ two main bands, two shadow bands, and four umklapp bands cross the Fermi level.

Figure 27 reproduces the Fermi-surface data and analysis of Aebi *et al.* (1994) for near optimally doped Bi2212. Panel (a) shows a plot of the spectral weight integrated within an energy window of 10 meV near the Fermi level (data were taken with an energy resolution of 30–40 meV). This was the first time that a detailed momentum-space E_F map was carried out on a cuprate superconductor. The authors concluded that the Fermi surface is a holelike piece, as indicated by the heavy lines in Fig. 27(b). The complications in the intensity map stem from the superposition of shadow surfaces that are offset from the main Fermi surface by (π,π), as shown in Fig. 27(c) and discussed above. Aebi *et al.* (1994) also concluded that there were no BiO Fermi-surface pockets, which had been predicted on the basis of band-structure calculations as shown in Fig. 27(d) (Massidda *et al.*, 1988). As a matter of fact, one additional problem with Bi2212 is that there are no reliable band calculations: all theoretical results predict a BiO Fermi surface that has not been convincingly observed (Shen and Dessau, 1995). The work of Aebi *et al.* (1994) represents the beginning of a very different approach in the field: instead of analyzing the data in terms of energy scans at fixed momenta or *energy distribution curves* (EDC's) as usually done, these authors for the very first time made use of momentum scans at fixed energy or *angular distribution curves* [nowadays more commonly referred to as *momentum distribution curves* (MDC's) after Valla, Fedorov, Johnson, Wells, *et al.* (1999), who used this approach to extract self-energy corrections from the ARPES data; see Fig. 7 and Sec. VIII]. In a series of papers, Aebi, Osterwalder, and co-workers used this approach to identify the superstructure periodicity and the intensity and dispersion of both main and shadow bands (Aebi *et al.*, 1994; Osterwalder *et al.*, 1995; Schwaller *et al.*, 1995).

The results of Aebi *et al.* (1994) are different from those of the early work by Dessau *et al.* (1993), which indicated another main Fermi-surface crossing in the $(\pi,0)$ region: the detection of two pieces of Fermi surface, one electronlike and the other holelike, was interpreted as a signature of bonding-antibonding splitting in a bilayer system due to the presence of two CuO_2 planes per unit cell (Dessau *et al.*, 1993). Subsequently, in a set of two papers, Ding, Bellman, *et al.* (1996) and Ding, Norman, *et al.* (1997) argued against bilayer splitting [a result that was taken as key supporting evidence for the interlayer tunneling mechanism for high-temperature superconductivity (Anderson, 1995, 1997, 1998)], and in favor of a Fermi surface characterized by a simple holelike barrel. They attributed the additional Fermi-surface crossing identified by Dessau *et al.* (1993) along the (0,0)-$(\pi,0)$ line to complications arising from the presence of a superstructure in the BiO layers (i.e., umklapp bands), as shown in Fig. 28. In particular, main and umklapp bands were identified in the complicated $(\pi,0)$ region on the basis of their different polarization dependence. In contrast with the case of LSCO, where a crossover from a holelike to an electronlike Fermi surface is observed near optimal doping (Ino *et al.*, 1999, 2002), Ding *et al.* (1997) suggested that a single holelike

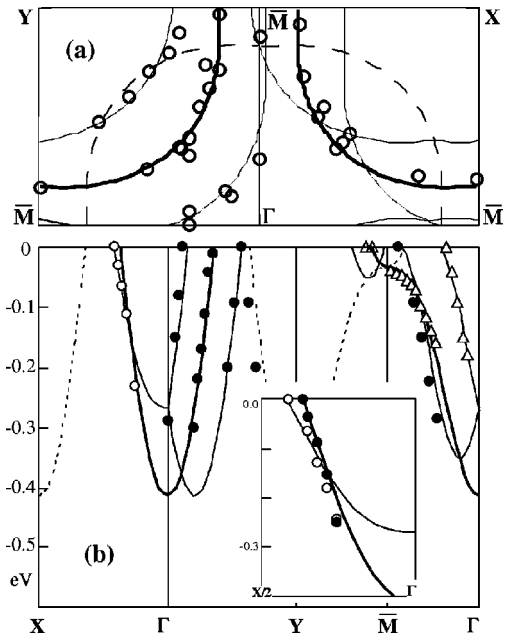

FIG. 28. Photoemission data from Bi2212 (T_c=87 K): (a) Fermi surface; (b) dispersion measured in the normal state at 95 K (the various symbols denote different polarizations conditions). Thick lines are the result of a tight-binding fit of the main band dispersion. Thin and dashed lines represent umklapp and shadow bands, respectively. The inset shows a blowup of Γ-X. From Ding, Bellman, *et al.*, 1996.

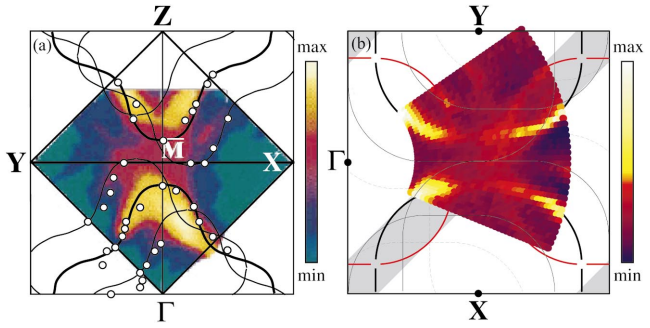

FIG. 29. Bi2212 near-E_F ARPES intensity maps: (a) comparison between the integrated intensity map (50 meV at E_F; Saini *et al.*, 1997) and Fermi surface crossings (white circles) determined by several methods from 33-eV data on slightly overdoped Bi2212. Thick and thin black lines indicate the main electronlike Fermi surface and its umklapp replicas (from Chuang *et al.*, 1999). (b) Normal-state E_F intensity map for Bi2212 obtained with 21.2-eV photons by normalizing the ARPES spectra with respect to the total integrated intensity. Main and shadow Fermi surfaces are indicated by thick black and red lines: first- and second-order umklapp surfaces by thin and dashed black lines (from Borisenko *et al.*, 2000) (Color).

sheet of Fermi surface is characteristic of all the studied doping levels. In addition, no shadow band was detected for the underdoped sample ($T_c=15$ K). This was taken as evidence ruling out the idea of a Fermi-surface pocket presented in Fig. 15(c), and also the explanations in terms of antiferromagnetic correlations for shadow bands observed near optimal doping by Aebi *et al.* (1994). However, the ARPES spectra from the $T_c=15$ K underdoped Bi2212 sample are characterized by a very broad line shape, indicating strong many-body effects on the spectral function which, as a consequence, is completely incoherent. Threrefore, the Fermi surface extracted from those ARPES data should be viewed with caution, in particular concerning the lack of bilayer splitting and of Fermi-surface pockets (or shadow bands).

After the initial debate, an agreement was reached concerning the absence of the BiO pockets predicted for Bi2212 by band-structure calculations. The general consensus was in favor of a holelike Fermi surface centered at (π,π) from under to overdoped samples (T_c between 15 and 67 K), with a volume consistent with the electron density in accordance with Luttinger's theorem (Luttinger, 1960). Recently, however, other reports have questioned this simple picture, arguing that this may not be a complete characterization of the low-lying excitations in Bi2212 (Chuang *et al.*, 1999; Feng *et al.*, 1999; Gromko *et al.*, 2000; Bogdanov *et al.*, 2001). These studies revealed a pronounced photon energy dependence of the low-energy spectral weight in the $(\pi,0)$ region and suggested an electronlike Fermi surface centered at the Γ point, as shown in Fig. 29(a) (Chuang *et al.*, 1999; Gromko *et al.*, 2000); or alternatively two coexisting electronic components resulting in electron and holelike surfaces (Feng *et al.*, 1999), similar to what was originally proposed by Dessau *et al.* (1993). These suggestions were opposed by other groups, who claimed that only a universal holelike Fermi surface is supported by the ARPES data once the effects of photon energy dependence of the matrix elements in the $(\pi,0)$ region are taken into account (Borisenko *et al.*, 2000, 2001; Fretwell *et al.*, 2000; Mesot, Randeria, *et al.*, 2001). As a matter of fact, first-principles simulations of the ARPES spectra performed within the one-step model, for an idealized tetragonal Bi2212 structure (i.e., no superstructure modulation), indicate a strong nontrivial dependence of the low-energy photoemission intensity on photoelectron momentum, and energy/polarization of the incident photons (Bansil and Lindroos, 1999). Therefore photoemission matrix elements may largely dominate the momentum dependence of the ARPES intensity and should be taken into account, especially when attempting to estimate the momentum distribution function $n(k)$ from the integrated photoemission intensity (see also Secs. II.C and II.D).

A new generation of photoemission data with superior momentum resolution beautifully shows the complexity of the ARPES results from Bi2212 [Figs. 29(b) and 30]. In particular, along Γ-Y all the features characterizing the ARPES spectra from Bi2212 can be unambiguously identified in the energy distribution curves, as it is along this direction that the different bands are most clearly separated [see Figs. 30(a) and (b), where the dispersive bands are labeled as indicated in the caption]. However, because of the superposition of several contri-

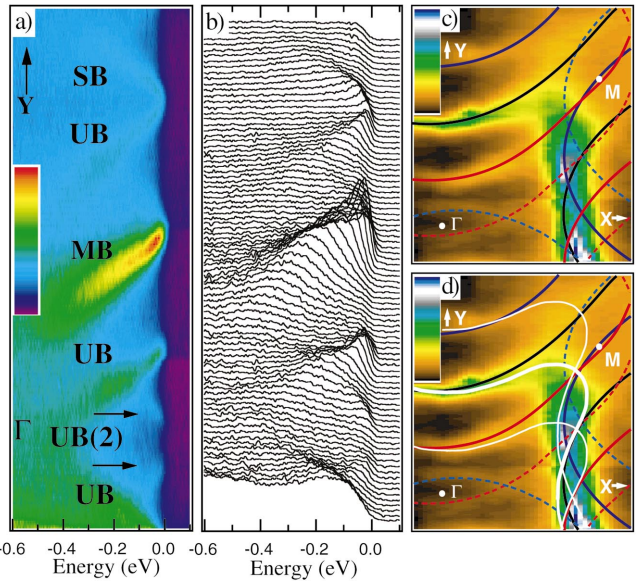

FIG. 30. ARPES results from optimally doped Bi2212 ($T_c=90$ K) measured along Γ-Y with 33 eV photons at 40 K: (a) intensity $I(\mathbf{k},\omega)$; (b) corresponding ARPES spectra; MB, main band; UB, umklapp band; UB(2), second-order umklapp band; SB, shadow band; (c) integrated intensity map (± 100 meV at E_F) together with holelike MB (black), UB (blue/red), and UB(2) (dashed blue/red) Fermi surfaces obtained from a tight-binding fit of the data (from Fretwell *et al.*, 2000); (d) same as (c) but with the addition of electronlike MB and UB Fermi surfaces indicated by thin and thick white lines (from Gromko *et al.*, 2000) (Color).

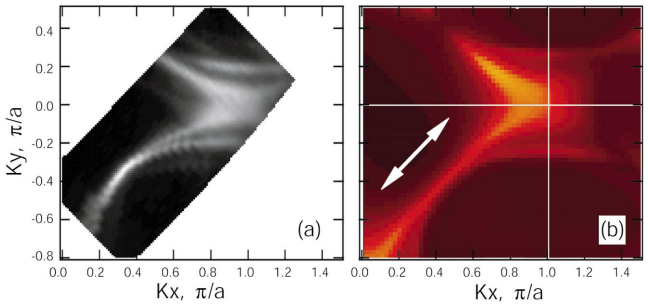

FIG. 31. ARPES data compared to theoretical simulations: (a) intensity map at 12-meV binding energy from overdoped Bi2212, obtained with 22-eV photons at 20 K with the superconducting gap already opened (from Bogdanov *et al.*, 2001); (b) first-principles simulation for the same experimental geometry (from Bansil and Lindroos, 1999) (Color).

butions and especially because of matrix element effects, not even the most detailed intensity maps are very clear around $(\pi,0)$, as shown in Fig. 29, and in particular in Figs. 30(c) and (d) where holelike and electronlike scenarios are compared with respect to the same set of data. In turn, any interpretation necessarily rests on the extrapolation of results obtained away from this region.

Very recently it became evident that one of the key ingredients in the debate on the topology of Bi2212 is actually the unresolved bilayer splitting of the in-plane electronic structure. In this regard, as will be discussed in greater detail in the next section, an essential piece of information comes from ARPES data obtained with improved angular resolution in the very overdoped regime: two Fermi-surface sheets are resolved, which originate from the bonding-antibonding splitting of the in-plane electronic structure caused by interaction between the layers (Chuang *et al.*, 2001a; Feng *et al.*, 2001). In this context, the cleanest experimental results have been obtained on very overdoped Pb-Bi2212 ($T_c=70$ K), in which Pb substitutes in the BiO planes, suppressing the superstructure and in turn the intensity of the umklapp bands (Bogdanov *et al.*, 2001). As shown in Fig. 31, where the ARPES data are compared to the theoretical simulations of Bansil and Lindroos (1999) for the same experimental geometry, two different sheets of Fermi surface are clearly resolved. With respect to the $\Gamma=(0,0)$ point, the outer sheet is the bonding surface, while the inner piece is the antibonding one. The bonding pocket is holelike, similar to what was reported many times before for Bi2212. The antibonding Fermi surface, on the other hand, has its Van Hove singularity near $(\pi,0)$ and is thus very close to the holelike/electronlike boundary. Therefore the experiments indicating a single holelike or electronlike Fermi surface in Bi2212 might simply be more sensitive to the bonding or antibonding sheet, respectively, as a consequence of sample doping and/or experimental conditions (such as the polarization and energy of the incident photons).

2. Bilayer band splitting

Independently of the controversy on the Fermi surface of Bi2212, whether the electronic structure of the cuprates can be influenced by interaction between CuO_2 planes has been an issue of interest for a long time, because one of the proposed mechanisms for high-temperature superconductivity is interlayer pair tunneling (Chakravarty *et al.*, 1993; Anderson, 1997). Within this model, interlayer hopping is suppressed because of correlations and only electron pairs can tunnel between the planes. Coherent pair tunneling will drive the system into the superconducting state via the lowering of kinetic energy perpendicular to the planes. As discussed above, an early ARPES study on Bi2212 claimed the absence of bilayer splitting (Ding, Bellman, *et al.*, 1996). This report attracted much interest as it provided crucial support for the interlayer tunneling model, although with hindsight the momentum resolution was not sufficient to address this issue. Recently, new ARPES data with improved angular resolution have suggested that bilayer splitting can be detected for overdoped Bi2212 (Chuang *et al.*, 2001a; Feng *et al.*, 2001). Below, we discuss this issue in detail. As for the interlayer tunneling model, it has to be mentioned that strong evidence against it was reported on the basis of direct imaging of magnetic-flux vortices by scanning SQUID microscopy (Moler *et al.*, 1998) and by optical measurements on $Tl_2Ba_2CuO_{6+\delta}$ (Tsvetkov *et al.*, 1998). On the other hand, a subsequent optical study provided direct evidence for the lowering of the kinetic energy parallel to the planes across the superconducting transition, supporting the view that superconductivity in the cuprates is indeed unconventional (Molegraaf *et al.*, 2002).

Figure 32(a) presents the normal-state data from a $T_c=65$ K overdoped Bi2212 sample (Feng *et al.*, 2001). Two Fermi surfaces are observed for the main electronic structure, bonding (BB) and antibonding (AB), as well as their superstructure replica (BB′ and AB′). These

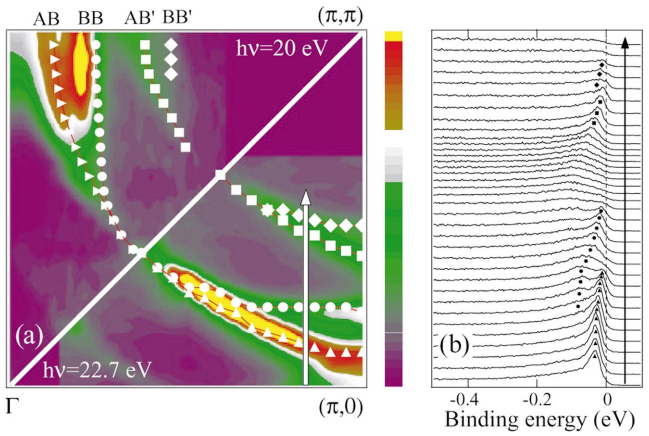

FIG. 32. Bilayer band splitting in overdoped Bi2212 ($T_c=65$ K): (a) integrated E_F intensity map (integration window $[-20$ meV, 10 meV$]$). The data were measured above T_c at 22.7 eV (lower right, $T=75$ K) and 20 eV (upper left, $T=80$ K). White symbols are the Fermi-surface crossings estimated directly from the dispersion of the peaks. BB and AB refer to primary bonding and antibonding bands, and BB′ and AB′ to the corresponding superstructure replicas. (b) ARPES spectra along the cut indicated by the white arrow in panel (a). After Feng, Armitage, *et al.*, 2001 (Color).

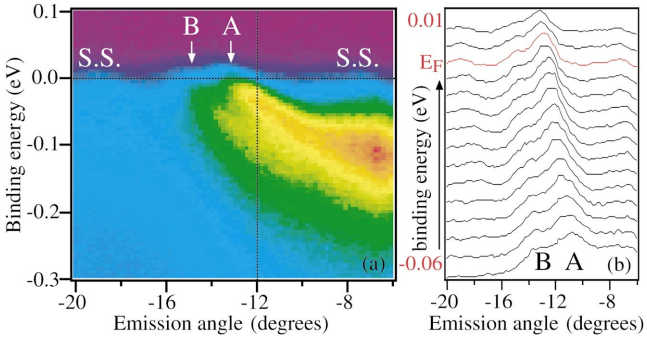

FIG. 33. Bonding (B) and antibonding (A) bands in overdoped Bi2212 (T_c=85 K): (a) E-k image plot of the ARPES intensity near (π,0); (b) corresponding momentum distribution curves (MDC's). From Chuang *et al.*, 2001a (Color).

surfaces correspond to four well-resolved quasiparticle peaks [Fig. 32(b)], whose dispersion can be clearly followed in the ARPES spectra taken along the k-space cut indicated by the arrow in Fig. 32(a). As expected on the basis of symmetry arguments (Chakravarty *et al.*, 1993; Andersen *et al.*, 1995) no splitting was detected along the nodal direction (even with the best achievable angular resolution of about 0.12°); the splitting increases upon approaching (π,0), where it exhibits the largest value of about 88 meV. The different photon energy dependence of BB and AB bands, revealed by the relative intensity change in the two mappings presented in Fig. 32(a) (top left and bottom right), is consistent with the different symmetry of the two bands along the c axis (odd and even for AB and BB, respectively). Analogous

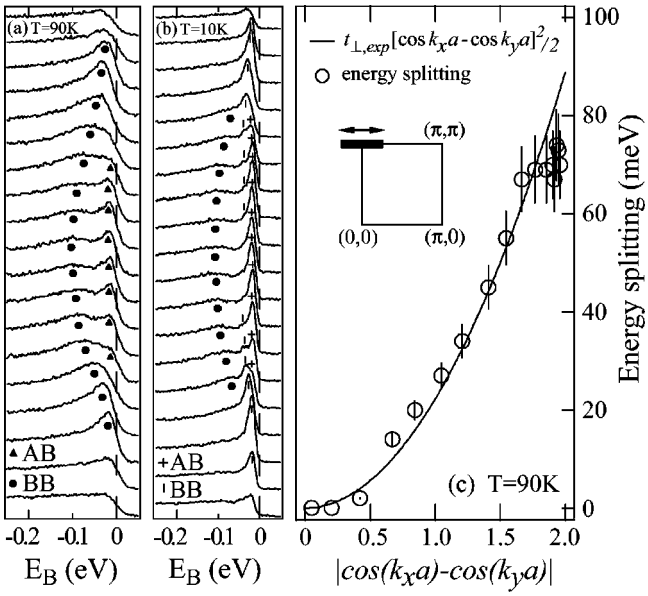

FIG. 34. ARPES spectra from overdoped Bi2212, (T_c =65 K) measured with 21.2-eV photons (HeI) along the $(-0.24\pi,\pi)$-$(0.24\pi,\pi)$ direction: (a) normal-state; (b) superconducting-state; (c) magnitude of the bilayer splitting along the antibonding Fermi surface (normal-state data). The curve is a fit to $t_{\perp,\mathrm{exp}}[\cos(k_x a)-\cos(k_y a)]^2/2$ obtained with $t_{\perp,\mathrm{exp}}=44\pm5$ meV. After Feng *et al.*, 2001.

conclusions were independently obtained by Chuang *et al.* (2001a) from an analysis in terms of momentum distribution curves of similar ARPES data [see Fig. 33, where BB and AB bands can be observed both in the image plot of the ARPES intensity near (π,0) and in the corresponding momentum distribution curves]. All together, the different studies indicate a normal-state bilayer splitting of the order of 70–100 meV in overdoped Bi2212 (Bogdanov *et al.*, 2001; Chuang *et al.*, 2001a; Feng *et al.*, 2001). As shown in Fig. 34(c), where the magnitude of the normal-state bilayer splitting along the antibonding Fermi surface is plotted, the observed energy splitting agrees well with the functional form $2t_\perp(\mathbf{k})=t_\perp[\cos(k_x a)-\cos(k_y a)]^2/2$ predicted on the basis of bilayer LDA calculations (Andersen *et al.*, 1995). However, the experimental value of 88 meV ($2t_{\perp,\mathrm{exp}}$) is much smaller than the 300 meV ($2t_{\perp,LDA}$) predicted by the bilayer LDA calculations. It is actually in better agreement with bilayer Hubbard model calculations (Liechtenstein *et al.*, 1996), which predict an energy splitting of similar momentum dependence and with a maximum value of about 40 meV. This smaller value reflects reduced hopping and is a direct consequence of the on-site Coulomb repulsion U explicitly included in the model. The fact that the splitting is underestimated as compared to experiment suggests that a smaller value of U should be used for this system.

Feng *et al.* (2001) also investigated the effect of the superconducting transition on the ARPES spectra at (π,0), where bilayer splitting is stronger. The data measured above and below T_c are presented in Figs. 34(a) and (b), respectively. Note that the peak-dip-hump structure in Fig. 34(a) is totally unrelated to superconductivity (Sec. VI), as the data were taken well above T_c; instead it corresponds to the bonding and antibonding split bands (indicated by circles and triangles, respectively). In the superconducting state [Fig. 34(b)], the two bands reach the same minimum binding energy (16 meV), indicating the opening of a superconducting gap with similar amplitude for both surfaces (Sec. V). Furthermore, while no change was seen for the antibonding band at high binding energy [see black circles in Figs. 34(a) and (b)], a double-peak structure was detected close to E_F at certain momenta [see crosses and bars in Fig. 34(b)]. The appearance of a second sharp peak near E_F below T_c presumably corresponds to the sharpening of a structure that could not be resolved in the normal state. A possible origin of this effect may be coupling between the bonding state and a low-energy collective mode (either phononic or electronic in nature), which would result in the transfer of spectral weight to the characteristic energy of the mode (see Sec. VIII), or the sudden drop of the electronic scattering rate due to the opening of the superconducting gap.

At this point the obvious question is: Why has a clear bilayer splitting never been observed before by ARPES, despite the intense effort? Obviously this achievement would not have been possible without the recent improvements in energy and momentum resolution. However, in this case the major breakthrough was probably

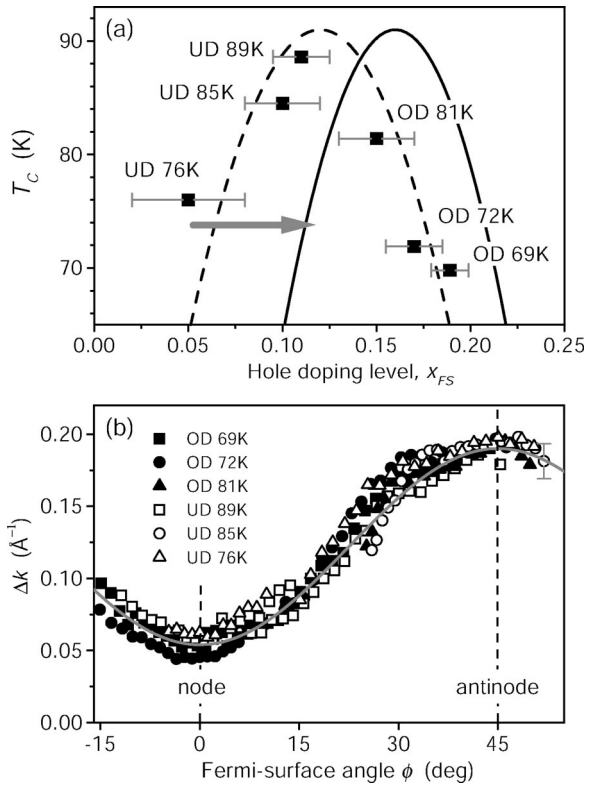

FIG. 35. Apparent violation of Luttinger's theorem in Bi2212: (a) T_c plotted vs the hole concentration x_{FS} as inferred from the volume of the Fermi surface determined by ARPES (symbols). The solid line is the universal empirical T_c-x relation (from Tallon *et al.*, 1995). (b) Momentum distribution curve width at E_F from along the 300-K Fermi surface (ϕ is the angle defined with respect to the nodal direction). The solid gray line is a fit to a functional form proportional to $\sin^2(2\phi)$. After Kordyuk *et al.*, 2002a.

the recent progress in high-pressure annealing techniques. This allowed the synthesis of heavily overdoped single crystals of Bi2212, which appear to exhibit much better defined quasiparticle peaks and thus provided the opportunity for the clear and unambiguous detection of bilayer split bands. One could then speculate that the absence of two well-defined features in the spectra of less overdoped samples does not necessarily indicate the complete absence of bilayer splitting effects, which may be hidden in the breadth of the line shapes. Indeed, this speculation is supported by many recent ARPES results (Chuang *et al.*, 2001b; Feng, Kim, *et al.*, 2002; Kordyuk *et al.*, 2002a, 2002b). For example, using the HeI line as the excitation energy, Kordyuk *et al.* (2002a) could only observe one large holelike Fermi surface centered at (π,π). However, as shown in Fig. 35(a), the experimentally determined Fermi-surface volume would correspond to a doping level 5–7 % off the expected value [see gray arrow in Fig. 35(a)]. This apparent violation of Luttinger's theorem (Luttinger, 1960) could be understood by considering that the second sheet of Fermi surface resulting from bilayer splitting might have escaped detection due to matrix elements. This explanation is supported by the results reported for the evolution of the momentum distribution width along the Fermi surface. As shown in Fig. 35(b), the angular dependence of the width does not change with doping and is thus unlikely to be due to many-body effects; in addition, its functional form is proportional to $\sin^2(2\phi)$, which is in agreement with a bilayer splitting of the form $[\cos(k_x a) - \cos(k_y a)]^2$, as determined in the overdoped regime (Chuang *et al.*, 2001a; Feng *et al.*, 2001).

Evidence for bilayer splitting at underdoping and optimal doping is also provided by systematic ARPES investigations performed as a function of doping and photon energy (Chuang *et al.*, 2001b; Feng, Kim, *et al.*, 2002; Gromko, Fedorov, *et al.*, 2002; Kordyuk *et al.*, 2002a, 2002b). As shown in Fig. 36(a), the BB and AB bands which are clearly resolved in overdoped Bi2212 with 22-eV photons become indistinguishable upon underdoping the system. However, in spectra taken with different photon energy at a given doping, the centroid is found at different positions; it moves from close to E_F to higher binding energies as the photon energy is changed from 47 to 22 eV [Fig. 36(a)]. This behavior indicates the presence of two different components in the spectra, with opposite photon energy dependence, as expected for BB and AB bands, which have opposite symmetry along the c axis with respect to the midpoint between the two CuO_2 planes (Chuang *et al.*, 2001b; Feng, Kim, *et al.*, 2002). Additional signatures of bilayer splitting can be observed by comparing spectra from Bi2212 and $Bi_2Sr_2CuO_{6+\delta}$ (Bi2201) at similar doping levels [Fig. 36(b)]. While in the nodal region the spectra have very similar line shapes (not shown), the situation is much more complicated close to $(\pi,0)$. Note that in Fig. 36(b), while the $(\pi,0)$ spectrum from overdoped Bi2212 (OD63, where 63 refers to $T_c = 63$ K) shows both BB and AB peaks, the one at $(\pi,0.2\pi)$ reduces to only the

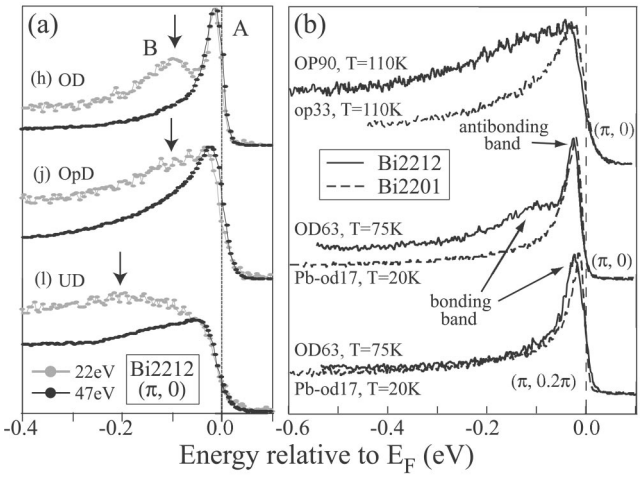

FIG. 36. Investigations of the bilayer splitting in Bi2212 as a function of doping and photon energy: (a) ARPES spectra from Bi2212 at $(\pi,0)$, for different doping levels [overdoping (OD), optimal doping (OpD), and underdoping (UD)] and photon energies (Chuang *et al.*, 2001b); (b) ARPES spectra from Bi2212 and Bi2201 measured with 22.7-eV photons near $(\pi,0)$, for various doping levels (Feng, Kim, *et al.*, 2002). All data were measured in the normal state.

BB peak because the AB band is already above E_F. As a consequence, the spectra from Bi2212 and Bi2201 match almost perfectly at $(\pi,0.2\pi)$ but not at $(\pi,0)$. In this context, the mismatch between optimally doped Bi2212 and Bi2201 spectra at $(\pi,0)$ and, in particular, the additional spectral weight at high energy observed in Bi2212 can be naturally attributed to the presence of the BB band. On the basis of these results, it was concluded that the broad line shape observed in the normal state for underdoped and optimally doped Bi2212 at $(\pi,0)$ has significant contributions from bilayer splitting effects (Chuang *et al.*, 2001b; Feng, Kim, *et al.*, 2002). It was also proposed that BB and AB bands may become directly detectable in the superconducting state due to the sharpening of the peaks (Gromko, Federov, *et al.*, 2002; Kordyuk *et al.*, 2002b), which provides a possible explanation for the so-called peak-dip-hump structure typically detected only below T_c at those doping levels (see Secs. VI and VIII.C.3).

3. Summary

Despite the controversy over the details of the Fermi surface, many of the ARPES results from Bi2212 are still reliable and the same holds for the qualitative descriptions that were developed based on them. This is particularly true with regard to doping-dependent studies performed under identical experimental conditions. For example, the magnitude and symmetry of the superconducting gap (Sec. V) and of the normal state excitation gap or pseudogap (Sec. VII) are relatively insensitive to the details of Fermi-surface topology.

Due to the limited doping range investigated, the ARPES results from Bi2212 are insufficient to conclude in favor of any of the four scenarios summarized in Fig. 15. While the Fermi surface of optimally doped Bi2212 resembles that reported in Figs. 15(a) and 15(d) (let us here neglect the issue of bilayer splitting), in the underdoped region, due to the opening of the pseudogap along the underlying Fermi surface (Sec. VII), the data are reminiscent of the models depicted in Figs. 15(b) and (c). The distinction between Figs. 15(a) and (d) has to be determined on the basis of the behavior near $(\pi,0)$, while between the models described in Figs. 15(b) and (c) it lies in the detection of the shadow surface [dashed line in Fig. 15(c)]. Although it has been argued that the case of Fig. 15(c) does not apply to Bi2212 (Ding, Norman, *et al.*, 1997), in contrast to an earlier report (Aebi *et al.*, 1994), no consensus has as yet been reached.

D. $Bi_2Sr_2CuO_{6+\delta}$

The investigation of low-energy electronic structure should be an easier task for the single-layer system $Bi_2Sr_2CuO_{6+\delta}$ (Bi2201) than for Bi2212. First, the ARPES spectra are free from possible complications arising from bilayer splitting. Second, Bi2201 has a lower T_c which allows measurements at lower temperature (i.e., less thermal broadening), without complications due to the opening of the superconducting gap. Furthermore, as in the case of Bi2212, the partial substitution of Pb for Bi in Bi2201 introduces additional disorder in the BiO planes which, in turn, suppresses the superstructural modulation and the intensity of the umklapp bands. All these characteristics would make Bi2201 an ideal candidate for studying the evolution of the Fermi-surface topology with doping, providing a valuable comparison for the more complex case of Bi2212. On the other hand, as in the Bi2212 case, no data are available in the extremely underdoped regime, and therefore the study of Bi2201 does not provide any more detailed information about the metal-insulator transition.

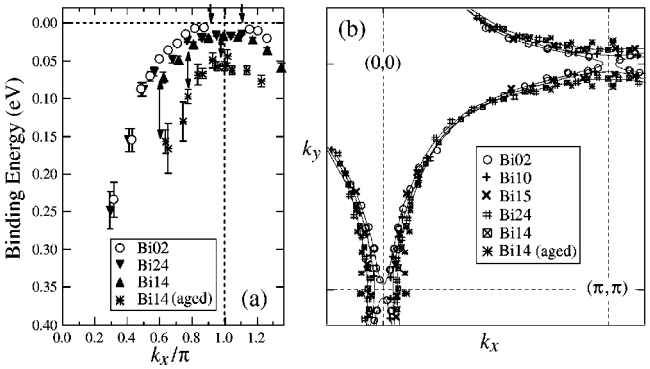

FIG. 37. Photoemission data from Pb-Bi2201: (a) dispersion along (0,0)-$(\pi,0)$; (b) Fermi-surface crossings for Pb-Bi2201 at various dopings (numbers in the legends indicate the values of T_c). An electronlike Fermi surface is observed for the overdoped sample with $T_c<2$ K. After Takeuchi *et al.*, 2001.

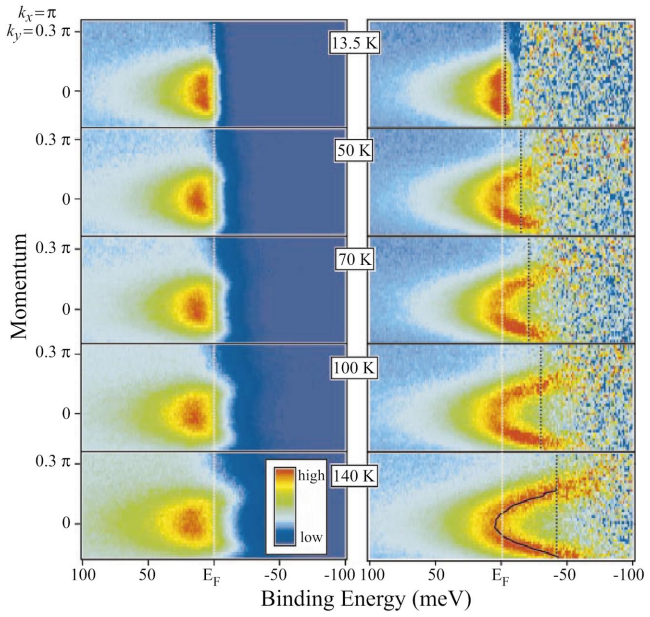

FIG. 38. E-k image plots for overdoped Pb-Bi2201 ($T_c<4$ K), along $(\pi,0)$-(π,π), at several temperatures: left panels, raw ARPES intensity; right panels, intensity divided by the Fermi-Dirac distribution function. The black dotted lines indicate the energy at which the Fermi-Dirac function has a value of 0.03, and the black solid line for $T=140$ K represents the peak positions obtained by fitting the data (Sato, Kamiyama, Takahashi, Mesot, *et al.*, 2001b) (Color).

Recently, two independent investigations of the low-energy electronic structure of Pb-doped Bi2201 for various dopings were reported by Takeuchi, *et al.* (2001) and by Sato *et al.* (Sato, Kamiyama, Naitoh, *et al.*, 2001; Sato, Kamiyama, Takahashi, *et al.*, 2001b). The ARPES spectra are characterized by a well-defined quasiparticle band whose dispersion can be easily followed and is reported for different doping levels in Fig. 37(a), while panel (b) presents the Fermi surface determined by various methods (Takeuchi *et al.*, 2001): by symmetrizing the spectra with respect to E_F (Norman, Randeria, *et al.*, 1998) and by dividing out the Fermi distribution broadened by the experimental resolution (Greber *et al.*, 1997). In underdoped and optimally doped samples the Fermi surface is characterized by a single hole barrel centered at (π,π), in good agreement with the expectation [Fig. 37(b)]. As doping is increased, the volume of the Fermi surface also increases (counting holes). In the overdoped regime and, in particular, for the overdoped Pb-Bi2201 sample characterized by $T_c<2$ K, the quasiparticle band crosses E_F before $(\pi,0)$ as shown in Fig. 37(a), defining an electronlike surface centered at (0,0), in agreement with the rigid-band picture [Fig. 37(b)]. The results reported by Takeuchi *et al.* (2001) represent the first direct observation of a continuous doping evolution of the Fermi-surface topology of Bi2201 from holelike to electronlike, similar to that seen for LSCO.

This topological crossover was not observed by Sato, Kamiyama, Naitoh, *et al.* (2001) or by Sato, Kamiyama, Takahashi, *et al.* (2001b), possibly due to a slightly lower doping level of the samples (instead in the underdoped and optimally doped regimes, the results from the two different groups are essentially the same). To determine whether the saddle point at $(\pi,0)$ is above or below E_F, Sato, Kamiyama, Takahashi, *et al.* (2001b) performed a detailed temperature dependence study. The left panels of Fig. 38 present data that indicate the presence of spectral weight below the Fermi level. From the bare data it is hard, however, to judge whether the quasiparticle band is indeed below E_F or the intensity corresponds to the broadened tail of a band located just above E_F. This issue can be addressed in a more conclusive way by dividing the spectra by the Fermi-Dirac distribution function at each temperature. The results are presented in the right panels of Fig. 38 and show the actual dispersion in a much clearer fashion. It is now obvious that the saddle point is located approximately 5 meV below E_F (which indicates that the difference between the results reported by the two groups is very subtle). As a more general remark, it should be emphasized that this kind of analysis appears to be a better method than the simple tracking of the ARPES intensity in determining the position of a quasiparticle band very close to the Fermi energy, especially in borderline cases such as in proximity to a topological transition.

E. $Bi_2Sr_2Ca_2Cu_3O_{10+\delta}$

Very recently, the first ARPES studies of the trilayer cuprate superconductors $Bi_2Sr_2Ca_2Cu_3O_{10+\delta}$ (Bi2223) have been carried out by several groups (Feng, Damascelli, *et al.*, 2002; Müller *et al.*, 2002; Sato, Matsui, *et al.*, 2002). As shown in Fig. 39, where normal-state data from nearly optimally doped Bi2223 are presented, dispersive quasiparticle peaks were detected by ARPES (including the umklapp features due to the superstructure of the BiO layers, already discussed for Bi2212 and Bi22201). The Fermi surface obtained by integrating the ARPES spectra in a ± 10-meV energy window at E_F is a large holelike pocket centered at the (π,π) point [see Fig. 39(d)]. At present, no clear evidence of additional sheets of Fermi surface due to interlayer coupling has been reported, contrary to what is theoretically predicted. In particular, one would expect the Fermi surface to be comprised of bonding (BB), nonbonding (NB), and antibonding (AB) sheets (see, for example, Mori *et al.*, 2002). Whether or not the three sheets would have the same topology depends on the details of the system (such as, e.g., the doping level). In particular, one could expect the bonding and nonbonding surfaces to be holelike in character, while the antibonding could be electronlike. However, because of the short escape depth of the outgoing photoelectrons, the photoemission intensity is expected to be dominated by the signal from the outer CuO_2 plane and, in turn, from the nonbonding sheet of Fermi surface (the nonbonding wave function has the highest probability density on the outer CuO_2 plane because, in contrast to the bonding and antibonding ones, it is the antisymmetric combination of the wave functions of *only* the two outer planes within a trilayer block). This could be the reason why a single holelike Fermi surface was observed by ARPES for Bi2223 [Fig. 39(d)]. The above speculation, however, needs to be tested by more extensive experiments.

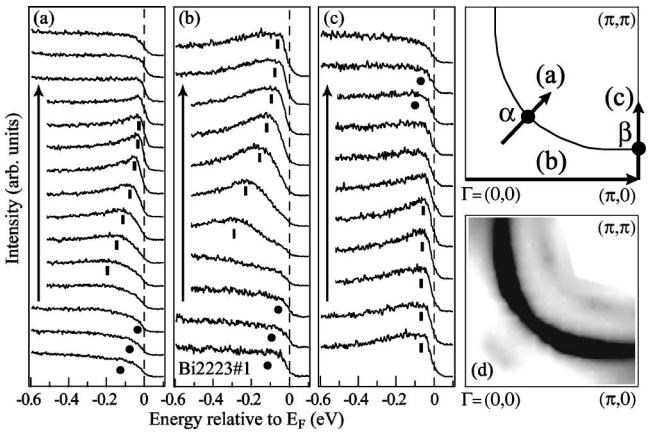

FIG. 39. Normal-state ARPES spectra from Bi2223 (a)–(c) taken along the high-symmetry lines as shown in the Brillouin-zone sketch ($T=125$ K, $h\nu=21.2$ eV). The main bands are marked with bars, umklapp bands with circles. (d) Momentum-space map of the spectral weight at E_F (± 10 meV). After Feng, Damascelli, *et al.*, 2002.

F. $YBa_2Cu_3O_{7-\delta}$

The Y-based copper oxides are probably the most important family of high-T_c superconductors. In fact

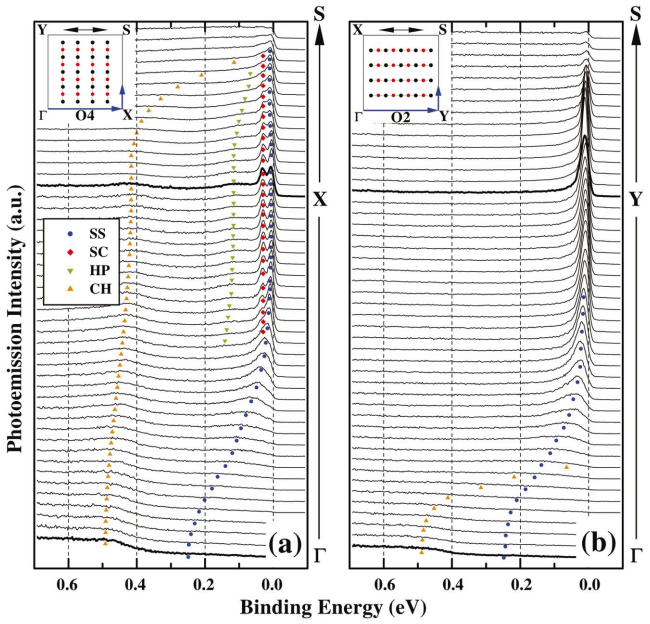

FIG. 40. ARPES spectra from untwinned Y123 measured at 10 K with 28-eV photons. Polarization (black arrows) and CuO chain directions are indicated in the insets. Labels: SS, surface state; SP, superconducting peak; HP, hump; CH, chain state. From Lu *et al.*, 2001 (Color).

$YBa_2Cu_3O_{7-\delta}$ (Y123) was the first compound for which superconductivity with $T_c > 77$ K (i.e., the liquid-nitrogen boiling point) was discovered (Wu *et al.*, 1987). Furthermore, it is on the Y-based cuprates that some of the most important experiments were preformed. One specific feature of Y123 is that, unlike the other cuprate superconductors, the reservoir layers in these materials contain CuO chains aligned along the Γ-Y direction (see Figs. 12 or 40 for the Brillouin-zone notations). Because of the presence of the CuO chain layer, Y123 possesses an orthorhombic crystal structure (Jorgensen *et al.*, 1987), which, according to band calculations, should result in significant anisotropy of the in-plane electronic structure (Andersen *et al.*, 1995). Compared to other compounds, in recent years relatively little photoemission work was done on Y123, in particular as far as the doping evolution of the electronic structure is concerned [Liu *et al.* (1995); see also Shen and Dessau (1995); Lynch and Olson (1999)]. This is partly due to the natural twinning of Y123 crystals (i.e., domains orthogonal to each other with respect to the CuO chain orientation are present) and to generic sample quality issues which are responsible for the poor quality of the cleaved surface (Edwards *et al.*, 1992; Schabel *et al.*, 1998a). However, the most serious problem in performing photoemission experiments on Y123 is the presence of a very narrow and intense surface-state peak located 10 meV below E_F at both X and Y (Schabel *et al.*, 1998a). This feature, which was initially interpreted as an extended Van Hove singularity analogous to that observed in the Bi-based superconductors (Gofron *et al.*, 1994), dominates over the low-energy bulk signal, hindering the study of the intrinsic electronic structure.

More detailed work on untwinned samples was carried out only near optimal doping. The most important results are the identification of the surface state, k_z dispersion, and the superconducting gap (Schabel *et al.*, 1997, 1998a, 1998b). The establishment of the surface-state nature of the intense peak just below E_F [originally proposed on the basis of the dependence of its intensity on photon energy/polarization, as well as on O, Co, and Pr doping (Schabel *et al.*, 1998a)] is crucial in order to understand the data, and in particular to extract information on the superconducting state (Sec. V.E).

Recently, Lu *et al.* (2001) reported significant progress in the investigation of Y123 by ARPES, made possible by the improvement in sample quality (Liang *et al.*, 1998) and instrumental resolution. Figure 40 presents the energy distribution curves from Y123 along the high-symmetry directions in the Brillouin zone, for polarization perpendicular [Fig. 40(a)] and parallel [Fig. 40(b)] to the direction of the CuO chains. Figures 41(a)–(f) present intensity plots of the second derivative with respect to the binding energy of the ARPES spectra, which allow one to follow the dispersion of the broader and weaker electronic bands. Lu *et al.* (2001) identified the four dispersive features summarized in Fig. 41(g): surface state (SS), superconducting peak (SC), hump (HP), and chain state (CH). As one can see in Fig. 40,

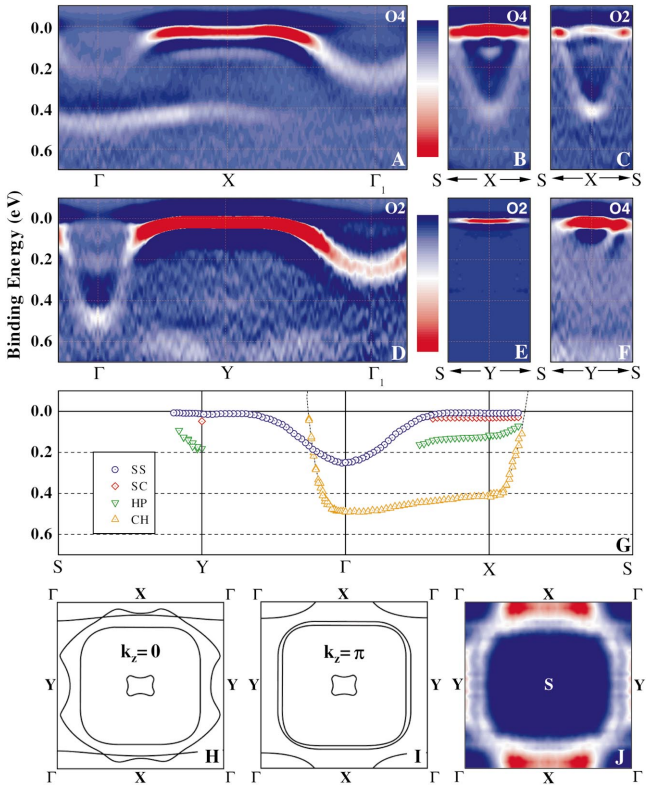

FIG. 41. Electronic dispersion and Fermi surface of Y123: (a)–(f) Second derivative with respect to the binding energy of the raw ARPES spectra from Y123 (sample orientations as in Fig. 40); (g) summary of all the dispersive bands; (h),(i) Fermi surface of Y123 from band-structure calculations (Andersen *et al.*, 1991, 1994); (j) integrated photoemission intensity map (50 meV at E_F). After Lu, *et al.*, 2001 (Color).

the surface state at X and Y is the most pronounced feature in the spectra. It has to be emphasized that while the surface-state nature of this peak has received strong support from its high sensitivity to surface degradation at elevated temperatures (Lu *et al.*, 2001), the precise origin of this state is not well understood at present: on the one hand, the scenario of a chain-related surface state proposed by Schabel *et al.* (1998a) appears to be consistent with recent scanning tunneling microscopy data (Derro *et al.*, 2002); on the other hand, this assignment is difficult to reconcile with the 2D dispersion of this feature along Γ-X and Γ-Y [blue symbols in Fig. 41(g)]. The broad feature at 400 meV below E_F at the X point [yellow symbols in Fig. 41(g)] was assigned by Lu *et al.* (2001) to a bulk chain-derived state, rather than to a bonding σ state as previously suggested (Schabel *et al.*, 1998a). This interpretation is based on the quasi-1D character of this feature (i.e., much larger dispersion along the chain direction than perpendicular to it) and the good agreement with band-structure calculations (Andersen *et al.*, 1995). Two more features, clearly detected at the X point, are marked with red and green symbols in Figs. 40(a) and 41(g). These are related to the electronic structure of the CuO_2 planes and will be further discussed in Sec. V.E.

In summary, the ARPES results from Y123 reveal bulk bands originating from the CuO chains and the CuO_2 planes, and a surface-state band. As shown in Figs. 41(h)–(j), the Fermi surface estimated from the integrated intensity near E_F is consistent with the band-structure results (Andersen *et al.*, 1991, 1994): a large holelike surface centered at S is observed, along with a 1D Fermi surface related to the bulk CuO chains (obviously this can only be an approximate comparison, as the experimental data were taken in the superconducting state and the intensity at X and Y is significantly affected by the presence of the surface state). This results in two Fermi-surface crossings along Γ-S, one due to the chain and the other to the plane electronic bands. Lastly, it has to be stressed that because of the reassignment of the 400-meV dispersive peak to a bulk chain state rather than a CuO_2 plane state, at present there is no consensus for bilayer splitting in Y123, contrary to what had been previously suggested by Schabel *et al.* (1998a). Also, no evidence of shadow bands is seen in Y123, which possibly supports a structural rather than a magnetic origin for these additional features in Bi2212.

G. $Nd_{2-x}Ce_xCuO_4$

Having discussed the ARPES results from many hole-doped (or p-type) systems, in this final section of our overview of the doping evolution of the normal-state electronic structure of the high-T_c cuprates we shall focus on the electron-doped (or n-type) superconductor $Nd_{2-x}Ce_xCuO_4$ (NCCO). As shown in Fig. 1, the undoped material is an antiferromagnetic insulator. When Ce is substituted for Nd, the antiferromagnetic ordering temperature drops precipitously, approaching $x=0.13$, and superconductivity occurs between $0.14<x<0.18$ for

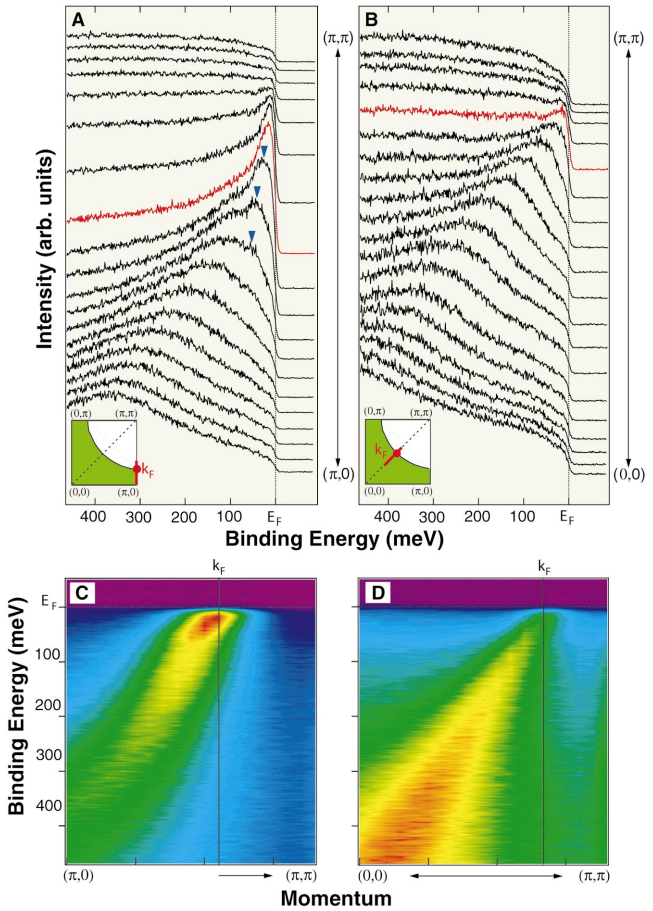

FIG. 42. Photoemission data from superconducting NCCO ($x=0.15$, $T_c=22$ K): (a),(b) ARPES spectra measured at 10 K with 21.2-eV photons (HeI); (c),(d) corresponding image plots. After Sato, Kamiyama, Takahashi, *et al.*, 2001a (Color).

oxygen-reduced samples. Note that there is only an approximate symmetry in the temperature/doping phase diagram about the zero-doping line between p-type and n-type systems, as the antiferromagnetic phase is much more robust in the electron-doped material and persists to much higher doping levels. At the same time, superconductivity occurs in a much narrower doping range. The relevance of a comparative study of n- and p-type cuprate superconductors is as a verification of the symmetry, or lack thereof, between antiferromagnetic insulators doped with electrons or holes. This issue has important theoretical implications, as most models thought to capture the essence of high-T_c superconductivity implicitly assume electron-hole symmetry.

After the early investigations by Anderson *et al.* (1993) and King *et al.* (1993), high-energy and momentum resolution ARPES data on superconducting NCCO ($x=0.15$, $T_c=22$ K) were reported only very recently (Armitage *et al.*, 2000; Armitage, Lu, Feng, *et al.*, 2001; Armitage, Lu, Kim, *et al.*, 2001; Sato, Kamiyama, Takahashi, *et al.*, 2001a; Armitage *et al.*, 2002). Figure 42 presents the ARPES spectra [(a) and (b)] and the corresponding image plots [(b) and (c)] reported by Sato, Kamiyama, Takahashi, *et al.* (2001a). The results are

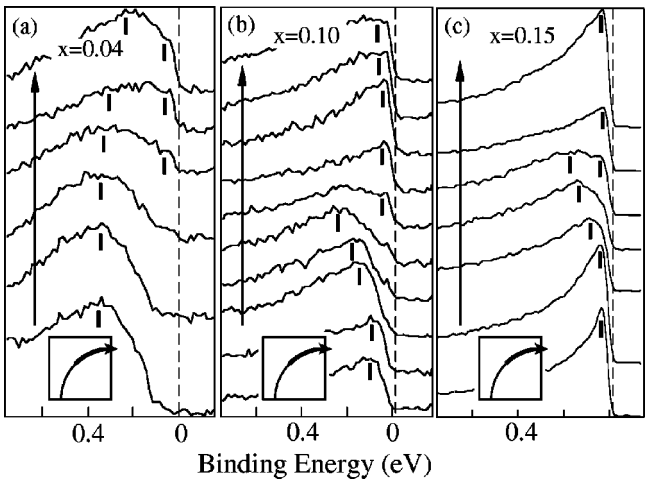

FIG. 43. ARPES spectra measured with 16.5-eV photons on (a)–(c) 4%-, 10%-, and 15%-doped NCCO from along the putative band-structure Fermi surface. From Armitage *et al.*, 2002.

analogous to those obtained by Armitage, Lu, Kim, *et al.* (2001). Along the (0,0)-(π,π) direction, NCCO shows a dispersion which is ubiquitous among the cuprates, with a quasiparticle peak dispersing quickly towards E_F and crossing it at about ($\pi/2$,$\pi/2$). Similarly, a peak disperses and crosses E_F along (π,0)-(π,π), in agreement with the expected holelike Fermi surface [see insets of Figs. 42(a) and (b)]. However, while in the p-type cuprates at (π,0) the quasiparticle peak forms a flat band just below E_F, in NCCO the flat band is located at 300 meV below E_F.

Studies of the doping evolution of the electronic structure were recently carried out by Armitage *et al.* (2002). As a starting point, these authors identified a charge-transfer band feature in the undoped insulator Nd_2CeO_4, which has the same dispersion as that found in the parent compounds of the p-type high-T_c superconductors (such as $Ca_2CuO_2Cl_2$; Sec. IV.A). This indicates that the electronic structure of the CuO_2 plane in these two compounds is the same, although one can be doped with electrons and the other with holes. More interestingly, the charge-transfer band in Nd_2CeO_4 is at about 1.2 eV below E_F, which is comparable to the charge-transfer gap energy if the chemical potential is pinned close to the conduction-band minimum. Data for different dopings are presented in Fig. 43, which shows the ARPES spectra from along the Fermi-surface contour expected from band-structure calculations. At low doping (4%), the spectra are gapped near ($\pi/2$,$\pi/2$) over an energy scale of about 200 meV and exhibit a broad maximum around 300 meV [Fig. 43(a)]. Moving towards (π,0), the 300-meV feature remains more or less at the same energy, and additional spectral weight develops near E_F. As the doping level is increased, the ARPES features become sharper and the one at ($\pi/2$,$\pi/2$) moves closer to E_F. At optimal doping (15%), the spectra are characterized by a sharp quasiparticle peak at E_F both at (π,0) and at ($\pi/2$,$\pi/2$), but not in the region in between where the line shape is still very broad [Fig. 43(c)]. The momentum dependence of the E_F spectral weight (integrated from -40 to $+20$ meV) is displayed for the different doping levels in Fig. 44. At 4% the low-energy weight is concentrated in a small pocket around (π,0), with a volume approximately consistent with the nominal doping level x. Upon increasing doping, one can observe both modification of the pockets and the emergence of low-lying spectral weight around ($\pi/2$,$\pi/2$); eventually (at 15%), the E_F intensity evolves into a large holelike Fermi surface centered at (π,π) with a volume given by $(1+x)$. In the lower panels of Fig. 44 one can follow the evolution of the overall electronic structure across the (charge-transfer) insulator-to-metal transition. In the insulator the valence-band maximum is found at ($\pi/2$,$\pi/2$). At 4% doping, spectral weight develops inside the gap (blue) in addition to the low-energy feature (red), which gives rise to the (π,0) pockets discussed above; at the same time, one can still observe some remanent of the charge-transfer band of the insulator. At higher doping values the latter disappears and the incoherent spectral weight evolves into dispersive quasiparticle bands, which define the large holelike Fermi surface centered at (π,π).

It should be emphasized that although 15%-doped NCCO appears to have a large Fermi surface with a volume given by $(1+x)$ counting electrons, in agreement with Luttinger's theorem (Luttinger, 1960), the data still present some unexpected features. What catches one's eye in Fig. 44(c) are the distinct regions of reduced intensity along the Fermi-surface contour near (0.65π,0.3π) and (0.3π,0.65π), in which the ARPES spectra are extremely broad even at E_F [Fig. 43(c)]. This behavior appears to be an intrinsic property of the spectral function of NCCO, as revealed by a comparison of data obtained for different photon energies and experimental geometries (Armitage, Lu, Kim, *et al.*, 2001). Although some effects due to the energy and polarization

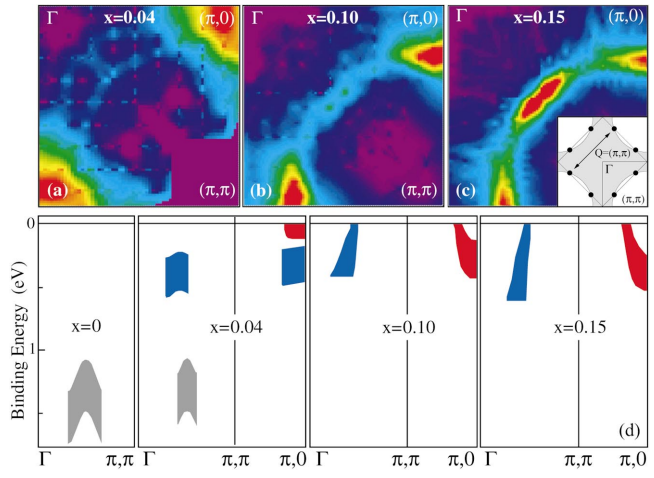

FIG. 44. The momentum dependence of the low-energy electronic structure of NCCO for different doping levels: (a)–(c) momentum-space maps of the low-lying spectral weight integrated between -40 and 20 meV, for $x=0.04$, 0.10, and 0.15; inset of panel (c): regions of the Fermi surface that can be coupled by (π,π) scattering; (d) energy dispersion of the detected features. After Armitage *et al.*, 2002 (Color).

dependence of the photoemission matrix elements are present, the overall systematics does not change. As noted by Armitage, Lu, Kim, *et al.* (2001), the regions of suppressed weight correspond to the intersections between the Luttinger Fermi surface and the antiferromagnetic Brillouin-zone boundaries [see inset of Fig. 44(c)]. These regions, connected by a $Q=(\pi,\pi)$ scattering vector, are referred to in the literature as *hot spots* (Kampf and Schrieffer, 1990a, 1990b; Pines, 1997; Schmalian *et al.*, 1998). The (π,π) scattering experienced by the charge carriers has been proposed to be the origin of the pseudogap observed in the underdoped p-type high-T_c superconductors near $(\pi,0)$. What is seen in NCCO is reminiscent of that behavior (Sec. VII), although in the present case the effects are detected at $(0.65\pi,0.3\pi)$. This could merely be a consequence of the different Fermi-surface volume and, in turn, of the intersections between the Fermi surface and the antiferromagnetic zone being pushed away from $(\pi,0)$ for NCCO. In this view, magnetic fluctuations would be a natural source of (π,π) scattering. More generally, however, any umklapp scattering would result in a breakdown of Fermi-liquid theory and in a segmented Fermi surface, as in Fig. 15(b) (Furukawa and Rice, 1998; Furukawa *et al.*, 1998; Honerkamp *et al.*, 2001).

It should be stressed that the doping dependence of the ARPES data from NCCO suggests the absence of particle-hole symmetry in the low-energy electronic structure of the cuprates. In fact, the lowest-energy states in p-type materials are located at $(\pi/2,\pi/2)$, while they appear at $(\pi,0)$ in the n-type systems. This constitutes the first direct evidence for the Mott-Hubbard gap not being a direct gap and it is actually consistent with calculations performed within the t-t'-t''-J model (successfully used to describe the undoped insulator data; Sec. IV.A), in which the breaking of particle-hole symmetry results from the inclusion of the t' term. In particular, the asymmetry seen by ARPES between undoped and 4% doped NCCO is well reproduced by a mean-field solution of the t-t'-t''-U model (Kusko *et al.*, 2002). Of course, the dynamic aspects of the data (e.g., the development of spectral weight inside the gap) cannot be obtained within a mean-field approach; rather, the transfer of spectral weight upon doping is generally found in cluster-model calculations.

H. Discussion

The most complete ARPES investigations of the doping evolution of the normal-state electronic structure have been performed on LSCO, which can be studied over a wide doping range. The results from this system have been extensively interpreted in the stripe scenario, which provides a possible explanation for many of the experimentally observed features:

(i) the two-component electronic structure seen in the very underdoped regime, which is suggestive of the creation of new electronic states inside the Mott-Hubbard gap;

(ii) the lack of chemical potential shift in the very underdoped regime;

(iii) the straight Fermi-surface segments observed under certain experimental geometries that are indicative of 1D electronic behavior.

However, there are aspects of the data that are difficult to reconcile with a naive stripe picture. Such aspects include the Fermi-arc feature and the nodal quasiparticles observed in ARPES experiments at very low doping levels, which originate from the lowest-energy feature of the two-component electronic structure (Yoshida *et al.*, 2002). Furthermore, as doping is increased, LSCO becomes more of a bandlike system with an LDA-like Fermi surface, and the signatures of stripes weaken; near optimal doping, the distinction between the pictures reported in Figs. 15(a) and 15(d) would become blurred.

For the Bi-based cuprates, on the other hand, there are no extensive reliable data in the underdoped regime and, in particular, near the metal-insulator transition boundary. To date, those features which have been discussed as possible signatures of a charge-ordered state in extremely underdoped LSCO have not been observed in other systems. In the case of Bi2212, long straight segments of Fermi surface have been observed for the bonding band along the direction (0,0)-$(\pi,0)$. This was already noted in the early low-resolution data (Feng *et al.*, 1999), but it is more clearly displayed by the recent data taken with improved momentum resolution (Kordyuk *et al.*, 2002a). The presence of nested Fermi-surface segments could give rise to a charge-density wave instability. This scenario, however, is different from the stripe interpretation of somewhat similar features observed in LSCO. In the latter case, the straight Fermi-surface segments would be the result and not the cause of the formation of quasi-1D stripes. Furthermore, it has to be emphasized that the persistence of partial Fermi-surface nesting well into the overdoped regime in Bi2212 makes a connection with a simple stripe instability less realistic (Kordyuk *et al.*, 2002a). On the other hand, why the nesting of Fermi surfaces does not lead to a charge-density wave instability is an interesting problem. And the presence of the antibonding sheet of Fermi surface might play an important role, which would be worth studying.

At this stage of the research on the high-T_c superconductors and their undoped parent compounds, it does not seem possible to conclude firmly in favor of one particular comprehensive theoretical model, in spite of the considerable progress made in recent years. This situation is emphasized by the longstanding puzzle concerning a fundamental question, i.e., how does the doping of a Mott insulator take place (Fig. 14)? On the one hand, contrary to the early report by Allen *et al.* (1990), very recent angle-integrated photoemission results from NCCO (Harima *et al.*, 2001; Steeneken, 2001) favor a scenario based on a shift of the chemical potential, which is also consistent with the ARPES data from NCCO. Actually, this would be in agreement with

t-t'-t''-J model calculations, which reproduce the substantial deformation of the quasiparticle band structure upon doping and suggest a unifying point of view for both the undoped insulator and the high-T_c superconductors (Eder *et al.*, 1997; Kusko *et al.*, 2002). The chemical-potential shift scenario is also supported by the data available on Na-CCOC, which show a quasiparticle dispersion strikingly similar to that of undoped CCOC. On the other hand, the lack of chemical-potential shift observed in LSCO in the underdoped regime and the detection of multiple electronic components support the formation of in-gap states upon doping the systems and, consequently, the need for a completely new approach. Further scrutiny is required to establish whether the evolution from Mott insulator to high-T_c superconductor is truly accounted for by one of the existing models or whether a different approach, maybe beyond a purely electronic description, is required (e.g., in which other factors, such as the underlying structural distortions, are explicitly included).

V. SUPERCONDUCTING GAP

The ability of ARPES to detect spectral changes across the superconducting phase transition is a remarkable testimony to the improvement in resolution over recent years, and is the key to the success of this technique in the study of the cuprate superconductors. The most important results obtained in the superconducting state are (i) the detection of an anisotropic d-wave gap along the normal-state Fermi surface, which contributed to the debate on the pairing mechanism [for a recent review of the pairing symmetry in the cuprate high-T_c superconductors, see Tsuei and Kirtley (2000a)]; (ii) the dramatic changes in the spectral line shape near $(\pi,0)$. In this section, we shall review point (i) for several systems, while we shall come back to (ii) later, within the discussion of the superconducting peak (Sec. VI.A) and of the self-energy corrections (Sec. VIII).

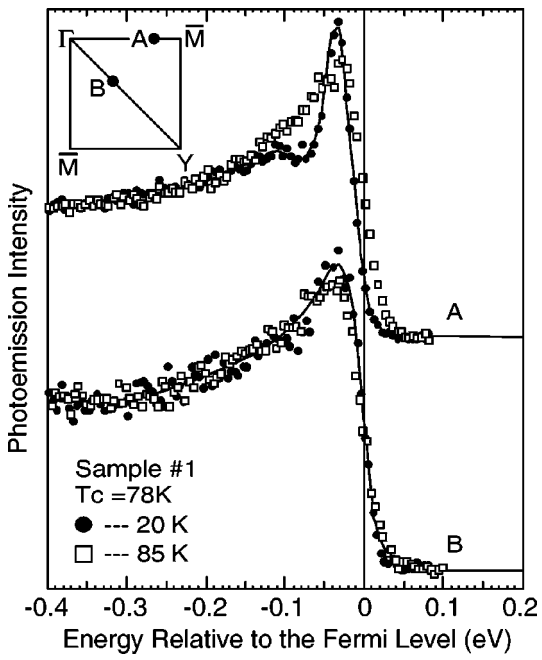

FIG. 45. Temperature dependent ARPES spectra from Bi2212 (T_c=88 K): A, measured close to $(\pi,0)$; B, measured in the nodal region, as sketched in the inset. From Shen *et al.*, 1993.

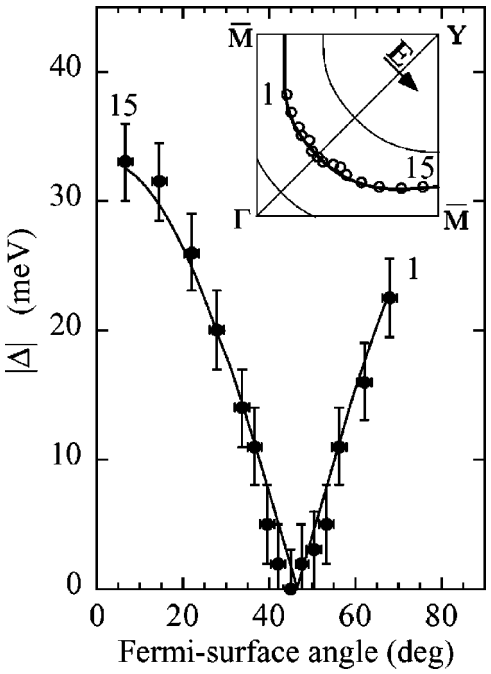

FIG. 46. Superconducting gap measured at 13 K on Bi2212 (T_c=87 K) plotted vs the angle along the normal-state Fermi surface (see sketch of the Brillouin zone), together with a d-wave fit. From Ding, Norman, *et al.*, 1996.

A. $Bi_2Sr_2CaCu_2O_{8+\delta}$

Figure 45 shows the early ARPES data from an overdoped Bi2212 sample at two different momenta in the Brillouin zone (Shen *et al.*, 1993). In the nodal region (B), the spectra taken above and below T_c are very similar, indicating a small or vanishing superconducting gap. Near the $(\pi,0)$ point (A), on the other hand, the normal- and superconducting-state spectra are clearly very different: in addition to the obvious line-shape evolution, note the shift of the leading edge, which reflects the opening of a sizable energy gap. These results strongly suggest that the superconducting gap is anisotropic and, in particular, consistent with a d-wave order parameter (Scalapino, 1995). Together with the microwave penetration depth results (Hardy *et al.*, 1993), this direct evidence for gap anisotropy played a major role in the early debate on the pairing symmetry (Levi, 1993).

Initially the magnitude of the gap was quantified simply on the basis of the position of the leading-edge midpoint of the ARPES spectra, which has since become a standard procedure (Tinkham, 1996). In particular, one could either follow the leading-edge shift of the spectra measured on the superconducting material above and below T_c or compare, at the same temperature below T_c, the positions of leading edges for the superconductor and a polycrystalline noble metal like Pt or Au (a caveat here is that the comparison between the nontrivial line shape measured on a single crystal of a high-

T_c superconductor and the structureless Fermi edge from a polycrystalline metal may be quantitatively inaccurate). Subsequently, some effort has been invested in a more detailed analysis of the superconducting gap. In principle, the gap Δ_k could be estimated by measuring the quasiparticle dispersion in the vicinity of the Fermi level, which, within the BCS framework (Schrieffer, 1964), is predicted to change from ϵ_k to $E_k=\sqrt{\epsilon_k^2+\Delta_k^2}$ upon entering the superconducting state. However, the determination of Δ_k on the basis of a change in the dispersion is a very difficult task because the cuprates are not conventional Fermi-liquid metals in the normal state and, as a consequence, ϵ_k cannot be determined with sufficient accuracy. Furthermore, this analysis is also complicated by the dramatic change in quasiparticle line shape that takes place across the phase transition (Fig. 45). Nonetheless, by fitting energy distribution curves at different momenta with a phenomenologically broadened BCS spectral function, Ding *et al.* (1995a, 1995b) and Ding, Norman, *et al.* (1996) obtained the momentum dependence of the gap along the normal-state Fermi surface (Fig. 46). The results agree with the $d_{x^2-y^2}$ functional form $\Delta(\mathbf{k})=\Delta_0[\cos(k_x a)-\cos(k_y a)]$ extremely well.

It has to be emphasized that such a good fit to the d-wave gap functional form as the one of Fig. 46 is the exception rather than the norm. In most cases, and especially in the underdoped regime, instead of the "V"-shaped cusp seen in the data of Fig. 46, one finds an extended area around the nodal region characterized by gapless excitations.[18] In this regard, it is also important to mention that very recent high-momentum-resolution results from underdoped Pb-Bi2212 ($T_c=77$ K), for which the bilayer splitting could be resolved making the analysis more reliable, indicated a "U" rather than a "V" shape for the superconducting gap along the bonding Fermi surface (Borisenko *et al.*, 2002).[19] In order to account for this behavior Mesot *et al.* (1999) suggested that higher harmonics consistent with d-wave symmetry, such as $[\cos(2k_x a)-\cos(2k_y a)]$, should be included in the expansion of the gap function $\Delta(\mathbf{k})$, in addition to the simple "V"-like $[\cos(k_x a)-\cos(k_y a)]$ first term (Wenger and Östlund, 1993). At present, however, this is still an open issue that deserves further study for its significant theoretical implications.

B. $Bi_2Sr_2CuO_{6+\delta}$

The angular dependence of the superconducting gap in Bi2201 was first investigated by Harris *et al.* (1997). As in the case of Bi2212, the results from Bi2201 appear to be consistent with a d-wave pairing symmetry, although a larger region of gapless excitations was observed close to the nodal direction. The overall magnitude of the superconducting gap ($\sim$10 meV at optimal doping) is approximately a factor of 3 smaller than for Bi2212 at similar doping levels, consistent with the observed reduction in transition temperature. More recently, the superconducting gap was investigated with improved resolution by Sato, Kamiyama, Naitoh, *et al.* (2001). By comparing the data obtained in the nodal and antinodal regions, these authors also concluded in favor of a d-wave symmetry order parameter with a maximum size of 10–15 meV at $(\pi,0)$.

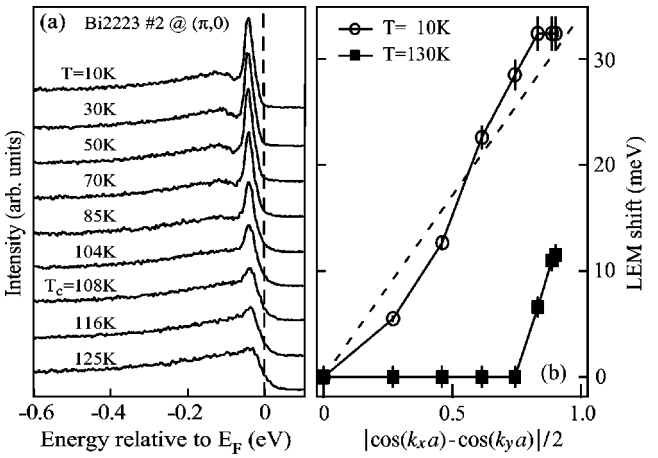

FIG. 47. The superconducting gap in nearly optimally doped Bi2223 ($T_c=108$ K): (a) temperature-dependent $(\pi,0)$ ARPES spectra measured with 21.2-eV photons; (b) position of the leading-edge midpoint above and below T_c along the normal-state Fermi surface. The dashed line represents the d-wave functional form. From Feng, Damascelli, *et al.*, 2002.

C. $Bi_2Sr_2Ca_2Cu_3O_{10+\delta}$

The superconducting gap in Bi2223 was recently measured by several groups (Feng, Damascelli, *et al.*, 2002; Müller *et al.*, 2002; Sato, Matsui, *et al.*, 2002). In Fig. 47(a), where the temperature dependence of the $(\pi,0)$ ARPES spectra is presented, one can clearly observe the remarkable change of quasiparticle line shape that takes place for $T<T_c$, as well as the opening of the superconducting gap. Figure 47(b) shows the angular dependence of the superconducting gap as determined from the shift of the leading-edge midpoint along the normal-state Fermi surface. The results are consistent with a d-wave symmetry order parameter, with the largest magnitude for the leading-edge gap so far reported among the Bi-based cuprate superconductors.

D. $La_{2-x}Sr_xCuO_4$

The superconducting gap in LSCO is much smaller than in Bi2212 and, so far, no detailed investigations have been reported. As we already mentioned in Sec. IV.B when discussing the data of Fig. 26, the presence of

[18]For instance, see Dessau *et al.* (1993); Ding, Norman, *et al.* (1996); Harris *et al.* (1996); Norman, Ding, *et al.* (1998); and Mesot *et al.* (1999).

[19]Note that although an identical gap was detected for both bilayer split Fermi surfaces in the antinodal region, the complete momentum dependence along the antibonding one could not be investigated in detail.

a finite superconducting gap was signaled by the shift of the leading-edge midpoint of the spectra along the normal-state Fermi surface (Ino *et al.*, 1999). On the basis of this behavior Ino *et al.* (1999) estimated a superconducting gap for optimally doped LSCO of about 10–15 meV, in agreement with the results from other techniques (Chen *et al.*, 1994; Yamada *et al.*, 1995; Nakano *et al.*, 1998). Furthermore, it appears that the measured gap is qualitatively consistent with a d-wave scenario. Similar conclusions were reached by Sato, Yokoya, *et al.* (1999) on the basis of a detailed fit of angle-integrated photoemission data.

E. $YBa_2Cu_3O_{7-\delta}$

Information on the superconducting state of Y123 by ARPES can be obtained only after identification of the surface state (Sec. IV.F), which dominates the photoemission spectra at both X and Y points in the Brillouin zone (note that it is at these momenta that a gap, if d-wave like, would have its maximum amplitude). By investigating the X region, where the surface state was weaker in that specific experimental geometry, Schabel *et al.* (1997) provided supporting evidence for a superconducting gap whose momentum dependence is consistent with the d-wave form. In that study, however, due to sample quality issues, the surface was not stable enough to allow cycling the temperature.

Recently, the substantial improvement in sample quality and instrumental resolution has allowed the convincing detection of superconductivity-related features in Y123 (Lu *et al.*, 2001). As shown in Figs. 48(a) and (b), after subtracting the surface-state contribution by means of a phenomenological fitting procedure, the remainder of the fitted function looks strikingly similar to the line shape typically observed in Bi2212 at $(\pi,0)$ in the superconducting state [see Fig. 48(c) and Sec. VI.A]. Direct evidence for the second peak being related to superconductivity comes from measurements performed by cycling the temperature, which show that this feature consistently disappears above T_c. This behavior is summarized for several overdoped samples ($T_c=89$ K) and both X and Y momenta in Fig. 48(d), where the normalized superconducting peak intensity is plotted [note that in Fig. 48(d) SPR refers to *superconducting peak ratio*, which will be defined in Sec. VI.A].

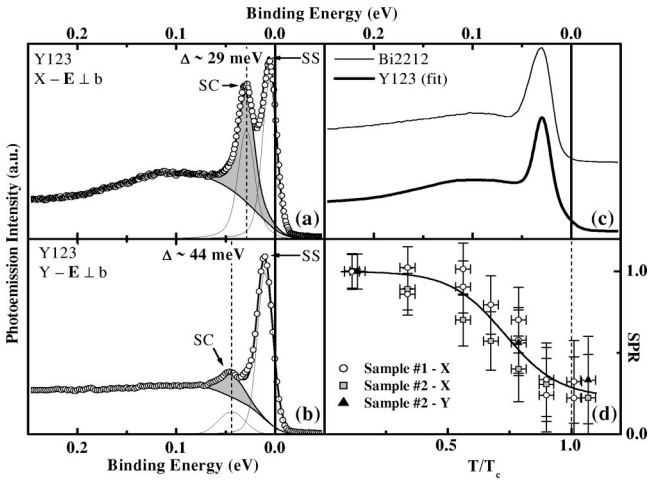

FIG. 48. Superconducting state results from overdoped Y123 ($T_c=89$ K): (a),(b) ARPES spectra measured at X and Y ($T=10$ K), with corresponding fitting curves; (c) comparison of the Y123 fit at X (surface-state peak subtracted) with the $(\pi,0)$ spectrum from overdoped Bi2212 ($T_c=84$ K); (d) temperature dependence of the normalized superconducting-peak intensity. From Lu *et al.*, 2001.

An interesting finding, which is specific to Y123, is the strong a-b anisotropy of the in-plane electronic structure. In fact, as determined by Lu *et al.* (2001), the energy positions of peak and hump for overdoped Y123 are 29 meV (Δ_x) and 120 meV (ω_x) at X, and 44 meV (Δ_y) and 180 meV (ω_y) at Y. These results, in agreement with those from other techniques (Polturak *et al.*, 1993; Liminov *et al.*, 2000), indicate a 50% difference in the gap magnitude Δ between X and Y, a remarkable deviation from the ideal $d_{x^2-y^2}$ gap form.

F. $Nd_{2-x}Ce_xCuO_4$

The improved experimental resolution also allowed the successful detection of the superconducting gap in the electron-doped superconductor NCCO (Armitage, Lu, Feng, *et al.*, 2001; Sato, Kamiyama, Takahashi, *et al.*, 2001a), a task that was not possible before (Anderson *et al.*, 1993; King *et al.*, 1993). This investigation is of particular relevance because, whereas for the hole-doped high-T_c superconductors it is now generally accepted that the order parameter has the dominant component of d-wave symmetry (see, for example, Tsuei and Kirtley, 2000a), for electron-doped systems this issue is less clear. On the one hand, an isotropic superconducting gap was supported by early evidence of tunneling (Huang *et al.*, 1990), microwave penetration depth (Wang *et al.*, 1990; Wu *et al.*, 1993), and Raman experiments (Stadlober *et al.*, 1995). On the other hand, this picture has been seriously questioned by recent scanning superconducting quantum interference device (SQUID) microscopy measurements on tricrystal films, which provided direct evidence for an order parameter with a large d-wave component (Tsuei and Kirtley, 2000b).

In order to investigate the superconducting gap by ARPES, Armitage, Lu, Kim, *et al.* (2001) focused on the Fermi-surface crossings near $(\pi/2,\pi/2)$ and $(\pi,0.3\pi)$ in the Brillouin zone [see Figs. 49(a) and (b)], where a $d_{x^2-y^2}$ superconducting gap is expected to be zero and maximum, respectively. The blue and red curves in Figs. 49(c) and (d) are data collected below and above $T_c=24$ K, respectively. Near the $(\pi/2,\pi/2)$ region [Fig. 49(c)], one does not see a shift of the leading edge of the spectra with temperature, indicating minimal or zero gap. Near $(\pi,0.3\pi)$ on the other hand, all curves show a clear shift below T_c of about 1.5–2 meV, in agreement with the opening of a superconducting gap [Fig. 49(d)]. Systematic estimates for the leading-edge midpoint shift were obtained by means of a phenomenological fitting procedure and are indicated, for the different spectra, in

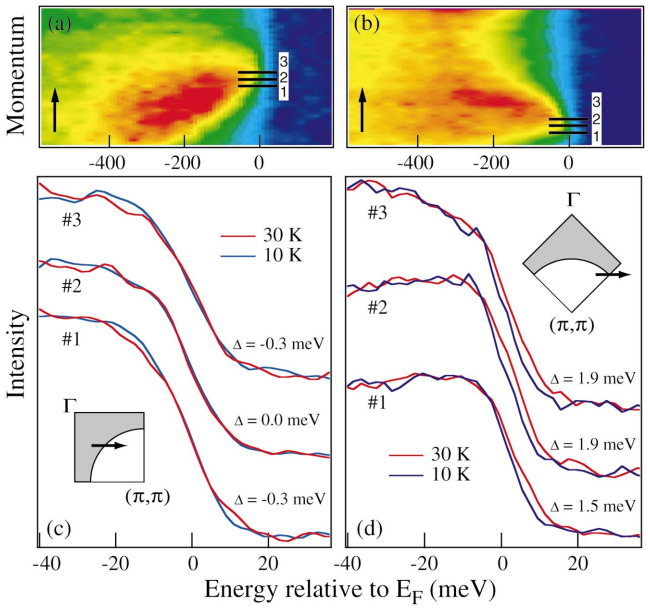

FIG. 49. Investigation of the superconducting gap in NCCO (T_c=24 K): (a),(b) image plots of the ARPES spectra from near (π/2,π/2) and (π/2,0.3π) along the cuts indicated by arrows in the Brillouin-zone sketches of (c) and (d), respectively; (c), (d) normal- and superconducting-state spectra from the E-k regions marked by the black bars in (a) and (b), respectively. The gap values obtained by fitting are also indicated. After Armitage, Lu, Feng, *et al.*, 2001 (Color).

Figs. 49(c) and (d). Armitage, Lu, Feng, *et al.* (2001) concluded that, although an anisotropic s-wave order parameter with a small amplitude in the nodal region could not be completely excluded, these results provide support for a d-wave pairing state in NCCO. As the leading-edge analysis can underestimate the superconducting gap value by as much as a factor of 2 (Ding, Campuzano, *et al.*, 1995a; Loeser *et al.*, 1997), a gap of about 4 meV would be consistent with the ARPES data, in agreement with other techniques (Huang *et al.*, 1990; Wang *et al.*, 1990; Wu *et al.*, 1993; Stadlober *et al.*, 1995; Kokales *et al.*, 2000; Prozorov *et al.*, 2000).

Similar results were also reported by Sato, Kamiyama, Tokahashi, *et al.* (2001a). In this case, the authors did not perform temperature-dependent measurements on NCCO across the phase transition but relied on a comparison, at one fixed temperature below T_c, between the Fermi edges measured on polycrystalline Pt and on a single-crystal of NCCO. Sato, Kamiyama, Takahashi, *et al.* (2001a) detected for NCCO a leading-edge shift of about 2–3 meV at the Fermi crossing along (π,0)-(π,π) and no shift at the Fermi crossing along (0,0)-(π,π). By fitting the data with a phenomenologically broadened BCS spectral function (Ding, Campuzano, *et al.*, 1995a, 1995b; Ding, Norman, *et al.*, 1996), they concluded in favor of a d-wave gap of about 5 meV, in agreement with the estimate by Armitage, Lu, Feng, *et al.* (2001).

G. Discussion

From the results presented in this section it is clear that the cuprate high-T_c superconductors are characterized by an overall d-wave pairing symmetry, although further scrutiny is required for specific issues such as the existence of an area of gapless excitations in the nodal region, which would hint at significant deviations from a pure $d_{x^2-y^2}$ symmetry. Furthermore, as summarized in Fig. 50 where ARPES as well as tunneling spectroscopy results are presented for several families of cuprates, at optimal doping the gap magnitude of the different systems scales linearly with the corresponding T_c (Sato, Kamiyama, Naitoh, 2001; Feng, Damascelli, *et al.*, 2002; Sato, Matsui, *et al.* 2002). In particular, as shown in Fig. 50, the gap versus T_c data obtained from the position of the leading-edge midpoint can be fitted by a line across the origin corresponding to the ratio $2\Delta_0/k_BT_c \simeq 5.5$ (Feng, Damascelli, *et al.*, 2002).

At this stage, a system that seems to stand out is Y123 because of the 50% anisotropy between its gap amplitudes at X and Y. As discussed by Lu *et al.* (2001), this anisotropy could originate from the orthorhombicity of the CuO_2 planes in Y123 which, according to band-structure calculations, should affect the normal-state electronic structure (Andersen *et al.*, 1995). Alternatively, it could be a consequence of the presence of the CuO chains which, for strong chain-plane hybridization, can directly affect the CuO_2-plane-derived electronic structure (Atkinson, 1999). Whatever the cause of this anisotropy, it seems that for Y123, rather than a pure $d_{x^2-y^2}$ symmetry, alternative models should be considered (Atkinson, 1999; Wu, 2002).

Although not detected by ARPES, significant deviations from a simple $d_{x^2-y^2}$ symmetry may be present in the case of NCCO. In fact, a nonmonotonic d-wave superconducting order parameter has been recently proposed on the basis of Raman experiments (Blumberg *et al.*, 2002). These results, whose interpretation was recently questioned (Venturini *et al.*, 2002), were taken as an indication that the absolute maximum in gap magnitude may be located at the intersection between the

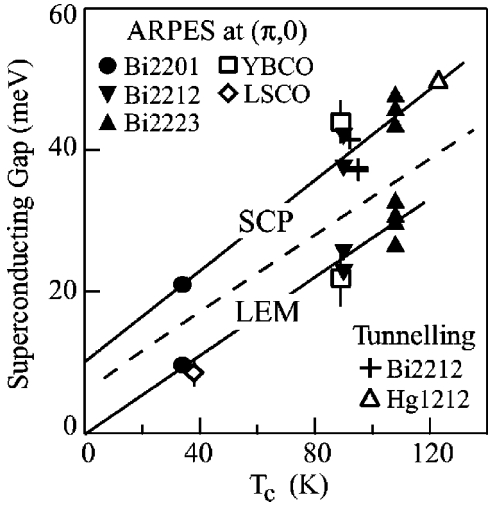

FIG. 50. Superconducting gap magnitude estimated from the superconducting peak position and the leading-edge midpoint shift (separated by the dashed line), plotted vs T_c for various optimally doped materials. From Feng, Damascelli, *et al.*, 2002.

holelike Fermi surface and the antiferromagnetic zone boundary [the so-called hot spots indicated in the inset of Fig. 44(c)], rather than at $(\pi,0)$ as in the p-type cuprate superconductors. In this regard, as for the possible deviations from a V-like cusp in the nodal region for p-type materials (Mesot *et al.*, 1999), it has been proposed that high-order harmonics should be included in the expansion of the gap function (Guinea *et al.*, 2002). This would account for the doping evolution of the gap anisotropy and, in particular, for the maximum gap amplitude's being pushed away from $(\pi,0)$ in optimally doped NCCO. However, in order to address these issues conclusively, more detailed ARPES studies of the momentum dependence of the superconducting gap in both n- and p-type superconductors are required.

VI. SUPERCONDUCTING PEAK

We now move on to the second well-known phenomenon observed in the ARPES data below T_c, namely, the dramatic change in line shape of the $(\pi,0)$ spectra, first seen in Bi2212 (Dessau *et al.*, 1991; Hwu *et al.*, 1991): a sharp quasiparticle peak develops at the lowest binding energies, followed by a dip and a broader hump, giving rise to the so-called *peak-dip-hump structure*. This evolution can be clearly seen in Fig. 51, or in Fig. 45 where the normal-state and superconducting-state spectra from $(\pi,0)$ and $(\pi/2,\pi/2)$ are compared. While the opening of the superconducting gap has been observed in many different cuprate high-T_c superconductors, for a long time the emergence of a sharp peak below T_c appeared to be a phenomenon unique to Bi2212. Only

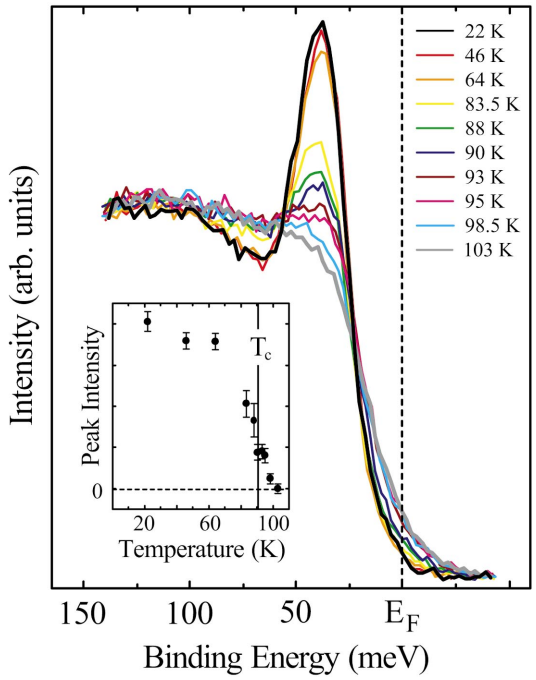

FIG. 51. Temperature-dependent photoemission spectra from optimally doped Bi2212 ($T_c=91$ K), angle integrated over a narrow cut at $(\pi,0)$. Inset: superconducting-peak intensity vs temperature. After Fedorov *et al.*, 1999 (Color).

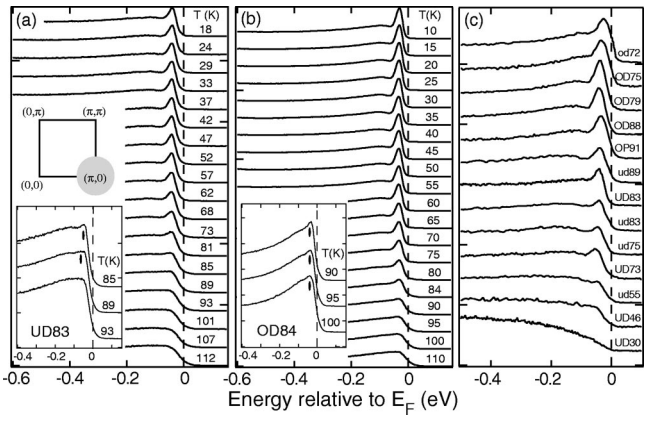

FIG. 52. Temperature and doping dependence of the photoemission data from Bi2212: (a),(b) temperature-dependent ARPES spectra from underdoped ($T_c=83$ K) and overdoped ($T_c=84$ K) Bi2212, respectively, angle-integrated over the area around $(\pi,0)$ shaded in gray in the Brillouin-zone sketch; insets are enlarged views of spectra taken just above T_c; (c) doping dependence, from underdoped to overdoped (bottom to top), of the superconducting-state $(\pi,0)$ spectra from Bi2212, for $T \ll T_c$. From Feng *et al.*, 2000.

very recently a similar feature has been detected below T_c in Y123 and Bi2223 (see Secs. V.E and VI.B, respectively). However, as it is on Bi2212 that the most extensive body of work for doping, temperature, and momentum dependence of this feature is available, we shall mainly focus on that material in this section.

Because the emergence of the peak-dip-hump structure in the Bi2212 $(\pi,0)$ spectra is the most remarkable effect seen across T_c, much work has been devoted to the experimental and theoretical investigation of this behavior. However, as we shall discuss in more detail below and in Sec. VIII, the line-shape analysis of ARPES spectra from Bi2212 is a very controversial subject and is currently a matter of intense debate. In particular, the recent observation of bilayer band splitting in Bi2212 (Sec. IV.C.2) suggests that the peak-dip-hump structure near $(\pi,0)$ needs to be completely reexplored. It is indeed possible that its main features could be interpretable as bilayer splitting effects. Nonetheless, due to the present uncertainty and the inherent interest of this issue, in this section we shall review previous analyses, focusing mainly on the experimental phenomenology.

A. $Bi_2Sr_2CaCu_2O_{8+\delta}$

The connection between the emergence of the peak-dip-hump structure and the onset of superconductivity has been documented by detailed temperature-dependent investigations by Loeser *et al.* (1997), and more recently by others.[20] Although it starts to manifest itself slightly above T_c, it is below T_c that the quasiparticle peak really stands out. This can be clearly observed

[20]See Franz and Millis (1998); Fedorov *et al.* (1999); Millis (1999); Feng *et al.* (2000); and Ding *et al.* (2001).

in the high-resolution ($\Delta E = 8$ meV) data from optimally doped Bi2212 presented in Fig. 51, which indicate an intrinsic width for this peak of about 14 meV (Fedorov *et al.*, 1999). Temperature-dependent data from underdoped and overdoped Bi2212 are presented in Figs. 52(a) and (b) (Feng *et al.*, 2000). As shown in particular in the insets of Fig. 52, the superconducting peak turns on slightly above T_c, in striking contrast to the pseudogap, which behaves very differently in underdoped and overdoped samples (e.g., it opens up well above T_c on the underdoped side, as discussed in Sec. VII). The results obtained at low temperatures ($\sim$10 K) for different doping levels are displayed in Fig. 52(c). The peak, not resolved in the very underdoped samples [bottom curve in Fig. 52(c)], grows with doping.

At the experimental level, the momentum dependence of the peak-dip-hump structure is a more complicated and controversial issue than the doping or temperature dependence. As we shall see below, this is mostly a consequence of the superstructure and bilayer splitting effects (Sec. IV.C), which are particularly pronounced in the $(\pi,0)$ region of momentum space. Another reason is that this investigation requires many spectra to be recorded as a function of momentum and temperature, which is technically more challenging, especially if one is going after small effects. For instance, Shen *et al.* (1998) reported a 2–5 % temperature-induced spectral weight transfer with momentum $\mathbf{Q} \simeq (0.45\pi,0)$. This was observed in samples with lower T_c, which in turn is due to the presence of impurities or the sample being underdoped, but not in those characterized by the highest T_c. It was interpreted as a consequence of stripe formation. It was later realized that this

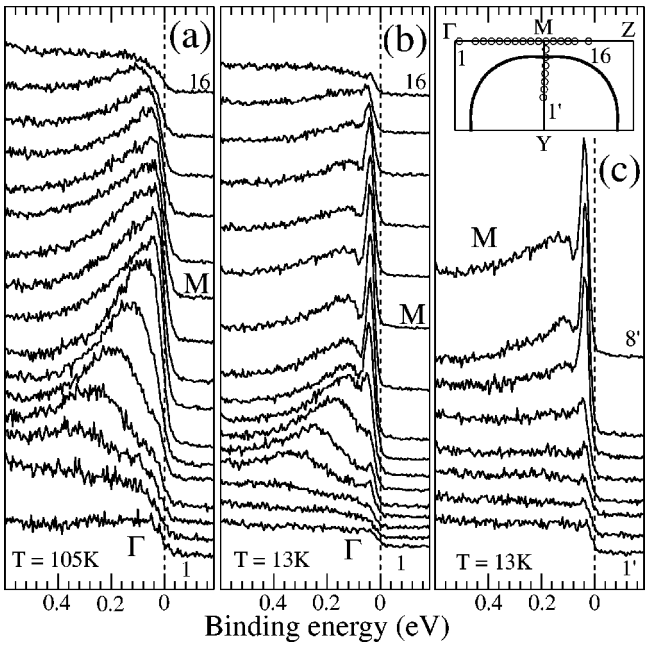

FIG. 53. ARPES spectra from overdoped Bi2212 ($T_c = 87$ K) along the high-symmetry directions: (a) normal- and (b),(c) superconducting state data measured at the k points indicated in the inset of (c). Momentum-space notations are defined as in Fig. 12. After Norman *et al.*, 1997.

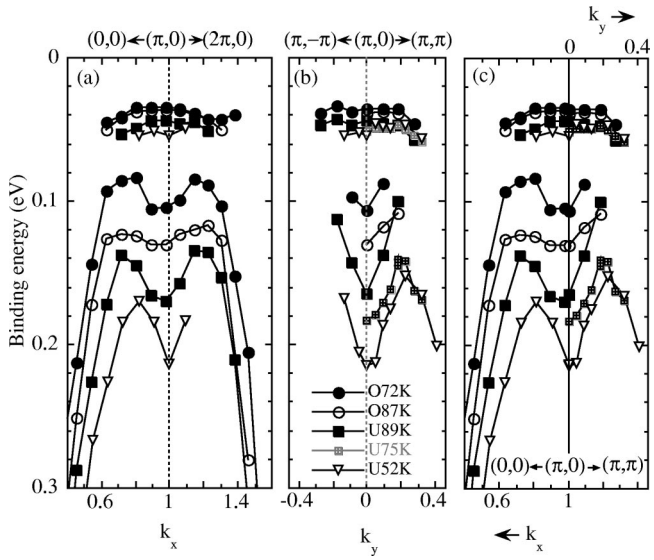

FIG. 54. Peak and hump dispersion in the superconducting state of Bi2212, for several dopings from underdoped to overdoped (bottom to top). From Campuzano *et al.*, 1999.

effect might more likely be an experimental artifact due to the aging of the sample surface, as suggested by ARPES experiments performed on samples containing impurities whose surface was intentionally and systematically aged (White *et al.*, 1999). Alternatively, this may be due to a structural transition taking place in underdoped samples in the measured in the measured temperature range, which could affect the amplitude of the superstructure modulation (Anderson *et al.*, 1997; Miles *et al.*, 1997).

Figure 53 presents ARPES spectra from Bi2212 along the high-symmetry lines (Norman *et al.*, 1997), which suggest that the sharp superconducting peak persists in a very large momentum-space region around $(\pi,0)$. However, as was later recognized, the low-energy peak observed at those k points at which the hump has dispersed to binding energies larger than 200 meV stems from the superstructure contamination discussed in Sec. IV.C. The actual experimental phenomenology is that the superconducting peak occurs only in those momentum-space regions where the normal-state band is within 100–150 meV of E_F and has a very weak dispersion. This can be seen in Fig. 54, which presents the quasiparticle dispersion reported for different doping levels by Campuzano *et al.* (1999).

The detection of the peak-dip-hump structure has generated a tremendous amount of interest, as it is thought to carry critical information about the superconducting transition.[21] In particular, it has given the main impetus for a phenomenological description of single-

[21]See, for example, Harris *et al.* (1996); Loeser *et al.* (1997); Norman *et al.* (1997); Shen and Schrieffer (1997); Chubukov and Morr (1998); Franz and Millis (1998); Shen *et al.* (1998); Campuzano *et al.* (1999); Fedorov *et al.* (1999); Eschrig and Norman (2000); Feng *et al.* (2000); Ding *et al.* (2001); and Kaminski *et al.* (2001).

particle excitations in terms of an interaction between quasiparticles and collective modes, which is of fundamental relevance to the nature of superconductivity and of the pairing mechanism in the high-T_c superconductors (see, for example, Eschrig and Norman, 2002a). However, as we shall discuss in more detail in Sec. VIII, different interpretative scenarios were proposed, which are still matter of intense debate. In this regard, it is important to point out that the main constituents of the peak-dip-hump structure have also been interpreted as possible fingerprints of the bilayer splitting of the electronic structure of Bi2212, with peak and hump corresponding to antibonding and bonding bands, respectively. As shown in Sec. IV.C.2, this assignment was particularly obvious for normal-state and superconducting-state data from overdoped Bi2212 (see Fig. 34). For the optimally doped and underdoped cases it has been suggested that in the normal state, due to the breadth of the line shapes, the two bands can only be recognized on the basis of their different photon energy dependence (see Fig. 36); in the superconducting state, on the other hand (see also Sec. VIII.C.3), bonding and antibonding bands can be resolved directly due to the sharpening and/or spectral weight increase of the peaks (Gromko, Fedorov, *et al.*, 2002; Kordyuk *et al.*, 2002b). In this context, it should be noted that the complex line shape observed in the $(\pi,0)$ spectra from YBCO (Fig. 48) and Bi2223 (Fig. 47) may indicate multilayer splitting effects.

Despite the degree of uncertainty in the line-shape analysis of the peak-dip-hump structure as a whole, and regardless of bilayer splitting effects, the detailed study of the temperature and doping dependence of this feature may still provide valuable information. Feng *et al.* (2000) used a phenomenological fitting procedure to quantify the temperature and doping evolution of the intensity of the lowest-energy peak at $(\pi,0)$. In particular, the ratio between the area of the peak and that of the spectrum integrated between -0.5 and 0.1 eV was considered, in an attempt to extract more systematic information (i.e., independent of artifacts due to k dependence of matrix elements and/or different experimental conditions for the different samples). The doping and temperature dependence of this quantity, referred to as *superconducting peak ratio* (SPR), are presented in Figs. 55(a) and (d). The comparison by Feng *et al.* (2000) of many superfluid-related quantities measured on Bi2212, Y123, and LSCO suggests that

(i) the remarkable similarities between the data presented in Fig. 55 hint at a universality in the superconducting properties of the cuprates;
(ii) ARPES, which probes single-particle excitations of the condensate and therefore directly measures the strength of the pairing (i.e., superconducting gap), may also provide information on the phase coherence of the superconducting state (note that in principle this can only be inferred from techniques that directly probe the collective motion of the condensate).

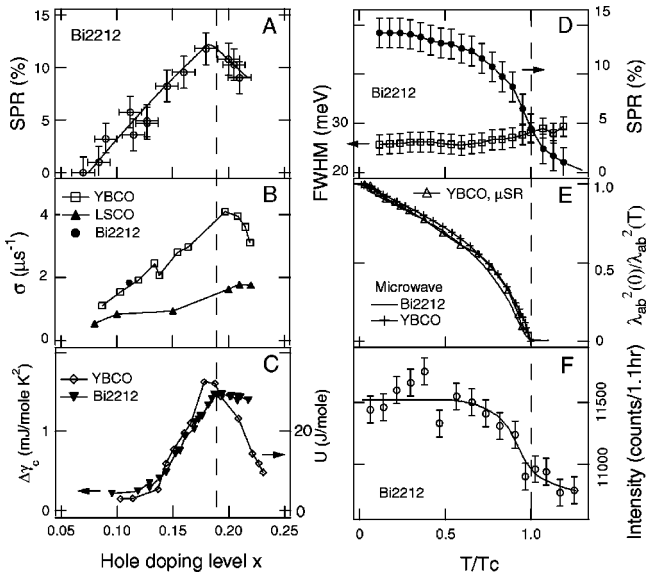

FIG. 55. Doping and temperature dependence of many different superconductivity-related quantities: Doping dependence for $T<T_c$: (a) SPR for the (Bi2212) spectra of Fig. 52(c); (b) μSR relaxation rate ($\sigma \propto n_s$) (Uemura *et al.*, 1991; Tallon *et al.*, 1999); (c) Bi2212 specific-heat coefficient jump $\Delta\gamma_c=\gamma(T_c)-\gamma(120\ \mathrm{K})$ (Tallon *et al.*, 2000), and (Y123) condensation energy U (Tallon *et al.*, 1999); T dependence: (d) SPR and peak-width of Bi2212 [sample OD84 in Fig. 52(b)]; (e) $\lambda_{ab}^2(0)/\lambda_{ab}^2(T)$ ($\propto n_s$) (Bonn *et al.*, 1994; Jacobs *et al.*, 1995; Sonier *et al.*, 1999), where λ_{ab} is the in-plane penetration depth; (f) intensity of the neutron (π,π) mode (He *et al.*, 2001). After Feng *et al.*, 2000.

This latter point is evidenced by the similar behavior observed, as a function of hole concentration, in SPR, superfluid density n_s measured by μSR [Fig. 55(b)], condensation energy U from the specific heat, and jump in the specific-heat coefficient [Fig. 55(c)], as well as in the similar temperature dependence of the SPR and n_s measured by microwave or μSR spectroscopy [Figs. 55(d) and (e)]. Furthermore, contrary to what is expected within the Fermi-liquid-BCS framework (Schrieffer, 1964), the SPR and superfluid density exhibit an abrupt drop near T_c (i.e., disappearance of phase coherence) rather than at T^* (the opening of the pseudogap in the underdoped regime) and grow with the hole concentration x while the gap magnitude, as determined by ARPES (see Sec. VII and Fig. 62), scales with $(1-x)$.

Similar observations were made by Ding *et al.* (2001), who also found an increase in the peak intensity with doping, as shown in Fig. 56(a) (here the quantity z_A, referred to by the authors as *coherent quasiparticle weight*, is defined exactly as the above SPR and is therefore a phenomenological quantity without rigorous theoretical implications). It was observed that the product $z_A\Delta_m$, where Δ_m is the superconducting gap estimated by the peak position at $(\pi,0)$ for $T=14$ K [Fig. 56(b)], is directly proportional to the superconducting transition temperature [Fig. 56(c)]. On the basis of these results, Ding *et al.* (2001) concluded that superconductivity is mainly controlled by the quasiparticle coherence z_A in

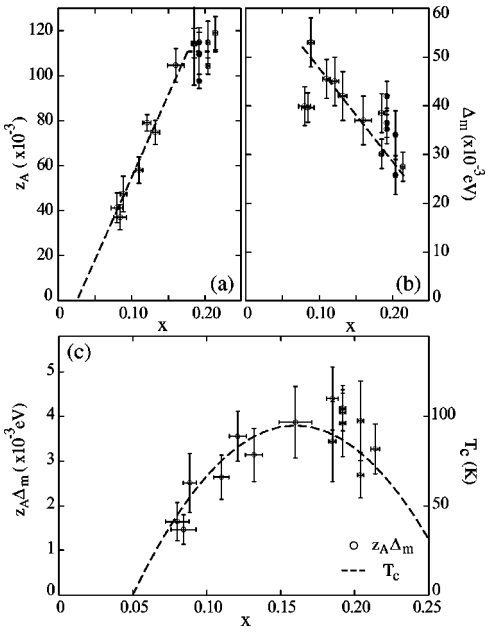

FIG. 56. Doping dependence, as estimated at 14 K, of (a) coherent quasiparticle weight z_A; (b) maximum gap size Δ_m; and (c) $z_A\Delta_m$. In (c) the empirical relation between T_c and x (Presland *et al.*, 1991) is also shown. After Ding *et al.*, 2001.

the underdoped regime and by the superconducting gap in the overdoped regime, and suggested that a new quantity, $z_A\Delta_m(T=0)$, may be the true superconducting order parameter in the high-T_c superconductors.

The emergence of a sharp quasiparticle peak below T_c has been taken as evidence for some form of coherent transition, which was also the spirit of the phenomenological analyses discussed above. While in the BCS framework (Schriffer, 1964), the superconducting transition and the opening of a superconducting gap in the single-particle excitation spectrum are due to an effective attractive interaction between Fermi-liquid quasiparticles which are already well defined above T_c, in the case of the high-T_c superconductors coherent quasiparticles may be formed only upon entering the superconducting state (see, for example, Shen and Sawatzky, 1999). Theoretical examples of this kind of transition in the literature include dimensional crossover (Carlson *et al.*, 2000), condensation of chargons (Senthil and Fisher, 1999), quantum confinement, and Bose condensation (Nagaosa and Lee, 2000). Note, however, that the above discussed interpretations by Feng *et al.* (2000) and Ding *et al.* (2001) are not universally accepted. Notably, Norman, Kaminski, *et al.* (2001) suggested that the temperature dependence of the ARPES spectra is not due to a decrease in spectral weight of the low-energy peak with increasing temperature above T_c, but is instead a reflection of the *quasiparticle lifetime catastrophe* (Kuroda and Varma, 1990; Norman and Ding, 1998; Abanov and Chubukov, 1999; Norman, Kaminski, *et al.*, 2001). The disappearance of the sharp peak above T_c would be a consequence of the reduction of the low-energy electron lifetime, which broadens the quasiparticles out of existence once the superconducting gap has closed. At this stage, it is hard to judge which interpretation is more appropriate. On the one hand, the analysis by Norman, Kaminski, *et al.* (2001) is more detailed than the phenomenological one presented in the two experimental papers (Feng *et al.*, 2000; Ding *et al.*, 2001). On the other hand, this alternative scenario seems to be in contrast with the experimental observation that, at least in the optimally-doped/overdoped regime [see Fig. 55(d) where the FWHM is plotted], the width of the superconducting peak does not appear to change significantly across the superconducting transition (Fedorov *et al.*, 1999; Feng *et al.*, 2000; Ding *et al.*, 2001).

B. $Bi_2Sr_2Ca_2Cu_3O_{10+\delta}$ and $Bi_2Sr_2CuO_{6+\delta}$

The temperature dependence seen for the quasiparticle peak in Bi2212 also seems to be confirmed by the data reported for optimally doped Bi2223 [Figs. 47(a) and 64], in which once again the quasiparticle peak disappears at temperatures slightly larger than $T_c=108$ K (Feng, Damascelli, *et al.*, 2002; Sato, Matsui, *et al.*, 2002). Furthermore, as shown in Fig. 57 where the superconducting state $(\pi,0)$ ARPES spectra from one-, two-, and three-CuO_2-plane Bi-cuprates are presented, it appears that the superconducting peak intensity increases with T_c, supporting the idea that it is related to the strength of superconductivity in the system. In particular, Feng, Damascelli, *et al.* (2002) showed that both the peak intensity and the superconducting gap increase approximately linearly with T_c in this family of compounds, which seems to indicate that both phase coherence and pairing strength scale with the number of CuO_2 planes. In this regard, it has to be mentioned that for Bi2201, presumably due to the lower superfluid density of the single-layer compound, only very recently some evidence was collected for the presence of a sharp peak at

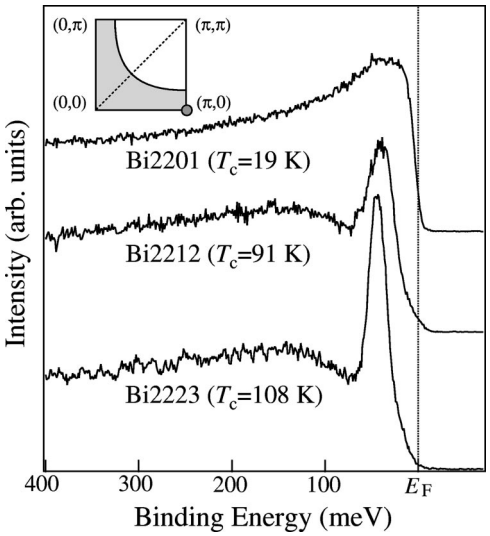

FIG. 57. Superconducting state $(\pi,0)$ ARPES spectra from Bi2201 ($T_c=19$ K), Bi2212 ($T_c=91$ K), and Bi2223 ($T_c=108$ K). The data were taken with 21.2-eV photons at 13.5 K for Bi2201, and 40 K for both Bi2212 and Bi2223. From Sato, Matsui, *et al.*, 2002.

low temperatures, which indeed is much weaker than in the case of Bi2212 and Bi2223 (Lanzara, 2002).

VII. PSEUDOGAP

One of the most important contributions of ARPES to the investigation of the high-T_c superconductors, is the identification of the normal-state excitation gap or *pseudogap* by Marshall *et al.* (1996) and Loeser *et al.* (1996), and then by Ding, Yokoya, *et al.* (1996). Similar to what we discussed in Sec. V for the superconducting gap, the pseudogap can be simply described as the opening of an energy gap along the underlying Fermi surface, but detected in this case in the normal state. In fact, for the underdoped cuprates it was found that the Fermi level crossings were absent over a large portion of the Fermi surface due to the opening of an excitation gap at temperatures considerably higher than T_c itself. This phenomenon was first recognized in the photoemission spectra by King *et al.* (1995) in attempting to connect the Bi2212 data to those from undoped SCOC (Wells *et al.*, 1995). The pseudogap has been observed in many of the cuprate superconductors, but has been most extensively studied in Bi2212. As we shall discuss in detail later, the main characteristics of the normal-state pseudogap can be summarized as follows (Randeria and Campuzano, 1997; Shen *et al.*, 1997): (i) the effect is strong in underdoped samples, persists to optimal doping, and disappears in overdoped samples (Levi, 1996). (ii) The gap has two energy scales, with the low-energy one given by the location of the leading-edge midpoint (which shows a clear gap), and the higher-energy one by the position of a broad peak near the $(\pi,0)$ point (the expected sharp quasiparticle peak at E_F is converted into a broad feature over $\sim$100 meV and the low-energy spectral weight is suppressed). The lower-energy scale has a d-wave-like momentum dependence similar to that of the superconducting gap, with a gapless arc near the nodal region. As a function of doping, the two energy scales track each other (Harris *et al.*, 1996; Marshall *et al.*, 1996; White *et al.*, 1996; Norman, Ding, *et al.*, 1998; Campuzano *et al.*, 1999). (iii) As the hole concentration is reduced, the size of the leading-edge pseudogap increases, in contrast to the decreasing of T_c. This is believed to be an important piece of evidence for the non-BCS behavior of the superconducting transition in the underdoped regime of the high-T_c superconductors.

A. $Bi_2Sr_2CaCu_2O_{8+\delta}$

The first specific study of the pseudogap effect in Bi2212 was performed by Marshall *et al.* (1996). Figure 58 reproduces the key data that illustrate the basic phenomenology. For optimally doped or overdoped samples, Fermi crossings around the entire Fermi surface were observed [solid squares in Fig. 58(a)]. For underdoped samples, well-defined Fermi-surface crossings were detected only within an arc segment centered on the (0,0)-(π,π) line [open circles in Fig. 58(a)], while they were completely missing near $(\pi,0)$. When the results from underdoped and optimally doped Dy-Bi2212 are compared [Fig. 58(b)], it is clear that the spectra from the underdoped samples pull towards higher binding energy in the entire $(\pi,0)$ region. As the Fermi surface should be a continuous surface in momentum space, this behavior was interpreted as the opening of an anisotropic gap. It has to be emphasized that the pseudogap phenomenon is relatively insensitive to the details of the Fermi-surface topology in this region (Sec. IV.C). The magnitude of the gap is rather large, and the spectra from underdoped samples are pulled back over an extended momentum-space region $(\pi,0)$, which is characterized by a weak band dispersion [see Figs. 58(c), (d), where the dispersion is summarized for several doping levels]. Hence the normal-state gap and its doping dependence are robust features in the ARPES spectra.

Marshall *et al.* (1996) suggested two different ways of characterizing the normal-state pseudogap: by the position of the leading edge (20–30 meV) or by the position of the broad maximum of the spectra (100–200 meV), which identify, respectively, low-energy and high-energy pseudogaps. While the former is well defined at intermediate low-doping levels but not in the deeply underdoped regime, the latter is particularly useful in the very underdoped cases. As we shall discuss below, it is gener-

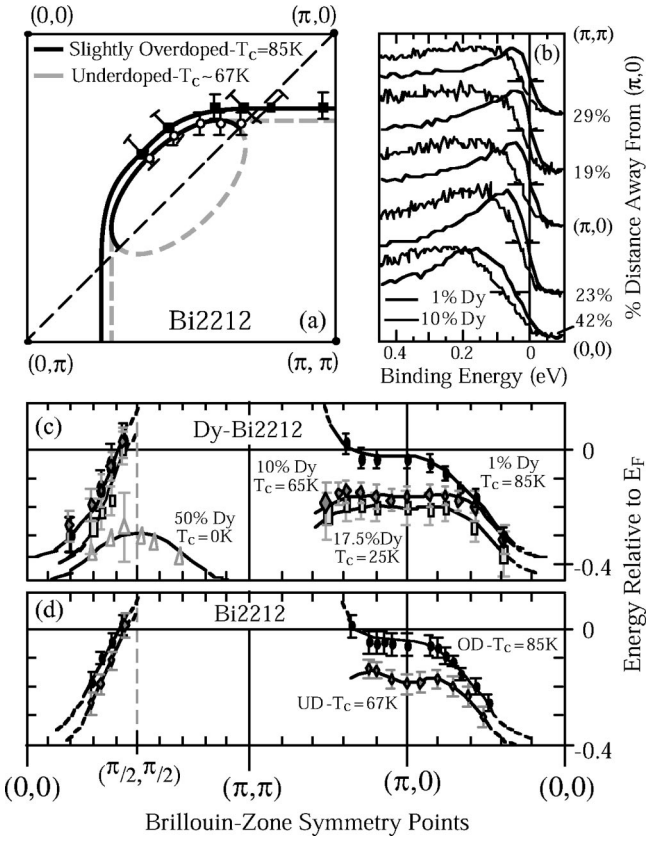

FIG. 58. The pseudogap phenomenology in Bi2212: (a) Fermi-surface crossings for Bi2212; (b) leading-edge midpoint shifts for Dy-Bi2212; (c),(d) dispersions determined from the peak centroids for Dy-Bi2212 and Bi2212, respectively, for different doping levels. After Marshall *et al.*, 1996.

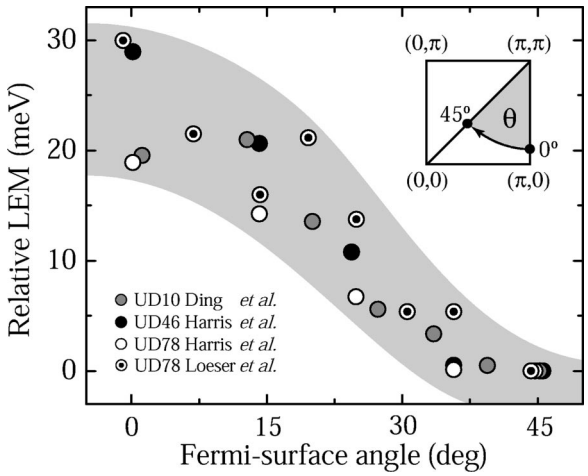

FIG. 59. Momentum dependence of the pseudogap along the expected Fermi surface for underdoped Bi2212 (numbers indicate T_c): UD10 (Ding, Yokoya, *et al.*, 1996); UD46, UD78 (Harris *et al.*, 1996); UD78 (Loeser *et al.*, 1996). The leading-edge midpoint positions are plotted *relative* to the value at 45°.

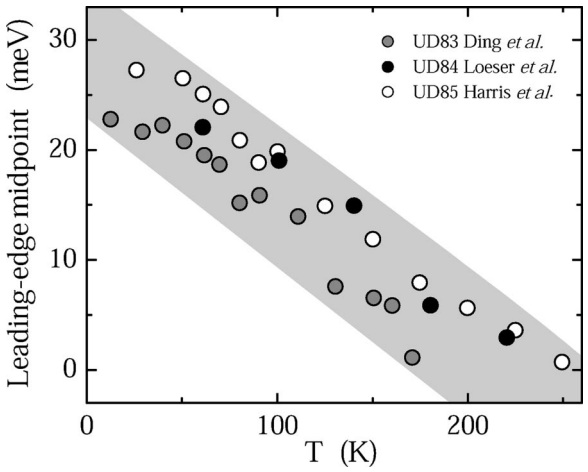

FIG. 60. Temperature dependence of the pseudogap near $(\pi,0)$ for underdoped Bi2212: UD83 (Ding, Yokoya, *et al.*, 1996); UD84 (Loeser *et al.*, 1997); UD85 (Harris *et al.*, 1996).

ally believed that the low- and high-energy scales of the normal-state gap naturally connect to the gaps of the superconductor and the antiferromagnetic insulator, respectively. In this regard, of particular relevance are the momentum-dependence studies of these features.

(i) For the low-energy pseudogap, detailed results were reported by Loeser *et al.* (1996) and Ding, Yokoya, *et al.* (1996). Although the spectra are characterized by a peak not as sharp as that seen in the superconducting state (Sec. VI.A), the compilation of data presented in Fig. 59 shows that the k dependence of the magnitude of the low-energy pseudogap is similar to that of the d-wave superconducting gap (Sec. V.A), which suggests the interesting possibility that the two gaps may originate from the same underlying mechanism.

(ii) As for the high-energy pseudogap, it was suggested that this feature exhibits the same dispersion along the (0,0)-$(\pi,0)$ and (π,π)-$(\pi,0)$ directions (Campuzano *et al.*, 1999). As these orthogonal directions are equivalent only in the reduced antiferromagnetic Brillouin zone, it was argued that the high-energy pseudogap is a remnant of the antiferromagnetic undoped insulator [a similar point was made by Ronning *et al.* (1998), following the proposal of Laughlin (1995, 1997)]. However, this conclusion rests on the assumption that the dispersion of the high-energy pseudogap is equivalent to that of the hump detected in the superconducting state (see Sec. VI.A and, in particular, Figs. 53 and 54). In light of the recent detection of bilayer splitting in Bi2212 (Sec. IV.C), and of the possible correspondence of peak and hump features to antibonding and bonding bilayer split bands, this interpretation of the dispersion of the hump and high-energy pseudogap should be reconsidered (then again, as we shall discuss in Secs. VII.D and VII.E, a similar behavior has also been observed on single-layer underdoped cuprates).

Important insights also come from studies of the pseudogap as a function of temperature. Figure 60 summarizes the temperature dependence of the leading-edge midpoint positions near $(\pi,0)$ for underdoped samples with T_c of about 85 K, which shows that at these dopings the pseudogap opens up around T^* ~200 K (Ding, Yokoya, *et al.*, 1996; Harris *et al.*, 1996; Loeser *et al.*, 1996). More specifically, as reported by Norman, Ding, *et al.* (1998) in a subsequent paper, we

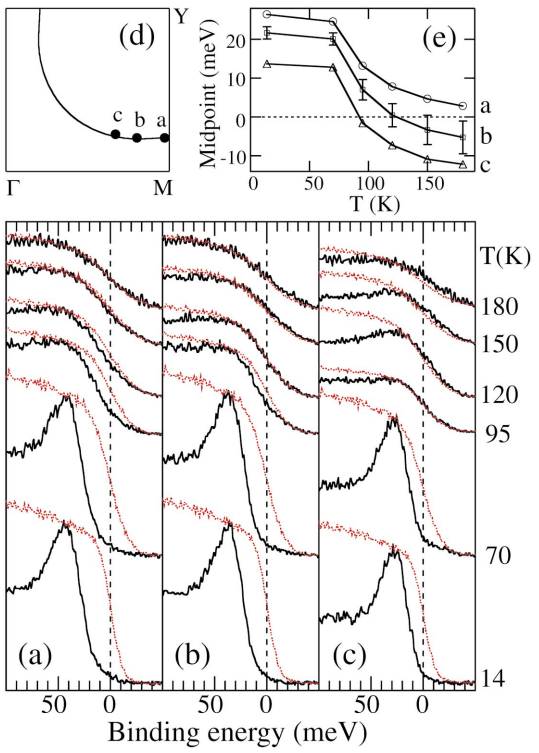

FIG. 61. Temperature and momentum dependence of the ARPES data from underdoped Bi2212 (T_c=85 K): (a)–(c) (black lines) spectra taken at different k points as sketched in (d), together with reference spectra from polycrystalline Pt (red lines). (e) Temperature dependence of the Bi2212 leading-edge midpoints. After Norman, Ding, *et al.*, 1998 (Color).

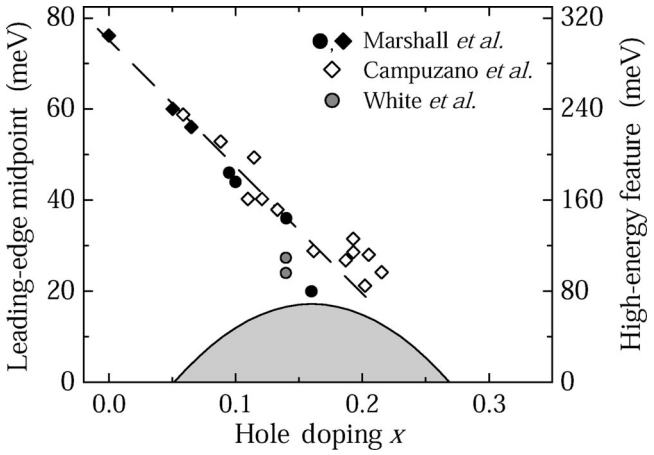

FIG. 62. Doping dependence of the pseudogap as determined by the position of leading-edge midpoint (circles, left axis) and high-energy feature (diamonds, right axis) in the $(\pi,0)$ ARPES spectra from $Bi_2Sr_2CaCu_2O_{8+\delta}$ (Bi2212) [the dome represents the d-wave mean-field approximation $\Delta(x)=4.3k_BT_c(x)/2$, left scale (Won and Maki, 1994)]. Data from Marshall *et al.* (1996); White *et al.* (1996); Campuzano *et al.*, (1999).

are dealing with a highly anisotropic gap that closes nonuniformly in momentum space as the temperature is increased. In fact, as shown in Fig. 61, the temperature at which the leading-edge midpoint coincides with the reference Fermi energy obtained from a polycrystalline Pt sample is very different for Bi2212 spectra taken at k-space points (a), (b), and (c). In particular, this happens at about 150 K at (a) and 95 K at (c). Since these results were obtained on a $T_c=85$ K underdoped sample, they indicate that gaps are already present at (a) and (b) at temperatures well above T_c.

The next important issue is the doping dependence of the normal-state gap magnitude. Figure 62 compiles data from several studies, which indicate that the pseudogap decreases monotonically upon doping. Here, in order to estimate the normal-state gap energy, we used both the position of the leading-edge midpoint and

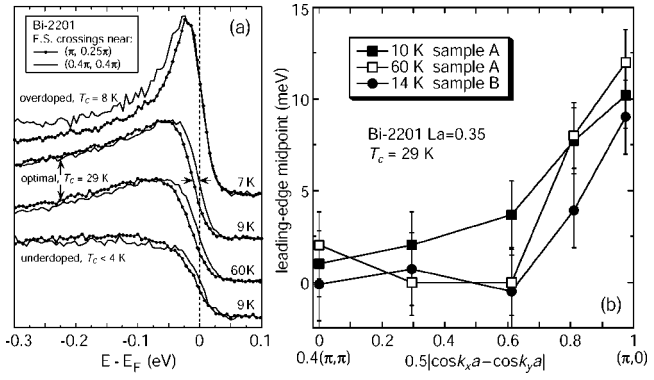

FIG. 63. Evidence for a d-wave-like pseudogap in Bi2201: (a) Bi2201 ARPES spectra measured, for different doping levels, at the Fermi surface crossings in the nodal region and close to $(\pi,0)$; (b) leading-edge midpoint shifts for slightly underdoped Bi2201 ($T_c=29$ K). After Harris *et al.*, 1997.

of the high-energy feature. Concerning the different doping dependence of the experimentally determined pseudogap and T_c lines in the underdoped regime, two alternative scenarios are usually discussed: (i) phase fluctuations and (ii) quantum critical point. The phase-fluctuation picture refers to the idea that superconductivity in the underdoped regime is determined by the phase stiffness of the superfluid,[22] which is consistent with the experimental observation that T_c in the underdoped samples is proportional to the superfluid density (Uemura *et al.*, 1991). In this view, the pseudogap would be a reflection of incoherent pair fluctuations above T_c[23] and would not scale with T_c itself. Given the similarity in the momentum dependence between the pseudogap and the superconducting gap, earlier photoemission data were mostly interpreted along these lines. In the case of the quantum-critical-point scenario, the superconducting and normal-state gaps would have different origins,[24] and the suppression of T_c in the underdoped regime would be due to the development of a competing order responsible for magnetic correlations independent of the Cu spins (Sonier *et al.*, 2001). In this context, possible microscopic descriptions for the pseudogap phase include the circulating-current phase (Varma, 1997, 1999), the charge-density wave (Castellani *et al.*, 1995), and the d-density-wave short-range fluctuations (Chakravarty *et al.*, 2001). It has to be mentioned that, in addition to scenarios (i) and (ii), there is also a class of pairing theories that explain the normal-state d-wave gap as a signature of pairing in the spin channel. These theories stem from the spin-density-wave/spin-bag approach[25] and from the strong-coupling version of the t-J or Hubbard models,[26] in which the pseudogap results from antiferromagnetic spin fluctuations and spinon pairing, respectively. Finally, there is the interpretation of the pseudogap in terms of umklapp scattering truncation of the Fermi surface near the location of the hot spots, as summarized in Fig. 15(b).[27]

B. $Bi_2Sr_2CuO_{6+\delta}$

Clear evidence for a d-wave-like pseudogap for underdoped and optimally doped Bi2201 was reported by Harris *et al.* (1997), as shown in Fig. 63 (no gap was observed for the overdoped material). On the basis of

[22]See, for instance, Doniach and Inui (1990); Uemura *et al.* (1991); Imada (1993); Emery and Kivelson (1995a, 1995b); and Kivelson *et al.* (1998).

[23]Pre-formation of Cooper pairs at the crossover temperature $T^*>T_c$ with no phase coherence, which is established only when they condense into the coherent superconducting state.

[24]See Tallon *et al.* (1999, 2000); and Tallon and Loram (2001).

[25]See, in particular, Kampf and Schrieffer (1990a, 1990b); and Kusko *et al.* (2002).

[26]See Kotliar and Liu (1988); Suzumura *et al.* (1988); Tanamoto *et al.* (1992); and Wen and Lee (1996).

[27]See Furukawa and Rice (1998); and Furukawa *et al.* (1998).

the leading-edge midpoint shift, the gap amplitude was estimated to be ~10 meV for the optimally doped sample, thus much smaller than in Bi2212 (~20–30 meV; see Fig. 62). As discussed for the case of Bi2212 (Sec. VII.A), the momentum dependence and magnitude of the normal-state pseudogap are similar to those of the superconducting gap, which may imply a common origin for the two features. Furthermore, as we shall see in Sec. VII.D, the magnitude of the pseudogap in Bi2201, in particular as estimated from the position of the leading-edge midpoint, is comparable to the results obtained for LSCO. Given that Bi2201 and LSCO are characterized by a similar value of $T_c^{\max} \simeq 34-38$ K, much lower than the ~95 K of Bi2212 [see, for example, Eisaki *et al.* (2002)], these findings suggest a direct correlation between $T_c^{\max}$ and the size of the pseudogap (and/or superconducting gap) for the different families of cuprates.

C. $Bi_2Sr_2Ca_2Cu_3O_{10+\delta}$

The pseudogap in Bi2223 has been recently studied by Feng, Damascelli, *et al.* (2002) and Sato, Matsui, *et al.* (2002), on nearly optimally doped samples ($T_c = 108$ K). The (π,0) ARPES spectra and the results obtained by symmetrizing the spectra with respect to E_F [as defined by Norman, Randeria, *et al.* (1998)] are presented as a function of temperature in Figs. 64(a) and (b). At low temperature, a large superconducting gap is clearly visible, as discussed in Sec. V.C. However, as emphasized by the direct comparison between the 170-K symmetrized spectrum and those taken at $T \geqslant 125$ K [Fig. 64(b)], the gap is still open at $T \simeq T_c$ and it does not close until $T^* \simeq 135$ K (as revealed by the suppression of the low-energy spectral weight). Note that the absolute difference between T_c and T^* is rather small in this case, presumably because the doping level is very close to optimal. Similar results were reported by Feng, Damascelli, *et al.* (2002), who showed that a gap is present at spectra taken above T_c near (π,0) but not along the nodal direction, which suggests a *d*-wave symmetry for the pseudogap in Bi2223.

D. $La_{2-x}Sr_xCuO_4$

The investigation of the normal-state pseudogap in LSCO by ARPES has been complicated by the poor stability of the cleaved surface at temperatures higher than T_c, even in ultrahigh vacuum. Therefore the first evidence for this phenomenon in LSCO was reported by Ino *et al.* (1998) on the basis of angle-integrated photoemission experiments, in which clean surfaces were obtained by repeatedly scraping (i.e., every 40 min) the sample surface *in situ* with a diamond file (procedure which obviously prevents the acquisition of angle-resolved spectra, due to the roughness of the scraped surface). These data show a systematic depression of the density of states (more pronounced at lower dopings), which was considered indicative of a pseudogap with an energy scale of 100–200 meV at 5–10 % doping.

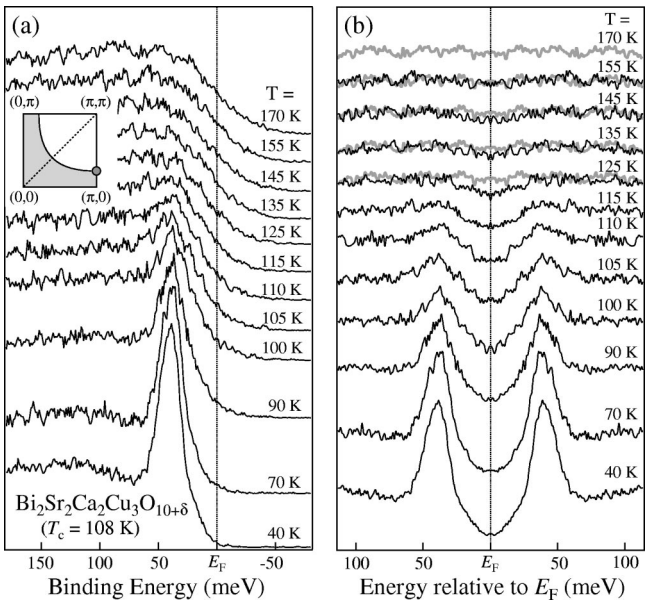

FIG. 64. Temperature dependent ARPES spectra measured on Bi2223 in correspondence with the underlying Fermi-surface crossing along the (π,0)-(π,π) direction: (a) raw spectra; (b) symmetrized spectra (the 170-K spectrum, gray thick line, is superimposed to those taken at $T \geqslant 125$ K for comparison). From Sato, Matsui, *et al.*, 2002.

Using a similar procedure, Sato, Yokoya, *et al.* (1999) investigated the temperature dependence of the pseudogap in optimally doped LSCO ($x = 0.15$, $T_c = 38$ K). In order to extract a more direct representation of the density of states near the Fermi level, these authors divided the spectra by the Fermi-Dirac distribution function (at the corresponding temperature) convoluted with a Gaussian (to account for the instrumental resolution of 7 meV). In contrast to what is observed in a normal metal like Au (inset of Fig. 65), on LSCO the intensity close to the Fermi level ($\leqslant 30$ meV) increased smoothly as the temperature was raised (Fig. 65). This effect was observable over a temperature range much larger than T_c, and thus provided direct evidence for the existence of a normal-state pseudogap.

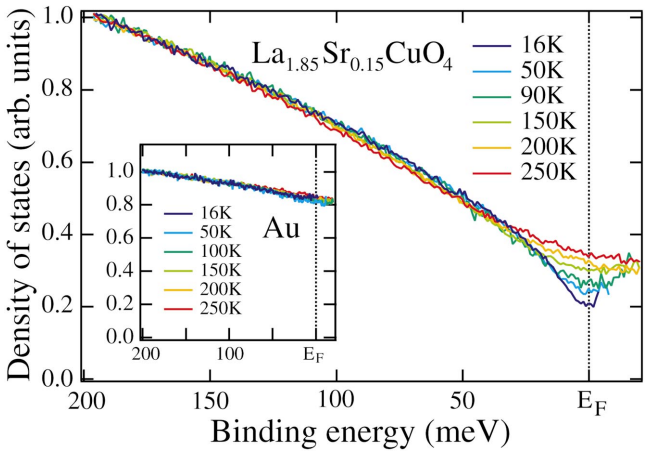

FIG. 65. Density of states for optimally doped LSCO ($T_c = 38$ K) and polycrystalline Au. After Sato *et al.*, 1999 (Color).

Detailed angle-resolved investigations of the pseudogap in LSCO were recently reported by Ino *et al.* (2002) and Yoshida (2001). As shown in Fig. 66(a), where the shift of the leading-edge midpoint along the underlying Fermi surface is presented for 10%-doped LSCO, a clear gap is observable close to $(\pi,0)$ but not at $(\pi/2,\pi/2)$, with an overall momentum dependence consistent with the d-wave functional form [Fig. 66(b)]. Note that the spectra presented in Fig. 66 were taken at the temperature of 30 K, not much higher than $T_c = 29$ K. This was necessary in order to avoid aging of the sample surface over the time required to obtain a complete set of data in momentum space. It has to be emphasized, however, that temperature-dependent ARPES experiments restricted to the $(\pi,0)$ region show that the gap is still open at temperatures as high as 90 K and therefore well into the normal state, consistent with the results presented in Fig. 65. Regarding the absolute magnitude of the pseudogap and its doping evolution, detailed estimates could also be obtained from angle-resolved experiments [Fig. 67(a)]. The results for the high-energy pseudogap at $(\pi,0)$ and the low-energy pseudogap at the underlying Fermi vector near $(\pi,0)$ are presented in Figs. 67(b) and (c), respectively. As in the case of the Bi-based high-T_c superconductors, these findings support the picture of a smooth evolution of the pseudogap into the superconducting gap as the doping is increased. Furthermore, as mentioned in Sec. VII.B, the results from these two different families indicate a direct scaling of the leading-edge pseudogap with $T_c^{\max}$.

It was noted that the doping dependence of the high-energy pseudogap [Fig. 67(b)] indicates that this effect is intimately related to the anomalous behavior seen in thermodynamics and transport properties. For $x < 0.2$ along with the opening of the pseudogap, one observes a suppression of the electronic specific heat and a decrease of the effective mass (Ino *et al.*, 1998, 2002). This suggests that a decrease in the density of states (or carriers) is responsible for the metal-insulator transition in LSCO, and not a divergence of the effective mass

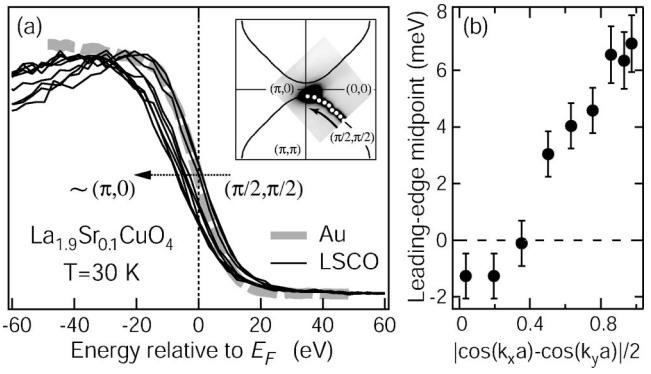

FIG. 66. Angle-resolved investigations of the pseudogap in LSCO: (a) ARPES spectra from along the Fermi-surface contour (see inset) measured at 30 K with 55.5-eV photons on 10%-doped LSCO ($T_c = 29$ K); a spectrum from polycrystalline Au is shown for comparison; (b) corresponding momentum dependence of the leading-edge gap. After Yoshida, 2001.

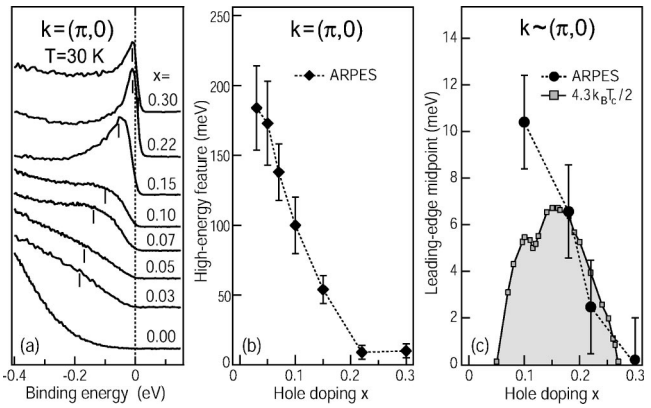

FIG. 67. Doping dependence of (a) the LSCO ARPES spectra ($h\nu = 55.5$ eV); (b) the high-energy feature at $(\pi,0)$; and (c) the leading-edge midpoint in correspondence with the underlying Fermi surface near $(\pi,0)$. The points in (c) and the spectra in (a) are only apparently at variance (see, for example, $x = 0.1$): the results are not from the exact same momenta (Yoshida, 2001). The dome in (c) is the d-wave mean-field approximation $\Delta(x) = 4.3 k_B T_c(x)/2$ (Won and Maki, 1994).

(Imada *et al.*, 1998), which is consistent with the decrease of coherent quasiparticle weight observed upon reducing the doping level [Fig. 67(a)].

E. $Ca_{2-x}Na_xCuO_2Cl_2$

Many attempts have been made to connect the electronic structure of the doped high-T_c superconductors to that of an insulator. This is also the case in the context of the pseudogap discussion, as many believe that the pseudogap is a quantity that can already be defined in an insulator. Since the best insulator data were collected on SCOC and CCOC, and the best metal data were obtained on Bi2212, it is natural that the possibility of such a connection has been most intensively explored for these two families of materials. The first explicit attempt in this direction was made by Laughlin (1995), who showed that the $(\pi,0)$ ARPES spectra evolve continuously from one system to another, making a strong case for the high-energy broad peak's being derived from the insulator. The idea of a pseudo or remnant Fermi surface discussed in Sec. IV.A.2 was inspired by this approach, which suggested considering the evolution of the $(\pi,0)$ spectra in terms of a gap evolution rather than a trivial band dispersion in the insulator.

The $(\pi,0)$ spectra from Bi2212, Dy-Bi2212, and CCOC are compared in Fig. 68(b) (Ronning *et al.*, 1998), which shows a smooth evolution of line shapes and peak positions (see arrows): with underdoping, the quasiparticle peak at $(\pi,0)$ broadens and shifts to higher binding energies. Note that for CCOC the zero in energy does not correspond to E_F but to the peak position at $(\pi/2,\pi/2)$ which, in turn, corresponds to the top of the valence band located ~ 700 meV below E_F because of the presence of the Mott-Hubbard gap. The high-energy pseudogap [Fig. 68(b)] is characterized by a d-wave-like dispersion not only in the underdoped systems but also

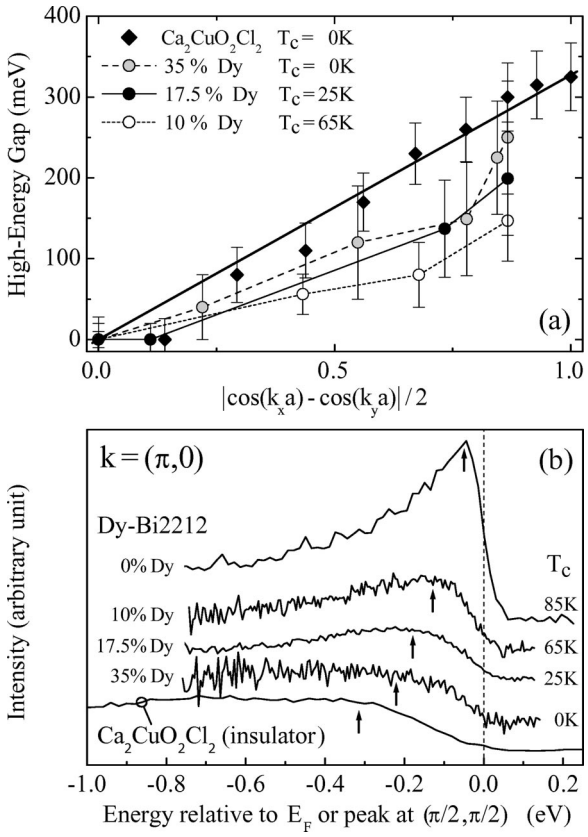

FIG. 68. Comparison of the pseudogap behavior in several cuprates: (a) high-energy pseudogap plotted vs $|\cos k_x - \cos k_y|/2$ for CCOC and Dy-Bi2212; (b) doping dependence of the $(\pi,0)$ ARPES spectra measured at 100 K with 25.2-eV photons on CCOC, and at 110 K with 22.4-eV photons on Dy-Bi2212. After Ronning *et al.*, 1998.

in the undoped insulator. This is shown in Fig. 68(a), where the dispersion of the high-energy pseudogap along the Fermi surface (remnant Fermi surface for CCOC) is plotted against the d-wave functional form (a fit for CCOC is shown). Although their sizes vary, the superconducting gap, the pseudogap of the underdoped system, and the gap of the insulator have a similar d-wave form, suggesting a common origin (Zacher, Hanke, *et al.*, 2000). This is consistent with the idea of one underlying symmetry principle that unifies the antiferromagnetic insulator and the d-wave superconductor (Zhang, 1997; Zacher, Hanke, *et al.*, 2000).

Recently, single crystals of Na-doped CCOC have been made available (as discussed earlier in Sec. IV.A), which allowed the study of the doping evolution from insulator to superconductor within the same material family (Kohsaka *et al.*, 2002; Ronning, Sasagawa, *et al.*, 2003). The $(\pi,0)$ spectra from 10%-doped Na-CCOC [Fig. 20(a)] and CCOC [Fig. 68(b)] exhibit the same line shape, although the insulator data are shifted below E_F by $\sim$700 meV (Ronning, Sasagawa, *et al.*, 2003). Furthermore, as shown in Fig. 21(b), the 10%-Na-doped sample is characterized by a Fermi arc centered around the nodal region, while around $(\pi,0)$ the spectra are pushed to much higher energies. This behavior is almost identical to that seen for underdoped Bi2212 in Fig. 58, which supports the earlier conclusions based on the comparison between CCOC and Bi2212 at various dopings. Hence these findings make a strong case for the high-energy pseudogap having its origin in the electronic structure of the insulator. In addition, regarding possible complications due to bilayer splitting effects in the $(\pi,0)$ data from Bi2212, it has to be emphasized that the similar behavior observed for single-layer Na-CCOC and bilayer Bi2212 provides further support for the presence of two energy scales in the pseudogap phenomenon and for their observed doping evolution.

F. Discussion

The results from Bi2201, Bi2212, and LSCO, with the presence of two-energy scales for both single- and double-layer materials, indicate the generality of the pseudogap phenomenology. The low-energy pseudogap smoothly evolves into the superconducting gap upon going from the underdoped to the overdoped regime. Both gaps exhibit the same overall d-wave symmetry. Furthermore, the magnitude of the leading-edge pseudogap scales with the maximum T_c of the different high-T_c superconductor families. The high-energy pseudogap, which allows a more meaningful description of the data in the very underdoped regime, seems to originate from the antiferromagnetic insulator, as first proposed on the basis of CCOC and Bi2212 data. In this regard, more direct evidence is provided by the results from Na-CCOC. The similar d-wave forms observed for the superconducting gap, the pseudogap of the underdoped system, and the angular-dependent part of the gap along the remnant Fermi surface of the insulator suggest a common origin for these different excitation gaps (Zacher, Hanke, *et al.*, 2000) and the existence of a unifying symmetry principle for the antiferromagnetic insulator and the d-wave superconductor (Zhang, 1997; Zacher, Hanke, *et al.*, 2000). However, as discussed in detail by Ronning, Kim, *et al.* (2003), an important caveat is the rounded electronic dispersion observed near the nodes of the d-wave functional form for both the superconducting and the normal-state gap. This finding, which is also consistent with the observations of Fermi arcs rather than a uniformly gapped Fermi surface in the pseudogap regime (Figs. 21, 58, and 61), suggests that high-order harmonics may have to be included in the expansion of the gap function (Mesot *et al.*, 1999; Guinea *et al.*, 2002), as already discussed in Secs. V.A and V.G. This would in fact account for the lack of a well-defined V-like cusp in the gap momentum dependence in the nodal region. The presence or absence of such a cusp is critical in discriminating between different microscopic models connecting the antiferromagnetic insulator to the d-wave superconductor.

Note that the detection of a d-wave-like pseudogap and, in particular, an increase in its maximum amplitude at $(\pi,0)$ upon reducing doping, emphasize the inadequacy of a rigid-band description of the electronic structure of the high-T_c superconductors (King *et al.*, 1995). In other words, the evolution from insulator to

overdoped metal cannot be described in terms of a simple shift of the chemical potential in a rigid-band picture. As shown in Fig. 19, in the insulator the binding energies of the lowest-energy states at $(\pi/2,\pi/2)$ and $(\pi,0)$ differ by $\sim$300 meV, while in the overdoped metal a Fermi level crossing can be found near both momenta; the rigid shift of chemical potential would instead result in Fermi-surface pockets closed around $(\pi/2,\pi/2)$.

VIII. SELF-ENERGY AND COLLECTIVE MODES

As discussed in Sec. II.C, the introduction of the electron self-energy $\Sigma(\mathbf{k},\omega)=\Sigma'(\mathbf{k},\omega)+i\Sigma''(\mathbf{k},\omega)$ is a powerful way to account for many-body correlations in solids. Its real and imaginary parts correspond, respectively, to energy renormalization with respect to the bare-band energy $\epsilon_{\mathbf{k}}$ and to the finite lifetime of the quasiparticles in the interacting system. Owing to the energy and momentum resolution now achievable (Sec. II.E), both components of the self-energy can in principle be estimated very accurately from an analysis of the ARPES intensity in terms of *energy distribution curves* (EDC's) and/or *momentum distribution curves* (MDC's).[28] In some cases the MDC analysis may be more effective than the analysis of the EDC's in extracting information on the self-energy, as noted by Valla, Fedorov, Johnson, Wells, *et al.* (1999), who first used this approach for Bi2212, as shown in Figs. 7 and 74 [in this regard it should be emphasized that the momentum space scan method to extract information about the electronic band structure was first introduced by Aebi, Osterwalder, and co-workers (Aebi *et al.*, 1994); Osterwalder *et al.*, 1995; Schwaller *et al.* 1995)]. In particular, the EDC's are typically characterized by a complex line shape (Fig. 7) because of the nontrivial ω dependence of the self-energy [see, for example, Eqs. (17) and (18)], the presence of additional background (Sec. II.D), and the low-energy cutoff due to the Fermi function. Furthermore, as can be seen by the generic expression for the spectral function $A(\mathbf{k},\omega)$ in Eq. (14), the EDC peak position is determined by $\Sigma'(\mathbf{k},\omega)$ as well as $\Sigma''(\mathbf{k},\omega)$, because both terms are strongly energy dependent. On the other hand, if the self-energy is independent of k normal to the Fermi surface (and the matrix elements are a slowly varying function of k), then the corresponding MDC's are simple Lorentzians centered at $k=k_F+[\omega-\Sigma'(\omega)]/v_F^0$ with FWHM given by $2\Sigma''(\omega)/v_F^0$, where v_F^0 is the bare Fermi velocity normal to the Fermi surface.[29] Indeed, Lorentzian line shapes were observed experimentally for the MDC's (Figs. 7 and 74), and this approach has been extensively used in the literature, as we shall see throughout this section. However, it has to be noted that, although the results of MDC and EDC analyses should coincide, differences in both dispersions and peak widths can be observed, in particular at high energies, due to the ω dependence of $\Sigma(\mathbf{k},\omega)$, or near the band maxima and minima (see, for example, the simulations in Fig. 72 below).

As we shall elaborate in Secs. VIII.B and VIII.C, the peak-dip-hump structure and the corresponding step edge in $\Sigma''(\mathbf{k},\omega)$ observed for the cuprates are the hallmarks of quasiparticles interacting with a dispersionless collective bosonic mode. As a matter of fact, this problem has been studied in great detail for the strong-coupling BCS superconductors, in which the bosonic mode is an Einstein phonon (Engelsberg and Schrieffer, 1963; Schrieffer, 1964; Scalapino, 1969). Therefore, before discussing the specific case of the cuprate high-temperature superconductors, in the following section we shall briefly review the effects of electron-phonon coupling on the ARPES spectra from simple metallic surfaces, for which, given that the electron-electron interaction is relatively unimportant, the established theoretical formalism can be applied very effectively.[30]

A. Electron-phonon coupling on metallic surfaces

The electron-phonon interaction involving surface phonons and the $\overline{\Gamma}$ surface state on the Be(0001) surface was investigated by two groups, who drew qualitatively similar conclusions (Balasubramanian *et al.*, 1998; Hengsberger, Fresard, *et al.*, 1999; Hengsberger, Purdie, *et al.*, 1999; LaShell *et al.*, 2000). Figure 69(a) shows the results of Hengsberger, Purdie, *et al.* (1999) for the Be(0001) surface state along the $\overline{\Gamma M}$ direction of the surface Brillouin zone; a feature is seen dispersing towards the Fermi level. Close to E_F, the spectral function exhibits a complex structure characterized by a broad hump and a sharp peak, with the latter being confined to within an energy range given by the typical bandwidth ω_{ph} of the surface phonons. This behavior corresponds to a two-branch splitting of the near-E_F dispersion, with a transfer of spectral weight between the two branches as a function of binding energy [this is more clearly shown by the simulation presented in Fig. 69(b)]. While the high-energy dispersion is representative of bare quasiparticles, at low energy the dispersion is renormalized by the electron-phonon interaction (this behavior is shown, for a similar electron-phonon coupled system, in the inset of Fig. 70). In other words, the weaker dispersion observed at energies smaller than ω_{ph} describes dressed quasiparticles with an effective mass enhanced by a factor of $(1+\lambda)$, where λ is the electron-phonon coupling parameter (Ashcroft and Mermin, 1976). This coupling can be estimated from the ratio of renormal-

[28]This is one of the features that make ARPES such a powerful tool for the investigation of complex materials, as exemplified by the recently reported experimental determinations of many-body effects in different systems. For reviews, see Gweon *et al.* (2001); Johnson, Fedorov, and Valla (2001); Kevan and Rotenberg (2001).

[29]This is obtained by approximating $\epsilon_{\mathbf{k}}\simeq v_F^0(k-k_F)$ in the spectral function $A(\mathbf{k},\omega)$ in Eq. (14) (Kaminski *et al.*, 2001).

[30]See Balasubramanian *et al.* (1998); Hofmann *et al.* (1998); Hengsberger, Fresard, *et al.* (1999); Hengsberger, Purdie, *et al.* (1999); Valla, Fedorov, Johnson, Wells, *et al.* (1999); LaShell *et al.* (2000); and Rotenberg *et al.* (2000).

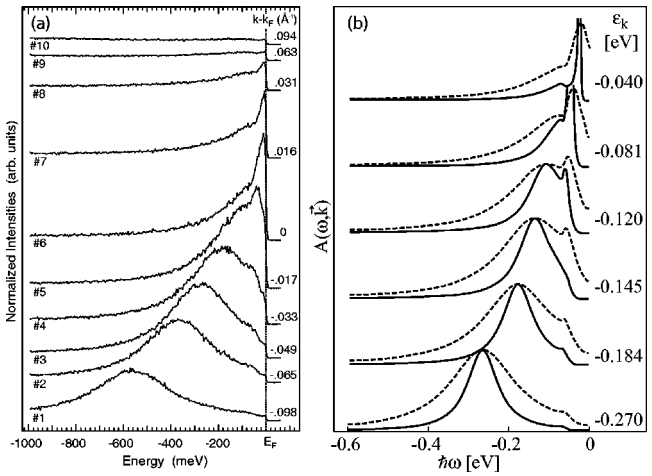

FIG. 69. The electron-phonon interaction on the Be(0001) surface: (a) ARPES spectra for the Be(0001) surface state measured at 12 K with (HeI) 21.2-eV photons (after Hengsberger, Purdie, *et al.*, 1999); (b) spectral function within the Debye model for $\omega_D = 65$ meV and $\lambda = 0.65$ with (dashed) and without (solid) impurity scattering. After LaShell *et al.*, 2000.

ized ($\mathbf{v_k}$) and bare ($\mathbf{v_k^0}$) quasiparticle velocities, according to the relation $\mathbf{v_k} = \hbar^{-1}\partial\varepsilon_\mathbf{k}/\partial\mathbf{k} = (1+\lambda)^{-1}\mathbf{v_k^0}$, which for the data presented in Fig. 69(a) gives the value $\lambda = 1.18$ [note that alternatively λ could be estimated from the temperature dependence of the linewidth near E_F (Balasubramanian *et al.*, 1998)]. In a followup paper, Hengsberger, Purdie, *et al.* (1999) provided a more detailed analysis of the data by also including the effects of impurities and electron-electron interactions, which, however, led to similar conclusions.

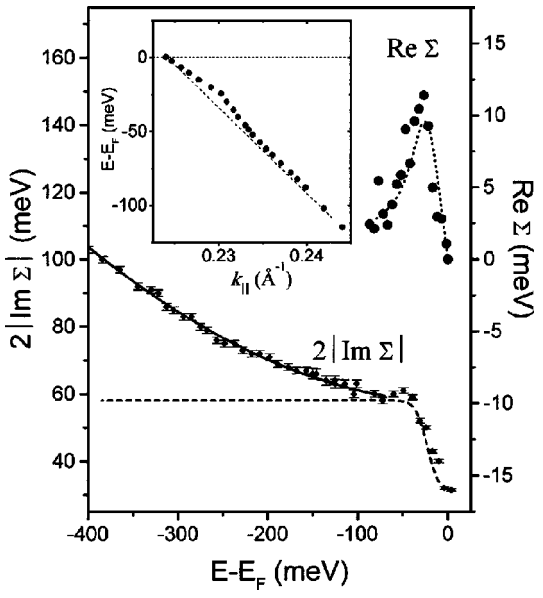

FIG. 70. Self-energy $\Sigma(\mathbf{k},\omega)$ estimated from the Mo(110) surface-state ARPES spectra, and corresponding quasiparticle dispersion (inset): dotted line, calculated electron-phonon contributions to the real part of $\Sigma(\mathbf{k},\omega)$; dashed line, contribution to the imaginary part of $\Sigma(\mathbf{k},\omega)$ (the latter was offset by 26 meV to account for impurity scattering). After Valla, Fedorov, Johnson, and Hulbert, 1999.

A slightly different analysis of similar data from Be(0001) was performed by LaShell *et al.* (2000). In this case, the authors used the isotropic zero-temperature Debye model with a constant electron-phonon interaction matrix element to express the Eliashberg coupling function (i.e., the phonon density of states weighted by the electron-phonon coupling strength) as $\alpha^2F(\omega) = \lambda(\omega/\omega_D)^2$, for $\omega < \omega_D$, and otherwise zero (here ω_D is the maximum phonon energy, and the dimensionless mass renormalization parameter λ represents the coupling strength). Within the above approximation the electron-phonon contribution to the self-energy $\Sigma(\mathbf{k},\omega)$, if effectively treated as momentum independent, can be calculated from $|\Sigma''(\omega)| = \pi\hbar\int\alpha^2F(\omega')d\omega'$. For real ($\Sigma'$) and imaginary ($\Sigma''$) parts one obtains

$$\Sigma'(\omega) = -(\lambda\hbar\omega_D/3)\times[(\omega/\omega_D)^3\ln|(\omega_D^2-\omega^2)/\omega^2| + \ln|(\omega_D+\omega)/(\omega_D-\omega)| + \omega/\omega_D],$$
$$|\Sigma''(\omega)| = \hbar\lambda\pi|\omega|^3/(3\omega_D^2), \quad |\omega| < \omega_D,$$
$$|\Sigma''(\omega)| = \hbar\lambda\pi\omega_D/3, \quad |\omega| > \omega_D. \tag{25}$$

The corresponding spectral function is shown in Fig. 69(b) for parameter values $\lambda = 0.65$ and $\omega_D = 65$ meV; it qualitatively reproduces the basic features of the ARPES spectra presented in Fig. 69(a), and in particular the double structure with a dip at approximately ω_D. By assuming the self-energy to be independent of (or weakly dependent on) momentum, a fact that is qualitatively consistent with the Lorentzian line shape of the MDC's (see previous section), LaShell *et al.* (2000) extracted $\Sigma(\omega)$ using only the free parameter ϵ_k, which they took as a second-order polynomial, imposing the additional condition that $\Sigma'(\omega)$ must vanish at $\omega = 0$ and $\omega \to \infty$. These results are in good agreement with theoretical simulations based on the Debye model.

Another example of an electron-phonon coupled system is the surface state of Mo(110) studied by Valla, Fedorov, Johnson, and Hulbert (1999). In this case, the real and imaginary parts of the self-energy shown in Fig. 70 were obtained directly from an EDC analysis: Σ'' corresponds to the EDC width and Σ' to the difference between the observed quasiparticle dispersion and a straight line approximating the dispersion of a noninteracting system (Fig. 70, inset). The steplike change at 30 meV in Σ'' is interpreted as the phonon contribution (dashed line), and the parabolic part at higher energies is attributed to electron-electron interactions. The phonon contribution to the real part of the self-energy is calculated from the Kramers-Kronig relations (see Sec. II.C) and agrees well with the data (dotted line). As an additional confirmation of the electron-phonon description, it was also noted that the observed temperature dependence of the scattering rate is well reproduced by the calculations (Valla, Fedorov, Johnson and Hulbert, 1999). The difference between the Mo(110) results and those from Be(0001), or the simulations presented in Fig. 69(b), is that no double structure is seen directly in the EDC's for the Mo(110) surface state, although one should expect it for the parameters extracted from the

experiment. The reason for this discrepancy probably lies in the energy scale of the Debye frequency, which is about 30 and 65 meV for Mo and Be, respectively. For $\omega_D = 30$ meV the complex line shape is probably smeared out because of impurities or finite resolution.

A similar manifestation of two-branch splitting in the ARPES spectra as a consequence of electron-phonon coupling was observed for hydrogen and deuterium adsorbed onto the W(110) surface (Rotenberg *et al.*, 2000). In this case, direct coupling between an adsorbate optical phonon and an intrinsic surface electronic state was signalled by the hydrogen/deuterium isotope effect.

B. Self-energy effects in the high-T_c superconductors

1. The (π,0) region

Earlier ARPES investigations of self-energy corrections in the cuprates focused on the antinodal (π,0) region of Bi2212, where across T_c the line shape evolves into the well-known peak-dip-hump structure discussed in Sec. VI.A. However, as recently recognized and elaborated in detail in Sec. IV.C.2, the (π,0) spectra from Bi2212 are severely distorted by bilayer splitting effects.[31] In particular, the results reported by Kordyuk *et al.* (2002b) and Gromko, Fedorov, *et al.* (2002) most convincingly suggested that the peak and hump observed in the superconducting state correspond to antibonding and bonding bilayer split bands, at *any* doping levels (i.e., even at underdoping and optimal doping). This invalidates much of the quantitative line-shape analysis of data from this momentum-space region. However, as the methodology is very instructive, we will nevertheless review the literature devoted to this issue.

There are two distinct approaches to obtaining a more detailed understanding of the peak-dip-hump structure seen at (π,0) in the superconducting state:

(i) The development of a way to extract self-energy information directly from the ARPES data. The essence of this approach is that one does not need input from any microscopic model. Thus it may in principle allow one to analyze the data with no preconceived judgment. The price to pay is that certain approximations are necessary and, as a consequence, one has to be cautious in the quantitative evaluation of the final results.[32]

(ii) The analysis of the photoemission data within the context of a specific microscopic model.[33] Within this approach, analogous to the case of the electron-phonon coupled systems discussed in Sec. VIII.A, the peak-dip-hump structure would result from coupling between the quasiparticles and a collective bosonic mode. In this case the latter is assumed to be electronic in nature and, in particular, the so-called $Q=(\pi,\pi)$ resonant magnetic mode observed in inelastic neutron-scattering experiments in YBCO (Rossat-Mignod *et al.*, 1991; Mook *et al.*, 1993; Fong *et al.*, 1995) and Bi2212 (Mook *et al.*, 1998; Fong *et al.*, 1999). Related to this scenario is the approach schematically summarized in Fig. 71, which emphasizes that the $Q\simeq(\pi,\pi)$ scattering will severely affect the (π,0) spectra (i.e., cause broadening due to the simultaneous excitation of collective modes). As a consequence of the sharpening of the quasiparticle pole in the superconducting state, a sharp peak would eventually emerge below T_c, as was observed in the experiments.

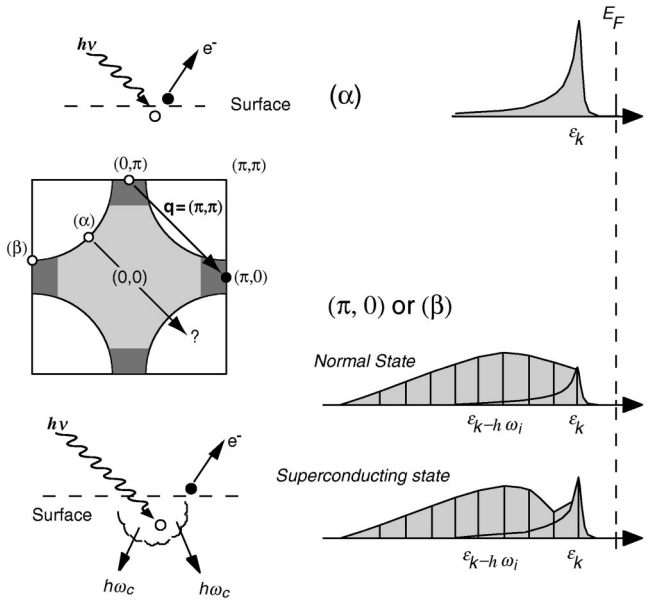

FIG. 71. Photoemission process and corresponding line shape for (α) weak coupling and (β) or (π,0) strong coupling. Phase-space considerations for quasiparticles coupled to (π,π) collective modes are sketched. From Shen and Schrieffer, 1997.

It should be noted that the connection between the (π,0) peak-dip-hump structure and a sharp electronic resonant mode in the cuprates was first proposed by Norman *et al.* (1997), following earlier work on electron-phonon coupling (Engelsberg and Schrieffer, 1963; Scalapino, 1969). Figure 72 reproduces the calculations performed at two different momenta in the superconducting state for electrons coupled to a collective mode of energy Ω_{res} as well as a gapped continuum, which accounts for the complete spin excitation spectrum (Eschrig and Norman, 2002a). As a result of the interaction, the spectral function is characterized by a peak-dip-hump-like line shape as well as a *break* and *two-branch behavior* (i.e., for peak and hump) in the EDC-derived quasiparticle dispersion. The energy of the dip and dis-

[31] See Chuang *et al.* (2001a, 2001b); Feng, Armitage, *et al.* (2001); Borisenko *et al.* (2002); Feng, Kim, *et al.* (2002); Gromko, Fedorov, *et al.* (2002); Kordyuk *et al.* (2002b).

[32] See Norman *et al.* (1997, 1999); Norman, Randeria, *et al.* (1998); Norman and Ding (1998); Norman (2001).

[33] See Norman *et al.* (1997); Shen and Schrieffer (1997); Norman and Ding (1998); Abanov and Chubukov (1999); Campuzano *et al.* (1999); Eschrig and Norman (2000, 2002a, 2002b); Norman (2001).

persion kink is comparable to that of the $(\pi,0)$ superconducting-state peak plus Ω_{res}. This behavior is particularly evident in the $(\pi,0)$ region [Figs. 72(a) and (b)], but similar although weaker effects can also be seen along the nodal direction [Figs. 72(c) and (d)]. An obvious difference between the two momentum-space regions in Fig. 72 comes from the anisotropy of the d-wave superconducting gap: while the quasiparticle peak crosses E_F with a linear dispersion along (0,0)-(π,π), it disperses backward losing spectral weight for $k>k_F$ around $(\pi,0)$, where the gap along the Fermi surface is maximum. In Fig. 72 it should also be noted that the two-branch behavior seen in the EDC's corresponds to a *kink* in the MDC-derived quasiparticle dispersion, which emphasizes the crossover between high- and low-energy branches.

The agreement between the above calculations and ARPES data such as those presented in Figs. 53, 54, and 76 was taken as evidence for the validity of this approach. Furthermore, as mentioned above, according to the magnetic-mode scenario the energy separation between peak and dip in the ARPES spectra [Fig. 73(a)] should correspond to the energy Ω_{res} of the mode itself (Campuzano *et al.*, 1999). Indeed, some correlation between these characteristic energies was experimentally observed over a broad doping range, as shown in Fig. 73(b), where ARPES and inelastic neutron-scattering data are compared. Campuzano *et al.* (1999) argued that these results, which have also been confirmed by more recent photoemission and neutron data reported for the very same sample by Mesot, Boehm, *et al.* (2001), provide more direct evidence for the bosonic mode's being the (π,π) resonant magnetic mode. However, in light of the recent detection of bilayer splitting effects that

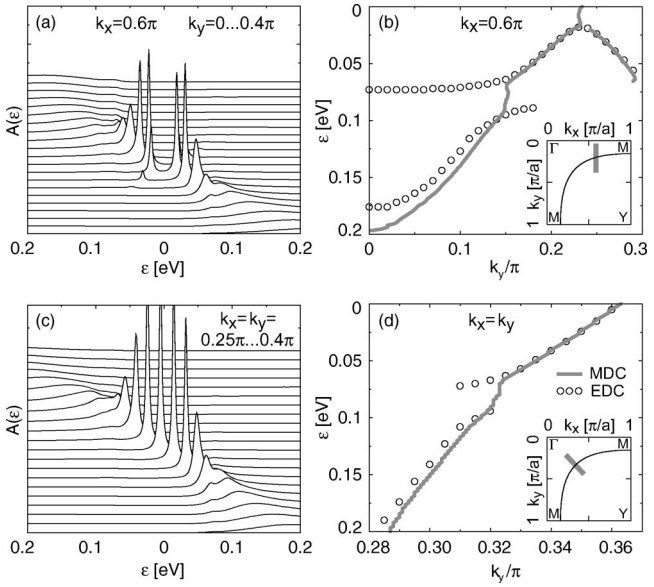

FIG. 72. Resonant magnetic-mode model calculations: (a), (c) electron removal and addition spectra; (b),(d) corresponding momentum-distribution-curve and energy-distribution-curve-derived dispersions, for momentum-space cuts parallel to M-Y (top panels) and to the nodal direction Γ-Y (bottom panels). After Eschrig and Norman, 2002a.

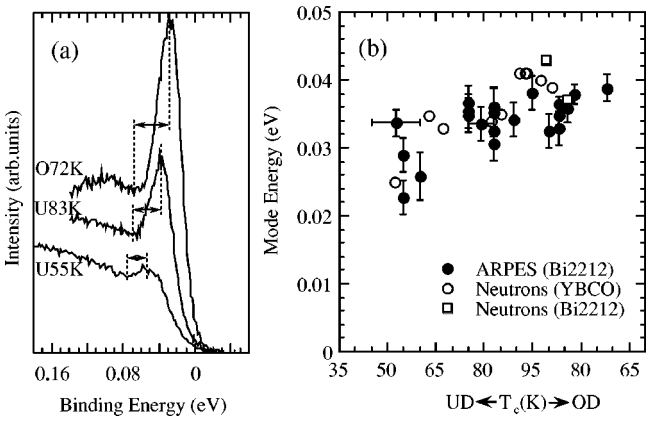

FIG. 73. Doping dependence of (a) the $(\pi,0)$ ARPES spectra from Bi2212; (b) the collective-mode energy as inferred from the ARPES spectra (i.e., difference between peak and dip positions) and neutron data. After Campuzano *et al.*, 1999.

dominate the $(\pi,0)$ spectra (with an energy scale coinciding with that of peak and hump), this quantitative comparison of neutrons and Bi2212 ARPES data needs to be carefully reevaluated (see, for example, Eschrig and Norman, 2002a, 2002b).

2. The nodal direction

As the data from Bi2212 along the (0,0)-(π,π) direction are not complicated by superstructure contaminations [at least along ΓY, as shown in Figs. 28 and 30(a) and (b)] or bilayer splitting effects (see Figs. 31 and 32), in principle the quasiparticle line-shape analysis in this region of momentum space should be more reliable. In this context, detailed ARPES studies of the single-particle self-energy have been very recently reported by several groups.[34] Interestingly, from a temperature dependence study on optimally doped Bi2212 (the corresponding ARPES data for the particular temperature of 48 K are shown in Fig. 7), Valla, Fedorov, Johnson, Wells, *et al.* (1999) reported that the width of the Lorentzian-like MDC's at E_F decreased linearly as a function of temperature (see Fig. 74), similar to what is observed for the scattering rate in normal-state resistivity data and consistent with the marginal Fermi-liquid (MFL) description (Varma *et al.*, 1989; see Sec. II.C). Furthermore, this behavior seemed to persist smoothly into the superconducting state in contrast to what is seen by transport and optical measurements. The linear dependence of the scattering rate on temperature (at small binding energies) and on energy (at large binding energies), with no indications of an extraneous energy scale set by conventional sources of quasiparticle scattering,

[34]See Valla, Fedorov, Johnson, Wells, *et al.* (1999); Bogdanov *et al.* (2000); Kaminski *et al.* (2000); Valla *et al.* (2000); Johnson and Valla (2001); Kaminski *et al.* (2001); Lanzara *et al.* (2001); and Yusof *et al.* (2002).

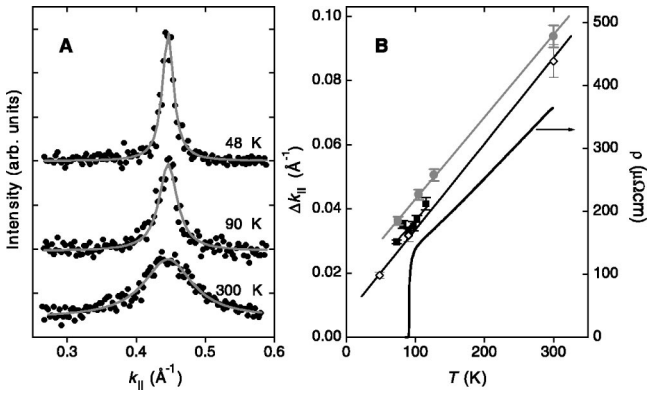

FIG. 74. Temperature-dependent photoemission results from optimally doped Bi2212 ($T_c = 91$ K): (a) momentum distribution curves (MDCs) at E_F measured along the nodal direction with 21.2-eV photons; (b) corresponding MDC widths vs temperature for three different samples (symbols), together with dc resistivity data (Valla, Fedorov, Johnson, Wells, *et al.*, 1999).

was considered by Valla, Fedorov, Johnson, Wells, *et al.* (1999) to be a signature of a nearby quantum critical point.[35]

However, evidence of an additional energy scale in the quasiparticle self-energy, at least below T_c, was later reported by two other groups (Bogdanov *et al.*, 2000; Kaminski *et al.*, 2000; Lanzara *et al.*, 2001). Kaminski *et al.* (2000) observed a clear drop in the low-energy scattering rate, in particular below T_c, as estimated from the width of the EDC's measured along the nodal direction on optimally doped Bi2212. This behavior is shown in Fig. 75, where the scattering rates obtained from ARPES and optical experiments are compared for two different temperatures above and below T_c. In addition, from an analysis of both EDC's and MDC's made on Bi2212 for several dopings along the (0,0)-(π,π) direction, Bogdanov *et al.* (2000) found a kink at approximately 50 ± 15 meV in the quasiparticle dispersion [see Fig. 78, which shows, in addition to the Bi2212 results, similar data reported by Lanzara *et al.* (2001) for a wide range of high-temperature superconductors]. This is counter to the linear dispersion predicted by band-structure calculations in this energy range (Krakauer and Pickett, 1988; Massidda *et al.*, 1988). The kink appeared to be more pronounced at low temperatures and in underdoped samples; below T_c, a drop in the EDC-derived quasiparticle scattering rate was observed at the kink energy, similar to that shown in Fig. 75.

It should be noted that a kink in the dispersion is also present in the superconducting-state results of Valla, Fedorov, Johnson, Wells, *et al.* (1999), although this aspect of the data was not considered by those authors (see white circles in Fig. 7). However, as the real and imaginary parts of the self-energy are related by Kramers-Kronig relations, the presence of a dispersion renormalization below a certain binding energy corresponds necessarily to a well-defined structure in the quasiparticle scattering rate, contrary to the initial claim that the temperature dependence of the scattering rate is linear in T_c and that there is no energy scale [as later recognized by those same authors (Johnson, Valla, *et al.*, 2001)].

C. Origin of the energy scale in the high-T_c superconductors

While there was initial disagreement, with one group arguing for the absence of an energy scale at all temperatures (Valla, Fedorov, Johnson, Wells, *et al.*, 1999), the field eventually converged to the conclusion that the kink in the dispersion and the change in the EDC width observed along the nodal direction indicate the presence of a well-defined energy scale in the electron self-energy for Bi2212, at least in the superconducting state. Furthermore, the coupling between the quasiparticles and some collective mode is considered to be the most likely origin of this phenomenon (Bogdanov *et al.*, 2000; Kaminski *et al.*, 2000, 2001; Johnson, Valla, *et al.*, 2001; Lanzara *et al.*, 2001). In fact, other possible causes, such as the opening of the superconducting gap, have been ruled out, as will be elaborated later. However, there is currently no consensus on whether or not these effects are limited to temperatures lower than T_c and, in turn, on the precise nature of the collective mode. As for the latter, in addition to the (π,π) resonant magnetic-mode scenario already discussed in relation to the self-energy effects in the $(\pi,0)$ region, lattice vibrations have also been proposed as a possible candidate. A direct comparison of these two competing scenarios will be presented in the following sections.

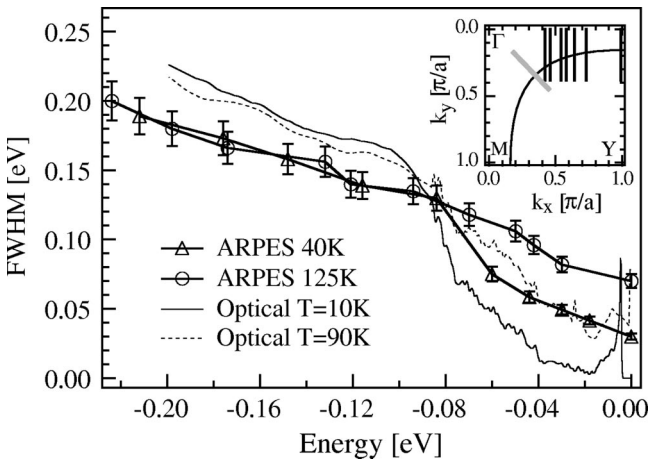

FIG. 75. Width of the energy distribution curves vs the quasiparticle binding energy for optimally doped Bi2212 ($T_c = 89$ K), from along the nodal direction (thick gray line in the Brillouin zone sketch), together with the frequency-dependent scattering rate from infrared reflectivity data (Puchkov *et al.*, 1996). After Kaminski *et al.*, 2000.

[35]See, for example, Chakravarty *et al.* (1989, 2001); Varma *et al.* (1989); Littlewood and Varma (1991); Sachdev and Ye (1992); Emery and Kivelson (1993b); Sokol and Pines (1993); Castellani *et al.* (1995); Varma (1997).

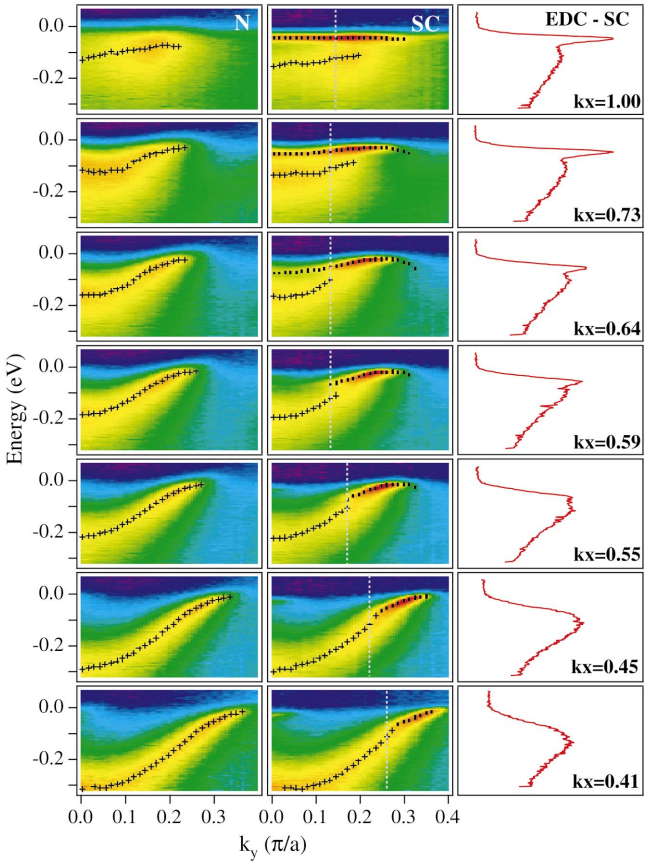

FIG. 76. ARPES intensity measured on optimally doped Bi2212 ($T_c=89$ K) with 22-eV photons: (left) normal state ($T=140$ K); (middle) superconducting state ($T=40$ K) (the location of the cuts in the Brillouin zone is indicated by the black lines in the sketch of Fig. 75); dots and crosses mark the position of peak and hump; (right) superconducting-state EDC's from the momenta indicated by the dashed lines in the middle panels. After Kaminski *et al.*, 2001 (Color).

1. Resonant magnetic-mode scenario

In the context of coupling between quasiparticles and a $Q=(\pi,\pi)$ mode, the strongest effects on the self-energy are expected around $(\pi,0)$, as emphasized in the inset of Fig. 71. However, as already discussed in relation to Fig. 72, Kaminski *et al.* (2001) argued that the coupling between quasiparticles and spin fluctuations could also be responsible for the drop in the scattering rate and the dispersion renormalization observed in the superconducting state of Bi2212 along the (0,0)-$(\pi,0)$ direction (Fig. 75, and Fig. 76 for $k_x=0.41$). This approach (Eschrig and Norman, 2000, 2002a; Kaminski *et al.*, 2001) provides a unified description of both the peak-dip-hump structure and two-branch behavior detected in the $(\pi,0)$ region (Fig. 76, top panels), and the quasiparticle renormalization observed along the nodal direction (Fig. 76, bottom panels). However, as already discussed in Sec. VIII.B.1, an important caveat is that the effects identified as due to self-energy corrections in the $(\pi,0)$ region could mostly be a direct manifestation of bonding and antibonding bilayer split bands.

Similar results and conclusions were later reported by Johnson, Valla, *et al.* (2001), who investigated the self-energy corrections along the nodal direction of Bi2212 for different doping levels, above and below T_c. Figure 77 shows the MDC-derived quasiparticle dispersion and an approximate estimate of the real part of the self-energy. This was obtained from the difference between the MDC-derived dispersion and the dashed straight lines that in Figs. 77(a)–(c) intersect the dispersion at k_F and at 200–250 meV, where Σ' is then set to zero. Strictly speaking, however, the true noninteracting dispersion should be used as a reference, which would not cross the interacting one. Although these results are not characterized by a strong temperature dependence [i.e., the main deviation from the dashed lines in Figs. 77(a)–(c) is already present in the normal state], Johnson, Valla, *et al.* (2001) argued that, while the normal-state dispersion shows only a smooth MFL-like renormalization (as defined in Sec. II.C), in the superconducting state the self-energy is characterized by the emergence of a sharp structure for underdoping and optimal doping. On the basis of this temperature and doping dependence, Johnson, Valla, *et al.* (2001) attributed the self-energy change across T_c (green symbols in Fig. 77) to the contribution of the resonant magnetic-mode. Interestingly, it was also noted that for $\omega\geqslant 50$ meV the band velocity decreases with doping and that in the underdoped regime both EDC and MDC widths are larger than the corresponding binding energy. These results were discussed by Johnson, Valla, *et al.* (2001) as indicative of electron or hole fractionalization, following an earlier work by Orgad *et al.* (2001).

2. Electron-phonon coupling scenario

As an alternative to the magnetic-mode scenario discussed in the previous section, Lanzara *et al.* (2001) and

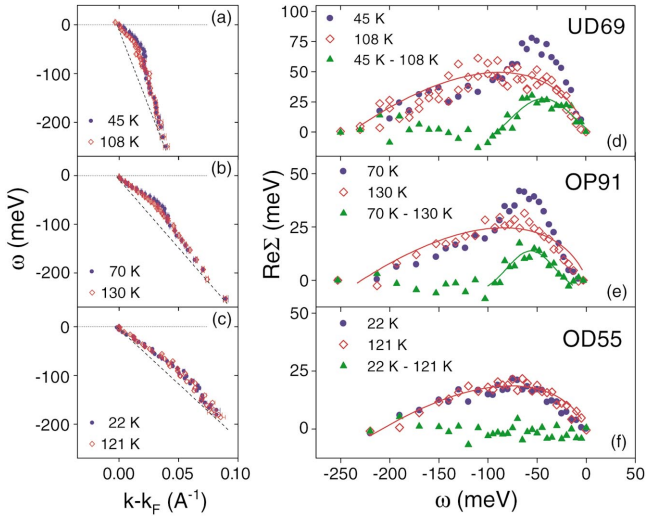

FIG. 77. MDC-derived quasiparticle dispersion along (0,0)-(π,π) for Bi2212: (a) underdoped; (b) optimally doped; (c) overdoped; (red) above T_c; (blue) below T_c; (d)–(f) Corresponding Σ': green symbols, difference between superconducting- and normal-state results; red lines, marginal-Fermi-liquid fits to the data. After Johnson, Valla, *et al.*, 2001 (Color).

Shen, Lanzara, *et al.* (2002) argued that the self-energy effects in the ARPES data from Bi2212 along the nodal direction can best be described in terms of electron-phonon coupling. This interpretation is based on the following observations. First, a kink in the quasiparticle dispersion as well as a drop in the scattering rate are seen in all the p-type cuprates studied, and the behavior is almost identical. This is shown in Figs. 78(a)–(c), which present the dispersion along (0,0)-(π,π) for LSCO, Bi2212, and Bi2201. In all cases one can observe a clear change in band velocity, which becomes more pronounced in the underdoped samples.[36] Note that the observation of a similar energy scale (50–80 meV) in systems characterized by very different gap energies (10–20 meV for LSCO and Bi2201, 30–50 meV for Bi2212) rules out the superconducting gap as a possible origin. Furthermore, this finding was taken by Lanzara *et al.* (2001) as strong evidence against the magnetic-mode interpretation and in favor of the phonon scenario. In fact, while the kink in the dispersion appears to be similar in the different families of compounds, the magnetic resonant mode behaves very differently. It is not seen in LSCO and is expected to have an energy three times lower in Bi2201 than in Bi2212 or YBCO, because its characteristic energy scales approximately with T_c. In contrast, the similar energy scale observed for the different compounds is consistent with coupling between quasiparticles and oxygen phonons. As revealed by neutron-scattering experiments (McQueeney *et al.*, 1999; Petrov *et al.*, 2000), these lattice vibrational modes are strongly coupled to the charge carriers and their characteristic frequencies fall in the same energy range as that of the kink observed in the quasiparticle dispersion [black arrows in Figs. 78(b)–(e)]. For instance, for LSCO the $(\pi,0)$ oxygen stretching mode has an energy of 70 meV, as indicated by the red arrow in Fig. 78(a) (McQueeney *et al.*, 1999), and coincides with the energy of the kink detected by ARPES.

A second important piece of evidence in favor of the phonon scenario comes from the temperature dependence of the kink in the quasiparticle dispersion. The data in Figs. 78(d) and (e) indicate that the effect smoothly evolves as the temperature is raised and persists well above T_c. This is particulary obvious in the 100-K data from LSCO, for which $T_c \simeq 38$ K. The inset in panel (e) presents the real part of the self-energy for optimally doped Bi2212 extracted with the same procedure as was used by Johnson, Valla, *et al.* (2001) for the data presented in Fig. 77. The results from the two groups are very similar except for a subtle difference: while both data sets show a slightly more pronounced structure at low temperature, the superconducting-state

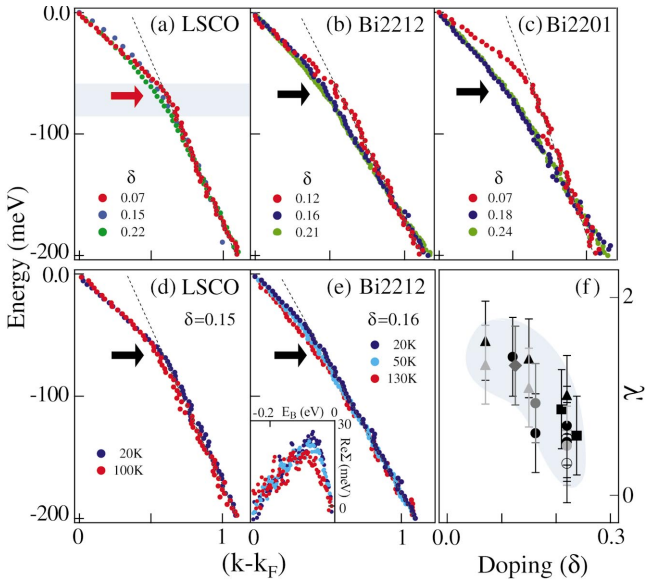

FIG. 78. Quasiparticle dispersion of Bi2212, Bi2201 and LSCO along the nodal direction, plotted vs the rescaled momentum for (a)–(c) different dopings, and (d),(e) different temperatures; black arrows indicate the kink energy; the red arrow indicates the energy of the $q=(\pi,0)$ oxygen stretching phonon mode; inset of (e): temperature-dependent Σ' for optimally doped Bi2212; (f) doping dependence of λ' along (0,0)-(π,π) for the different cuprates. From Lanzara *et al.*, 2001 (Color).

data by Johnson, Valla, *et al.* (2001) hint at a sharp peak superimposed on the normal-state result (Fig. 77), which could be taken as evidence for a qualitatively different effect below and above T_c. On the other hand, the data of Lanzara *et al.* (2001) show a more continuous evolution, with a persistence of the effect into the normal state. Therefore the temperature dependence of the ARPES data from Bi2212 and especially LSCO was taken by Lanzara *et al.* (2001) as direct and conclusive evidence against the magnetic-mode interpretation because the latter, as indicated by elastic neutron-scattering experiments, turns on below T_c (Dai *et al.*, 1996, 1999; Fong *et al.*, 1999; He *et al.*, 2001).

Figure 79 directly compares the low-temperature ARPES spectra taken with 55-eV photons on overdoped (OD), optimally doped (OP), and underdoped (UD) Bi2212. It should be emphasized that these data were recorded along the nodal direction, where the two bilayer split bands are degenerate in energy (Sec. IV.C.2). The most important feature is that these spectra are characterized by a clear peak-dip-hump structure, in strong resemblance to both the simulated spectral function for an electron-phonon coupled system (Fig. 79, right panel), and the results for the Be(0001) surface state presented in Fig. 69(a). Note that the peak-dip-hump structure is better resolved in these data than in those reported in an earlier publication (Bogdanov *et al.*, 2000) because of the improved signal-to-noise ratio and possibly the higher photon energy used in the more recent experiments. The dip energy, marked by dashed lines in Fig. 79, corresponds to that of the kink in the dispersion (Fig. 78). However, while the kink is still

[36]For the n-type cuprates no detailed study is available; at this stage, as shown in Fig. 42, no effect is detected on NCCO along the nodal direction (Sato, Kamiyama, *et al.*, 2001a; Shen, Lanzara, *et al.*, 2002), while a break in the dispersion at about 50 meV was observed along the $(\pi,0)$-(π,π) direction (Sato, Kamiyama, *et al.*, 2001a).

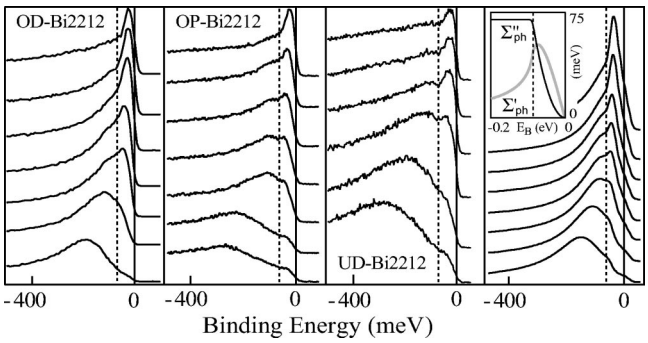

FIG. 79. Low-temperature spectra from overdoped (OD), optimally doped (OP), and underdoped (UD) Bi2212 along (0,0)-(π,π). Right panel: spectral function for an electron-phonon coupled system in the Debye model at $T=0$; $\Sigma'(\omega)$ and $\Sigma''(\omega)$ are shown in the inset, where the dashed line indicates the maximum phonon energy. From Lanzara *et al.*, 2001.

recognizable above T_c, the peak-dip-hump structure is smeared out at high temperature. Similar results have also been obtained along the nodal direction for LSCO (Zhou, 2001) and Bi2201 (Lanzara, 2002). In particular, for Bi2201 the peak-dip-hump structure could be clearly observed above T_c, as this is low enough that the system can be studied in the normal state, avoiding, at the same time, excessive thermal broadening.

From the ratio of the quasiparticle velocities at energies above and below the kink, Lanzara *et al.* (2001) estimated the quantity λ' which is proportional to the electron-phonon coupling parameter λ. Note that this is the same procedure already discussed in Sec. VIII.A for Be(0001); however, in the present case due to the underlying electron-electron correlations the quasiparticle velocity is already strongly renormalized over a large energy scale. The doping dependence of λ' is presented in Fig. 78(f) and it shows that the electron-phonon coupling increases in all three systems (i.e., LSCO, Bi2201, and Bi2212) as the doping level is reduced.

The ARPES results presented in this section indicate that in addition to electron self-energy corrections due to electron-electron correlations, which are responsible for the renormalization of the electronic structure of the cuprates over a large energy scale (see Sec. IV.A), the contribution from electron-phonon interaction must also be taken into account, as it appears to have a direct influence on the quasiparticle dynamics. In this regard Shen, Lanzara, *et al.* (2002) went a step further and, by considering both the diagonal and off-diagonal channels of electron-phonon coupling for *p* and *n*-type high-temperature cuprate superconductors, asserted that the electron-phonon interaction is also an essential ingredient to pairing (a more detailed discussion of this issue is, however, beyond the scope of our review).

3. Discussion

As we have seen throughout this section, the investigation of the self-energy corrections in Bi2212 is an extremely complex issue. There is now strong evidence that the normal-state and superconducting-state low-energy dispersion along the nodal direction is characterized by a sharp break accompanied by a double-peak structure in the EDC's (as indicated by the data not only from Bi2212 but also from Bi2201 and LSCO). This structure identifies an energy scale in the quasiparticle dynamics which is naturally explained as a consequence of relatively strong electron-phonon coupling. On the other hand, the results we discussed for the antinodal region are much less certain because of complications due to superstructure contaminations and bilayer splitting effects. Recently, new and more convincing evidence for the presence of a kink in the Bi2212 quasiparticle dispersion near $(\pi,0)$ below T_c has been reported by Gromko *et al.* (Gromko, Chuang, *et al.*, 2002; Gromko, Fedorov, *et al.*, 2002). As shown in Fig. 80(a), where the normal-state ARPES intensity from overdoped Bi2212 along the (π,π)-$(\pi,0)$-$(\pi,-\pi)$ direction is presented, Gromko *et al.* were able to clearly resolve the bonding and antibonding split bands as well as their superstructure replicas. Below $T_c=58$ K [Fig. 80(b)], they observed the opening of the superconducting gap and the sharpening and/or intensity increase of the low-energy peaks, which gave rise to the traditional $(\pi,0)$ peak-dip-hump structure. In addition, the bonding band MDC-derived dispersion, which is linear above T_c, is now characterized by a sharp kink at 40 meV [this is further substantiated by the detailed study of a $T_c=71$ K overdoped sample presented in Fig. 80(c)]. It should be emphasized that, on the one hand, this work confirms prior reports (e.g., Norman, Eschrig, *et al.*, 2001). On the other hand, while the kink in the $(\pi,0)$ region was earlier believed to be connected to the traditional peak-dip-hump structure, these results indicate the independence of the two phenomena, with the traditional peak-dip-hump structure being simply a bilayer splitting effect. Furthermore, Gromko, Chuang, *et al.* (2002) reported that the emergence of the $(\pi,0)$ kink at 40 meV in the bonding band was accompanied by the development of a separate antinodal peak-dip-hump structure much weaker than the traditional one, consistent with an earlier report [Feng *et al.*, 2001; see crosses and bars in Fig. 34(b)].

From a comparison of the results above and those presented in Sec. VIII.C, it is clear that the kinks in the antinodal and nodal dispersions have completely different origins: (i) while the former has a dramatic temperature dependence and is observed only below T_c [Fig. 80(c)], the latter is already seen above T_c and is essentially independent of temperature (Fig. 78); (ii) as summarized by Gromko, Fedorov, *et al.* (2002) in Fig. 80(d) where several energy scales are plotted versus doping, the antinodal kink has a characteristic energy significantly smaller than the nodal one; (iii) furthermore, also the doping dependence of their energy scale [Fig. 80(d)], and of the magnitude of the velocity renormalization (which is proportional to the coupling strength) are different; as for the latter in particular, while the nodal kink gets weaker with increasing doping, the antinodal one

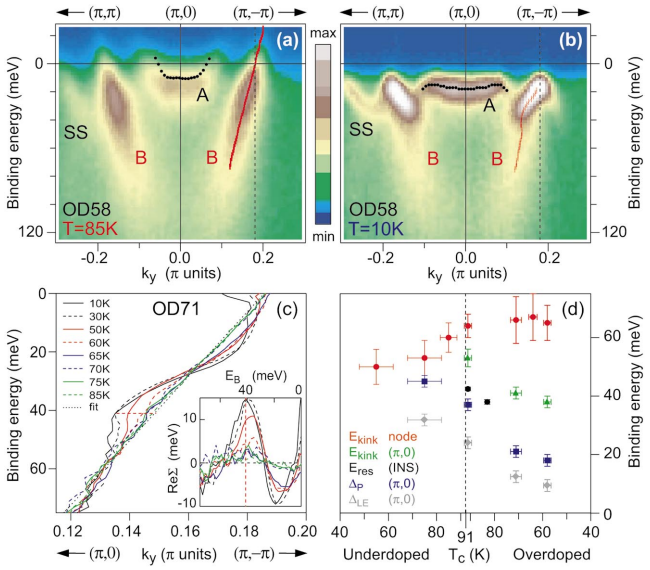

FIG. 80. Quasiparticle dispersion of overdoped Bi2212 (T_c = 85 K) near (π,0): (a) normal-state and (b) superconducting-state ARPES intensity measured with 20-eV photons [red and black lines: bonding (B) and antibonding (A) band dispersion; SS: superstructure replica]; (c) MDC-derived dispersion along (π,0)-(π,-π); inset: temperature dependence of $\Sigma'(\omega)$ defined as the difference between the data and the linear fit to the 85-K result; (d) doping dependence of kink energy, gap magnitude (from peak and leading-edge midpoint positions), and resonant-mode frequency (neutron-scattering data). After Gromko, Fedorov, *et al.*, 2002 (Color).

remains very strong in the overdoped regime.[37]

Because the antinodal kink is clearly associated with the onset of superconductivity and is limited to a small momentum-space region around (π,0) where the superconducting gap is maximum, Gromko, Fedorov, *et al.* (2002) suggested that this effect is due to coupling between the electrons and the $Q=(\pi,\pi)$ magnetic resonant mode. This, in turn, could be the source of pairing for high-T_c superconductivity. However, in this regard a few caveats have to be mentioned. First, there are alternative explanations for the observed effect that have to be ruled out, such as the very same opening of the superconducting gap and the dramatic change in quasiparticle dynamics associated with it (see Sec. VI). Furthermore, at this stage there is no experimental evidence from inelastic neutron-scattering experiments for the existence of a resonant mode in the extremely overdoped regime ($T_c \sim 58$ K), where the antinodal kink remain very strong. For a more conclusive assignment, a more detailed investigation of these issues is required.

[37]It is hard to judge whether there is an additional kink in the antinodal region at higher binding energies, similar to that observed along the nodal direction. This uncertainty is due to the very limited energy range of the data at (π,0), which is defined by the bottom of the bonding band (see Figs. 34 and 80).

IX. CONCLUDING REMARKS

The results discussed in the course of this review paper demonstrate that the high-T_c superconductors are complex materials characterized by many competing degrees of freedom. As a consequence, both the experimental investigation and the theoretical understanding are extremely difficult. However, the remarkable improvement of the ARPES technique has allowed the community to considerably deepen its knowledge of the electronic structure of the copper oxide superconductors, a fundamental step towards the development of a comprehensive theoretical description of these systems. In fact, looking back over the last decade, there are many topics on which the ARPES results have produced a general consensus and have profoundly impacted our understanding of the physics of the cuprates:

(i) The importance of electronic correlations (Mott physics) and the renormalization of the bandwidth from t to J scale for the undoped parent compounds of the high-T_c superconductors.

(ii) The existence of a well-defined Fermi surface for the overdoped metal in all the different families of cuprates; in this context, the observation of two bilayer split sheets of Fermi surface in Bi2212 is the most direct example of the remarkable precision achieved by these measurements.

(iii) The qualitative doping evolution of the electronic structure in the different high-T_c superconductor families, and the influence of antiferromagnetic correlations in p-type underdoped cuprates and especially in the n-type ones, in which the hot-spot physics is still observed at optimal doping.

(iv) The overall d-wave symmetry of the superconducting gap detected below T_c in both hole- and electron-doped systems, which supports the universality of the pairing nature in the high-T_c superconductors.

(v) The opening of a normal-state pseudogap at a temperature $T^* > T_c$ in the underdoped regime, with a d-wave functional form similar to that of the superconducting gap.

(vi) The emergence of a coherent quasiparticle peak below T_c near (π,0) in Bi2212, whose spectral weight scales with the doping level x and the superfluid density in the underdoped regime.

(vii) The presence of an energy scale of about 40–80 meV in the quasiparticle dynamics, as revealed by the sharp dispersion renormalization and drop in scattering rate observed at those energies at different momenta. Independently of its final interpretation, this latter effect is likely to be of great significance to pairing because its energy scale falls in between the values of J and Δ.

Looking towards the future, ARPES as a technique continues to develop rapidly. In gas-phase photoemission experiments, which are performed in a very different configuration, the energy resolution has now reached exceptional values of better than 0.01 meV

(Hollenstein *et al.*, 2001). One would expect further progress in solid-state experiments, as well. Significant technological advances include implementation of circularly polarized photon sources, spin-polarized detectors, and time-resolved systems. In this regard, it should be mentioned that most recently Kaminski *et al.* (2002), by detecting a difference in the ARPES intensity measured with left- and right-circularly polarized photons on Bi2212 at $(\pi,0)$, concluded that the opening of the normal-state pseudogap below T^* in the underdoped regime corresponds to a phase transition into a state characterized by spontaneously broken time-reversal symmetry (as suggested by Varma, 2000). In turn, this would imply that T^* identifies a new phase transition rather than a fluctuation regime for the superconducting order parameter. Although the validity of these conclusions remains to be tested, this and other new experiments, not only limited to the specific field of high-T_c superconductors (for a general overview see, Grioni, 2001), indicate that the study of the electronic structure of complex materials by ARPES will remain a vibrant and rapidly evolving field.

ACKNOWLEDGMENTS

We would first like to express our gratitude to the current and former members of the Stanford photoemission group for their cooperation, daily discussions, and many useful comments: N. P. Armitage, P. Bogdanov, Y. Chen, T. Cuk, D. S. Dessau, H. Eisaki, D. L. Feng, S. L. Friedmann, M. Z. Hasan, J. M. Harris, N. J. C. Ingle, S. A. Kellar, C. Kim, D. M. King, A. Lanzara, W. S. Lee, A. G. Loeser, D. H. Lu, D. S. Marshall, A. Y. Matsuura, T.-U. Nahm, C.-H. Park, A. V. Puchkov, F. Ronning, M. C. Schabel, K. M. Shen, Z. Y. Wang, B. O. Wells, P. J. White, W. L. Yang, and X. J. Zhou. We would also like to take this opportunity to acknowledge our collaborators in the field: A. V. Balatsky, R. J. Birgeneau, D. A. Bonn, E. W. Carlson, J. N. Eckstein, V. J. Emery, A. Fujimori, M. Greven, W. N. Hardy, A. Ino, A. Kapitulnik, M. A. Kastner, K. Kishio, S. A. Kivelson, R. Liang, S. Maekawa, Y. Maeno, L. L. Miller, T. Mizokawa, N. Nagaosa, D. Orgad, F. Parmigiani, G. A. Sawatzky, J. R. Schrieffer, W. E. Spicer, H. Takagi, S. Tajima, T. Timusk, T. Tohyama, Y. Tokura, S. Uchida, D. van der Marel, T. Yoshida, R. Yosjizaki, and Z.-X. Zhao. Over the years, we have benefited tremendously from scientific discussions with S. Doniach, R. B. Laughlin, and S.-C. Zhang, as well as many other colleagues: E. Abrahams, P. Aebi, P. B. Allen, O. K. Andersen, P. W. Anderson, E. Arrigoni, A. Bansil, M. R. Beasley, A. Bianconi, J. C. Campuzano, S. Chakravarty, C. W. Chu, A. V. Chubukov, E. Dagotto, J. C. Davis, H. Ding, Y. Endoh, M. E. Flatté, H. Fukuyama, T. H. Geballe, W. Hanke, W. A. Harrison, M. Imada, P. D. Johnson, B. Keimer, H. Keller, D.-H. Lee, P. A. Lee, Yu Lu, R. S. Markiewicz, J. Mesot, A. J. Millis, K. A. Moler, H. A. Mook, K. A. Müller, M. R. Norman, N. P. Ong, J. Orenstein, J. Osterwalder, S. H. Pan, M. Randeria, S. Sachdev, D. J. Scalapino, N. V. Smith, M. Tachiki, J. M. Tranquada, Y. J. Uemura, C. M. Varma, M. G. Zacher, and J. Zaanen. Finally, it is a pleasure to thank E. Abrahams, P. Aebi, N. P. Armitage, E. Arrigoni, T. Cuk, N. J. C. Ingle, D. H. Lu, D. W. Lynch, R. S. Markiewicz, N. Nagaosa, M. R. Norman, F. Ronning, K. M. Shen, and J. van den Brink for critical readings of this review article. This project was carried out at the Stanford Synchrotron Radiation Laboratory (SSRL) which is operated by the DOE Office of Basic Energy Sciences, Division of Chemical Sciences. The Office's Division of Materials Science has provided funding for this project. The Stanford work was also supported by NFS Grant No. DMR0071897 and ONR Grant No. N00014-98-1-0195. The work of the Advanced Light Source was supported by the DOE Office of Basic Energy Science, Division of Material Science.

REFERENCES

Abanov, A., and A. V. Chubukov, 1999, Phys. Rev. Lett. **83**, 1652.

Abrahams, E., and C. M. Varma, 2000, Proc. Natl. Acad. Sci. U.S.A. **97**, 5714.

Abrikosov, A. A., J. C. Campazuno, and K. Gofron, 1993, Physica C **214**, 73.

Abrikosov, A. A., L. P. Gor'kov, and I. E. Dzyaloshinskii, 1965, *Quantum Field Theoretical Methods in Statistical Physics* (Pergamon, Oxford).

Aebi, P., J. Osterwalder, P. Schwaller, H. Berger, C. Beeli, and L. Schlapback, 1995, J. Phys. Chem. Solids **56**, 1845.

Aebi, P., J. Osterwalder, P. Schwaller, L. Schlapbach, M. Shimoda, T. Mochiku, and K. Kadowaki, 1994, Phys. Rev. Lett. **72**, 2757.

Affleck, I., and J. B. Martson, 1988, Phys. Rev. B **37**, 3774.

Allen, J. W., C. G. Olson, M. B. Maple, J. S. Kang, L. Z. Liu, J. H. Park, R. O. Anderson, W. P. Ellis, J. T. Markert, Y. Dalichaoch, and R. Liu, 1990, Phys. Rev. Lett. **64**, 595.

Andersen, O. K., O. Jepsen, A. I. Liechtenstein, and I. I. Mazin, 1994, Phys. Rev. B **49**, 4145.

Andersen, O. K., A. I. Liechtenstein, O. Jepsen, and F. Paulsen, 1995, J. Phys. Chem. Solids **56**, 1573.

Andersen, O. K., A. I. Liechtenstein, O. Rodriguez, I. I. Mazin, O. Jepsen, V. P. Aantropov, O. Gunnarsson, and S. Gopalan, 1991, Physica C **185-189**, 147.

Anderson, A. R., P. A. Miles, G. D. Gu, G. J. Russell, S. J. Kennedy, and N. Koshizuka, 1997, Physica C **281**, 356.

Anderson, P. W., 1950, Phys. Rev. **79**, 350.

Anderson, P. W., 1959, Phys. Rev. **115**, 2.

Anderson, P. W., 1987, Science **235**, 1196.

Anderson, P. W., 1995, Science **268**, 1154.

Anderson, P. W., 1997, *The Theory of Superconducting in the High-T_c Cuprates* (Princeton University, Princeton).

Anderson, P. W., 1998, Science **279**, 1196.

Anderson, P. W., 2000, Science **288**, 480.

Anderson, R. O., R. Claessen, J. W. Allen, C. G. Olson, C. Janowitz, L. Z. Liu, J.-H. Park, M. B. Maple, Y. Dalichaouch, M. C. de Andrade, R. F. Jardim, E. A. Early, *et al.*, 1993, Phys. Rev. Lett. **70**, 3163.

Armitage, N. P., D. H. Lu, D. L. Feng, C. Kim, A. Damascelli, K. M. Shen, F. Ronning, Z.-X. Shen, Y. Onose, Y. Taguchi, and Y. Tokura, 2001, Phys. Rev. Lett. **86**, 1126.

Armitage, N. P., D. H. Lu, C. Kim, A. Damascelli, K. M. Shen, F. Ronning, D. L. Feng, P. Bogdanov, Z.-X. Shen, Y. Onose, Y. Taguchi, Y. Tokura, *et al.*, 2001, Phys. Rev. Lett. **87**, 147003.

Armitage, N. P., D. H. Lu, C. Kim, A. Damascelli, K. M. Shen, F. Ronning, Y. Onose, Y. Taguchi, Y. Tokura, and Z.-X. Shen, 2000, Physica C **341-348**, 2083.
Armitage, N. P., F. Ronning, D. H. Lu, C. Kim, A. Damascelli, K. M. Shen, D. L. Feng, H. Eisaki, Z.-X. Shen, P. K. Mang, N. Kaneko, and M. Greven, *et al.*, 2002, Phys. Rev. Lett. **88**, 257001.
Ashcroft, N. W., and N. D. Mermin, 1976, *Solid State Physics* (Saunders College, Philadelphia).
Atkinson, W. A., 1999, Phys. Rev. B **59**, 3377.
Auerbach, A., 1994, *Interacting Electrons and Quantum Magnetism* (Springer, Berlin).
Bachrach, R. Z., 1992, *Synchrotron Radiation Research*, Advances in Surface and Interface Science Vol. 1 (Plenum, New York).
Balasubramanian, T., E. Jensen, X. L. Wu, and S. L. Hulbert, 1998, Phys. Rev. B **57**, 6866.
Balents, L., M. P. A. Fisher, and C. Nayak, 1998, Int. J. Mod. Phys. B **12**, 1033.
Balents, L., M. P. A. Fisher, and C. Nayak, 1999, Phys. Rev. B **60**, 1654.
Balents, L., M. P. A. Fisher, and C. Nayak, 2000, Phys. Rev. B **61**, 6307.
Bansil, A., and M. Lindroos, 1995, J. Phys. Chem. Solids **56**, 1855.
Bansil, A., and M. Lindroos, 1998, J. Phys. Chem. Solids **59**, 1879.
Bansil, A., and M. Lindroos, 1999, Phys. Rev. Lett. **83**, 5154.
Bardeen, J., L. N. Cooper, and J. R. Schrieffer, 1957, Phys. Rev. **108**, 1175.
Beamson, G., D. Briggs, S. F. Davies, I. W. Fletcher, D. T. Clark, J. Howard, U. Gelius, B. Wannberg, and P. Balzer, 1990, Surf. Interface Anal. **15**, 541.
Bednorz, J. G., and K. A. Müller, 1986, Z. Phys. B: Condens. Matter **64**, 189.
Belinicher, V. I., A. L. Chernyshev, and V. A. Shubin, 1996, Phys. Rev. B **54**, 14 914.
Bergemann, C., S. R. Julian, A. P. Mackenzie, S. NishiZaki, and Y. Maeno, 2000, Phys. Rev. Lett. **84**, 2662.
Berglund, C. N., and W. E. Spicer, 1964, Phys. Rev. **136**, A1030.
Bianconi, A., N. L. Saini, A. Lanzara, M. Missori, T. Rossetti, H. Oyanagi, H. Yamaguchi, K. Oka, and T. Ito, 1996, Phys. Rev. Lett. **76**, 3412.
Blumberg, G., A. Koitzsch, A. Gozar, B. S. Dennis, C. A. Kendziora, P. Fournier, and R. L. Greene, 2002, Phys. Rev. Lett. **88**, 107002.
Bogdanov, P. V., A. Lanzara, S. A. Kellar, X. J. Zhou, E. D. Lu, W. J. Zheng, G. Gu, J.-I. Shinoyama, K. Kishio, H. Ikeda, R. Yoshizaki, Z. Hussain, *et al.*, 2000, Phys. Rev. Lett. **85**, 2581.
Bogdanov, P. V., A. Lanzara, X. J. Zhou, S. A. Kellar, D. L. Feng, E. D. Lu, H. Eisaki, J. Shimoyama, K. Kishio, Z. Hussain, and Z.-X. Shen, 2001, Phys. Rev. B **64**, 180505.
Bonn, D. A., S. Kamal, K. Zhang, R. Liang, D. J. Baar, E. Klein, and W. N. Hardy, 1994, Phys. Rev. B **50**, 4051.
Borisenko, S. V., M. S. Golden, S. Legner, T. Pichler, C. Dürr, M. Knupfer, J. Fink, G. Yang, S. Abell, and H. Berger, 2000, Phys. Rev. Lett. **84**, 4453.
Borisenko, S. V., A. A. Kordyuk, T. K. Kim, S. Legner, K. A. Nenkov, M. Knupfer, M. S. Golden, J. Fink, H. Berger, and R. Follath, 2002, Phys. Rev. B **66**, 140509.
Borisenko, S. V., A. A. Kordyuk, S. Legner, C. Dürr, M. Knupfer, M. S. Golden, J. Fink, K. Nenkov, D. Eckert, G. Yang, S. Abell, H. Berger, *et al.*, 2001, Phys. Rev. B **64**, 094513.
Braun, J., 1996, Rep. Prog. Phys. **59**, 1267.
Brookes, N. B., G. Ghiringhelli, O. Tjernberg, L. H. Tjeng, T. Mizokawa, T. W. Li, and A. A. Menovsky, 2001, Phys. Rev. Lett. **87**, 237003.
Brundle, C. R., and A. D. Baker, 1977, *Electron Spectroscopy: Theory, Techniques, and Applications*, Vol. 1 (Academic, New York).
Brundle, C. R., and A. D. Baker, 1978, *Electron Spectroscopy: Theory, Techniques, and Applications*, Vol. 2 (Academic, New York).
Buckingham, M. J., 1950, Phys. Rev. **80**, 704.
Bulut, N., D. J. Scalapino, and S. R. White, 1994, Phys. Rev. Lett. **73**, 748.
Campuzano, J. C., H. Ding, M. R. Norman, H. M. Fretwell, M. Randeria, A. Kaminski, J. Mesot, T. Takeuchi, T. Sato, T. Yokoya, T. Takahashi, T. Mochiku, *et al.*, 1999, Phys. Rev. Lett. **83**, 3709.
Campuzano, J. C., H. Ding, M. R. Norman, M. Randeira, A. F. Bellman, T. Yokoya, T. Takahashi, H. Katayama-Yoshida, T. Mochiku, and K. Kadowaki, 1996, Phys. Rev. B **53**, 14 737.
Cardona, M., and L. Ley, 1978, *Photoemission in Solids*, Vol. 1 (Springer, Berlin).
Carlson, E. W., D. Orgad, S. A. Kivelson, and V. J. Emery, 2000, Phys. Rev. B **62**, 3422.
Carlson, T. A., 1975, *Photoelectron and Auger Spectroscopy* (Plenum, New York).
Castellani, C., C. Di Castro, and M. Grilli, 1995, Phys. Rev. Lett. **75**, 4650.
Chakravarty, S., P. Aebi, J. Osterwalder, P. Schwaller, L. Schlapbach, M. Shimoda, T. Mochiku, and K. Kadowaki, 1995, Phys. Rev. Lett. **74**, 1885.
Chakravarty, S., B. I. Halperin, and D. R. Nelson, 1989, Phys. Rev. B **39**, 2344.
Chakravarty, S., R. B. Laughlin, D. K. Morr, and C. Nayak, 2001, Phys. Rev. B **63**, 094503.
Chakravarty, S., A. Sudbo, P. W. Anderson, and S. Strong, 1993, Science **261**, 337.
Chen, X. K., J. C. Irwin, H. J. Trodahl, T. Kimura, and K. Kishio, 1994, Phys. Rev. Lett. **73**, 3290.
Chernyshev, A. L., A. H. Castro Neto, and A. R. Bishop, 2000, Phys. Rev. Lett. **84**, 4922.
Chuang, Y.-D., A. D. Gromko, D. S. Dessau, Y. Aiura, Y. Yamaguchi, K. Oka, A. J. Arko, J. Joyce, H. Eisaki, S. I. Uchida, S. I. Uchida, K. Nakamara, *et al.*, 1999, Phys. Rev. Lett. **83**, 3717.
Chuang, Y.-D., A. D. Gromko, A. Fedorov, Y. Aiura, K. Oka, Y. Ando, H. Eisaki, S. I. Uchida, and D. S. Dessau, 2001a, Phys. Rev. Lett. **87**, 117002.
Chuang, Y.-D., A. D. Gromko, A. V. Fedorov, Y. Aiura, K. Oka, Y. Ando, and D. S. Dessau, 2001b, e-print cond-mat/0107002.
Chubukov, A. V., 1995, Phys. Rev. B **52**, 3840.
Chubukov, A. V., and D. K. Morr, 1998, Phys. Rev. Lett. **81**, 4716.
Cooper, J. W., 1962, Phys. Rev. **128**, 681.
Courths, R., and S. Hüfner, 1984, Phys. Rep. **112**, 53.
Dagotto, E., 1994, Rev. Mod. Phys. **66**, 763.
Dagotto, E., A. Moreo, F. Ortolani, J. Riera, and D. J. Scalapino, 1991, Phys. Rev. Lett. **67**, 1918.
Dagotto, E., A. Nazarenko, and M. Boninsegni, 1994, Phys. Rev. Lett. **73**, 728.
Dagotto, E., A. Nazarenko, and A. Moreo, 1995, Phys. Rev. Lett. **74**, 310.

Dai, P., H. A. Mook, S. M. Hayden, G. Aeppli, T. G. Perring, R. D. Hunt, and F. Doğan, 1999, Science **284**, 1344.
Dai, P., M. Yethiraj, F. A. Mook, T. B. Lindemer, and F. Doğan, 1996, Phys. Rev. Lett. **77**, 5425.
Damascelli, A., D. H. Lu, and Z.-X. Shen, 2001, J. Electron Spectrosc. Relat. Phenom. **117-118**, 165.
Damascelli, A., D. H. Lu, K. M. Shen, N. P. Armitage, F. Ronning, D. L. Feng, C. Kim, Z.-X. Shen, T. Kimura, Y. Tokura, Z. Q. Mao, and Y. Maeno, 2000, Phys. Rev. Lett. **85**, 5194.
Damascelli, A., K. M. Shen, D. H. Lu, N. P. Armitage, F. Ronning, D. L. Feng, C. Kim, Z.-X. Shen, T. Kimura, Y. Tokura, Z. Q. Mao, and Y. Maeno, 2001, J. Electron Spectrosc. Relat. Phenom. **114-116**, 641.
Damascelli, A., K. M. Shen, D. H. Lu, and Z.-X. Shen, 2001, Phys. Rev. Lett. **87**, 239702.
Day, C., 2001, Phys. Today **54** (4), 17.
Derro, D. J., E. W. Hudson, K. M. Lang, S. H. Pan, J. C. Davis, J. T. Markert, and A. L. de Lozanne, 2002, Phys. Rev. Lett. **88**, 097002.
Dessau, D. S., Z.-X. Shen, D. M. King, D. S. Marshall, L. W. Lombardo, P. H. Dickinson, A. G. Loeser, J. DiCarlo, C.-H. Park, A. Kapitulnik, and W. E. Spicer, 1993, Phys. Rev. Lett. **71**, 2781.
Dessau, D. S., B. O. Wells, Z.-X. Shen, W. E. Spicer, A. J. Arko, R. S. List, D. B. Mitzi, and A. Kapitulnik, 1991, Phys. Rev. Lett. **66**, 2160.
Dickinson, P. H., and S. Doniach, 1993, Phys. Rev. B **47**, 11 447.
Dietz, E., H. Becker, and U. Gerhardt, 1976, Phys. Rev. Lett. **36**, 1397.
Ding, H., A. F. Bellman, J. C. Campuzano, M. Randeria, M. R. Norman, T. Yokoya, T. Takahashi, H. Katayama-Yoshida, T. Mochiku, K. Kadowaki, G. Jennings, and G. P. Brivio, 1996, Phys. Rev. Lett. **76**, 1533.
Ding, H., J. C. Campuzano, A. F. Bellman, T. Yokoya, M. R. Norman, M. Randeria, T. Takahashi, H. Katayama-Yoshida, T. Mochiku, K. Kadowaki, and G. Jennings, 1995a, Phys. Rev. Lett. **74**, 2784.
Ding, H., J. C. Campuzano, A. F. Bellman, T. Yokoya, M. R. Norman, M. Randeria, T. Takahashi, H. Katayama-Yoshida, T. Mochiku, K. Kadowaki, and G. Jennings, 1995b, Phys. Rev. Lett. **75**, 1425.
Ding, H., J. R. Engelbrecht, Z. Wang, J. C. Campuzano, S.-C. Wang, H.-B. Yang, R. Rogan, T. Takahashi, K. Kadowaki, and D. G. Hinks, 2001, Phys. Rev. Lett. **87**, 227001.
Ding, H., M. R. Norman, J. C. Campuzano, M. Randeria, A. F. Bellman, T. Yokoya, T. Takahashi, T. Mochiku, and K. Kadowaki, 1996, Phys. Rev. B **54**, 9678.
Ding, H., M. R. Norman, T. Yokoya, T. Takeuchi, M. Randeria, J. C. Campuzano, T. Takahashi, T. Mochiku, and K. Kadowaki, 1997, Phys. Rev. Lett. **78**, 2628.
Ding, H., T. Yokoya, J. C. Campuzano, T. Takahashi, M. Randeria, M. R. Norman, T. Mochiku, K. Hadowaki, and J. Giapintzakis, 1996, Nature (London) **382**, 51.
Di Stasio, M., K. A. Müller, and L. Pietronero, 1990, Phys. Rev. Lett. **64**, 2827.
Doniach, S., and M. Inui, 1990, Phys. Rev. B **41**, 6668.
Duò, L., S. De Rossi, P. Vavassori, F. Ciccacci, G. L. Olcese, G. Chiaia, and I. Lindau, 1996, Phys. Rev. B **54**, 17 363.
Dürr, C., S. Legner, R. Hayn, S. V. Borisenko, Z. Hu, A. Theresiak, M. Knupfer, M. S. Golden, J. Fink, F. Ronning, Z.-X. Shen, H. Eisaki, *et al.*, 2001, Phys. Rev. B **63**, 014505.
Eastman, D. E., 1972, in *Techniques of Metal Research*, edited by E. Passaglia (Interscience, New York), Vol. VI, Part I.
Eberhardt, W., and F. J. Himpsel, 1980, Phys. Rev. B **21**, 5572.
Economou, E. N., 1983, *Green's Functions in Quantum Physics*, Springer Series in Solid State Science Vol. 7 (Springer, Berlin).
Eder, R., Y. Ohta, and G. A. Sawatzky, 1997, Phys. Rev. B **55**, 3414.
Edwards, H. L., J. T. Markert, and A. L. de Lozanne, 1992, Phys. Rev. Lett. **69**, 2967.
Einstein, A., 1905, Ann. Phys. (Leipzig) **31**, 132.
Eisaki, H., N. Kaneko, D. L. Feng, A. Damascelli, P. K. Mang, K. M. Shen, M. Greven, and Z.-X. Shen, 2002, "Effect of inherent chemical inhomogeneity in the Bi-based copper oxide superconductors," Standford University preprint.
Emery, V. J., 1987, Phys. Rev. Lett. **58**, 2794.
Emery, V. J., and S. A. Kivelson, 1993a, Physica C **209**, 597.
Emery, V. J., and S. A. Kivelson, 1993b, Phys. Rev. Lett. **71**, 3701.
Emery, V. J., and S. A. Kivelson, 1995a, Nature (London) **374**, 434.
Emery, V. J., and S. A. Kivelson, 1995b, Phys. Rev. Lett. **74**, 3253.
Emery, V. J., S. A. Kivelson, and J. M. Tranquada, 1999, Proc. Natl. Acad. Sci. U.S.A. **96**, 8814.
Engelsberg, S., and J. R. Schrieffer, 1963, Phys. Rev. **131**, 993.
Eroles, J., G. Ortiz, A. V. Balatsky, and A. R. Bishop, 2001, Phys. Rev. B **64**, 174510.
Eschrig, M., and M. R. Norman, 2000, Phys. Rev. Lett. **85**, 3261.
Eschrig, M., and M. R. Norman, 2002a, e-print cond-mat/0202083.
Eschrig, M., and M. R. Norman, 2000b, Phys. Rev. Lett. **89**, 277005.
Eskes, H., and R. Eder, 1996, Phys. Rev. B **54**, 14 226.
Fan, H. Y., 1945, Phys. Rev. **68**, 43.
Fedorov, A. V., T. Valla, P. D. Johnson, Q. Li, G. D. Gu, and N. Koshizuka, 1999, Phys. Rev. Lett. **82**, 2179.
Feibelman, P. J., and D. E. Eastman, 1974, Phys. Rev. B **10**, 4932.
Feng, D. L., N. P. Armitage, D. H. Lu, A. Damascelli, J. P. Hu, P. Bogdanov, A. Lanzara, F. Ronning, K. M. Shen, H. Eisaki, C. Kim, Z.-X. Shen, *et al.*, 2001, Phys. Rev. Lett. **86**, 5550.
Feng, D. L., A. Damascelli, K. M. Shen, N. Motoyama, D. H. Lu, H. Eisaki, K. Shimizu, J. Shimoyama, K. Kishio, N. Kaneko, M. Greven, G. D. Gu, *et al.*, 2002, Phys. Rev. Lett. **88**, 107001.
Feng, D. L., C. Kim, H. Eisaki, D. H. Lu, K. M. Shen, F. Ronning, N. P. Armitage, A. Damascelli, N. Kaneko, M. Greven, J. Shimoyama, K. Kishio, *et al.*, 2002, Phys. Rev. B **65**, 220501.
Feng, D. L., D. H. Lu, K. M. Shen, C. Kim, H. Eisaki, A. Damascelli, R. Yoshizaki, J. Shimoyama, K. Kishio, G. D. Gu, S. Oh, A. Andrus, *et al.*, 2000, Science **289**, 277.
Feng, D. L., W. J. Zheng, K. M. Shen, D. H. Lu, F. Ronning, J. Shimoyama, K. Kishio, G. Gu, D. V. der Marel, and Z.-X. Shen, 1999, e-print cond-mat/9908056.
Fetter, A. L., and J. D. Walecka, 1971, *Quantum Theory of Many-Particle Systems* (McGraw-Hill, New York).
Feuerbacher, B., B. Fitton, and R. F. Willis, 1978, *Photoemission and the Electronic Properties of Surfaces* (Wiley, New York).
Feuerbacher, B., and R. F. Willis, 1976, J. Phys. C **9**, 169.
Fink, J., N. Nücker, H. A. Romberg, and J. C. Fuggle, 1989, IBM J. Res. Dev. **33**, 372.

Fleck, M., A. I. Lichtenstein, E. Pavarini, and A. M. Oleś, 2000, Phys. Rev. Lett. **84**, 4962.
Fong, H. F., P. Bourges, Y. Sidis, L. P. Regnault, A. Ivanov, G. D. Gul, N. Koshizuka, and B. Keimer, 1999, Nature (London) **398**, 588.
Fong, H. F., B. Keimer, P. W. Anderson, D. Reznik, F. Doğan, and I. A. Aksay, 1995, Phys. Rev. Lett. **75**, 316.
Franz, M., and A. J. Millis, 1998, Phys. Rev. B **58**, 14 572.
Fretwell, H. M., A. Kaminski, J. Mesot, J. C. Campuzano, M. R. Norman, M. Randeria, T. Sato, R. Gatt, T. Takahashi, and K. Kadowaki, 2000, Phys. Rev. Lett. **84**, 4449.
Fulde, P., 1995, *Electron Correlations in Molecules and Solids* (Springer, Berlin).
Furukawa, N., and T. M. Rice, 1998, J. Phys.: Condens. Matter **10**, L381.
Furukawa, N., T. M. Rice, and M. Salmhofer, 1998, Phys. Rev. Lett. **81**, 3195.
Gadzuk, J. W., and M. Šunjić, 1975, Phys. Rev. B **12**, 524.
Garnier, M., K. Breuer, D. Purdie, M. Hengsberger, Y. Baer, and B. Delley, 1997, Phys. Rev. Lett. **78**, 4127.
Gavaler, J. R., 1973, Appl. Phys. Lett. **23**, 480.
Gobeli, G. W., F. G. Allen, and E. O. Kane, 1964, Phys. Rev. Lett. **12**, 94.
Gofron, K., J. C. Campuzano, A. A. Abrikosov, M. Lindroos, A. Bansil, H. Ding, D. Koelling, and B. Dabrowski, 1994, Phys. Rev. Lett. **73**, 3302.
Gofron, K., J. C. Campuzano, H. Ding, C. Gu, R. Liu, B. Dabrowski, B. W. Veal, W. Cramer, and G. Jennings, 1993, J. Phys. Chem. Solids **54**, 1193.
Golden, M. S., C. Dürr, A. Koitzsch, S. Legner, Z. Hu, S. Borisenko, M. Knupfer, and J. Fink, 2001, J. Electron Spectrosc. Relat. Phenom. **117-118**, 203.
Greber, T., T. J. Kreutz, and J. Osterwalder, 1997, Phys. Rev. Lett. **79**, 4465.
Greven, M., R. J. Birgeneau, Y. Endoh, M. A. Kastner, B. Keimer, M. Matsuda, G. Shirane, and T. R. Thurston, 1994, Phys. Rev. Lett. **72**, 1096.
Grioni, M., 2001, Ed., J. Electron Spectrosc. Relat. Phenom. **117-118**, special issue on Strongly Correlated Systems.
Gromko, A. D., Y.-D. Chuang, D. S. Dessau, K. Nakamura, and Y. Ando, 2000, e-print cond-mat/0003017.
Gromko, A. D., Y.-D. Chuang, A. V. Fedorov, Y. Aiura, Y. Yamaguchi, K. Oka, Y. Ando, and D. S. Dessau, 2002, e-print cond-mat/0205385.
Gromko, A. D., A. V. Fedorov, Y.-D. Chuang, J. D. Koralek, Y. Aiura, Y. Yamaguchi, K. Oka, Y. Ando, and D. S. Dessau, 2002, e-print cond-mat/0202329.
Guinea, F., R. S. Markiewicz, and M. A. H. Vozmediano, 2002, e-print cond-mat/0206208.
Gweon, G.-H., J. D. Denlinger, J. W. Allen, R. Claessen, C. G. Olson, H. Höchst, J. Marcus, C. Schlenker, and L. F. Schneemeyer, 2001, J. Electron Spectrosc. Relat. Phenom. **117-118**, 481.
Haas, S., A. Moreo, and E. Dagotto, 1995, Phys. Rev. Lett. **74**, 4281.
Haffner, S., D. M. Brammeier, C. G. Olson, L. L. Miller, and D. W. Lynch, 2001, Phys. Rev. B **63**, 212501.
Haffner, S., C. G. Olson, L. L. Miller, and D. W. Lynch, 2000, Phys. Rev. B **61**, 14 378.
Han, J. H., Q.-H. Wang, and D.-H. Lee, 2001, Int. J. Mod. Phys. B **15**, 1117.
Hansen, E. D., T. Miller, and T.-C. Chiang, 1997a, Phys. Rev. Lett. **78**, 2807.
Hansen, E. D., T. Miller, and T.-C. Chiang, 1997b, Phys. Rev. B **55**, 1871.
Hardy, W. N., D. A. Bonn, D. C. Morgan, R. Liang, and K. Zhang, 1993, Phys. Rev. Lett. **70**, 3999.
Harima, N., A. Fujimori, T. Sugaya, and I. Terasaki, 2002, e-print cond-mat/0203154.
Harima, N., J. Matsuno, A. Fujimori, Y. Onose, Y. Taguchi, and Y. Tokura, 2001, Phys. Rev. B **64**, 220507.
Harris, J. M., Z.-X. Shen, P. J. White, D. S. Marshall, M. C. Schabel, J. N. Eckstein, and I. Bozovic, 1996, Phys. Rev. B **54**, 15 665.
Harris, J. M., P. J. White, Z.-X. Shen, H. Ikeda, R. Yoshizaki, H. Eisaki, S. Uchida, W. D. Si, J. W. Xiong, Z.-X. Zhao, and D. S. Dessau, 1997, Phys. Rev. Lett. **79**, 143.
He, H., Y. Sidis, P. Bourges, G. D. Gu, A. Ivanov, N. Koshizuka, B. Liang, C. T. Lin, L. P. Regnault, E. Schoenherr, and B. Keimer, 2001, Phys. Rev. Lett. **86**, 1610.
Hedin, L., and S. Lundqvist, 1969, in *Solid State Physics: Advances in Research and Applications*, edited by H. Ehrenreich, F. Seitz, and D. Turnbull (Academic, New York), Vol. 23.
Hengsberger, M., R. Fresard, D. Purdie, P. Segovia, and Y. Baer, 1999, Phys. Rev. B **60**, 10 796.
Hengsberger, M., D. Purdie, P. Segovia, M. Garnier, and Y. Baer, 1999, Phys. Rev. Lett. **83**, 592.
Hermanson, J., 1977, Solid State Commun. **22**, 9.
Hertz, H., 1887, Ann. Phys. (Leipzig) **17**, 983.
Himpsel, F. J., 1983, Adv. Phys. **32**, 1.
Hiroi, Z., N. Kobayashi, and M. Takano, 1994, Nature (London) **371**, 139.
Hiroi, Z., N. Kobayashi, and M. Takano, 1996, Physica C **266**, 191.
Hodges, C., H. Smith, and J. W. Wilkins, 1971, Phys. Rev. B **4**, 302.
Hofmann, P., Y. Q. Cai, C. Grütter, and J. H. Bilgram, 1998, Phys. Rev. Lett. **81**, 1670.
Hollenstein, U., R. Seiler, H. Schmutz, M. Andrist, and F. Merkt, 2001, J. Chem. Phys. **115**, 5461.
Honerkamp, C., M. Salmhofer, N. Furukawa, and T. M. Rice, 2001, Phys. Rev. B **63**, 035109.
Horsch, P., and W. Stephan, 1993, *Electronic Properties of High-T_c Supercondcutors,* Springer Series in Solid State Science, Vol. 113, p. 351.
Horsch, P., W. H. Stephan, K. v. Szczepanski, M. Ziegler, W. von der Linden, 1989, Physica C **162-164**, 783.
Huang, Q., J. F. Zasadzinski, N. Tralshawala, K. E. Gray, D. G. Hinks, J. L. Peng, and R. L. Greene, 1990, Nature (London) **347**, 369.
Hubbard, J., 1964a, Proc. R. Soc. London, Ser. A **277**, 237.
Hubbard, J., 1964b, Proc. R. Soc. London, Ser. A **281**, 401.
Hüfner, S., 1995, *Photoelectron Spectroscopy* (Springer, Berlin).
Hwu, Y., L. Lozzi, M. Marsi, S. La Rosa, M. Winokur, P. Davis, M. Onellion, H. Berger, F. Gozzo, F. Levy, and G. Margaritondo, 1991, Phys. Rev. Lett. **67**, 2573.
Ichioka, M., and K. Machida, 1999, J. Phys. Soc. Jpn. **68**, 4020.
Imada, M., 1993, J. Phys. Soc. Jpn. **62**, 1105.
Imada, M., A. Fujimori, and Y. Tokura, 1998, Rev. Mod. Phys. **70**, 1039.
Inglesfield, J. E., and B. W. Holland, 1981, in *The Chemical Physics of Solid Surfaces and Heterogeneous Catalysis*, edited by D. A. King and D. P. Woodruff (Elsevier Scientific, Amsterdam), Vol. 1.

Ino, A., C. Kim, T. Mizokawa, Z.-X. Shen, A. Fujimori, M. Takaba, K. Tamasaku, H. Eisaki, and S. Uchida, 1999, J. Phys. Soc. Jpn. **68**, 1496.
Ino, A., C. Kim, M. Nakamura, T. Yoshida, T. Mizokawa, A. Fujimori, Z.-X. Shen, T. Kakeshita, H. Eisaki, and S. Uchida, 2002, Phys. Rev. B **65**, 094504.
Ino, A., C. Kim, M. Nakamura, T. Yoshida, T. Mizokawa, Z.-X. Shen, A. Fujimori, T. Kakeshita, H. Eisaki, and S. Uchida, 2000, Phys. Rev. B **62**, 4137.
Ino, A., T. Mizokawa, A. Fujimori, K. Tamesaku, H. Eisaki, S. Uchida, T. Kimura, T. Sasagawa, and K. Kishio, 1997, Phys. Rev. Lett. **79**, 2101.
Ino, A., T. Mizokawa, K. Kobayashi, A. Fujimori, T. Sasagawa, T. Kimura, K. Kishio, K. Tamasaku, H. Eisaki, and S. Uchida, 1998, Phys. Rev. Lett. **81**, 2124.
Ioffe, L. B., and A. J. Millis, 1996, Phys. Rev. B **54**, 3645.
Jacobs, T., S. Sridhar, Q. Li, G. D. Gu, and N. Koshizuka, 1995, Phys. Rev. Lett. **75**, 4516.
Jahn, H. A., and E. Teller, 1937, Proc. R. Soc. London, Ser. A **61**, 220.
Johnson, P. D., A. V. Fedorov, and T. Valla, 2001, J. Electron Spectrosc. Relat. Phenom. **117-118**, 153.
Johnson, P. D., T. Valla, A. V. Fedorov, Z. Yusof, B. O. Wells, Q. Li, A. R. Moodenbaugh, G. D. Gu, N. Koshizuka, C. Kendziora, S. Jian, and D. G. Hinks, 2001, Phys. Rev. Lett. **87**, 177007.
Jorgensen, J. D., M. A. Beno, D. G. Hinks, L. Soderholm, K. J. Volin, R. L. Hitterman, J. D. Grace, I. K. Schuller, C. U. Segrè, K. Zhang, and M. S. Kleefisch, 1987, Phys. Rev. B **36**, 3608.
Joyce, J. J., A. J. Arko, J. Lawrence, P. C. Canfield, Z. Fisk, R. J. Bartlett, and J. D. Thompson, 1992, Phys. Rev. Lett. **68**, 236.
Kaindl, G., M. Domke, C. Laubschat, E. Weschke, and C. Xue, 1992, Rev. Sci. Instrum. **63**, 1234.
Kaminski, A., J. Mesot, H. Fretwell, J. C. Campuzano, M. R. Norman, M. Randeria, H. Ding, T. Sato, T. Takahaski, T. Mochiku, K. Kadowaki, and H. Hoechsts, 2000, Phys. Rev. Lett. **84**, 1788.
Kaminski, A., M. Randeria, J. C. Campuzano, M. R. Norman, H. Fretwell, J. Mesot, T. Sato, T. Takahashi, and K. Kadowaki, 2001, Phys. Rev. Lett. **86**, 1070.
Kaminski, A., S. Rosenkranz, H. M. Fretwell, J. C. Campuzano, Z. Li, H. Raffy, W. G. Cullen, H. You, C. G. Olson, C. M. Varma, and H. Höchst, 2002, Nature (London) **416**, 610.
Kampf, A., and J. R. Schrieffer, 1990a, Phys. Rev. B **41**, 6399.
Kampf, A. P., and J. R. Schrieffer, 1990b, Phys. Rev. B **42**, 7967.
Kevan, S. D., 1992, *Angle Resolved Photoemission—Theory and Current Applications* (Elsevier Science, Amsterdam).
Kevan, S. D., and E. Rotenberg, 2001, J. Electron Spectrosc. Relat. Phenom. **117-118**, 57.
Kim, C., 2001, J. Electron Spectrosc. Relat. Phenom. **117-118**, 503.
Kim, C., A. Y. Matsuura, Z.-X. Shen, N. Motoyama, H. Eisaki, S. Uchida, T. Tohyama, and S. Maekawa, 1996, Phys. Rev. Lett. **77**, 4054.
Kim, C., F. Ronning, A. Damascelli, D. L. Feng, Z.-X. Shen, B. O. Wells, Y. J. Kim, R. J. Birgeneau, M. A. Kastner, L. L. Miller, H. Eisaki, and S. Uchida, 2002, Phys. Rev. B **65**, 174516.
Kim, C., Z.-X. Shen, N. Motoyama, H. Eisaki, S. Uchida, T. Tohyama, and S. Maekawa, 1997, Phys. Rev. B **56**, 15 589.
Kim, C., P. J. White, Z.-X. Shen, T. Tohyama, Y. Shibata, S. Maekawa, B. O. Wells, Y. J. Kim, R. J. Birgeneau, and M. A. Kastner, 1998, Phys. Rev. Lett. **80**, 4245.
Kimura, H., K. Hirota, C.-H. Lee, K. Yamada, and G. Shirane, 2000, J. Phys. Soc. Jpn. **69**, 851.
King, D. M., D. S. Dessau, A. G. Loeser, Z.-X. Shen, and B. O. Wells, 1995, J. Phys. Chem. Solids **56**, 1865.
King, D. M., Z.-X. Shen, D. S. Dessau, B. O. Wells, W. E. Spicer, A. J. Arko, D. S. Marshall, J. DiCarlo, A. G. Loeser, C. H. Park, E. R. Ratner, J. L. Peng, *et al.*, 1993, Phys. Rev. Lett. **70**, 3159.
Kipp, L., K. Rossnagel, C. Solterbeck, T. Strasser, W. Schattke, and M. Skibowski, 1999, Phys. Rev. Lett. **83**, 5551.
Kittel, C., 1996, *Introduction to Solid State Physics* (Wiley, New York).
Kivelson, S. A., E. Fradkin, and V. J. Emery, 1998, Nature (London) **393**, 550.
Koch, E.-E., G. V. Marr, G. S. Brown, D. E. Moncton, S. Ebashi, M. Koch, and E. Rubenstein, 1991, Eds., *Handbook on Synchrotron Radiation* (Elsevier Science, Amsterdam).
Kohsaka, Y., T. Sasagawa, F. Ronning, T. Yoshida, C. Kim, T. Hanaguri, M. Azuma, M. Takano, Z.-X. Shen, and H. Takagi, 2002, e-print cond-mat/0209339.
Kokales, J. D., P. Fournier, L. V. Mercaldo, V. V. Talanov, R. L. Greene, and S. M. Anlage, 2000, Phys. Rev. Lett. **85**, 3696.
Kordyuk, A. A., S. V. Borisenko, M. S. Golden, S. Legner, K. A. Nenkov, M. Knupfer, J. Fink, H. Berger, L. Forro, and R. Follath, 2002, Phys. Rev. B **66**, 014502.
Kordyuk, A. A., S. V. Borisenko, T. K. Kim, K. Nenkov, M. Knupfer, M. S. Golden, J. Fink, H. Berger, and R. Follath, 2002, Phys. Rev. Lett **89**, 077003.
Kotliar, G., and J. Liu, 1988, Phys. Rev. Lett. **61**, 1784.
Krakauer, H., and W. E. Pickett, 1988, Phys. Rev. Lett. **60**, 1665.
Kuroda, Y., and C. M. Varma, 1990, Phys. Rev. B **42**, 8619.
Kusko, C., R. S. Markiewicz, M. Lindroos, and A. Bansil, 2002, Phys. Rev. B **66**, 140513.
Kyung, B., and R. A. Ferrell, 1996, Phys. Rev. B **54**, 10 125.
Landau, L. D., 1956, Sov. Phys. JETP **3**, 920.
Landau, L. D., 1957, Sov. Phys. JETP **5**, 101.
Landau, L. D., 1959, Sov. Phys. JETP **8**, 70.
Lanzara, A., 2002, Standford University preprint.
Lanzara, A., P. V. Bogdanov, X. J. Zhou, S. A. Kellar, D. L. Feng, E. D. Lu, T. Yoshida, H. Elsaki, A. Fujimori, K. Kishio, J. Shimoyama, T. Noda, *et al.*, 2001, Nature (London) **412**, 510.
La Rosa, S., I. Vobornik, F. Zwick, H. Berger, M. Grioni, G. Margaritondo, R. J. Kelley, M. Onellion, and A. Chubukov, 1997, Phys. Rev. B **56**, 525.
LaShell, S., E. Jensen, and T. Balasubramanian, 2000, Phys. Rev. B **61**, 2371.
Laughlin, R. B., 1995, J. Low Temp. Phys. **99**, 443.
Laughlin, R. B., 1997, Phys. Rev. Lett. **79**, 1726.
Leckey, R. C. G., 1982, Appl. Surf. Sci. **13**, 125.
Lee, D.-H., 2000, Phys. Rev. Lett. **84**, 2694.
Lee, P. A., and N. Nagaosa, 1992, Phys. Rev. B **46**, 5621.
Lee, T. K., and C. T. Shih, 1997, Phys. Rev. B **55**, 5983.
Lema, F., and A. A. Aligia, 1997, Phys. Rev. B **55**, 14 092.
Leung, P. W., B. O. Wells, and R. J. Gooding, 1997, Phys. Rev. B **56**, 6320.
Levi, B. G., 1990, Phys. Today **43** (3), 20.
Levi, B. G., 1993, Phys. Today **46** (5), 17.
Levi, B. G., 1996, Phys. Today **49** (1), 19.

Ley, L., and M. Cardona, 1979, *Photoemission in Solids*, Vol. II (Springer, Berlin).
Liang, R., D. A. Bonn, and W. N. Hardy, 1998, Physica C **304**, 105.
Lieb, E. H., and F. Y. Wu, 1968, Phys. Rev. Lett. **20**, 1445.
Liebsch, A., 1976, Phys. Rev. B **13**, 544.
Liebsch, A., 1978, in *Electron and Ion Spectroscopy of Solids*, edited by L. Fiermans, J. Vennik, and W. Dekeyser (Plenum, New York).
Liechtenstein, A. I., O. Gunnarsson, O. K. Andersen, and R. M. Martin, 1996, Phys. Rev. B **54**, 12 505.
Limonov, M. F., A. I. Rykov, S. Tajima, and A. Yamanaka, 2000, Phys. Rev. B **61**, 12 412.
Lindau, I., and W. E. Spicer, 1980, in *Synchrotron Radiation Research*, edited by H. Winick and S. Doniach (Plenum, New York).
Lindroos, M., and A. Bansil, 1995, Phys. Rev. Lett. **75**, 1182.
Lindroos, M., and A. Bansil, 1996, Phys. Rev. Lett. **77**, 2985.
Lindroos, M., S. Sahrakorpi, and A. Bansil, 2002, Phys. Rev. B **65**, 054514.
Littlewood, P. B., and C. M. Varma, 1991, J. Appl. Phys. **69**, 4979.
Liu, R., B. W. Veal, C. Gu, A. P. Paulikas, P. Kostic, and C. G. Olson, 1995, Phys. Rev. B **52**, 553.
Liu, Z., and E. Manousakis, 1992, Phys. Rev. B **45**, 2425.
Loeser, A. G., Z.-X. Shen, D. S. Dessau, D. S. Marshall, C. H. Park, P. Fournier, and A. Kapitulnik, 1996, Science **273**, 325.
Loeser, A. G., Z.-X. Shen, M. C. Schabel, C. Kim, M. Zhang, A. Kapitulnik, and P. Fournier, 1997, Phys. Rev. B **56**, 14185.
Lu, D. H., D. L. Feng, N. P. Armitage, K. M. Shen, A. Damascelli, C. Kim, F. Ronning, Z.-X. Shen, D. A. Bonn, R. Liang, W. N. Hardy, A. I. Rykov, *et al.*, 2001, Phys. Rev. Lett. **86**, 4370.
Lu, D. H., M. Schmidt, T. R. Cummins, S. Schuppler, F. Lichtenberg, and J. G. Bednorz, 1996, Phys. Rev. Lett. **76**, 4845.
Luttinger, J. M., 1960, Phys. Rev. **119**, 1153.
Luttinger, J. M., 1961, Phys. Rev. **121**, 942.
Lynch, D. W., and C. G. Olson, 1999, *Photoemission Studies of High-Temperature Superconductors* (Cambridge University, Cambridge).
Mackenzie, A. P., S. R. Julian, A. J. Diver, G. J. Mcmullan, M. P. Ray, G. G. Lonzarich, Y. Maeno, S. Nishizaki, and T. Fujita, 1996, Phys. Rev. Lett. **76**, 3786.
Maekawa, S., T. Matsuura, Y. Isawa, and H. Ebisawa, 1988, Physica C **152**, 133.
Mahan, G. D., 1970, Phys. Rev. B **2**, 4334.
Mahan, G. D., 1978, in *Electron and Ion Spectroscopy of Solids*, edited by L. Fiermans, J. Vennik, and W. Dekeyser (Plenum, New York).
Mahan, G. D., 1981, *Many-Particle Physics* (Plenum, New York).
Makinson, R. E. B., 1949, Phys. Rev. **75**, 1908.
Margaritondo, G., and J. H. Weaver, 1983, in *Methods of Experimental Physics: Surfaces*, edited by M. G. Legally and R. L. Park (Academic, New York).
Markiewicz, R. S., 1991, Int. J. Mod. Phys. B **5**, 2037.
Markiewicz, R. S., 1997, J. Phys. Chem. Solids **58**, 1179.
Markiewicz, R. S., 2000, Phys. Rev. B **62**, 1252.
Marshall, D. S., D. S. Dessau, A. G. Loeser, C.-H. Park, A. Y. Matsuura, J. N. Eckstein, I. Bozovic, P. Fournier, A. Kapitulnik, W. E. Spicer, and Z.-X. Shen, 1996, Phys. Rev. Lett. **76**, 4841.
Martensson, N., P. Baltzer, P. A. Bruhwiler, J.-O. Forsell, A. Nilsson, A. Stenborg, and B. Wannberg, 1994, J. Electron Spectrosc. Relat. Phenom. **70**, 117.
Massidda, S., J. Yu, and A. J. Freeman, 1988, Physica C **152**, 251.
Mattheiss, L. F., 1987, Phys. Rev. Lett. **58**, 1028.
Matzdorf, R., Z. Fang, Ismail, J. Zhang, T. Kimura, Y. Tokura, K. Terakura, and E. W. Plummer, 2000, Science **289**, 746.
Mazin, I. I., and D. J. Singh, 1997, Phys. Rev. Lett. **79**, 733.
McQueeney, R. J., Y. Petrov, T. Egami, M. Yethiraj, G. Shirane, and Y. Endoh, 1999, Phys. Rev. Lett. **82**, 628.
Meinders, M. B. J., 1994, Ph.D. thesis (University of Groningen, The Netherlands).
Mesot, J., M. Boehm, M. R. Norman, M. Randeria, N. Metoki, A. Kaminski, S. Rosenkranz, A. Hiess, H. M. Fretwell, J. C. Campuzano, and K. Kadowaki, 2001, e-print cond-mat/0102339.
Mesot, J., M. R. Norman, H. Ding, M. Randeria, J. C. Campuzano, A. Paramekanti, H. M. Fretwell, A. Kaminski, T. Takeuchi, S. Yokoya, T. Sato, T. Takahashi, *et al.*, 1999, Phys. Rev. Lett. **83**, 840.
Mesot, J., M. Randeria, M. R. Norman, A. Kaminski, H. M. Fretwell, J. C. Campuzano, H. Ding, T. Takeuchi, T. Sato, T. Yokoya, T. Takahashi, I. Chong, *et al.*, 2001, Phys. Rev. B **63**, 224516.
Miles, P. A., S. J. Kennedy, A. R. Anderson, G. D. Gu, G. J. Russell, and N. Koshizuka, 1997, Phys. Rev. B **55**, 14 632.
Miller, T., W. E. McMahon, and T.-C. Chiang, 1996, Phys. Rev. Lett. **77**, 1167.
Millis, A. J., 1999, Nature (London) **398**, 193.
Mitchell, K., 1934, Proc. R. Soc. London, Ser. A **146**, 442.
Mitton, S., 1995, Science Watch **6** (1), 1.
Mitton, S., 1998, Science Watch **9** (2), 1.
Molegraaf, H. J. A., C. Presura, D. van der Marel, P. H. Kes, and M. Li, 2002, Science **295**, 2239.
Moler, K. A., J. R. Kirtley, D. G. Hinks, T. W. Li, and M. Xu, 1998, Science **279**, 1193.
Molodtsov, S. L., S. V. Halilov, V. D. P. Servedio, W. Schneider, S. Danzenbächer, J. J. Hinarejos, M. Richter, and C. Laubschat, 2000, Phys. Rev. Lett. **85**, 4184.
Mook, H. A., F. Doğan, and B. C. Chakoumakos, 1998, e-print cond-mat/9811100.
Mook, H. A., M. Yethiraj, G. Aeppli, T. E. Mason, and T. Armstrong, 1993, Phys. Rev. Lett. **70**, 3490.
Moraghebi, M., C. Buhler, S. Yunoki, and A. Moreo, 2001, Phys. Rev. B **63**, 214513.
Mori, M., T. Tohyama, and S. Maekawa, 2002, Phys. Rev. B **66**, 064502.
Mott, N. F., 1949, Proc. Phys. Soc., London, Sect. A **62**, 416.
Mott, N. F., 1956, Can. J. Phys. **34**, 1356.
Mott, N. F., 1974, *Metal Insulator Transition* (Taylor and Francis, London).
Müller, K. A., 2000, in *Stripes and Related Phenomena,* edited by A. Bianconi and N. L. Saini (Kluwer Academic/Plenum, New York).
Müller, R., C. Janowitz, M. Schneider, R.-S. Unger, A. Krapf, H. Dwelk, A. Müller, L. Dudy, R. Manzke, and H. Hoechst, 2002, J. Supercond. **15**, 147.
Nagamatsu, J., N. Nakagawa, T. Muranaka, Y. Zenitani, and J. Akimitsu, 2001, Nature (London) **410**, 63.
Nagaosa, N., and P. A. Lee, 2000, Phys. Rev. B **61**, 9166.
Nakano, T., N. Momono, M. Oda, and M. Ido, 1998, J. Phys. Soc. Jpn. **67**, 2622.

Nazarenko, A., K. J. E. Vos, S. Haas, E. Dagotto, and R. J. Gooding, 1995, Phys. Rev. B **51**, 8676.
Nemoshkalenko, V. V., and V. G. Aleshin, 1979, *Electron Spectroscopy of Crystals* (Plenum, New York).
Norman, M. R., 2001, Phys. Rev. B **63**, 092509.
Norman, M. R., and H. Ding, 1998, Phys. Rev. B **57**, 11 089.
Norman, M. R., H. Ding, J. C. Campuzano, T. Takeuchi, M. Randeria, T. Yokoya, T. Takahashi, T. Mochiku, and K. Kadowaki, 1997, Phys. Rev. Lett. **79**, 3506.
Norman, M. R., H. Ding, H. Fretwell, M. Randeria, and J. C. Campuzano, 1999, Phys. Rev. B **60**, 7585.
Norman, M. R., H. Ding, M. Randeria, J. C. Campuzano, T. Yokoya, T. Takeuchi, T. Takahashi, T. Mochiku, K. Kadowaki, P. Guptasarma, and D. G. Hinks, 1998, Nature (London) **392**, 157.
Norman, M. R., M. Eschrig, A. Kaminski, and J. C. Campuzano, 2001, Phys. Rev. B **64**, 184508.
Norman, M. R., A. Kaminski, J. Mesot, and J. C. Campuzano, 2001, Phys. Rev. B **63**, 140508.
Norman, M. R., M. Randeria, H. Ding, and J. C. Campuzano, 1998, Phys. Rev. B **57**, 11 093.
Nozières, P., 1964, *Theory of Interacting Fermi Systems* (Benjamin, New York).
Oguchi, T., 1995, Phys. Rev. B **51**, 1385.
Olson, C. G., R. Liu, D. W. Lynch, R. S. List, A. J. Arko, B. W. Veal, Y. C. Chang, P. Z. Jiang, and A. P. Paulikas, 1990, Phys. Rev. B **42**, 381.
Olson, C. G., R. Liu, A.-B. Yang, D. W. Lynch, A. J. Arko, R. S. List, B. W. Veal, Y. C. Chang, P. Z. Jiang, and A. P. Paulikas, 1989, Science **245**, 731.
Orenstein, J., and A. J. Millis, 2000, Science **288**, 468.
Orgad, D., S. A. Kivelson, E. W. Carlson, V. J. Emery, X. J. Zhou, and Z.-X. Shen, 2001, Phys. Rev. Lett. **86**, 4362.
Osterwalder, J., P. Aebi, P. Schwaller, L. Schlapbach, M. Shimoda, T. Mochiku, and K. Kadowaki, 1995, Appl. Phys. A: Mater. Sci. Process. **60A**, 247.
Patthey, F., J.-M. Imer, W.-D. Schneider, H. Beck, Y. Baer, and B. Delley, 1990, Phys. Rev. B **42**, 8864.
Pendry, J. B., 1975, J. Phys. C **8**, 2413.
Pendry, J. B., 1976, Surf. Sci. **57**, 679.
Petrov, Y., T. Egami, R. J. McQueeney, M. Yethiraj, H. A. Mook, and F. Doğan, 2000, e-print cond-mat/0003414.
Pickett, W. E., 1989, Rev. Mod. Phys. **61**, 433.
Pines, D., 1997, Z. Phys. B: Condens. Matter **103**, 129.
Pines, D., and P. Nozières, 1966, *The Theory of Quantum Liquids*, Vol. 1 (Benjamin, New York).
Plummer, E. W., and W. Eberhardt, 1982, in *Advances in Chemical Physics*, edited by I. Prigogine and S. A. Rice (Wiley, New York), Vol. XLIV.
Polturak, E., G. Koren, D. Cohen, and E. Aharoni, 1993, Phys. Rev. B **47**, 5270.
Presland, M. R., J. L. Tallon, R. G. Buckley, R. S. Liu, and N. E. Flower, 1991, Physica C **176**, 95.
Preuss, R., W. Hanke, and W. von der Linden, 1995, Phys. Rev. Lett. **75**, 1344.
Prozorov, R., R. W. Giannetta, P. Fournier, and R. L. Greene, 2000, Phys. Rev. Lett. **85**, 3700.
Puchkov, A. V., D. N. Basov, and T. Timusk, 1996, J. Phys.: Condens. Matter **8**, 10 049.
Puchkov, A. V., Z.-X. Shen, T. Kimura, and Y. Tokura, 1998, Phys. Rev. B **58**, 13 322.
Randeria, M., and J.-C. Campuzano, 1997, e-print cond-mat/9709107.
Randeria, M., H. Ding, J. C. Campuzano, A. Bellman, G. Jennings, T. Tokoya, T. Takahashi, H. Katayama-Yoshida, T. Mochiku, and K. Kadowaki, 1995, Phys. Rev. Lett. **74**, 4951.
Rao, C. N. R., and B. Raveau, 1995, *Transition Metal Oxides* (VCH, New York).
Rickayzen, G., 1991, *Green's Functions and Condensed Matter in Techniques of Physics*, Vol. 7 (Academic, London).
Ronning, F., C. Kim, D. L. Feng, D. S. Marshall, A. G. Loeser, L. L. Miller, J. N. Eckstein, L. Bozovic, and Z.-X. Shen, 1998, Science **282**, 2067.
Ronning, F., C. Kim, K. M. Shen, N. P. Armitage, A. Damascelli, D. H. Lu, D. L. Feng, Z.-X. Shen, L. L. Miller, Y.-J. Kim, F. Chou, and I. Terasaki, 2003, Phys. Rev. B **67**, 035113.
Ronning, F., T. Sasagawa, Y. Kohsaka, K. M. Shen, A. Damascelli, C. Kim, T. Yoshida, N. P. Armitage, D. H. Lur, D. L. Feng, L. L. Miller, H. Takagi, *et al.*, 2003, e-print cond-mat/0301024.
Rossat-Mignod, J., L. P. Regnault, C. Vettier, P. Bourges, P. Burlet, J. Bossy, J. Y. Henry, and G. Lapertot, 1991, Physica C **185-189**, 86.
Rossnagel, K., L. Kipp, M. Skibowski, C. Solterbeck, T. Strasser, W. Schattke, D. VoS, P. Krüger, A. Mazur, and J. Pollmann, 2001, Phys. Rev. B **63**, 125104.
Rotenberg, E., J. Schaefer, and S. D. Keven, 2000, Phys. Rev. Lett. **84**, 2925.
Sachdev, S., 2000, Science **288**, 475.
Sachdev, S., and J. Ye, 1992, Phys. Rev. Lett. **69**, 2411.
Saini, N. L., J. Avila, A. Bianconi, A. Lanzara, M. C. Asensio, S. Tajima, G. D. Gu, and N. Koshizuka, 1997, Phys. Rev. Lett. **79**, 3467.
Saitoh, Y., T. Nakatani, T. Matsushita, T. Miyahara, M. Fujisawa, K. Soda, T. Muro, S. Ueda, H. Harada, A. Sekiyama, S. Imada, H. Daimon, *et al.*, 1998, J. Synchrotron Radiat. **5**, 542.
Salkola, M. I., V. J. Emery, and S. A. Kivelson, 1996, Phys. Rev. Lett. **77**, 155.
Sato, T., T. Kamiyama, Y. Naitoh, T. Takahashi, I. Chong, T. Terashima, and M. Takano, 2001, Phys. Rev. B **63**, 132502.
Sato, T., T. Kamiyama, T. Takahashi, K. Kurahashi, and K. Yamada, 2001a, Science **291**, 1517.
Sato, T., T. Kamiyama, T. Takahashi, J. Mesot, A. Kaminski, J. C. Campuzano, H. M. Fretwell, T. Takeuchi, H. Ding, I. Chong, T. Terashima, and M. Takano, 2001b, Phys. Rev. B **64**, 054502.
Sato, T., H. Matsui, S. Nishina, T. Takahashi, T. Fujii, T. Watanabe, and A. Matsuda, 2002, Phys. Rev. Lett. **89**, 067005.
Sato, T., L. T. Yokoya, Y. Naitoh, T. Takahashi, K. Yamada, and Y. Endoh, 1999, Phys. Rev. Lett. **83**, 2254.
Sawatzky, G. A., 1989, Nature (London) **342**, 480.
Scalapino, D. J., 1969, in *Superconductivity*, edited by R. D. Park (Decker, New York), Vol. 1.
Scalapino, D. J., 1995, Phys. Rep. **250**, 330.
Schabel, M. C., C.-H. Park, A. Matsuura, Z.-X. Shen, D. A. Bonn, R. Liang, and W. N. Hardy, 1997, Phys. Rev. B **55**, 2796.
Schabel, M. C., C.-H. Park, A. Matsuura, Z.-X. Shen, D. A. Bonn, R. Liang, and W. N. Hardy, 1998a, Phys. Rev. B **57**, 6090.
Schabel, M. C., C.-H. Park, A. Matsuura, Z.-X. Shen, D. A. Bonn, R. Liang, and W. N. Hardy, 1998b, Phys. Rev. B **57**, 6107.
Schaich, W. L., and N. W. Ashcroft, 1971, Phys. Rev. B **3**, 2452.

Schilling, A., M. Cantoni, J. D. Guo, and H. R. Ott, 1993, Nature (London) **363**, 56.
Schmalian, J., D. Pines, and B. Stojković, 1998, Phys. Rev. Lett. **80**, 3839.
Schrieffer, J. R., 1964, *Theory of Superconductivity* (Addison-Wesley, New York).
Schwaller, P., P. Aebi, H. Berger, C. Beeli, J. Osterwalder, and L. Schlapbach, 1995, J. Electron Spectrosc. Relat. Phenom. **76**, 127.
Seah, M. P., and W. A. Dench, 1979, Surf. Interface Anal. **1**, 2.
Sekiyama, A., T. Iwasaki, K. Matsuda, Y. Saitoh, Y. Onuki, and S. Suga, 2000, Nature (London) **403**, 396.
Senthil, T., and M. P. A. Fisher, 1999, e-print cond-mat/9912380.
Shen, K. M., A. Damascelli, D. H. Lu, N. P. Armitage, F. Ronning, D. L. Feng, C. Kim, Z.-X. Shen, D. J. Singh, I. I. Mazin, S. Nakatsuji, Z. Q. Mao, *et al.*, 2001, Phys. Rev. B **64**, 180502.
Shen, Z.-X., and D. S. Dessau, 1995, Phys. Rep. **253**, 1.
Shen, Z.-X., D. S. Dessau, B. O. Wells, D. M. King, W. E. Spicer, A. J. Arko, D. Marshall, L. W. Lombardo, A. Kapitulnik, P. Dickinson, S. Doniach, J. DiCarlo, *et al.*, 1993, Phys. Rev. Lett. **70**, 1553.
Shen, Z.-X., J. M. Harris, and A. G. Loeser, 1997, Hyperfine Interact. **105**, 13.
Shen, Z.-X., A. Lanzara, S. Ishihara, and N. Nagaosa, 2002, Philos. Mag. B **82**, 1349.
Shen, Z.-X., and G. A. Sawatzky, 1999, Phys. Status Solidi B **215**, 523.
Shen, Z.-X., and J. R. Schrieffer, 1997, Phys. Rev. Lett. **78**, 1771.
Shen, Z.-X., P. J. White, D. L. Feng, C. Kim, G. D. Gu, H. Ikeda, R. Yoshizaki, and N. Koshizuka, 1998, Science **280**, 259.
Shirley, D. A., 1972, Phys. Rev. B **5**, 4709.
Siegbahn, K., K. Siegbahn, C. Nordling, G. Johansson, J. Hedman, P. F. Heden, K. Hamrin, U. I. Gelius, T. Bergmark, L. O. Werme, R. Manne, and Y. Baer, 1969, *ESCA Applied to Free Molecules* (North-Holland, Amsterdam).
Sigmund, E., and K. A. Müller, 1994, Eds., *Phase Separation in Cuprate Superconductors* (Springer Verlag, Berlin).
Singh, D. J., 1995, Phys. Rev. B **52**, 1358.
Singh, D. J., and W. E. Pickett, 1995, Phys. Rev. B **51**, 3128.
Smith, K. E., and S. D. Kevan, 1991, Prog. Solid State Chem. **21**, 49.
Smith, N. V., 1971, CRC Crit. Rev. Solid State Sci. **2**, 45.
Smith, N. V., and F. J. Himpsel, 1983, in *Handbook on Synchrotron Radiation*, edited by E.-E. Koch (North-Holland, Amsterdam), Vol. Ib.
Smith, N. V., P. Thiry, and Y. Petroff, 1993, Phys. Rev. B **47**, 15 476.
Sokol, A., and D. Pines, 1993, Phys. Rev. Lett. **71**, 2813.
Sonier, J. E., J. H. Brewer, R. F. Kiefl, R. I. Miller, G. D. Morris, C. E. Stronach, J. S. Gardner, S. R. Dunsiger, D. A. Bonn, W. N. Hardy, R. Liang, and R. H. Heffner, 2001, Science **292**, 1692.
Sonier, J. E., J. H. Brewer, R. F. Kiefl, G. D. Morris, R. I. Miller, D. A. Bonn, J. Chakhalian, R. H. Heffner, W. N. Hardy, and R. Liang, 1999, Phys. Rev. Lett. **83**, 4156.
Stadlober, B., G. Krug, R. Nemetschek, R. Hackl, J. L. Cobb, and J. T. Markert, 1995, Phys. Rev. Lett. **74**, 4911.
Steeneken, P., 2001, University of Groningen preprint.
Straub, T., R. Claessen, P. Steiner, S. Hüfner, V. Eyert, K. Friemelt, and E. Bucher, 1997, Phys. Rev. B **55**, 13 473.
Strocov, V. N., R. Claessen, G. Nicolay, S. Hüfner, A. Kimura, A. Harasawa, S. Shin, A. Kakizaki, P. O. Nilsson, H. I. Starnberg, and P. Blaha, 1998, Phys. Rev. Lett. **81**, 4943.
Strocov, V. N., H. I. Starnberg, P. O. Nilsson, H. E. Brauer, and L. J. Holleboom, 1997, Phys. Rev. Lett. **79**, 467.
Sushkov, O. P., G. A. Sawatzky, R. Eder, and H. Eskes, 1997, Phys. Rev. B **56**, 11 769.
Suzuki, T., T. Goto, K. Chiba, T. Shinoda, T. Fukase, H. Kimura, K. Yamada, M. Ohashi, and Y. Yamaguchi, 1998, Phys. Rev. B **57**, 3229.
Suzumura, Y., Y. Hasegawa, and H. Fukuyama, 1988, J. Phys. Soc. Jpn. **57**, 2768.
Takahashi, T., H. Matsuyama, H. Katayama-Yoshida, Y. Okabe, S. Hosoya, K. Seki, H. Fujimoto, M. Sata, and H. Inokuchi, 1988, Nature (London) **334**, 691.
Takeuchi, T., T. Yokoya, S. Shin, K. Jinno, M. Matsuura, T. Kondo, H. Ikuta, and U. Mizutani, 2001, J. Electron Spectrosc. Relat. Phenom. **114-116**, 629.
Tallon, J. L., C. Bernhard, H. Shaked, R. L. Hitterman, and J. D. Jorgensen, 1995, Phys. Rev. B **51**, 12 911.
Tallon, J. L., and J. W. Loram, 2001, Physica C **349**, 53.
Tallon, J. L., J. W. Loram, G. V. M. Williams, J. R. Cooper, I. R. Fisher, J. D. Johnson, M. P. Staines, and C. Bernhard, 1999, Phys. Status Solidi B **215**, 531.
Tallon, J. L., G. V. M. Williams, and J. W. Loram, 2000, Physica C **338**, 9.
Tanamoto, T., H. Kohno, and H. Fukuyama, 1992, J. Phys. Soc. Jpn. **61**, 1886.
Tarascon, J. M., W. R. McKinnon, P. Barboux, D. M. Hwang, B. G. Bagley, L. H. Greene, G. W. Hull, Y. LePage, N. Stoffel, and M. Giroud, 1988, Phys. Rev. B **38**, 8885.
Testardi, L. R., J. H. Wernick, and W. A. Royer, 1974, Solid State Commun. **15**, 1.
Tinkham, M., 1996, *Introduction to Superconductivity* (McGraw-Hill, New York).
Tjeng, L. H., N. B. Brookes, and B. Sinkovic, 2001, J. Electron Spectrosc. Relat. Phenom. **117-118**, 189.
Tohyama, T., and S. Maekawa, 2000, Supercond. Sci. Technol. **13**, R17.
Tohyama, T., S. Nagai, Y. Shibata, and S. Maekawa, 1999, Phys. Rev. Lett. **82**, 4910.
Tohyama, T., Y. Shibata, S. Maekawa, Z.-X. Shen, N. Nagaosa, and L. L. Miller, 2000, J. Phys. Soc. Jpn. **69**, 9.
Tokura, Y., and N. Nagaosa, 2000, Science **288**, 462.
Tranquada, J. M., B. J. Sternlieb, J. D. Axe, Y. Nakamura, and S. Uchida, 1995, Nature (London) **375**, 561.
Tsuei, C. C., and J. R. Kirtley, 2000a, Rev. Mod. Phys. **72**, 969.
Tsuei, C. C., and J. R. Kirtley, 2000b, Phys. Rev. Lett. **85**, 182.
Tsvetkov, A. A., D. van der Marel, K. A. Moler, J. R. Kirtley, J. L. de Boer, A. Meetsma, Z. F. Ren, N. Koleshnikov, D. Dulić, A. Damascelli, M. Grüninger, J. Schützmann, *et al.*, 1998, Nature (London) **395**, 360.
Uemura, Y. J., L. P. Le, G. M. Luke, B. J. Sternlieb, W. D. Wu, J. H. Brewer, T. M. Riseman, C. L. Seaman, M. B. Maple, M. Ishikawa, D. G. Hinks, J. D. Jorgensen, *et al.*, 1991, Phys. Rev. Lett. **66**, 2665.
Valla, T., A. V. Fedorov, P. D. Johnson, and S. L. Hulbert, 1999, Phys. Rev. Lett. **83**, 2085.
Valla, T., A. V. Fedorov, P. D. Johnson, Q. Li, G. D. Gu, and N. Koshizuka, 2000, Phys. Rev. Lett. **85**, 828.
Valla, T., A. V. Fedorov, P. D. Johnson, B. O. Wells, S. L. Hulbert, Q. Li, G. D. Gu, and N. Koshizuka, 1999, Science **285**, 2110.

van Veenendaal, M. A., G. A. Sawatzky, and W. A. Groen, 1994, Phys. Rev. B **49**, 1407.
Varma, C. M., 1997, Phys. Rev. B **55**, 14 554.
Varma, C. M., 1999, Phys. Rev. Lett. **83**, 3538.
Varma, C. M., 2000, Phys. Rev. B **61**, 3804.
Varma, C. M., P. B. Littlewood, S. Schmitt-Rink, E. Abrahams, and A. E. Ruckenstein, 1989, Phys. Rev. Lett. **63**, 1996.
Varma, C. M., P. B. Littlewood, S. Schmitt-Rink, E. Abrahams, and A. E. Ruckenstein, 1990, Phys. Rev. Lett. **64**, 497.
Varma, C. M., S. Schmitt-Rink, and E. Abrahams, 1987a, in *Novel Mechanisms of Superconductivity*, edited by S. A. Wolf and V. Z. Kresin (Plenum, New York), p. 355.
Varma, C. M., S. Schmitt-Rink, and E. Abrahams, 1987b, Solid State Commun. **62**, 681.
Venturini, F., R. Hackl, and U. Michelucci, 2000, e-print cond-mat/0205415.
Wang, S. H., Q. Song, B. P. Clayman, J. L. Peng, L. Zhang, and R. N. Shelton, 1990, Phys. Rev. Lett. **64**, 1067.
Wells, B. O., Z.-X. Shen, D. S. Dessau, W. E. Spicer, D. B. Mitzi, L. Lombardo, A. Kapitulnik, and A. J. Arko, 1992, Phys. Rev. B **46**, 11 830.
Wells, B. O., Z.-X. Shen, A. Matsuura, D. M. King, M. A. Kastner, M. Greven, and R. J. Birgeneau, 1995, Phys. Rev. Lett. **74**, 964.
Wen, X.-G., and P. A. Lee, 1996, Phys. Rev. Lett. **76**, 503.
Wendin, G., 1981, *Breakdown of the One-Electron Pictures in Photoelectron Spectroscopy* (Springer, Berlin).
Wenger, F., and S. Östlund, 1993, Phys. Rev. B **47**, 5977.
Wertheim, G., 1978, in *Electron and Ion Spectroscopy of Solids*, edited by L. Fiermans, J. Vennik, and W. Dekeyser (Plenum, New York).
Weschke, E., C. Laubschat, T. Simmons, M. Domke, O. Strebel, and G. Kaindl, 1991, Phys. Rev. B **44**, 8304.
White, P. J., Z.-X. Shen, D. L. Feng, C. Kim, M. Z. Hasan, J. M. Harris, A. G. Loeser, H. Ikeda, R. Yoshizaki, G. D. Gu, and N. Koshizuka, 1999, e-print cond-mat/9901349.
White, P. J., Z.-X. Shen, C. Kim, J. M. Harris, A. G. Loeser, P. Fournier, and A. Kapitulnik, 1996, Phys. Rev. B **54**, 15 669.
White, S. R., and D. J. Scalapino, 2000, Phys. Rev. B **61**, 6320.
Williams, R. H., G. P. Srivastava, and I. T. McGovern, 1980, Rep. Prog. Phys. **43**, 1357.
Withers, R. L., J. S. Anderson, B. G. Hyde, J. G. Thompson, L. R. Wallenberg, J. D. FitzGerald, and A. M. Stewart, 1988, J. Phys. C **21**, L417.
Won, H., and K. Maki, 1994, Phys. Rev. B **49**, 1397.
Wu, D. H., J. Mao, S. N. Mao, J. L. Peng, X. X. Xi, T. Venkatesan, R. L. Greene, and S. M. Anlage, 1993, Phys. Rev. Lett. **70**, 85.
Wu, M. K., J. R. Ashburn, C. J. Torng, P. H. Hor, R. L. Meng, L. Gao, Z. J. Huang, Y. Q. Wang, and C. W. Chu, 1987, Phys. Rev. Lett. **58**, 908.
Wu, W. C., 2002, Phys. Rev. B **65**, 052508.
Xiang, T., and J. M. Wheatley, 1996, Phys. Rev. B **54**, 12 653.
Xu, J.-H., T. J. Watson-Yang, J. Yu, and A. J. Freeman, 1987, Phys. Lett. A **120**, 489.
Yamada, K., S. Wakimoto, G. Shirane, C. H. Lee, M. A. Kastner, S. Hosoya, M. Greven, Y. Endoh, and R. J. Birgeneau, 1995, Phys. Rev. Lett. **75**, 1626.
Yamamoto, A., M. Onoda, E. Takayama-Muromachi, F. Izumi, T. Ishigaki, and H. Asano, 1990, Phys. Rev. B **42**, 4228.
Yeh, J. J., and I. Lindau, 1985, At. Data Nucl. Data Tables **32**, 1.
Yokoya, T., A. Chainani, T. Takahashi, H. Ding, J. C. Campuzano, H. Katayama-Yoshida, M. Kasai, and Y. Tokura, 1996a, Phys. Rev. B **54**, 13 311.
Yokoya, T., A. Chainani, T. Takahashi, H. Kayatama-Yoshida, M. Kasai, and Y. Tokura, 1996b, Phys. Rev. Lett. **76**, 3009.
Yokoya, T., T. Kiss, T. Watanabe, S. Shin, M. Nohara, H. Takagi, and T. Oguchi, 2000, Phys. Rev. Lett. **85**, 4952.
Yoshida, T., 2001, Ph.D. thesis (University of Tokyo).
Yoshida, T., X. J. Zhou, M. Nakamura, S. A. Kellar, P. V. Bogdanov, E. D. Lu, A. Lanzara, Z. Hussain, A. Ino, T. Mizokawa, A. Fujimori, H. Eisaki *et al.*, 2001, Phys. Rev. B **63**, 220501.
Yoshida, T., X. J. Zhou, T. Sasagawa, W. L. Yang, P. V. Bogdanov, A. Lanzara, Z. Hussain, T. Mizokawa, A. Fujimori, H. Eisaki, Z.-X. Shen, T. Kakeshita, *et al.*, 2002, e-print cond-mat/0206469.
Yusof, Z. M., B. O. Wells, T. Valla, A. V. Fedorov, P. D. Johnson, Q. Li, C. Kendziora, S. Jian, and D. G. Hinks, 2002, Phys. Rev. Lett. **88**, 167006.
Zaanen, J., 1999, Science **286**, 251.
Zaanen, J., and O. Gunnarsson, 1989, Phys. Rev. B **40**, 7391.
Zaanen, J., G. A. Sawatzky, and J. W. Allen, 1985, Phys. Rev. Lett. **55**, 418.
Zacher, M. G., R. Eder, E. Arrigoni, and W. Hanke, 2000, Phys. Rev. Lett. **85**, 2585.
Zacher, M. G., W. Hanke, E. Arrigoni, and S.-C. Zhang, 2000, Phys. Rev. Lett. **85**, 824.
Zhang, F. C., and T. M. Rice, 1988, Phys. Rev. B **37**, 3759.
Zhang, S.-C., 1997, Science **275**, 1089.
Zhou, X. J., 2001, Stanford University preprint.
Zhou, X. J., P. Bogdanov, S. A. Kellar, T. Noda, H. Eisaki, S. Uchida, Z. Hussain, and Z.-X. Shen, 1999, Science **286**, 268.
Zhou, X. J., T. Yoshida, S. A. Kellar, P. V. Bogdanov, E. D. Lu, A. Lanzara, M. Nakamura, T. Noda, T. Kakeshita, H. Eisaki, S. Uchida, A. Fujimori, *et al.*, 2001, Phys. Rev. Lett. **86**, 5578.